

Development of an *in vitro* model of peri-implantitis

Thesis submitted by

Elham Hazeim Abdulkareem

BDS, MSc Oral & Maxillofacial Surgery (Baghdad)

For the degree of

DOCTOR OF PHILOSOPHY

In the Faculty of Medicine,

University College London

Department of Microbial Diseases,

UCL Eastman Dental Institute,

256 Gray's Inn Road

London WC1X 8LD

-2013-

Abstract

Introduction

Peri-implantitis is a bacterially induced inflammatory reaction surrounding dental implants leading to loss of supporting bone. Microbial biofilm development seems to play an important role in altering the biocompatibility of the implant surface leading to loss of the implant.

Aims

The aim of this study was to develop an *in vitro* model of peri-implantitis.

Material and Methods

Microcosm biofilms were grown on titanium discs in a constant depth film fermentor (CDFF). Artificial saliva and peri-implant sulcular fluid (PISF) were delivered to simulate three communities associated with dental implants (health, peri-implant mucositis and peri-implantitis). The intact biofilms were visualised by confocal laser scanning microscope (CLSM) at different time points. Biofilms were cultured on non-selective and selective media. PCR-cloning and comparative sequencing of the 16S rRNA gene was carried out to determine bacterial richness. To quantify bacterial species, multiplex qPCR was used for a range of important oral species; qPCR probes were designed, tested and used to quantify *Capnocytophaga* in the communities. Evaluation of current and novel treatment modalities, to eliminate the microcosm biofilm, on commercial titanium surfaces (polished, SLA and SLActive surfaces) was carried out. Furthermore, novel antimicrobial surfaces were prepared and initial biofilm formation assessed by cultural analysis and CLSM.

Results

The biofilms shifted from coccid dense communities, to those dominated by rods and long filaments. The clones shifted from healthy to mixed pathogens. The qPCR revealed significant differences between a healthy and disease conditions. The combined treatment (mechanical and chemical) revealed the greatest reduction of biofilm on all surfaces tested. The antibacterial surfaces showed promotion towards a healthy community on old mature biofilm.

Discussion/Conclusion

The CDFF allowed successful growth of microbial communities and the ability to monitor the bacterial shifts between three communities associated with dental implants. In addition, it has allowed the testing of a range of titanium surfaces and treatment modalities. This model will allow further understanding of the

Abstract

microbiology of peri-implantitis and provide appropriate biofilm communities for testing surfaces infection and treatments.

Declaration

Declaration

I hereby certify that the work embodied in this thesis is entirely the result of my own investigations. This research project has not been submitted either in part or in full for a degree or diploma to this or any other University or examination board elsewhere.

Elham Hazeim Abdulkareem

2013

Dedication

**To my Mama & Daddy, Sisters, Brothers
&
their respective families**

Acknowledgement

It is indeed a great honour and privilege to have been supervised by Dr David Spratt and Dr Jonathan Pratten. They have been stood by me through thick and thin, generously giving of their time, support and encouragement. Their most humane and unstinting approach in guiding me through this period of research from the initial to the final level enabled me to develop an understanding of the subject. I am heartily thankful to them and owe them this PhD.

I fully acknowledge the guidance and support of Professor Nikos Donos, Head of Periodontology department, Eastman Dental Institute, University College London.

I fully acknowledge the support, help and collaboration of Professor Rob Allaker University of Bart's and the London, Queen Mary's School of Medicine.

I would like to thank all Doctors in the microbiology unit, in particular Dr Anna Tymon, Dr Lena Ceric, Dr Derren Ready and Dr Haitham Hussain for their time and patience especially during the early days of the project.

I would like to thank Dr Nicky Mordan for her time and help during CLSM and SEM imaging techniques, Biomaterials & Engineering, Eastman Dental Institute, University College London.

I would like to thank Dr Jie Huang, Kaveh Memarzadeh and Dr Megul Vergus for their help during antibacterial samples preparation, Department of Mechanical Engineering, University College London.

I would like to thank Dr Aviva Petrie for her time and help during statistical analysis, Statistical analysis department, Eastman Dental Institute, University College London.

I would like to thank Dr Daniel Ciantar of the Anatomy department, University College London.

Acknowledgement

I fully acknowledge the guidance and support of Dr Nickos Mardas during periodontology clinic sessions, Periodontology department, Eastman Dental Institute, University College London.

I thank Dr Mohammed Parker of the department of Biomaterials & Engineering for his time and help in the laboratory.

I thank all my colleagues in the Microbial Diseases department, Eastman Dental Institute, University College London.

I fully acknowledge the funding provided for this project by the Iraqi Ministry of Higher Education and Scientific Research. I appreciate the period of study sponsorship by Iraq, which made it is possible for me to undertake research at the Eastman Dental Institute.

The greatest gratitude is due to my parents, for their love, support (both psychological and financial), guidance and encouragement, throughout my life in general and throughout this PhD in particular. I would not have come this far without you. This is your PhD as much as it is mine. If all parents were like you the world would be such a better place.

Considerable credit is also due to my sisters Noor, Marwa, Ola and my brothers Omar, Ahmed and Ali. Despite us being in different parts of the world, their support flowed through e-mail and telephone calls.

Above all I thank **Allah** for giving me the possibility to undertake this adventurous journey in science which gave me some insight into His Creation.

Index of contents

Abstract.....	2
Declaration.....	4
Dedication.....	5
Acknowledgement.....	6
Index of contents.....	8
List of figures.....	18
List of tables.....	30
List of presentations pertaining to this research	32
Chapter 1	34
Literature review	34
Overview.....	35
1.1 History of osseointegration	35
1.2 Peri-implantitis (PI).....	36
1.2.1 Definition	36
1.2.2 Classification	37
1.2.3 Diagnosis.....	37
1.2.4 Clinical signs and symptoms	38
1.2.5 Prevalence of peri-implantitis	39
1.2.6 Etiopathogenesis.....	41
1.2.7 Peri-implant microbiota.....	43
1.2.7.1 Microbiota associated with healthy peri-implant tissues	43
1.2.7.2 Microbiota associated to peri-implant infection	43
1.3 Importance of saliva in oral hygiene	45
1.4 Peri-implant sulcular fluid (PISF)	46
1.5 Biofilms	47
1.5.1 Oral biofilm formation	48
1.5.2 Supragingival biofilm architecture on natural teeth	50

1.5.3 Subgingival biofilm architecture on natural teeth.....	51
1.6 Identification of organisms in peri-implant disease	54
1.6.1 Culture dependent techniques	54
1.6.2 Culture independent techniques.....	55
1.6.2.1 Polymerase chain reaction (PCR) and 16S rRNA genes	55
1.6.2.2 Quantitative polymerase chain reaction (qPCR).....	57
1.6.2.3 Pyrosequencing	61
1.7 Structural analysis of dental plaque	63
1.7.1 Electron microscopy	63
1.7.2 Transmission electron microscopy (TEM)	63
1.7.3 Scanning electron microscopy (SEM)	64
1.7.4 Confocal laser scanning microscopy (CLSM)	65
1.8 Treatment of peri-implantitis	66
1.8.1 Non-surgical therapy	66
1.8.1.1 Antiseptic agents	67
1.8.1.2 Antibiotic use in peri-implantitis	69
1.8.1.3 Mechanical therapy for peri-implantitis	70
1.8.1.4 Laser application for treatment of peri-implant infections	71
1.8.1.5 Photodynamic therapy (PDT)	73
1.8.2 Surgical therapy	76
1.8.3 Cumulative interceptive supportive therapy (CIST)	77
1.9 Modelling dental plaque and plaque related diseases	79
1.9.1 Microplates	79
1.9.2 Flow cells	79
1.9.3 The constant depth film fermentor (CDFF)	80
1.10 Aims of study	82
1.11 Schematic plan of study.....	82
Chapter 2	84
Materials and Methods	84

2.1 Growth media.....	85
2.2 Constant depth film fermentor set up.....	87
2.2.1 Microcosm biofilms.....	89
2.2.2 <i>In vitro</i> model parameters.....	89
2.2.3 Inoculation of the CDFF	90
2.2.4 Biofilm sampling	90
2.2.5 Conditions used for running the CDFF	90
2.3 Identification of cultivable species by comparative 16S rRNA gene sequencing.....	92
2.3.1 DNA extraction	92
2.3.1.1 DNA extraction procedure	92
2.3.1.2 Polymerase chain reaction (amplifying the DNA)	93
2.3.1.3 Agarose gel electrophoresis	93
2.3.1.4 Purification of PCR products.....	94
2.3.2 16S rRNA gene cloning.....	94
2.3.2.1 Culturing	94
2.3.2.2 Colony counting of isolates.....	95
2.3.2.3 Extraction of DNA from clones.....	95
2.3.2.4 Sequencing reactions	95
2.4 Quantitative PCR analysis of biofilm samples	95
2.4.1 Preparation of DNA for standard curve generation	95
2.4.2 QPCR assay set up	96
2.4.3 PCR conditions.....	96
2.4.4 Analysis of qPCR results.....	96
2.4.5 Standard curve	97
2.5 Biofilm imaging.....	97
2.5.1 Confocal laser scanning microscopy (CLSM)	97
2.5.1.1 Sample preparation	97
2.5.1.2 Image analysis.....	97
Chapter 3	98

Development of an <i>in vitro</i> biofilm model of health and peri-implant mucositis.....	98
3.1 Introduction	99
3.2 Materials & Methods	102
3.2.1 Inoculation of the CDFF	102
3.2.2 Changes in environmental parameters from a healthy implant and progressing to peri-implant mucositis.....	102
3.2.3 Structural analysis of biofilms using CLSM	103
3.3 Results	104
3.3.1 Inoculum analysis.....	104
3.3.2 Culture analysis.....	105
3.3.3 Structural analysis of biofilms using CLSM data	108
3.3.4 Biofilm thickness analysis.....	112
3.4 Discussion.....	113
3.5 Conclusion	117
Chapter 4	118
Development of an <i>in vitro</i> microcosm model to simulate a healthy dental implant, peri-implant mucositis and peri-implantitis	118
4.1 Introduction	119
4.2 Materials & Methods	121
4.2.1 Culture media.....	121
4.2.2 Inoculation of the CDFF	121
4.2.3 Production of the biofilm	121
4.2.4 Culture methods	122
4.2.5 Confocal laser scanning microscopy, viability mapping and image analysis.....	122
4.2.6 16S rRNA gene cloning and sequencing	122
4.3 Results	124
4.3.1 Culture analysis.....	124
4.3.1.1 Aerobe and anaerobe viable counts	125
4.3.1.2 Selective media	125

4.3.2 Structural analysis of biofilm using CLSM	129
4.3.2.1 CLSM and image analysis of experiment CDFF 4 and 5.....	129
4.3.2.1.1 Health conditions.....	130
4.3.2.1.2 Peri-implant mucositis conditions	131
4.3.2.1.3 Peri-implantitis conditions	135
4.3.2.2 Viability mapping.....	139
4.3.3 Biofilm thickness.....	153
4.3.4 Comparisons between experiment 4 and experiment 5	154
4.3.5 16S rRNA gene PCR, gene cloning and sequencing.....	156
4.4 Discussion.....	158
4.4.1 Culture analysis.....	158
4.4.2 Characterisation of biofilm architecture	159
4.4.3 Characterisation of biofilm using comparative 16S rRNA gene cloning and sequencing	161
4.5 Conclusions	163
Chapter 5	164
Characterization of microcosm biofilm associated with healthy, peri-implant mucositis and peri-implantitis conditions using multiplex qPCR	164
5.1 Introduction	165
5.2 Materials & Methods	168
5.2.1 Preparation of DNA for standard curve generation	168
5.2.2 Quantitative PCR analysis of biofilm samples.....	168
5.2.3 Oligonucleotide primers and TaqMan probes	168
5.2.4 QPCR assay.....	169
5.2.5 Statistical analysis	170
5.3 Results	171
5.3.1 Standard curve	171
5.3.2 Quantification of bacteria by qPCR	172

5.3.2.1 Detection of <i>Fusobacterium nucleatum</i>	173
5.3.2.2 Detection of <i>Lactobacillus casei</i>	174
5.3.2.3 Detection of <i>Veillonella dispar</i>	175
5.3.2.4 Detection of <i>Neisseria subflava</i>	176
5.3.2.5 Detection of <i>Actinomyces naeslundii</i>	177
5.3.2.6 Detection of <i>Prevotella intermedia</i>	178
5.3.2.7 Detection of <i>Streptococcus sanguinis</i>	179
5.3.2.8 Detection of <i>Streptococcus mutans</i>	180
5.3.3 CDFF peri-implant biofilm communities	181
5.4 Discussion.....	185
5.6 Conclusions	187
Chapter 6	189
Design and evaluation of a quantitative PCR assay for the detection of <i>Capnocytophaga</i> spp.	189
6.1 Introduction	190
6.2 Materials and Methods.....	192
6.2.1 Evaluation of qPCR primers	192
6.2.1.1 Bacterial strains and culture conditions	192
6.2.1.2 Design of oligonucleotide primers.....	192
6.2.1.3 Genomic DNA extraction	196
6.2.1.4 Optimization of qPCR amplification	196
6.2.1.5 Real time PCR assays and melting curve	197
6.2.1.6 Melting curve cycling conditions	197
6.2.1.7 TaqMan probe assay for qPCR data collection	198
6.2.1.8 Standard curve for <i>Capnocytophaga</i> species	198
6.2.1.9 Reproducibility and Reliability	198
6.2.1.10 Quantitative PCR analysis of biofilm samples	198
6.3 Results	199
6.3.1 Agarose gel electrophoresis of PCR products	199

6.3.2 Melting curve	199
6.3.3 Specificity of primers and TaqMan probe	201
6.3.4 Standard curve	203
6.3.5 Quantification of <i>Capnocytophaga</i> species	204
6.3.6 CDFF peri-implant biofilm communities	205
6.4 Discussion.....	206
6.5 Conclusion	208
Chapter 7	209
An <i>in vitro</i> assessment of antibacterial treatment strategies, which are currently available against peri-implantitis biofilms.....	209
7.1 Introduction	210
7.1.1 Objectives.....	214
7.2 Materials and Methods.....	215
7.2.1 Commercial titanium (Ti) discs	215
7.2.2 Microcosm biofilms.....	215
7.2.3 Medium and Inoculum	215
7.2.4 CDFF set up	216
7.2.5 <i>In vitro</i> model parameters.....	217
7.2.6 Conditions used for running the CDFF	217
7.2.7 Titanium surface decontamination	217
7.2.7.1 Non-mechanical cleaning	217
7.2.7.1.1 Reduced transport fluid (control untreated biofilms)	217
7.2.7.1.2 Chlorhexidine	217
7.2.7.1.3 Photodynamic therapy (PDT).....	218
7.2.7.1.3.1 Light Source	218
7.2.7.2 Mechanical cleaning	219
7.2.7.2.1 Titanium brush (TB)	219

7.2.7.2.2 Combination of titanium brush followed by photodynamic therapy (TiBrush + PDT).....	220
7.2.8 Biofilm sampling	220
7.2.9 Confocal laser scanning microscope.....	220
7.2.10 Biocompatibility test.....	221
7.2.10.1 Standard curve of MG-63 cells	221
7.2.10.2 MG-63 cells on decontamination surfaces.....	221
7.2.10.3 Fluoroscan assay.....	223
7.2.10.4 Scanning electron microscopy (SEM).....	223
7.3 Results	225
7.3.1 Cultural analysis	225
7.3.2 Substratum	225
7.3.2.1 Peri-implant mucositis conditions	225
7.3.2.2 Peri-implantitis conditions	229
7.3.3 Biofilm analysis using CLSM	232
7.3.3.1 Biofilm thickness	239
7.3.4 Cell morphology	240
7.3.5 Surface biocompatibility	249
7.4 Discussion.....	253
7.4.1 Microbial culture data	253
7.4.2 CLSM analysis	256
7.4.3 SEM.....	258
7.4.4 Cell culture	259
7.5 Conclusions	260
Chapter 8	261
Assessment of novel nanotechnology surface implant coatings to reduce biofilm formation.....	261
8.1 Introduction	262
8.2 Material and Methods	265

8.2.1 Nanoparticles	265
8.2.2 Electrohydrodynamic (EHD) spraying	265
8.2.3 CDFF set up	268
8.2.4 Biofilm sampling	268
8.2.5 Characterisation of nanocoatings surfaces	268
8.2.6 Confocal laser scanning microscopy (CLSM)	269
8.3 Results	270
8.3.1 Culture analysis	270
8.3.2 Culture analysis of substratum	270
8.3.3 Characterisation of nanoparticles	273
8.3.4 Biofilm structure analysis using CLSM	274
8.3.5 Biofilm thickness analysis	279
8.4 Discussion	280
8.4.1 Characterization of nanoparticles modified titanium surface	280
8.4.2 Culture data	280
8.4.3 CLSM data	282
8.5 Conclusions	282
Chapter 9	283
General discussion and conclusions	283
9.1 General discussion	284
9.1.1 Development of an <i>in vitro</i> model of peri-implantitis	288
9.1.2 Assessing the change in proportions and total of specific bacteria in biofilms of the three communities using multiplex qPCR assays	290
9.1.3 Design of novel TaqMan probe and primers to assess the proportions of <i>Capnocytophaga</i> species	291
9.1.4 Testing of current and future decontamination modalities	292
9.1.5 To assess the initial attachment of bacterial biofilm on novel nanocoatings surfaces	294
9.1.6 Conclusions	294

Index of contents

9.1.7 Clinical relevance	295
9.1.8 Future work	295
References.....	297
Appendix.....	349

List of figures

Figure 1.1. Plastic probe inserted around an implant abutment (Gattani and Ansari, 2010) 37

Figure 1.2. A: Clinical photograph of early peri-implantitis around an implant at the maxillary left lateral incisor position. B: Peri-apical radiograph of maxillary lateral incisor with bone loss, depicting early peri-implantitis. C: Bleeding on probing was noted following removal of the probe (white arrow). D: Peri-apical radiograph depicting moderate peri-implantitis with bone loss (white arrow) (Froum and Rosen, 2012) 38

Figure 1.3. A. Clinical view of a peri-implantitis lesion. B. Peri-apical radiograph exhibiting peri-implantitis with crater shaped (cup or cavity) bone defects (yellow arrow) (Gattani and Ansari, 2010) 39

Figure 1.4. This diagram represents the stages in oral biofilm formation. (A) Pellicle formation. The pellicle is a thin film derived from salivary glycoproteins attached to a clean tooth surface. (B) Initial adhesion. Pioneer bacteria in saliva recognize the binding proteins in acquired pellicle and attached to them. This adhesion is reversible. (C) Maturation. Different bacterial species coaggregate and mature biofilm forms. (D) Dispersion. Bacteria disperse from the biofilm surface and disseminate to colonize a new site 49

Figure 1.5. Localisation of the main bacteria found in supragingival biofilms. Bacteria double stained with probe EUB338 labelled with FITC or Cy3. Bars are 10 µm, taken from Zijnge (2010) 51

Figure 1.6. Showing the stratification and location of commonly found organisms in subgingival plaque. Biofilms were double-stained with probe EUB338 labelled with FITC or Cy3. The yellow colour results from the simultaneous staining with FITC and Cy3 labelled probes. Bars are 10 µm, taken from (Zijnge et al., 2010). Showing stratification that occurs from the base of the sulcus towards the gingival margin 52

Figure 1.7. A diagrammatic representation of subgingival microbiota complexes (Socransky et al., 1998) 53

Figure 1.8. Clinical application of antimicrobial photodynamic therapy in the treatment of peri-implantitis. A. Application of the photosensitizer. The photosensitizer was placed in the peri-implant pocket. B. Irradiation with the diode laser. C. The clinical situation of therapy after 6 months. The treated site

showed limited clinical improvement of peri-implant pocket and bleeding on probing occurred (Takasaki et al., 2009).....	74
Figure 1.9. Schematic of the flow cells models; 1: saliva-supplemented medium. 2: Tissue culture medium. 3: flow cells. 4: Peristaltic pump. 5: lower chamber effluent. 6: upper chamber effluent. Reproduced and image taken from (http://Flow+cells model source).....	80
Figure 1.10. Constant depth film fermentor with power supply (Pratten, 2007).	81
Figure 1.11. A summary schematic of the study.....	83
Figure 2.1. The constant depth film fermentor (CDFF): Diagram of vertical section through the fermentor (Pratten et al, 1998).	88
Figure 2.2. The constant depth film fermentor (CDFF) set-up.....	89
Figure 2.3. Schematic summary for development of the <i>in vitro</i> model of peri-implantitis showing the three stages of development (health, peri-implant mucositis and peri-implantitis).	91
Figure 3.1. Composition of biofilms (viable count data from 5 different media) sampled from the CDFF at different time points (6 h – 348 h). Error bars represent standard deviations ($n = 2$).....	105
Figure 3.2. Composition of biofilms (viable count data from 5 different media) sampled from the CDFF at different time points (6 h – 360 h). Error bars represent standard deviation ($n = 3$).	106
Figure 3.3. Composition of biofilms (viable count data from 5 different media) sampled from the CDFF at different time points (6 h – 438 h). Red vertical line represent time of introduction of microaerophilic gas mixture and increased flow rate of peri-implant sulcular fluid at 222 h. Error bars represent standard deviation ($n = 2$).....	107
Figure 3.4. Images were taken through the z axis within the biofilm, vertical panels are xy voxels and horizontal panels are xz voxel. CLSM images along the z plane of microcosm biofilms were grown for 348 h. At 6 h, the young biofilm is characterised by the presence of viable and non-viable chains (rods and cocci). Scale bar (20 μ m).	108
Figure 3.5. Images were taken through the z axis within the biofilm, vertical panels are xy voxels and horizontal panels are xz voxel. CLSM images were characterised by the presence of extensive numbers of filaments or 'fusiform-shaped' bacteria covering the Ti surface. Few rod or coccal shaped bacteria were evident beneath and those present appeared non-viable cells (red channel). Scale bar (20 μ m).	109

Figure 3.6. Images were taken through the z axis within the biofilm, vertical panels are xy voxels and horizontal panels are xz voxel. CLSM images were characterised by the presence of fusiform shapes which covered the Ti surface, with few rod or coccal shaped bacteria being evident beneath these cells, and when present were non-viable (red channel) cells. Scale bar (20 μ m). 110

Figure 3.7. Images were taken through the z axis within the biofilm, vertical panels are xy voxels and horizontal panels are xz voxel. CLSM images showing microcosm biofilm grown under microaerophilic environment with increased flow of PISF represented by 366 h, 414 h and 438 h. Scale bar (20 μ m). 111

Figure 3.8. The thickness of biofilm at different time points in μ m. At 222 h, a change in the environment to a microaerophilic atmosphere was initiated with increased introduction of PISF for experiment 3. 112

Figure 4.1. Viable counts of aerobe and anaerobe spp. of microcosm biofilm under health, peri-implant mucositis and peri-implantitis conditions. First black dash line represents the switch over to microaerophilic gas mixture and increased flow of PISF, second black dash line represents switch over to an anaerobic gas mixture and PISF only. Error bars represent standard deviation ($n = 4$). Graphs show data from experiments 4 and 5. 126

Figure 4.2. Viable counts of *Streptococcus* spp., *Actinomyces* spp., Gram negative anaerobe spp. and *Veillonella* spp. of microcosm biofilm under health, peri-implant mucositis and peri-implantitis conditions. First black vertical dash line represents the switch over to microaerophilic gas mixture and increased flow of PISF, second black dash line represents switch over anaerobic gas mixture and PISF only. Error bars represent standard deviation ($n = 4$). Graphs represent combined data from experiments 4 and 5. 127

Figure 4.3. Viable counts of *Candida* spp. and *Staphylococcus* spp. from microcosm biofilms under health, peri-implant mucositis and peri-implantitis conditions. First vertical black dash line represents the switch over to microaerophilic gas mixture and increased flow of PISF, second black dash line represents switch over anaerobic gas mixture and PISF only. Error bars represent standard deviation ($n = 4$). Graphs represent combined data from experiments 4 and 5. 128

Figure 4.4. Representative CLSM images of healthy dental implant biofilms sampled at 96 h with x, y and z planes presented. Scale bar (20 μ m). 130

Figure 4.5. Representative CLSM images of peri-implant mucositis biofilms sampled at 246 h with x, y and z planes presented. Scale bar (20 μ m). 131

Figure 4.6. Representative CLSM images of peri-implant mucositis biofilms sampled at 366 h with x, y and z planes. Scale bar (20 μ m).....	132
Figure 4.7. Representative CLSM images of peri-implant mucositis biofilms sampled at 390 h with x, y and z planes presented. Scale bar (20 μ m).....	133
Figure 4.8. Representative CLSM images of peri-implant mucositis biofilms sampled at 438 h with x, y and z planes presented. Scale bar (20 μ m).....	134
Figure 4.9. Representative CLSM images of peri-implantitis biofilms sampled at 540 h with x, y and z planes presented. Scale bar (20 μ m).	135
Figure 4.10. Representative CLSM images of peri-implantitis biofilms sampled at 588 h with x, y and z planes presented. Scale bar (20 μ m).	136
Figure 4.11. Representative CLSM images of peri-implantitis biofilms sampled at 612 h with x, y and z planes presented. Scale bar (20 μ m).	137
Figure 4.12. Representative CLSM images of peri-implantitis biofilms sampled at 714 h with x, y and z planes presented. Scale bar (20 μ m).	138
Figure 4.13. Fluorescent image intensity, blue line represents the total biomass intensity while the green and red lines represent the viable and non-viable channels from the CLSM stacks images; under health condition at 96 h, under peri-implant mucositis at 246 h, 366 h and 390 h. 4 and 5 represent individual experiments.....	141
Figure 4.14. Fluorescent image intensity, blue line represents the total biomass intensity while the green and red lines represent the viable and non-viable channels from the CLSM stacks images; under peri-implant mucositis at 438 h and under peri-implantitis at 540 h, 588 h. 4 and 5 represent individual experiments.....	142
Figure 4.15. Fluorescent image intensity, blue line represents the total biomass intensity while the green and red lines represent the viable and non-viable channels from the CLSM stacks images; under peri-implantitis at 612 h and 714 h. 4 and 5 represent individual experiments.....	143
Figure 4.16. Individual optical sections of biofilms sampled at 96 h from both experiments 4 and 5. Numbering is from 1 at the apex in 1 μ m increments until the titanium surface is reached.....	144
Figure 4.17. Individual optical sections of biofilms sampled at 246 h for both experiments 4 and 5. Numbering is from 1 at the apex in 1 μ m increments until the titanium surface is reached.....	145

Figure 4.18. Individual optical sections of biofilms sampled at 366 h for both experiments 4 and 5. Numbering is from 1 at the apex in 1 μm increments until the titanium surface is reached.....	146
Figure 4.19. Individual optical sections of biofilms sampled at 390 h from experiments 5. Numbering is from 1 at the apex in 1 μm increments until the titanium surface is reached.....	147
Figure 4.20. Individual optical sections of biofilms sampled at 438 h from both experiments 4 and 5. Numbering is from 1 at the apex in 1 μm increments until the titanium surface is reached.....	148
Figure 4.21. Individual optical sections of biofilms sampled at 540 h from both experiments 4 and 5. Numbering is from 1 at the apex in 1 μm increments until the titanium surface is reached.....	149
Figure 4.22. Individual optical sections of biofilms sampled at 588 h from both experiments 4 and 5. Numbering is from 1 at the apex in 1 μm increments until the titanium surface is reached.....	150
Figure 4.23. Individual optical sections of biofilms sampled at 612 h from both experiments 4 and 5. Numbering is from 1 at the apex in 1 μm increments until the titanium surface is reached.....	151
Figure 4.24. Individual optical sections of biofilms sampled at 714 h from both experiments 4 and 5. Numbering is from 1 at the apex in 1 μm increments until the titanium surface is reached.....	152
Figure 4.25. Changes in biofilm thickness (μm) over time. First black dash line represents the switch over to microaerophilic gas mixture, second black dash line represents switch over anaerobic gas mixture.....	153
Figure 5.1. The standard curve of <i>L. casei</i> generated from a plot C_t against log concentration for eight 10-fold serial dilutions.....	171
Figure 5.2. The linear slope of <i>L. casei</i> , with a slope of -3.337 and an R^2 of 0.99 for triplicate samples replicated three times.....	172
Figure 5.3. Total counts of bacteria obtained by qPCR represented by blue bars. Numbers of <i>F. nucleatum</i> obtained by qPCR are represented by the black line. The proportion of <i>F. nucleatum</i> is represented by the yellow line with data points labelled. At 222 h the environment was changed to a microaerophilic atmosphere with increased introduction of PISF. At 516 h, the change of environment to anaerobic atmosphere. <i>F. nucleatum</i> error bars represent standard deviation ($n = 6$). Universal error bars represent standard deviation ($n = 9$).....	173

Figure 5.4. Total counts of bacteria obtained by qPCR represented by blue bars. Numbers of *L. casei* obtained by qPCR are represented by the black line. The proportions of *L. casei* are represented by the yellow line with data points labelled. At 222 h the environment was changed to a microaerophilic atmosphere with increased introduction of PISF. At 516 h, the change of environment to anaerobic atmosphere. *L. casei* error bars represent standard deviation ($n = 6$). Universal error bars represent standard deviation ($n = 9$)..... 174

Figure 5.5. Total counts of bacteria obtained by qPCR represented by blue bars. Numbers of *V. dispar* obtained by qPCR are represented by the black line. The proportions of *V. dispar* are represented by the yellow line with data points labelled. At 222 h the environment was changed to a microaerophilic atmosphere with increased introduction of PISF. At 516 h, the change of environment to anaerobic atmosphere. *V. dispar* error bars represent standard deviation ($n = 6$). Universal error bars represent standard deviation ($n = 9$)..... 175

Figure 5.6. Total counts of bacteria obtained by qPCR represented by blue bars. Numbers of *N. subflava* obtained by qPCR are represented by the black line. The proportions of *N. subflava* are represented by the yellow line with data points labelled. At 222 h the environment was changed to a microaerophilic atmosphere with increased introduction of PISF. At 516 h, the change of environment to anaerobic atmosphere. *N. subflava* error bars represent standard deviation ($n = 6$). Universal error bars represent standard deviation ($n = 9$)..... 176

Figure 5.7. Total counts of bacteria obtained by qPCR represented by blue bars. Numbers of *A. naeslundii* obtained by qPCR are represented by the black line. The proportions of *A. naeslundii* are represented by the yellow line with data points labelled. At 222 h the environment was changed to a microaerophilic atmosphere with increased introduction of PISF. At 516 h, the change of environment to anaerobic atmosphere. *A. naeslundii* error bars represent standard deviation ($n = 6$). Universal error bars represent standard deviation ($n = 9$)..... 177

Figure 5.8. Total counts of bacteria obtained by qPCR represented by blue bars. Numbers of *P. intermedia* obtained by qPCR are represented by the black line. The proportions of *P. intermedia* are represented by the yellow line with data points labelled. At 222 h the environment was changed to a microaerophilic atmosphere with increased introduction of PISF. At 516 h, the change of environment to anaerobic atmosphere. *P. intermedia* error bars represent

standard deviation ($n = 6$). Universal error bars represent standard deviation ($n = 9$).....	178
Figure 5.9. Total counts of bacteria obtained by qPCR represented by blue bars. Numbers of <i>S. sanguinis</i> obtained by qPCR are represented by the black line. The proportions of <i>S. sanguinis</i> are represented by the yellow line with data points labelled. At 222 h the environment was changed to a microaerophilic atmosphere with increased introduction of PISF. At 516 h, the change of environment to anaerobic atmosphere. <i>S. sanguinis</i> error bars represent standard deviation ($n = 9$). Universal error bars represent standard deviation ($n = 9$).....	179
Figure 5.10. Total counts of bacteria obtained by qPCR represented by blue bars. Numbers of <i>S. mutans</i> obtained by qPCR are represented by the black line. The proportions of <i>S. mutans</i> are represented by the yellow line with data points labelled. At 222 h the environment was changed to a microaerophilic atmosphere with increased introduction of PISF. At 516 h, the change of environment to anaerobic atmosphere. <i>S. mutans</i> error bars represent standard deviation ($n = 9$). Universal error bars represent standard deviation ($n = 9$)....	180
Figure 6.1. Regions used as target for <i>Capnocytophaga</i> species. The primers and TaqMan probe based on alignment of the 16S rRNA gene sequence. The black forward primer position 357F (Lane, 1991) and red text is the reverse primer position. Blue text is the dual labelled probe position; [] represents locked nucleic acid bases; *** represents identical aligned sequences.....	194
Figure 6.2. Signature sequences for the closely and more distantly related reference strains were aligned by Clustal W2 program. The black forward primer position 357F (Lane, 1991) and red text is the reverse primer position. Blue text is the dual labelled probe position; [] represents locked nucleic acid bases; *** represents identical aligned sequences.	195
Figure 6.3. Gel electrophoresis image of <i>C. ochracea</i> PCR products. Expected size by: 224 bp, 1 by: <i>C. ochracea</i> (red arrow). 2 by: <i>F. nucleatum</i> , 3 by: <i>L. casei</i> , 4 by: <i>V. dispar</i> , 5 by: <i>N. subflava</i> , 6 by: <i>A. naeslundii</i> , 7 by: <i>P. intermedia</i> , 8 by: <i>S. sanguinis</i> , 9 by: <i>S. mutans</i> , 10 by: <i>P. gingivalis</i> , 11 by: <i>T. forsythia</i> , and 12 by: <i>A. actinomycetemcomitans</i> and M by: Hyperladder I.	199
Figure 6.4. A SYBR Green melt curve demonstrating the target amplicons have a T_m of around 84°C. The y axis represents the derivative of fluorescence changes and the x axis represents the temperature (°C).	200

Figure 6.5. <i>C. ochracea</i> amplification plot determined by qPCR using primers set and TaqMan probe shows the optimal probe concentration given the lowest C_t value with the highest fluorescent signal (red colour) triplicate samples and negative control samples (blue colour) at 60°C annealing temperature.....	200
Figure 6.6. The amplicon of <i>C. ochracea</i> (red colour) is specific at 60°C against all strains mentioned in section 6.2.1.1 except <i>V. dispar</i> (blue colour), <i>F. nucleatum</i> (yellow colour) and <i>P. gingivalis</i> (black colour).....	201
Figure 6.7. The amplicon of <i>C. ochracea</i> is specific at 63°C against all strains except <i>F. nucleatum</i> (green colour).....	202
Figure 6.8. The Amplicon is specific for <i>C. ochracea</i> at 64°C against all strains.	202
Figure 6.9. The standard curve is linear from 10^1 to 10^6 copies of <i>C. ochracea</i>	203
Figure 6.10. Total numbers of bacteria determined by qPCR represented by blue bars. Numbers of <i>Capnocytophaga</i> spp. obtained by qPCR are represented by the black line. The proportions of <i>Capnocytophaga</i> spp. are represented by the yellow line with data labelled. <i>Capnocytophaga</i> spp. error bars represents standard deviation ($n = 6$). Universal error bars represent standard deviation ($n = 9$).	204
Figure 7.1. The CDFF containing pans were autoclaved at 121°C for 15 min. A. The Ti discs were added aseptically to the pans through the sampling port with a flat-ended tool inside a flow cabinet. B. The pan was tapped down to the level of the turntable with a flat-ended tool.	216
Figure 7.2. Periowave photodisinfection system.	218
Figure 7.3. A. The Straumann TiBrush; B. The titanium brush (manufactured by Straumann); C. Slow speed NSK Contra angle handpiece (ERI 6i 16:1); D. Portable NSK Mio Coreless Micromotor System (120V).	219
Figure 7.4. A. MG-63 cells were placed onto a disc; B. 200 μ l of culture medium was added after 4 h of incubation of MG-63 cells.	222
Figure 7.5. 20 μ l of Alamar blue was added into the medium and incubated for 4 h prior to fluoroscan assay.	222
Figure 7.6. A. 100 μ l of sample (medium and Alamar blue) was removed and placed into each well of 96 wells. B. The optical densities of each sample were read at 530 nm (excitation) and 590 nm (emission) on a micro-plate reader (Fluoroscan II).	223

Figure 7.7. The composition of the biofilm microorganisms (CFU/ml) after decontamination techniques on polished titanium surfaces under peri-implant mucositis conditions. Error bars represent standard deviation ($n = 4$) 227

Figure 7.8. The composition of the biofilm microorganisms (CFU/ml) after decontamination techniques on SLA titanium surfaces under peri-implant mucositis conditions. Error bars represent standard deviation ($n = 4$) 227

Figure 7.9. The composition of the biofilm microorganisms (CFU/ml) after decontamination techniques on SLActive titanium surfaces under peri-implant mucositis conditions. Error bars represent standard deviation ($n = 4$) 228

Figure 7.10. The total counts of biofilm microorganisms (CFU/ml) after decontamination techniques on polished titanium surfaces under peri-implantitis conditions. Error bars represent standard deviation ($n = 4$) 230

Figure 7.11. The total counts of biofilm microorganisms (CFU/ml) after decontamination techniques on SLA surfaces under peri-implantitis conditions. Error bars represent standard deviation ($n = 4$) 230

Figure 7.12. The total counts of biofilm microorganisms (CFU/ml) after decontamination techniques on SLActive surfaces under peri-implantitis conditions. Error bars represent standard deviation ($n = 4$) 231

Figure 7.13. CLSM images showing viability of 612 h microcosm on control untreated biofilms (RTF) biofilms. Vertical view represents yz and sagittal view represents xz taken through layers of z axis. Scale bar represents 20 μm 234

Figure 7.14. CLSM images showing viability of 612 h microcosm (PDT) biofilms. Green represents viable bacteria. Red represents non-viable bacteria. Vertical view represents yz and sagittal view represents xz taken through layers of z axis. Scale bar represents 20 μm 235

Figure 7.15. CLSM images showing viability of 612 h microcosm (TB+PDT) biofilms. Red represents non-viable bacteria. Vertical view represents yz and sagittal view represents xz taken through layers of z axis. Scale bar represents 20 μm 236

Figure 7.16. CLSM images showing viability of 612 h microcosm (TiBrush) biofilm on three surfaces. Red represents non-viable bacteria. Vertical view represents yz and sagittal view represents xz taken through layers of z axis. Scale bar represents 20 μm 237

Figure 7.17. CLSM images showing viability of 612 h microcosm (CHX) biofilms. Green represents viable bacteria. Red represents non viable bacteria. Vertical

view represents yz and sagittal represents xz taken through layers of z axis. Scale bar represents 20 μm 238

Figure 7.18. Thickness of biofilm μm grown on the three titanium surfaces after treatment regimes. Biofilms were 612 h old and grown under peri-implantitis conditions. Error bars represent standard deviation ($n = 4$). 239

Figure 7.19. Sterile discs examined under SEM revealed that polished surfaces were relatively moderately smooth, whilst SLA and SLActive surfaces exhibited micropits, grooves and troughs (deemed moderately rough). Samples were viewed at $\times 200$ (Bar 200 μm). 242

Figure 7.20. MG-63 cells (red arrows) attaching on three different sterile structural surfaces. Samples were viewed at $\times 1500$, $\times 500$, and $\times 150$ (Bar 40 μm , 100 μm , 400 μm , respectively). 243

Figure 7.21. MG-63 cells grown on three untreated control biofilms surfaces (RTF) after 7 days in culture. Green arrow indicates residual biofilm, yellow arrow indicates organic layer made solid lamp, and red arrow indicates MG-63 cells. Samples were viewed at $\times 1500$, $\times 500$, and $\times 150$ (Bar 40 μm , 100 μm , 400 μm , respectively). 244

Figure 7.22. SEM images of MG-63 cell on three different titanium surfaces following PDT decontamination regimes after 7 days in culture. Red arrow indicates MG-63, yellow arrow indicates residual bacteria and biofilm, and green arrow indicates organic layer. Samples were viewed at $\times 1500$, $\times 500$, and $\times 150$ (Bar 40 μm , 100 μm , 400 μm , respectively). 245

Figure 7.23. SEM images of MG-63 cells grown on three different titanium surfaces following TiBrush and PDT decontamination regimes after 7 days in culture. Red arrows indicates MG-63 cells division on polished surface, MG-63 attaching to the surface on SLA, and MG-63 split from the surface due to SEM sample processing. Samples were viewed at $\times 1500$, $\times 500$, and $\times 150$ (Bar 40 μm , 100 μm , 400 μm , respectively). 246

Figure 7.24. MG-63 cells (red arrows) attaching to three different titanium surfaces following TiBrush decontamination regime. Samples were viewed at $\times 1500$, $\times 500$, and $\times 150$ (Bar 40 μm , 100 μm , 400 μm , respectively). 247

Figure 7.25. SEM images of MG-63 cells on three different titanium surfaces following CHX decontamination regimes after 7 days in culture. Red arrow indicates MG-63 attaching and splitting due to SEM process on SLA surface, yellow arrow indicate residual bacteria or biofilm, and green arrow indicates

organic materials. Samples were viewed at $\times 1500$, $\times 500$, and $\times 150$ (Bar 40 μm , 100 μm , 400 μm , respectively)	248
Figure 7.26. The standard curve of fluorescence and number of MG-63 cells after 4 h incubation with Alamar blue. The MG-63 cell number represents the mean \pm standard deviation ($n = 4$).....	249
Figure 8.1. Electrohydrodynamic Deposition (EHD). A, the coating setup shows the nanoparticles were placed into a syringe and needle arrangement on a syringe pump to allow a controlled flow rate. B, Ti discs were arranged within the nanoparticle spray. The yellow conical line illustrates the spray coverage.	266
Figure 8.2. A & B, nano coated Ti discs prior to heat treatment (600°C for 1 h). C. cooling at a rate of 1°C/min.	267
Figure 8.3. Total anaerobic bacteria counts on fastidious anaerobic agar under conditions simulating health for biofilm grown on control (uncoated polished titanium surfaces); ZnO surfaces, HA surfaces and combined ZnO + HA surfaces. Sampling points were 6, 24, 96 hours. Two separate experimental runs comprised of 4 replicates. Error bars represent the standard deviations ($n = 4$).	271
Figure 8.4. Total aerobic bacteria counts on blood agar under conditions simulating health for biofilm grown on control (uncoated polished titanium surfaces); ZnO surfaces, HA surfaces and combined ZnO + HA surfaces. Sampling points were 6, 24, 96 hours. Two separate experimental runs comprised of 4 replicates of each were used. Error bars represent the standard deviations ($n = 4$).....	272
Figure 8.5. Total <i>Streptococcus</i> spp. counts on mitis salivarius agar under conditions simulating health for biofilm grown on control (uncoated polished titanium surfaces); ZnO surfaces, HA surfaces and combined ZnO + HA surfaces. Sampling points were 6, 24, 96 hours. Two separate experimental runs comprised of 4 replicates. Error bars represent the standard deviations ($n = 4$).	272
Figure 8.6. Scanning electron micrograph showing the microstructure of the nano surfaces on the Ti substrate prepared using the electrosprayed technique. Nano spray surfaces are shown at magnification of $\times 120$ (scale bar 100 μm). Inserts are higher magnification ($\times 10,000$ with scale bar 1 μm). Pure Ti (control) disc is shown a higher magnification, scale bar 200 μm	273

Figure 8.7. The surface colour of the Ti coated discs after 600°C treatment. ZnO coating become purple, HA become dark blue and combined ZnO + HA become blue/grey colour)..... 273

Figure 8.8. Live/dead staining of 24 h biofilm on control and ZnO nanoparticles. The lowest total viable biomass volume was on ZnO followed by HA nanoparticles surfaces. The highest total viable biomass volume was on combined ZnO + HA nanoparticles followed by control (pure titanium) surfaces. Scale bars 20 μ m. 275

Figure 8.9. Live/dead staining of 24 h biofilm on HA and combined ZnO + HA nanoparticles. The lowest total viable biomass volume was on ZnO followed by HA nanoparticles surfaces. The highest total viable biomass volume was on combined ZnO + HA nanoparticles followed by control (pure titanium) surfaces. Scale bars 20 μ m. 276

Figure 8.10. Live/dead staining of 96 h biofilm on control, ZnO nanoparticles. The lowest total viable biomass volume was on combined ZnO + HA followed by ZnO and HA nanoparticles surfaces compared with total viable biomass volume was on control (pure titanium) surfaces. Scale bars 20 μ m. 277

Figure 8.11. Live/dead staining of 96 h biofilm on HA and combined ZnO + HA nanoparticles. The lowest total viable biomass volume was on combined ZnO + HA followed by ZnO and HA nanoparticles surfaces compared with total viable biomass volume was on control (pure titanium) surfaces. Scale bars 20 μ m... 278

Figure 8.12. Thickness in μ m of biofilms over time. Error bars represents the standard deviation ($n = 10$)..... 279

List of tables

Table 3.1. Composition of pooled saliva (inoculum) on selective and non-selective culture media for three experiments. Mean and \pm standard deviation of ($n = 2$).....	104
Table 4.1. Composition of pooled saliva (inoculum) on selective and non-selective culture media. Error bars represent standard deviation ($n = 2$).....	124
Table 4.2. The mean CFU/ml data of biofilm generated in experiment 4 and experiment 5 under healthy, peri-implant mucositis and peri-implantitis conditions.....	155
Table 4.3. Taxa detected by using 16S rRNA gene cloning and sequencing from microcosm biofilms grown on titanium surfaces in a CDFF at different time points 6 h and 96 h representing health, 246 h and 438 h representing peri-implant mucositis and, 540 h and 714 h representing peri-implantitis. Green shading refers to organisms commonly classified from the literature as being associated with healthy dental implants. Yellow shading refers to organisms associated with peri-implant mucositis and red shading refers to dominant organisms associated with peri-implantitis. Blue shading refers to organisms not normally associated with the resident oral microbiota.....	157
Table 5.1. Primers and probes used in the three triplex qPCR arrays. The triplex were composed of <i>F. nucleatum</i> , <i>L. casei</i> and <i>V. dispar</i> (FLV); <i>N. subflava</i> , <i>A. naeslundii</i> and <i>P. intermedia</i> (NAP); and <i>S. sanguinis</i> , <i>S. mutans</i> and universal (SSU) with few modifications to the assays previously reported (Ciric et al., 2010).....	169
Table 5.2. Numbers of each of the taxa investigated in microcosm biofilms samples under health conditions. \pm represents standard deviation.....	182
Table 5.3. Numbers of each of the taxa investigated in microcosm biofilms samples under peri-implant mucositis conditions. \pm represents standard deviation.....	183
Table 5.4. Numbers of each of the taxa investigated in microcosm biofilms samples under peri-implantitis conditions. \pm represents standard deviation.	184
Table 6.1. Lists of primers based on 16S rRNA gene sequence were designed in this study for detection and quantification of <i>Capnocytophaga</i> species.....	193
Table 6.2. Sequences of primers and probe were used with final concentration.	193
Table 6.3. qPCR assays reactions for single tube and 5 tubes.	197

Table 6.4. The mean value of <i>Capnocytophaga</i> species investigated by qPCR of microcosm biofilms grown in the CDFF under health, peri-implant mucositis and peri-implantitis conditions, \pm standard deviation ($n = 6$)	205
Table 7.1. The mean \pm standard deviation of CFU/ml ($n = 4$) of the salivary inoculum	225
Table 7.2. The number of cultured MG-63 cells on days 1, 4 and 7 on the three Ti surfaces. Biofilms were grown under peri-implant mucositis conditions prior to treatment. Control disc with untreated biofilm and sterile disc without biofilm; \pm standard deviation ($n = 2$).....	251
Table 7.3. The number of cultured MG-63 cells on day 1, day 4, day 7 on the three Ti surfaces. Biofilms were grown under peri-implantitis conditions prior to treatment. Control untreated biofilm surfaces and sterile without biofilm surfaces; \pm standard deviation ($n = 2$).....	252
Table 8.1. The mean \pm standard deviation ($n = 4$) (CFU/ml) of the salivary inoculum	270

List of presentations pertaining to this research

1. 10th European Oral Microbiology Workshop and Conference: oral presentation: 19-22 May 2011, Zeist, The Netherlands. An *in vitro* model of bacterial shifts associated with peri-implantitis. Elham Hazeim Abdulkareem*, Jonathan Pratten, Nicola Mordan, David Spratt.
2. Graduate school poster competition: poster presentation. 2011. University College London. An *in vitro* model of bacterial shifts associated with peri-implantitis. Elham Hazeim Abdulkareem*, Jonathan Pratten, Nicola Mordan, David Spratt.
3. European Association of Osseointegration Conference: oral presentation: Athens 2011. An *in vitro* model of bacterial shifts associated with peri-implantitis. Elham Hazeim Abdulkareem*, Jonathan Pratten, Nicola Mordan, David Spratt.
4. Graduate school poster competition: poster presentation. 2012. University College London. An *in vitro* model of bacterial shifts associated with peri-implantitis. Elham Hazeim Abdulkareem*, Jonathan Pratten, Nicola Mordan, David Spratt.
5. Oral Microbiology and Immunology Group: postgraduate meeting: oral presentation: Newcastle University, United Kingdom, 2012. An *in vitro* model of peri-implantitis. Elham Hazeim Abdulkareem*, Jonathan Pratten, Nicola Mordan, Anna Tymon, Nikos Donos, David Spratt.
6. 6th ASM conference on Biofilm. American Society for Microbiology: poster presentation: Miami, Florida, United State, 2012. Decontamination strategies of titanium surfaces using an *in vitro* model of peri-implantitis. Elham Hazeim Abdulkareem*, Nikos Donos, Jonathan Pratten, Nicola Mordan, Anna Tymon, David Spratt.
7. Oral Microbiology and Immunology Group: postgraduate meeting: oral presentation: University College London, Eastman Dental Institute, United Kingdom, 2013. Treatment strategies of titanium surfaces using an *in vitro* model of peri-implantitis. Elham Hazeim Abdulkareem*, Nikos Donos, Jonathan Pratten, Nicola Mordan, Anna Tymon, David Spratt.

- 8.** 2nd annual scientific meeting, Iraqi Association for Oral Research division of International association of Dental Research (IADR): oral presentation, London, United Kingdom, 2013. The assessment of antibacterial nano-coatings in an *in vitro* model of peri-implantitis. Elham Hazeim Abdulkareem*, K Memarzadeh, J. Pratten, M. Vergas, Huang J., R.P. Allaker, D. Spratt.
- 9.** International Team of Implantology (ITI) Italy Congress 2013. A novel *in vitro* model of peri-implantitis to study the efficacy of treatment protocols. Elham Hazeim Abdulkareem*, Jonathan Pratten, David Spratt.

Chapter 1
Literature review

Overview

Peri-implantitis is defined as irreversible mucosal inflammation around a dental implant associated with the loss of supporting bone. Implants, like teeth, are susceptible to bacterial plaque accumulation and calculus formation. The various complex composition of the peri-implantitis microbiota has been extensively reviewed. The first part of this review will report the history of osseointegration, and the investigations into the peri-implantitis microbiota to highlight how certain species came to be regarded as pathogens in peri-implant infections. In recent years, new methods have become available based on the direct examination of DNA from samples, which will also be reviewed. An overview of current *in vitro* methods which may be applicable to model dental implant infections in a defined manner will be given and finally, an assessment made on the impact of treatment modalities on peri-implantitis infections.

1.1 History of osseointegration

In the last four decades, the development of osseointegrated titanium implants has led to countless changes in the field of restorative dentistry. Therefore, the use of dental implants represents one of the most rapidly expanding areas of dentistry. The birth of modern implantology can be found in the late 1950s and early 1960s. Bränemark discovered in 1952 that titanium irreversibly bonds to living bone tissue and called the phenomenon osseointegration. The first practical application of new titanium roots in an edentulous patient was in 1965 (Adell et al., 1981). Zarb led the first international team to learn the principles of osseointegration, in the late 1970s. One implant described by Bränemark et al. (1977) and composed of commercially pure titanium has had considerable clinical success. The first published work in the area was by Adell et al. (1981) in the International Journal of Oral Surgery. The first commercial dental implants were called Biotes, but these were later renamed 'Bränemark' to reflect the inventor. Interestingly, these implants are still in use today. The term Osseointegration was originally coined by Bränemark, to describe direct contact between the implant and the bone tissue (Bränemark et al., 1983). In the early 1990s, Zarb and Bränemark introduced a new description: "A process whereby clinically asymptomatic rigid fixation of alloplastic materials is achieved and maintained in bone during functional loading" (Albrektsson and Wennerberg, 2005). Since the introduction of the Bränemark implant system (Nobel Biocare, Gothenburg, Sweden) in 1982, the number of patients with implant-supported prosthesis has grown exponentially.

Endosseous implants are available with various surface characteristics ranging from relatively smooth-machined surfaces to more roughened surfaces achieved by coating, blasting, acid treatments or a combination of these. The ultimate goal of modern implantology is satisfactory and fast osseointegration, which is largely dependent on the implant surface itself (Wennerberg and Albrektsson, 2000). Based on the scale of the features, the surface roughness of implants can be divided into macro-, micro- and nanosized topologies (Albrektsson, 1998). A bioinert surface is one which itself does not play a role in osseointegration. It merely forms a favourable substrate for the osseous deposition to occur, whereas, a bioactive surface is one which actively participates in the osseointegrative process due to the reaction between the chemically modified surface coating and the surrounding bone (Wennerberg and Albrektsson, 2000). Substrates such as calcium phosphate and hydroxyapatite (HA) coatings were classified as osteoinductive surfaces as they enhance bone regeneration and may even cause bone to grow or extend into an area where it is not normally found. Surface irregularities were produced through ablative/subtractive procedures or additives procedures. Ablative procedures include grit blasting, acid etching, anodizing and shot/laser peening (which is a mechanical method similar to sandblasting). Additive procedures include plasma spraying, electrophoretic deposition, sputter deposition, sol gel coating, pulsed laser deposition and biomimetic precipitation.

Current trends in implant surfaces have various topographies with a wide range of thickness, from nanometers to millimetres. Nanotechnology may produce surfaces with controlled topography and chemistry that would help in understanding biological interactions and developing novel implants surfaces with predictable tissue–integrative properties. Many have been reported with nanometer-controlled surfaces that have an effect on early events, such as adsorption of proteins, blood clot formation and cell behaviour occurring upon implantation of dental implants (Stanford, 2008).

1.2 Peri-implantitis (PI)

1.2.1 Definition

The term 'peri-implantite' occurred for the first time in the scientific literature as early as 1965 in a French article by Levignac: 'L'osteolyse periimplantaire, Periimplantose – Periimplantite'. It was not until two decades later, in the late 1980s, that the term appeared in English scientific literature (Mombelli et al., 1987) to describe a destructive inflammatory process affecting the soft and hard tissues around osseointegrated implants, leading to the formation of a peri-

implant pocket and loss of supporting bone. In the 1990s it was modified to describe an inflammatory disease that results in the loss of supporting bone around an implant (Mombelli and Mericske-Stern, 1990).

1.2.2 Classification

As with periodontitis and gingivitis, the term of 'peri-implant mucositis' has been defined as an inflammatory condition residing in the mucosa without clinical evidence of bone loss. Peri-implantitis is a general clinical term describing an inflammatory condition affecting mucosa around an osseointegrated implant in function (Lindhe and Meyle, 2008, Lindhe et al., 1992, Lang et al., 1993, Mombelli, 1999, Zitzmann and Berglundh, 2008).

1.2.3 Diagnosis

There are a number of clinical parameters used to evaluate periodontal conditions and these have also been used to assess peri-implantitis; these include:

- a) Peri-implant probing depth.
- b) Bleeding on probing.
- c) Exudation and suppuration from the peri-implant space.
- d) Swelling.

Many studies have shown that a successful implant generally allows a plastic probe penetration of approximately 3 mm to 4 mm in the healthy peri-implant sulcus and is illustrated in Figure 1.1. (Mombelli and Lang, 1998, Zarb and Alberktsson, 1990).

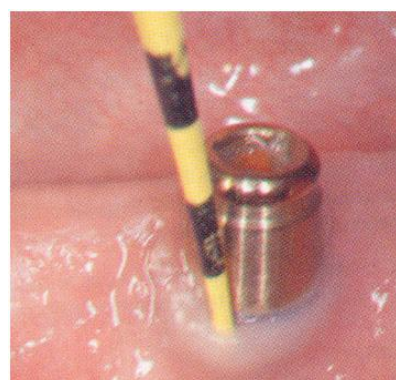


Figure 1.1. Plastic probe inserted around an implant abutment (Gattani and Ansari, 2010).

1.2.4 Clinical signs and symptoms

The inflammation of the soft tissues is associated with bleeding after gentle probing with a blunt instrument. There may be suppuration from the pocket. Swelling and redness of the marginal tissues are not always very prominent and there is usually no pain associated with peri-implantitis (Leonhardt et al., 1992, Mombelli, 1994, 1999, Lindhe et al., 2008, Zitzmann & Berglundh, 2008, Lang and Berglundh, 2011). The typical bone defect is “crater-like” (a cup shape or cavity on the bone) and runs all around the implant (Mombelli and Lang, 1998) (Figures 1.2 and 1.3).

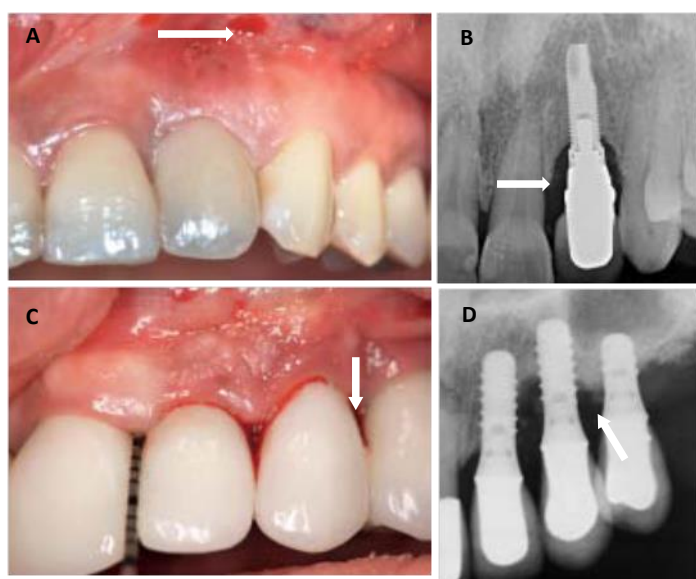


Figure 1.2. A: Clinical photograph of early peri-implantitis around an implant at the maxillary left lateral incisor position. B: Peri-apical radiograph of maxillary lateral incisor with bone loss, depicting early peri-implantitis. C: Bleeding on probing was noted following removal of the probe (white arrow). D: Peri-apical radiograph depicting moderate peri-implantitis with bone loss (white arrow) (Froum and Rosen, 2012).

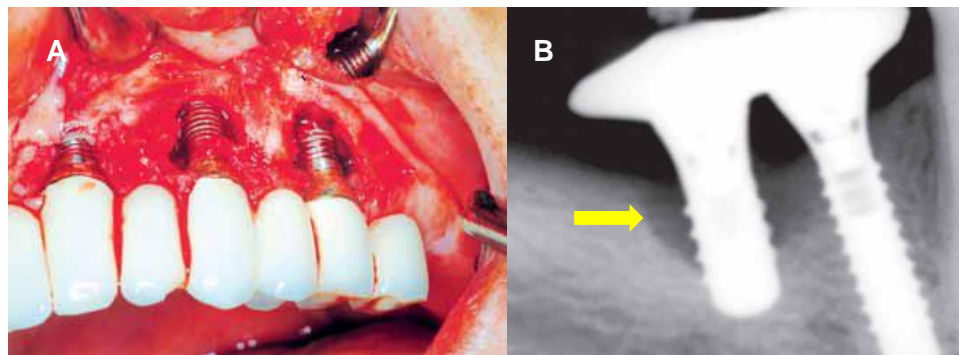


Figure 1.3. A. Clinical view of a peri-implantitis lesion. B. Peri-apical radiograph exhibiting peri-implantitis with crater shaped (cup or cavity) bone defects (yellow arrow) (Gattani and Ansari, 2010).

1.2.5 Prevalence of peri-implantitis

The use of dental implants has been widely recognized as a predictable treatment modality for the replacement of missing teeth (Aglietta et al., 2009). Bearing in mind that more than two million oral implants are placed annually (Klinge et al., 2005), peri-implant disease could affect more than half a million implants each year (Atieh et al., 2012). Several long-term studies have reported success rates greater than 90% over various time periods (Adell et al., 1981, 1986, Albrektsson et al., 1986, Buser et al., 1990, 1991, 2012). Indeed, despite frequent complications, patients demonstrate a high satisfaction rate of close to 90% with regard to cost. However, only around 24% of patients were 'very satisfied' (Simonis et al., 2010). Various studies have published success and survival rates of dental implants, after at least 10 years of functional loading, to range from 89% to 95% (Simonis et al., 2010). An accurate estimation of the true prevalence of peri-implant disease however, remains unclear. This could be attributed to the lack of standardized criteria for diagnosis of peri-implant mucositis and peri-implantitis, different implant systems being used, and that there are no reliable parameters to assess the biological and prosthetic complications (Simonis et al., 2010). A study by Taguchi et al. (2013) reported that the cumulative survival rate for an implant supporting a single crown was 97% after an observation period of 4 years (Taguchi et al., 2013). Success is defined as being free of all these complication over the entire observation period. Systematic reviews have shown a survival rate of 96.5% after 5 years for single tooth replacement, 95.4% for implant-implant fixed bridgework and 90.1% for implant reconstruction (Lang et al., 2004). There are several published studies to date aiming to analyse the prevalence of mucositis and peri-implantitis. The literature reports that peri-implantitis affects 7.8% - 43.3% of all implants (Berglundh et al., 2002; Ferreira et al., 2006, Roos-Jansäker et al., 2006,

Zitzmann & Berglundh, 2008, Koldsland et al., 2010). Roos-Jansäker et al. (2006) found that 16% of patients had peri-implantitis in a study of 218 patients, which involved a follow up period of 9-14 years. Whilst Zitzmann & Berglundh et al. (2008) reinterpreted these results using different diagnostic criteria for peri-implantitis and stated that the prevalence would be 55.6%. Mir-Mari et al. (2012) evaluated 524 implants placed in the maxilla and 440 implants placed in the mandible from 1-18 years post-implantation. The authors analysed the prevalence of patients with peri-implantitis and this ranged from between 12% and 22%, while 39% also had peri-implant mucositis. Another study by Ferreira et al. (2006) involving 221 patients over a 42 month period, showed the prevalence of peri-implantitis to be only 8.9%. Rinke et al. (2011) found the prevalence of peri-implantitis to be 11.2% and mucositis 44.9%. Kourtis et al. (2004) and Pjetursson et al. (2004) reported a peri-implantitis incidence of 8.6% within 5 years. Other studies by Berglundh et al. (2002) reported a prevalence of peri-implantitis of 6.4% in partially edentulous patients with a follow-up period of more than 5 years. Roos-Jansäker et al. (2003) reported that the prevalence of peri-implantitis varies between 1% and 19%. Jung et al. (2008) found peri-implantitis as a frequent complication with an incidence of 8.6% after observation period of 5 years and 17% after 10-16 years of function. Koldsland et al. (2010) reported that the prevalence of peri-implantitis ranged between 11% and 47%. The percentage of peri-implantitis after the first year of loading has been shown to account for 10% to 50% of implant failures (Esposito et al., 1998). Some have argued that these figures are “the tip of the iceberg” and that with better diagnosis they will increase. Peri-implantitis and periodontal diseases share some risk factors such as tobacco use, levels of oral hygiene and diabetes mellitus. Many patients who had periodontitis and subsequently were treated with implants may have greater risk of peri-implant disease (Klinge et al., 2005, Donos et al., 2012, Safii et al., 2010). The risk of peri-implantitis was reported to be five times higher in patients with a history of chronic periodontitis. Moimaz et al. (2009) reported that smoking, a recognized risk factor for periodontitis, is also the most important risk factor for the development of mucositis. There are data that indicate that smoking considerably increases the risk of failure of dental implants (Bain and Moy, 1993, Moimaz et al., 2009). An increased prevalence of peri-implant disease in the form of suppuration and loss of bone has also been reported in smokers (Lindquist et al., 1997).

1.2.6 Etiopathogenesis

The primary factor for peri-implantitis remains the colonization of the implant surface with pathogenic bacteria, similar to the aetiology of periodontitis (Heitz – Mayfield & Lang, 2010). The lack of direct attachment between the dental implant and the mucosa may facilitate migration of the microbiota along the implant surface and increase the risk of peri-implantitis and eventually loss of implant (Meffert, 1988, Mombelli & Lang, 1998, Esposito et al., 1998). These failures are classified into early (failure to establish osseointegration) and late (failure to maintain osseointegration) (Mombelli, 1999). One way to differentiate early and late failures is to define the early group as implants removed before prosthetic restoration, while those occurring after prosthetic rehabilitation are classified as late (Esposito et al., 1998). Early failures are characterized by minimal bone loss and are predominantly in female and younger patients. According to a study by Manor et al. (2009), the most common causes of late failures were peri-implantitis, and implant overloading and fracture. However, the principal cause of early failure was the lack of osseointegration. Early failures are caused by the inability to establish a close contact between bone and implant due to the absence of bone apposition and the formation of scar tissue between the surface of the implant and surrounding bone (Esposito et al., 2000). Esposito et al. (1998), noted that surgical trauma, bone quality and bone quantity were the most important etiological factors involved in early implant failures. In the majority of studies, success rates are calculated from the time of implant loading and full functionality, therefore little information is available on implant failures prior to loading (Kronström et al., 2000, Kronström et al., 2001). The causes and mechanisms of early implant failure are unclear; different studies (Kronström et al., 2000, Kronström et al., 2001) have found a variety of statistically significant factors associated with early implant failure, these are: age and sex (Sverzut et al., 2008), systemic diseases (Alsaadi et al., 2008), smoking (Sverzut et al., 2008), type of edentulous (Alsaadi et al., 2008), maxillary implant location (van Steenberghe et al., 2002), quantity and quality of bone (Shibli et al., 2007), and implant length and diameter (Noguerol et al., 2006). Immunological (Kronström et al., 2000) and genetic factors (Leite et al., 2008) have also been associated with early implant failure.

The weak point of dental implants is inadequate attachment of the gingiva which may lead to rapid adhesion of bacteria and biofilm formation in this region. The implant surface is susceptible to infection because of two main reasons namely, formation of a surface biofilm and compromised immune ability at the implant/tissue interface (Mombelli and Décailliet, 2011). Biocompatibility of

titanium implants can be attributed to a surface protein layer formed under physiological conditions. This protein layer makes the surface suitable for bacterial colonization and biofilm formation. The host immune response in the implant is consequently impaired. In the early phase after implantation, the local defence system is severely disturbed by surgical trauma, and hence it is the most likely time for infection. Even after completion of tissue integration, the host defence at the implant/tissue interface is still compromised because of the small number of blood vessels in this area. The reduced defence mechanism facilitates colonization of bacteria and infection may result. Mombelli et al. (1987) suggested that persistent bacterial contamination and functional overloading were the two key aetiological factors for chronic inflammation which lead to peri-implantitis and implant failure. Furthermore, bacterial peri-implant infections may arise as a result of non-microbial events which may subsequently favour the emergence of a pathogenic microbiota (Mombelli et al., 2012). For example, the fracture of an implant can give rise to secondary bacterial infection, and thus provoke peri-implant disease. Another example is peri-implant infection due to submucosal persistence of luting cement, where the presence of a foreign body gives rise to a bacterial infection. Wilson (2009) reported that excess dental cement was used in 81% of 39 of cases associated with clinical and/or radiographical signs of peri-implant infection.

After plaque accumulation begins, neutrophils move to the peri-implant crevice in response to chemotactic peptides, released from the bacteria. Furthermore, as bacteria damage epithelial cells, they induce cytokines, thereby attracting leukocytes (predominantly neutrophils) to the crevice. The neutrophils within the crevice can then phagocytose and digest bacteria removing these bacteria from the pocket. If the neutrophil becomes overloaded with bacteria, it degranulates. This cause tissue damage from toxic enzymes released from the neutrophils. In such instances, the gingival tissue will become inflamed, a process termed peri-implant mucositis. If the inflammation extends from the marginal gingiva into the supporting peri-implant tissues, this resulted in bone destruction and loss of attachment. The factors involved in bone destruction in peri-implant disease are bacterial and host mediated. Bacterial plaque products induce differentiation of bone progenitor cells into osteoclasts and stimulate gingival cells to release mediators that have the same effect (Norowski and Bumgardner, 2009).

1.2.7 Peri-implant microbiota

1.2.7.1 Microbiota associated with healthy peri-implant tissues

Most oral disease states, such as periodontal disease and peri-implantitis are related to dental plaque, a microbial biofilm consisting of a complex multispecies community of organisms formed on colonisable surfaces. Following exposure of the surface of the dental implant to the oral cavity, a biofilm is formed (Mombelli et al., 1987, Rosenberg et al., 1991, van Winkelhoff et al., 2000). The colonising organisms initially provide a surface for subsequent adhesion of periodontal pathogens and possible development of peri-implantitis (Heuer et al., 2007). Healthy peri-implant tissues are dominated by high numbers of coccoid cells, a low proportion of anaerobic species, a small number of Gram-negative species and a low proportion of periodontopathogenic bacteria (Ata-Ali et al., 2011). It is also possible to find low concentrations of anaerobic Gram-negative bacilli in some healthy implant sites (Heitz-Mayfield and Lang, 2010, Quirynen et al., 2002). It has been shown that Gram-positive facultative anaerobes are predominate in healthy peri-implant crevices of successful implants (Mombelli and Mericske-Stern, 1990). The authors reported that 52.8% of the organisms cultured were facultatively anaerobic cocci and 17.4% were facultatively anaerobic rods, while Gram-negative anaerobic rods accounted for only 7.3%. *Fusobacterium* spp. and *Bacteroides intermedius* were both found in 8.8% of the samples. Shibli et al. (2008) analysed supragingival and subgingival plaque were taken from the deepest sites of each implant and analyzed for the presence of 36 microorganisms by checkerboard DNA–DNA hybridization. The authors reported three host-compatible bacterial species including: *Actinomyces naeslundii*, *Streptococcus intermedius* and *Streptococcus mitis* and one putative periodontal pathogen (*Fusobacterium periodonticum*) were present at higher levels in the supragingival samples compared with the subgingival samples of the healthy implants. The authors also reported very similar pattern in terms of mean proportions of microbial complexes in the subgingival biofilm of subjects with chronic periodontitis has been described previously.

1.2.7.2 Microbiota associated to peri-implant infection

Generally, numerous different bacterial species are important in the aetiology of peri-implant mucositis and peri-implantitis (Pontoriero et al., 1994, Augthun and Conrads, 1997, Salcetti et al., 1997, Leonhardt et al., 1999, Quirynen et al., 2002).

Clinical studies have documented that sites of peri-implant infections present a microbiota very similar to that found in periodontal disease (Hultin et al., 2002).

High levels and proportions of periodontal pathogens including *Prevotella nigrescens*, *Campylobacter rectus*, *Aggregatibacter actinomycetemcomitans*, *Porphyromonas gingivalis*, *Tannerella forsythia* and *Treponema denticola* have been identified. Interestingly, some studies have identified organisms associated with peri-implantitis which are not commonly found in the oral cavity, including *Staphylococcus aureus*, enteric bacilli and frequently found in the oral cavity such as *Candida albicans* (Botero et al., 2005, Fürst et al., 2007). Chloroflexi, Tenericutes, and Synergistetes phyla were only detected at peri-implantitis sites (Koyanagi et al., 2010). Also *Parvimonas micra*, *Peptostreptococcus stomatis*, *Pseudoramibacter alactolyticus*, and *Solobacterium moorei* were only observed at peri-implantitis sites (Koyanagi et al., 2010). *Fusobacterium nucleatum* and *Granulicatella adiacens* were identified at all of the peri-implantitis sites (Koyanagi et al., 2010). Microbiological DNA-probe analysis has revealed that patients with peri-implantitis harbour high levels of periodontal pathogens like *A. actinomycetemcomitans*, *P. gingivalis*, *Prevotella intermedia*, *T. forsythus* and *T. denticola*. Also, subgingival spirochete levels in healthy implants have been reported to be low or even totally absent compared to that of failing implants (Hultin et al., 2002). Lower levels of the genera *Leptotrichia*, *Propionibacter* and *Prevotella* and higher levels of *Actinomyces*, *Peptococcus*, *Campylobacter*, *non-mutans Streptococcus*, *Butyrivibrio* and *Streptococcus mutans* were identified in peri-implantitis by 454 pyrosequencing techniques (Kumar et al., 2012). It has been reported that Gram-negative obligate anaerobes predominantly comprise the microbiota in peri-implantitis pockets as well as in periodontal pockets (Mombelli et al., 1987). The existing dental biofilm is an important source of bacteria colonizing the new inserted implants in partial edentulous patients. Periodontal bacteria around natural teeth act as a reservoir for spread to the whole oral cavity (Kolenbrander et al., 2006). In a complete edentulous cavity, the peri-implant microbiota source was from the oral mucous membranes (Danser et al., 1996) or could not be detected after full mouth extraction (Danser et al., 1994, Kocar et al., 2010). Recently, it has been confirmed that there is a predominance of Firmicutes and Bacteroidetes in peri-implantitis. *Dialister* spp. and *Eubacterium* spp. belonging to Firmicutes have a high prevalence and proportion at peri-implantitis sites (Koyanagi et al., 2013). Also *Peptostreptococcus* spp. were more abundant in peri-implantitis. Heavy colonization of *Fusobacterium* spp. and *Streptococcus* spp. were observed at peri-implantitis sites (Koyanagi et al., 2013). These bacteria are frequently observed in both peri-implantitis and periodontitis biofilms (Mombelli et al., 1987). The recent clinical study by Thierbach and Eger (2013) found that the distribution

of red complex periodontal pathogens (*F. nucleatum*, *T. forsythia*, *Treponema denticola*, *P. gingivalis*) in patients with peri-implantitis and suppuration had a higher prevalence than in patients with peri-implantitis and no suppuration formation. Although numerous studies have examined the presence of periodontopathic bacteria at PI sites, the prevalence varies between reports (Mombelli and Décailliet, 2011).

1.3 Importance of saliva in oral hygiene

Saliva is an important resource for evaluating physiological and pathological conditions in humans. The advantages of using saliva in laboratory diagnosis are that it is readily available, easy to collect, non-invasive, and has a simple low-cost storage when compared to blood collection. With the addition of modern techniques and chemical instrumentation equipment, there has been an increase in its use for laboratory investigations, applicable for basic and clinical analyses in the field of dentistry. It has been used as a diagnostic and monitoring method for periodontal disease (Kaufman and Lamster, 2000).

Water is the greatest component of saliva, representing 99% of its composition. Organic and inorganic molecules dissolved in the aqueous component vary widely from one individual to another, and also in the same individual at different of the day. Approximately 90% of saliva volume is produced by the salivary glands, and the remaining 10% is produced by minor salivary glands (Napeñas et al., 2009). Saliva contains several inorganic ions including sodium, potassium, calcium, chloride, bicarbonate and phosphate. Some of these ions can reduce the cariogenic effect of acids produced from bacterial metabolism of dietary carbohydrates by buffering system.

Other nitrogenous compound present in saliva are, for example, urea. The major organic constituents of submandibular/sublingual saliva are proteins and glycoproteins, such as mucin. Mucin are the glycoproteins primarily responsible for lubrication and may also bind to toxins, agglutinate bacteria, interact with host cells, and are important components of the acquired pellicle and plaque matrix formation (Dodds et al., 2005). Several antibacterial factors are present in saliva such as lysozyme, lactoferrin and the sailoperoxidase system which are important in controlling bacterial and fungal colonization of the oral cavity (Dodds et al., 2005). In the mouth, saliva participates in the activities of chewing, speaking and swallowing, as well as taste sensitivity, lubrication of tissues, mucosal protection and regulation of pH. Hog gastric mucin has been used as a model substitute of saliva because this mucin possesses the highest similarity in glycoprotein structure to human mucin (Bradshaw et al., 1994). Saliva harbours

as many as 10^8 bacteria per ml (Saxton, 1973). Bacteria found in saliva reflect the number and types of bacteria present on the teeth supragingivally as well as on the lateral and dorsal surfaces of the tongue (Asikainen et al., 1991).

1.4 Peri-implant sulcular fluid (PISF)

The gingival crevicular fluid (GCF) is a serum transudate that exudes through the sulcular and junctional epithelium. The GCF contains most of the components of serum which are present within the circulation, but in periodontitis it is selectively enriched with certain components as it passes through the resident inflammatory cell infiltrate, such as immunoglobulin which is secreted locally by the plasma cell population (Offenbacher, 1996). Since the GCF originates from plasma, its chemical composition corresponds to that of blood serum (Ficara et al., 1975). Several enzymes and cytokines have been associated with gingival inflammation and alveolar bone loss. Offenbacher (1996), found an increase in GCF levels of cytokines and prostaglandin E₂ in periodontitis patients. The Peri-implant crevicular fluid (PICF) has its origin at the base of the marginal gingival sulcus (Casado et al., 2013b). Periodontitis and peri-implantitis share similar features of inflammatory processes and both are associated with resorption of alveolar bone (Meffert, 1996). Adonogianaki et al. (1995) reported that both peri-implant sulcular fluid (PISF) and GCF are produced via similar mechanisms, have similar immune and inflammatory responses, and both contain components related to the nature of the bone. Several studies support a correlation between peri-implant infections and an increase of inflammatory mediators in the PISF (Heitz-Mayfield, 2008a). During inflammation the flow of crevicular fluid increases into the pocket. Apse et al. (1989) reported that the volume of GCF did not differ between implant sites and natural teeth, and the features of inflammation were similar. Another study by Behneke et al. (1997), confirmed the positive correlation between PISF volume and peri-implant bone loss. Several studies from the literature have supported the evidence that there is an increased volume of GCF (Rüdin et al., 1970) and PISF (Tözüm et al., 2008, Güncü et al., 2012) with inflamed implants/gingivitis compared to non-inflamed/healthy sites. The GCF flow rate *in vivo* per day is only a few millilitres (Wilson, 1999). For example, gingivitis subjects have GCF flow rates of 0.087 μ l/min, whereas for moderate periodontal pocket depth, a rate of 0.4 μ l/min has been reported (Goodson, 2003, Uitto, 2003). Another study by Heitz et al. (2004) showed that there was no significant change in GCF volume (week 1 = 0.14 μ l, week 2 = 0.09 μ l, week 3 = 0.07 μ l) on early healing following periodontal surgical procedures, including one-stage implant installations. PISF was shown to be a promising

medium for the detection of peri-implant activity; in addition it has successfully been used as a biochemical marker in peri-implant disease (Heitz-Mayfield, 2008b). It seems to reflect the degree of inflammatory reaction affecting the surrounding tissues, bone and mucosa, and the presence of biomechanical stress (Heitz-Mayfield, 2008b, Casado et al., 2013a).

1.5 Biofilms

Biofilms are defined as aggregations of microorganisms attached to each other or to a surface and enclosed in extracellular polymeric substance (EPS) produced by the bacteria themselves (Marsh, 2010). Dental plaque is a soft tenacious deposit forming on the surfaces of teeth, denture, restorations or the oral mucosa (Busscher et al., 2010). The oral cavity differs from all other human microbial habitats by the simultaneous presence of two types of surfaces for microbial colonization: shedding (mucosa) and non-shedding surfaces (teeth or restorative materials and dentures) (Busscher et al., 2010). The oral cavity is an open system. In the oro-phryngeal areas, a dynamic equilibrium exists between the adhesion capacity of microorganisms and a variety of removal forces such as swallowing, frictional removal by diet, tongue and oral hygiene intervention, and the cleansing actions of saliva.

In order to survive within the oro-phryngeal area, bacteria need to adhere either to the soft or hard tissues in order to resist shear forces (Marsh, 2005). The high turnover of the oral epithelial lining (shedding 3x /day) is an efficient defence mechanism as it prevents the accumulation of large masses of microorganisms. On the other hand, teeth, dentures, or endosseous implants provide non-shedding surfaces, which allow the formation of thick biofilms (Listgarten, 1994). The first step in the formation of a biofilm after the formation of a conditioning film has been studied on solid surfaces in the oral cavity. Microbial biofilms in the oral cavity are involved in the aetiology of various oral diseases such as caries, periodontal and endodontic disease and dental implant failures (Lee et al., 2012). It consists of a large aggregation of microorganisms embedded in an organic matrix comprised of material derived from the diet, the biological fluids and products of bacterial metabolism. Many biofilms are bathed by fluids, such as saliva flowing over dental plaque on a tooth surface in oral cavity. The mature plaque composed of approximately 70% of microbial contents with a concentration of organisms which may average 1.7×10^{11} organisms/g wet weight (Socransky, 1970). It has been reported that (EPS) matrix forms 75-80% volume of the biofilm (Haffajee and Socransky, 2005). EPS plays a prominent role in bacterial retention at a surface. Not only does the EPS form the sticky

matrix that can ultimately regulate the structural component of the biofilm, but it may also affect initial attachment. It is estimated that of the total organic carbon content of biofilms, 50%-90% comes from the EPS (Flemming et al., 2000) with 40% of the dry weight of dental biofilms being polysaccharide in nature (Paes Leme et al., 2006). There are different bacterial species in the mouth and species mainly colonize the teeth, tongue, oral mucosa, hard palate, carious lesions, periodontal pocket and peri-implant pocket. The distribution of microbiota in the oral cavity is not random and depends on the particular environment those sites provide, for example the anaerobic environment provided by the periodontal pocket.

1.5.1 Oral biofilm formation

The first step of oral biofilm formation is the attachment of acquired pellicle to a clean tooth surface (Marsh and Percival, 2006). The pellicle is a thin protein containing film derived from salivary glycoproteins. The second step of biofilm formation is bacterial adhesion to the pellicle. In this stage, the attachment is reversible and those organisms initially attached can easily be detached from the pellicle. As soon as the pioneer bacteria attach to the pellicle, EPS begins to be made, which helps the bacteria remain bound together. The main pioneer bacterial genera attaching to the tooth surface are *Actinomyces* spp., *Streptococcus* spp., *Haemophilus* spp., *Capnocytophaga* spp., *Veillonella* spp., and *Neisseria* spp. (Marsh, 2010). The early colonizing bacteria provide specific binding sites for subsequent bacterial colonisation and promote biofilm development. Later colonizing bacteria recognize polysaccharide receptors or proteins on the bacterial cell surfaces of early colonisers and attach to them (Kinniment et al., 1996a). When bacteria coaggregate (bacteria attach to one another via specific molecules) in a mature oral biofilm (Rickard et al., 2004), different morphological forms such as 'corn cob', bristle brush, or other forms may develop (Marsh and Percival, 2006). The attached bacterial species include *F. nucleatum*, *Treponema* spp., *T. forsythensis*, *P. gingivalis*, and *A. actinomycetemcomitans*. The mature biofilm microbial components are quite different from the initial biofilm. The shifts that occur during biofilm development include a reduction in streptococci and *Neisseria* spp. and an increase in *Actinomyces*, *Corynebacterium*, *Fusobacterium* and *Veillonella* species (Marsh, 1994). Dispersion of biofilm cells can occur when bacteria leave the biofilm by single cell detachment or a cluster of cells detaching in a mature biofilm. The dispersion model of biofilm takes place in different ways and includes erosion, sloughing and seeding. The possible reasons for detachment could be due to

limited nutrients present at the original site necessitating for bacteria to relocate, or it might be due to fluid shear force of saliva (Figure 1.4).

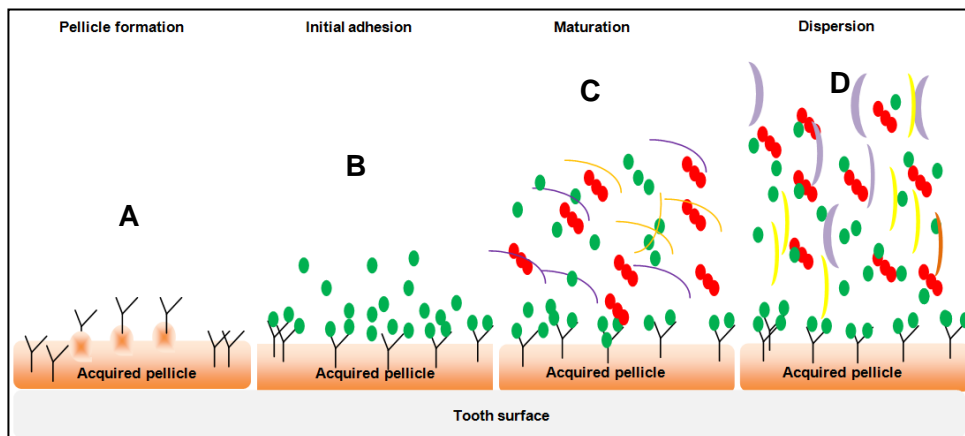


Figure 1.4. This diagram represents the stages in oral biofilm formation.

(A) Pellicle formation. The pellicle is a thin film derived from salivary glycoproteins attached to a clean tooth surface. (B) Initial adhesion. Pioneer bacteria in saliva recognize the binding proteins in acquired pellicle and attach to them. This adhesion is reversible. (C) Maturation. Different bacterial species coaggregate and mature biofilm forms. (D) Dispersion. Bacteria disperse from the biofilm surface and disseminate to colonize a new site.

1.5.2 Supragingival biofilm architecture on natural teeth

The complex architecture of oral biofilms in nature was highlighted by the work of Listgarten et al. (1963) who used light and electron microscopy on epoxy resin crowns and extracted teeth. The term “supragingival plaque” refers to those biofilms that form on the tooth surface above the level of the gingival margin (this also includes interdental biofilms). As this surface, unlike any other in the body, is non-shedding physical and chemical means are required to remove accumulated plaque. The initial plaque formation starts with the salivary pellicle adsorbed to the tooth surface. The acquired pellicle is rapidly adsorbed to the enamel surface within seconds of cleaning and continues to accumulate for approximately 2 hours to form a tenacious layer 0.1-1 μm thick (Listgarten, 1994). This pellicle conditioning film affects the order of microbial colonisation (Marsh, 2004). Figure 1.5, highlights the localisation and stratification of bacteria within supragingival plaque, with respect to the tooth surface. Within the first 24 hours of colonisation, oral streptococci have been shown to make up 60-90% of supragingival plaque (Nyvad and Kilian, 1987). The streptococci are joined by other initial colonizers such as *Actinomyces* spp., and *Lactobacillus* spp. (Listgarten, 1994). *Streptococcus salivarius* is often associated with building stability in the biofilm matrix via lactose uptake and urease enzymes (Sissons and Yakub, 2000). The earliest foci of bacterial accumulation is localized to surface pits and fissures, but can also be found on isolated protected portions of smooth surfaces (Newman, 1972a, Newman, 1972b). In time, the bacteria spread over larger sections of smooth surfaces with thicker accumulations at protected sites. Plaque development on smooth surfaces is favoured on interdental surfaces and on the gingival margin, where plaque is more protected from the frictional effects of the tongue and cheek.

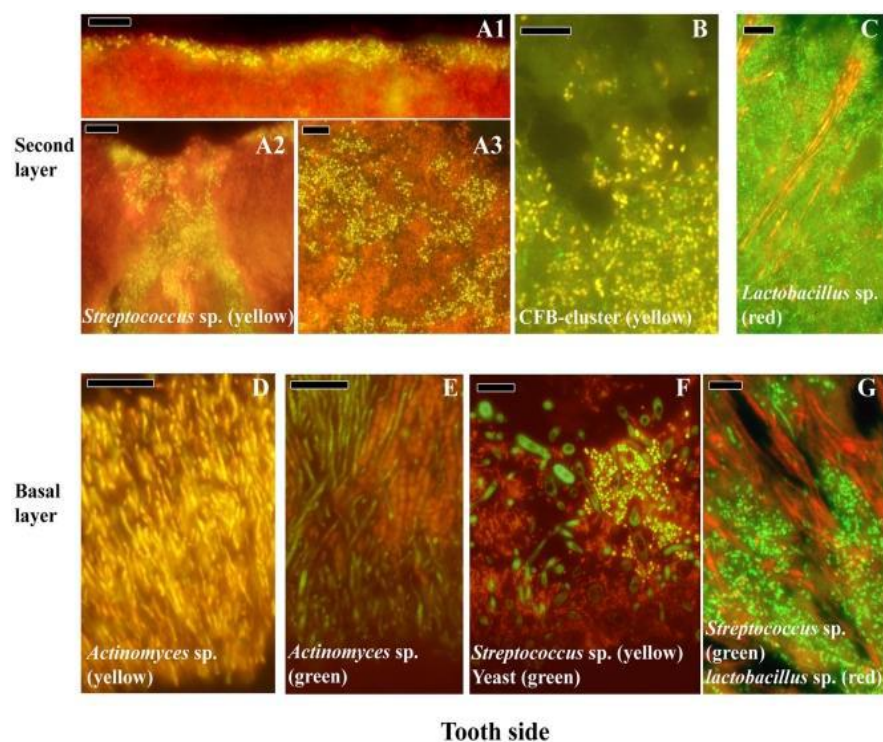


Figure 1.5. Localisation of the main bacteria found in supragingival biofilms. Bacteria double stained with probe EUB338 labelled with FITC or Cy3. Bars are 10 μ m, taken from Zijnge (2010).

1.5.3 Subgingival biofilm architecture on natural teeth

Subgingival plaque is formed in the protected environment between the gingival margin and the tooth surface. Due to this location, the main nutrition comes from gingival crevicular fluid (GCF), as well as potentially blood. An anaerobic environment can develop and lead to a predominance of more asaccharolytic species (Darveau et al., 1997). Figure 1.6, shows the stratification of the organisms that can occur in subgingival plaque within the periodontal pocket. The undisturbed growth of supragingival plaque on the gingival margins begins to cause inflammation, redness, and swelling. These changes result in the creation of a deepened gingival sulcus (pseudo-pocket), which provides a relatively anaerobic environment suitable for the growth of motile rods, Gram-negative filamentous bacteria and spirochetes (Listgarten, 1994). Much of the microbiota of the gingival sulcus area is motile and the structural organization of this microbial population is different from that seen in the supragingival region (Listgarten, 1994). The author observed formation of columnar micro-colonies with their long axis perpendicular to the crown surface. After one day of growth, Gram-positive cocci dominated these columns long with some isolated branching filaments. After one week, filaments appeared on top of the columns. After three weeks, filaments were seen fully colonising the biofilm and subsequently

replacing the coccus dominated population. Most of the subgingival microbiota were Gram-negative bacteria such as *P. gingivalis*, *P. intermedia*, and *P. nigrescens*. Most *Prevotella* sp. and *Parvimonas micra* colonize the biofilm in micro-colonies which are located on top or within the top layer of the biofilm. *P. gingivalis* and *Porphyromonas endodontalis* also appear mainly as micro-colonies within the top layer.

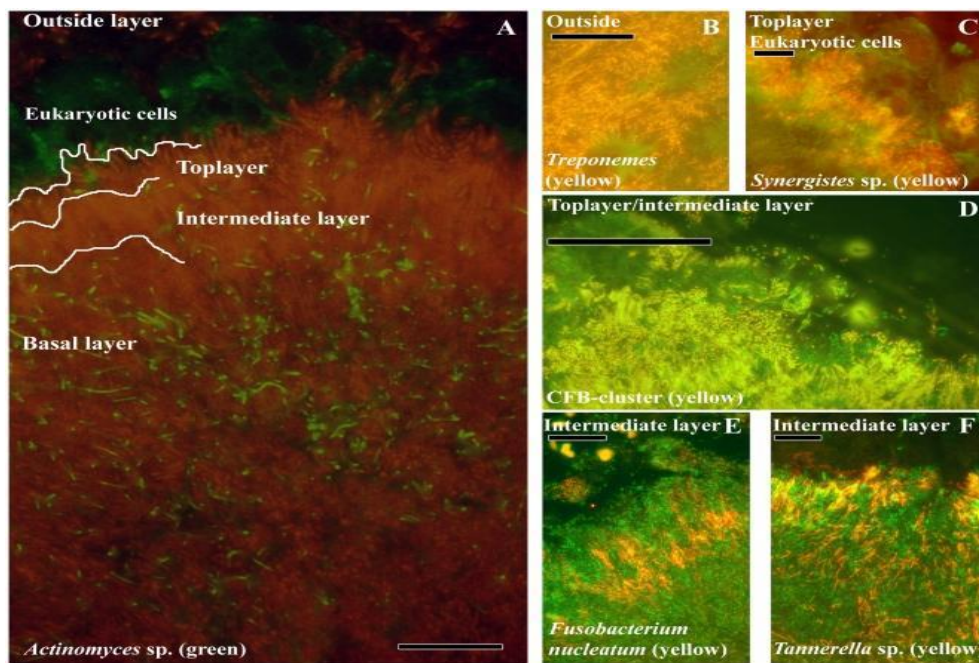


Figure 1.6. Showing the stratification and location of commonly found organisms in subgingival plaque. Biofilms were double-stained with probe EUB338 labelled with FITC or Cy3. The yellow colour results from the simultaneous staining with FITC and Cy3 labelled probes. Bars are 10 μ m, taken from (Zijng et al., 2010). Showing stratification that occurs from the base of the sulcus towards the gingival margin.

Different aggregate morphologies have been observed by Fluorescent *in situ* Hybridisation (FISH), for example, fine “test-tube brushes” composed of *T. forsythia* and *F. nucleatum* were arranged perpendicularly around lactobacilli or test-tube brushes composed of a complex mixture of cells like *T. forsythia*, *Campylobacter* sp., *P. micra* and *F. nucleatum* (Zijng et al., 2010).

Al-Ahmad et al. (2010) found that the composition of the biofilm was not influenced by which material surface it was grown on. The authors suggested that the acquired pellicle had a greater impact on the composition of the adherent bacteria and formed biofilm *in vivo* than the actual material of the surface itself and concluded that the biofilm formation on tooth enamel is similar to that which takes place on the implant materials. This is in accordance with

Tanner et al. (1997) who showed that the sequence of microbial colonization and biofilm formation on oral implants was similar to that of teeth.

A diagrammatic representation can be found in Figure 1.7 (Socransky et al., 1998). This complex microbiota can be further defined into clusters of organisms. The study reported that their term “red complex” microbiota, are indicative of increased periodontitis lesions in adults (Umeda et al., 1996). It has been shown that the species found in this red complex have been found to produce proteolytic enzymes, a contributing factor to periodontitis disease progression (Loesche, 1992), and have a strong capacity to coaggregate (Onagawa et al., 1994).

The “Orange complex” has been strongly associated with periodontitis. The authors found bacteria associated with a healthy gingival crevice such as *Streptococcus* spp., *Actinomyces* spp., *Capnocytophaga* spp., *Eubacterium* spp., *Fusobacterium* spp. and *Veillonella* spp. were predominant (Listgarten, 1994).

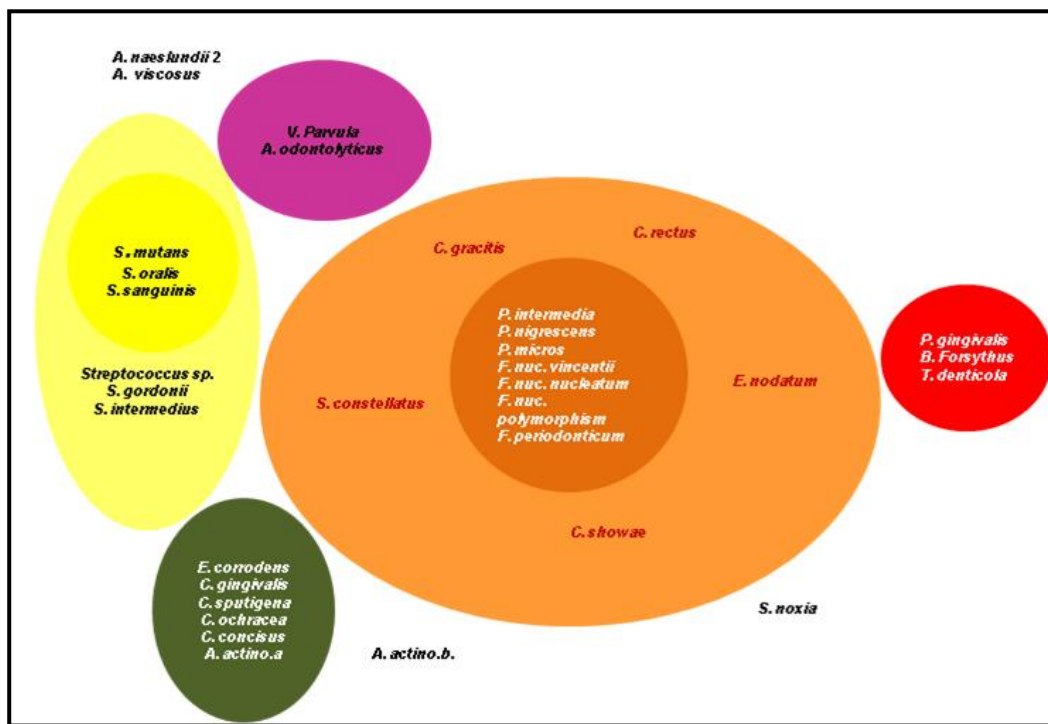


Figure 1.7. A diagrammatic representation of subgingival microbiota complexes (Socransky et al., 1998).

1.6 Identification of organisms in peri-implant disease

The detection of organisms associated with peri-implant disease has included numerous techniques ranging from electron microscopy (Rams and Link, 1983), culture dependent techniques (Rams et al., 1984), polymerase chain reaction (PCR), 16S rRNA gene cloning and comparative sequencing (Koyanagi et al., 2010), checkerboard DNA-DNA hybridization (Máximo et al., 2009, Al-Radha et al., 2012), through to 454 pyrosequencing (Kumar et al., 2012).

1.6.1 Culture dependent techniques

Bacterial culture is the traditional basis of identification and has been widely used in epidemiological and clinical studies. The main advantages of culture are its ability to detect multiple bacterial species and the possibility of obtaining relative and absolute counts of cultured species (Kazor et al., 2003). These techniques are effective when reliable selective media for a particular species or genera are available (Spratt, 2004).

Initial assessment of the microbial population involves the use of non-selective media such as blood agar, and fastidious anaerobic agar that allows the growth of a wide range of species. As many oral species have complex nutritional requirements, supplements such as serum, haemin, and menadione are often added to encourage the growth of a wider range of species. To enumerate specific species or genera, many selective media have been developed for oral species. These include *mitis salivarius* (MS) agar for the isolation of *Streptococcus* spp., and cadmium fluoride acriflavine tellurite (CFAT) agar for the isolation of *Actinomyces* spp. (Zylber and Jordan, 1982). Other examples of selective media are Gram-negative anaerobe medium supplemented with vancomycin to allow growth Gram negative rods and inhibit Gram-positive bacteria, and mannitol salt media for isolation of *Staphylococcus* and differentiation of *Staphylococcus aureus*.

A variety of special media and prolonged incubation periods under anaerobic conditions has allowed isolation of more diverse bacteria. The major problem of this technique is that requires highly skilled personnel with an extensive knowledge of bacteria culture and isolation techniques. Once cultured, the bacterial isolates need to be characterised and identified. There are various biochemical tests available to achieve this (Gram staining, oxidise test, catalyse test, coagulase test). However, these are very labour intensive but have been used in the study of the composition of dental plaque and are still generally used as the gold standard when determining the performance of new microbial tests in periodontal microbiology (Mombelli et al., 1990). Culture techniques have been

used comprehensively in early experimental peri-implantitis studies (Augthun and Conrads, 1997, Alcoforado et al., 1991, Sanz et al., 1990, Rams and Link, 1983, Rams et al., 1984, Nakou et al., 1987, Mombelli et al., 1988, Rosenberg et al., 1991, Nakazato et al., 1989, Danser et al., 1997, Ong et al., 1992). Isolated bacteria can be identified by molecular approaches. 16S rRNA gene analysis has been accepted as the current standard in definitive identification of oral bacteria (Tanner et al., 1994).

1.6.2 Culture independent techniques

1.6.2.1 Polymerase chain reaction (PCR) and 16S rRNA genes

The polymerase chain reaction (PCR) is a method first described by Kary Mullis in the late 1980s (Spratt, 2004). The application of PCR and sequencing revolutionized the detection and identification of bacteria. PCR is a technique, which uses a DNA polymerase enzyme to make a large number of copies of virtually any given piece of DNA or gene. The particular stretch of DNA to be amplified, called the target sequence, is identified by a specific pair of DNA primers, oligonucleotides usually about 20 nucleotides in length which designate the outer limits of the amplification product (Spratt, 2004).

There are a number of advantages and indeed disadvantages associated with the comparative sequencing technique. One advantage is that the single protocol is easily learned has relatively high through put and a good level of identification could be expected (Spratt, 2004). However, the misidentification of isolates can be an issue. For example, new un-named isolates can be placed into species isolates from very closely related groups can be misidentified, such as mitis group streptococci. Some bacterial groups are very closely related and the sequence information within the gene is not sufficient to resolve these taxa with any certainty (Spratt, 2004). Difficult groups to resolve which are relevant in endodontic infections include: mitis group streptococci (*S. mitis*, *S. oralis*, *S. sanguinis*, and *S. gordonii*), *Actinomyces* spp, (*A. naeslundii*, *A. israelii*, *A. meyeri*, *A. odontolyticus*, *A. viscosus*, *A. gerencseriae* and *A. radicidentis*), coagulase-negative staphylococci (*S. epidermidis*, *S. warneri*, *S. lentus* etc) and *Veillonella* spp (*V. parvula*, *V. atypica* and *V. dispar*) (Spratt, 2004). The candidate genes have been proposed and used for comparative sequence analysis studies. Manganese dependant superoxide dismutase (sodA) is one such gene that has been successfully used to identify the oral streptococci, including the mitis group (Poyart et al., 1998) and the coagulase-negative staphylococci (Poyart et al., 2001). The 16S (small subunit) rRNA gene was selected as a candidate molecule for a number of reasons: it is present in all

organisms, it is sequence sufficiently conserved and contains regions of conserved, variable and hypervariable sequence, it is of sufficient size (ca. 1500 bases) to be relatively easily sequenced but large enough to contain sufficient information for identification and phylogenetic analysis (Spratt, 2004). The use of 16S rRNA gene makes it possible to recognize phylogeny of all organisms on earth. For bacterial identification, 16S rDNA sequencing is particularly important in cases of bacteria with unusual phenotypic profiles, rare, slow growing bacteria, uncultivable bacteria and Gram-negative infections (Koyanagi et al, 2010). It presents some advantages when compared to other microbiologic tests because it is fast and simple means to produce relatively high numbers of copies of DNA molecules obtained from minimal amounts of fragments of microorganisms DNA. This approach allows the detection of almost every species in a given sample and is able to indicate the presence of previously uncultivated and unknown bacteria (Aas et al., 2005). It is the best method available at present for determining the diversity of microorganisms without cultivation. The method is based on isolation of DNA from the target environment or based on nucleic acids extracted directly from clinical samples. Polymerase chain reaction (PCR) amplification of the ribosomal rRNA gene, cloning the amplicons into *Escherichia coli*, and sequence analysis of the cloned 16S rRNA gene inserts (Woo et al., 2008). The use of specific PCR is equivalent to the use of selective media in culture dependent technique. It is use is increasing as result of ribosomal gene sequencing allowing identification of novel bacteria species from human sample. This approach allows working with samples containing many different species (mixed PCR products). 16S rDNA sequencing has played a pivotal role in the accurate identification of bacterial isolates and the discovery of novel bacteria in clinical microbiology laboratories (Spratt, 2004).

These approaches have been used for evaluation of peri-implant microbiota in edentulous patients and showed that the longer the implants were in the oral cavity, the higher the occurrence of *A. actinomycetemcomitans*, *P. gingivalis*, and *P. intermedia* in the peri-implant sulci of completely edentulous patients (Devides and Franco, 2006). It has been used for analysis of microbiota associated with peri-implantitis and showed that peri-implantitis sites had a more complex microbiota compared to periodontitis/healthy implant sites and that these were mainly composed of Gram-negative anaerobic bacteria (Koyanagi et al., 2010, Koyanagi et al., 2013). The main drawback of using the 16S rRNA gene for amplification is that the universal primers used in the PCR are not as universal as once hoped, for example selective amplification can arise with templates with a low GC content (Polz and Cavanaugh, 1998).

Overall, a major drawback with most of these techniques is that they do not provide access to the whole genome (Spratt, 2004). Spratt (2004) stated that these techniques (culture dependant and culture independent) are not exclusive to each other and should be used together by microbiologists in an informed polyphasic manner to understand the complex nature of dental infections.

1.6.2.2 Quantitative polymerase chain reaction (qPCR)

A recent advance in PCR technology has been the development of real-time PCR systems. The development had been facilitated by the earlier combination of the 5' nuclease assay developed by Holland et al. (1991) with fluorescence detection following cleavage of an internal (TaqMan) DNA probe (Livak et al., 1995), enabling the accumulation of amplicons to be monitored after each cycle and hence facilitating quantitative determination of the initial template gene (or transcript) numbers. The target specificity of any qPCR assay is determined by the design of the primers (and in some cases an internal probe), allowing quantification of taxonomic or functional gene markers present within a mixed community from the domain level down to the quantification of individual species or phylotypes (Smith and Osborn, 2009).

The qPCR works in essentially the same manner as end-point PCR. Multiple amplification cycles in which template DNA is initially denatured is followed by annealing of oligonucleotide primers (targeting specific sequences) is further followed extension of a complementary strand from each annealed primer. This is performed by a thermostable DNA polymerase. The multiple cycling, resulting in an exponential increase in amplicon number. However, in contrast to end-point PCR, the increase in amplicon numbers is quantified in “real-time” during the PCR via detection of a fluorescent reporter that indicates amplicon accumulation during every cycle.

Two reporter systems are commonly used, namely, the SYBR green assay (Wittwer et al., 1997) and the TaqMan probe system (Holland et al., 1991, Livak et al., 1995). Since SYBR green binds to all double-stranded DNA, it is essential to use primer pairs that are highly specific to their target sequence to avoid generation of nonspecific products that would contribute to the fluorescent signal, resulting in an overestimation of the target. Primer pairs that exhibit self-complementarity should also be avoided to prevent primer–dimer formation. A post-PCR melting curve analysis should be carried out to confirm that the fluorescence signal is generated only from target templates and not from the formation of nonspecific PCR products. A melting curve is constructed, and fluorescence levels are measured at each discrete temperature point. As the

double-stranded template is heated, it denatures, resulting in a corresponding decline in fluorescence due to SYBR green dissociation from the double-stranded product (Giglio et al., 2003). The TaqMan Real Time PCR assay is based on Taq Polymerase 5'-3' nuclease activity (Lyons et al., 2000, Asai et al., 2002, Nadkarni et al., 2002, Suzuki et al., 2004, Yoshida et al., 2004). The TaqMan Real Time PCR probe, which is labelled with two fluorescent dyes, is created within the amplicon defined by a gene-specific PCR primer pair. The 5' end is labelled with a reporter dye (usually 6-carboxy-fluorescein, FAM), while the 3' end is labelled with a second fluorescent dye (6-carboxy-tetramethyl-rhodamine, TAMRA). The TaqMan probe method utilizes a fluorescently labelled probe that hybridizes to an additional conserved region that lies within the target amplicon sequence. During the annealing step of each cycle of the PCR, primers and the intact probe bind to their target sequences. During subsequent template extension, the 5' exonuclease activity of the Taq polymerase enzyme cleaves the fluorophore from the TaqMan probe and a fluorescent signal is detected as the fluorophore is no longer in close proximity to the quencher.

The qPCR amplification curve can be subdivided into four stages, namely background noise, where the background fluorescence still exceeds that derived from initial exponential template accumulation, exponential amplification, linear amplification and a plateau stage. During the exponential phase of the amplification, the amount of target amplified is proportional to the starting template and it is during these cycles that gene numbers are quantified using the C_T method.

The C_T is reached when the accumulation of fluorescence (template) is significantly greater than the background level. During the initial cycles, the fluorescence signal due to background noise is greater than that derived from the amplification of the target template (Smith and Osborn, 2009). Once the C_T value is exceeded, the exponential accumulation of product can be measured. When the initial concentration of the target template is higher, the C_T will be reached at an earlier amplification cycle (Becker et al., 2000). The absolute value of C_T depends on the initial template copy number, the efficiency of both DNA amplification and cleavage of the TaqMan Real Time PCR probe (Price et al., 2007). For each standard curve, the r^2 value, the amplification efficiency, E derived from the slope of the standard curve and the y -intercept value indicates the sensitivity of the reaction; lower values indicate greater sensitivity of the qPCR amplification (Becker et al., 2000).

The gene and transcript numbers of the target gene of interest have been normalized to the numbers of 16S rRNA gene or transcripts (Kandeler et al.,

2006). 16S rRNA gene copy and transcript numbers are highly variable, with the number of 16S rRNA genes per operon varying dramatically between species (1–15 copies). A number of studies have reported that 16S rRNA gene numbers from environmental samples cannot be converted to cell numbers as the exact number of copies of the 16S rRNA gene in any given bacterial species varies (Klappenbach et al., 2001, Klappenbach et al., 2000). The quantification of gene copy number from an environmental DNA template should not be carried out if the resulting C_T values are greater than or equal to those of the no template control (NTC) (Suzuki et al., 2000). The sensitivity of qPCR allows quantification of very low numbers of target genes, with detection limits as low as two copies of a gene in a qPCR (Fey et al., 2004) although routinely this is perhaps 10 of copies.

The key considerations and recommendations for the use of qPCR are: the amplicons should be short, ideally between 50 and 150 bp in length, the GC content of the primers may range between 20% and 80% (although paired primers should have similar melting temperatures (T_m)), a high GC content will increase the specificity of the reaction. When designing a TaqMan probe, the probe should be situated as close as possible to the forward primer without overlapping. The probe should not have a guanine nucleotide at the 5' end or have more guanines than cytosine's as guanine residues are natural quenchers. The T_m of the probe should be 8–10 °C above the T_m of the primers. A full description of the standard curve (r^2 , slope, efficiency and y-intercept value) should be given when reporting gene and/or transcript numbers. Biological (not just technical) replication (at least $n = 3$) is essential for qPCR to enable statistical investigation of differences in gene or transcript numbers between samples or treatments (Smith and Osborn, 2009).

Multiple TaqMan probes and primer sets can be used in different qPCR assays to differentiate between closely related sequences (Smith and Osborn, 2009), or alternatively, probes can be labelled with different fluorophores, facilitating the development of multiplex qPCR protocols whereby different targets can be coamplified and quantified within a single reaction. For example, Baldwin et al. (2003) developed a multiplex qPCR assay targeting a number of different aromatic oxygenase genes using bacterial strains and then subsequently applied the assay to simultaneously quantify aromatic oxygenase genes in contaminated groundwater. The multiplex qPCR has also been used to identify and quantify 8 key taxa associated with health, gingivitis and dental caries (Ciric et al., 2010).

The qPCR, with species-specific primers and probes, represents a specific, sensitive, and quantitative tool to study periodontal pathogens (Boutaga et al.,

2007). The qPCR assays offer significant advantages over traditional culture techniques that can be both labour and time intensive and over conventional PCR assays that will only determine presence or absence. The methods allow quantitative identification of any bacterial species of interest including bacteria that may be very difficult to culture (Paster and Dewhirst, 2009). The TaqMan Real Time PCR significantly increases the specificity of the detection.

For the quantitative detection of DNA, specific sets of primers were designed that amplify unique nucleotide sequences of the target organism and a fluorescent signalling DNA probe was used for quantification and differentiation of periodontopathogens from subgingival plaque samples (Nonnenmacher et al., 2004).

The qPCR is more rapid, reliable and able to detect absolute number of bacterial cells from known standards (Paster and Dewhirst, 2009). Furthermore, they do not require post amplification handling of PCR products and results are obtained within hours from a wide variety of sample types.

The qPCR technique has been used for the identification of *P. gingivalis* (Lyons et al., 2000, Sakamoto et al., 2001, Boutaga et al., 2003), *A. actinomycetemcomitans* (Sakamoto et al. 2001), *T. denticola* (Sakamoto et al. 2001, Asai et al. 2002, Yoshida et al. 2004) and *T. forsythensis* (Sakamoto et al. 2001). Many studies have reported the usefulness and acceptance of this system for the identification of oral bacteria, detection and quantification (Maeda et al., 2003, Boutaga et al., 2007, Yoshida et al., 2004). Furthermore, qPCR can be used to quantify specific bacterial populations in plaque samples before and after treatment for monitoring therapeutic efficacy (Yoshida et al., 2004). The qPCR technique can provide results in 2 hours, whereas anaerobic cultures require 7-8 days to confirm the presence of putative periodontopathogens (Price et al., 2007).

The TaqMan probes are more expensive than using SYBR green chemistry and the former requires the presence of an additional conserved site within the short amplicon sequence to be present. Identification of three conserved regions within a short region (typically ca. <100 bp) may not always be possible, especially when primer/probe combinations are being designed to target divergent gene sequences. More advances in TaqMan probe technology have involved the introduction of the minor groove binder (MGB) probe (Kutyavin et al., 2000). The MGB molecule is attached to the 3' end of the probe and essentially folds back onto the probe. This will increases the stability of the probe, allowed the design of shorter probes (13–20 bp) than are required for traditional TaqMan probes (20–40 bp), and maintaining the required hybridization annealing temperature

(Kutyavin et al., 2000). Since molecular analysis of environmental microorganisms has repeatedly shown that the majority of microorganisms (and their genes) in the environment are highly divergent from those of most cultured organisms, this represents the development of new PCR-based assays.

Recently, ultra-high-throughput sequencing approaches such as pyrosequencing (Edwards et al., 2006). This pyrosequencing approach particularly, offers considerable benefits both in terms of providing much larger data sets than can be generated via library-based approaches, and as importantly, by avoiding potential sequence-specific cloning biases. Moreover, where pyrosequencing is used to target-specific genes (rRNA genes); (Sogin et al., 2006), such data sets provide only semi quantitative assessments of the diversity.

1.6.2.3 Pyrosequencing

Pyrosequencing is defined as a sequencing method based on real-time monitoring of the DNA synthesis. It is a four-enzyme DNA sequencing technology monitoring the DNA synthesis detected by bioluminescence (Ahmadian et al., 2000).

Pyrosequencing is becoming a common method used for determining richness and diversity complex bacterial communities. The identification of bacterial strains usually involves sequencing of the 16S rRNA gene. Several studies have reported the usefulness of pyrosequencing technology for bacterial typing by sequencing various the variable regions of the 16S rRNA gene. In the 454 pyrosequence system (Roche) (Wade, 2013), 16S rRNA genes are amplified by PCR from samples with universal primers and then mixed in equal proportions. The mixture is then amplified in an emulsion and distributed among wells on a plate to which are added beads containing the sequencing reagents. Nucleotide incorporation is detected by a CCD camera imaging system and around 0.8 million sequences, up to 750 base pairs long can be obtained in a single run. To enable multiple samples to be sequenced in the same run, primers with unique barcodes are used, typically 8–12 nucleotides, incorporated into the initial PCR primer. These barcodes are then incorporated into the final sequences obtained and can be easily sorted and assigned to source samples after sequencing (Wade, 2013). The use of pyrosequencing and alternative high throughput methods such as the Illumina system, which provides a higher numbers of sequences, although of shorter length, has revolutionised culture-independent analyses and has been the cornerstone of that part of the Human Microbiome Project devoted to determining the composition of the microorganisms at different human body sites (Consortium, 2012). These studies have shown that

each body site studied was colonised by a microbiome characteristic of that site but that the individual was the primary factor influencing the composition of the microbiome i.e. each individual is colonised by a unique microbiome (Segata et al., 2012). Within the mouth, samples from seven different surfaces were found to be colonised by three distinct bacterial communities: the buccal mucosa, gingiva and hard palate had similar microbiota while the saliva, tongue, tonsils and throat, and supra- and sub-gingival plaque each had distinctive communities (Segata et al., 2012). The use of recently developed molecular methods has greatly expanded our knowledge of the composition and function of the oral microbiome in health and disease. Technical advances in DNA and RNA sequencing will provide vast amounts of new data but analysing and interpreting the data will be extremely challenging (Wade, 2013).

1.7 Structural analysis of dental plaque

1.7.1 Electron microscopy

The electron microscope is a type of microscope that uses a beam of electrons to create an image of the specimen. It is capable of much higher magnifications and has a greater resolving power than a light microscope, allowing it to see much smaller objects in finer detail. Electron microscopy has been used previously for studying biofilm composition and structure because of these properties (Listgarten, 1976, Theilade et al., 1976). The disadvantages of this approach are that specimens require dehydration, fixing, embedding, and staining/coating which causes considerable distortion of the biofilm structure (cells, matrix and fluid filled spaces), leading to shrinkages of 50% during fixation and may change the relationship of one component with respect to another (Wood et al., 2000). It is laborious and can produce artefacts resulting from sample preparation. A significant amount of training is required in order to operate an electron microscope successfully. The samples need to be specially prepared by sometimes lengthy and difficult techniques to withstand the environment inside an electron microscope. In the life sciences, it is still mainly the specimen preparation that limits the resolution of what we can see in the electron microscope, rather than the microscope itself. The technique has however revealed a microscopic world previously unknown to us.

1.7.2 Transmission electron microscopy (TEM)

The original form of electron microscopy, Transmission Electron microscopy (TEM) involves a high voltage electron beam emitted by a cathode and formed by magnetic lenses. The electron beam that has been partially transmitted through the very thin (and so semi-transparent for electrons) specimen carries information about the structure of the specimen (Crawford and Burke, 2004). The spatial variation in this information (the "image") is then magnified by a series of magnetic lenses until it is recorded by hitting a fluorescent screen, photographic plate, or light sensitive sensor such as a CCD (charge-coupled device) camera. The image detected by the CCD may be displayed in real time on a monitor or computer. TEM produce two-dimensional, black and white images (Sugiyama and Sigesato, 2004). TEM resolution is about an order of magnitude better than the SEM resolution. The TEM can easily resolve details of 0.2 nm. The ability to determine the positions of atoms within materials has made the TEM an indispensable tool for nano-technologies research and development in many fields. For the TEM, samples are generally prepared by exposure to many chemicals, in order to give good ultra-structural detail which may result in

artefacts purely as a result of preparation (Sugiyama and Sigesato, 2004). This gives the problem of distinguishing artefacts from genuine structures within the specimen, particularly in biological samples.

There are a number of drawbacks to the TEM technique. Many materials require extensive sample preparation to produce a sample thin enough to be electron transparent, which makes TEM analysis a relatively time consuming process with a low throughput of samples (Sugiyama and Sigesato, 2004). The structure of the sample may also be changed during the preparation process. Also the field of view is relatively small, raising the possibility that the region analysed may not be characteristic of the whole sample (Sugiyama and Sigesato, 2004). There is potential that the sample may be damaged by the electron beam, particularly in the case of biological materials. Previous studies on dental plaque structure carried out at high resolution by TEM suggested that the biofilm architecture appeared to be relatively dense, although it was not easy to attribute inter-bacterial space to either matrix or fluid-filled space with this technology (Wood et al., 2000).

1.7.3 Scanning electron microscopy (SEM)

The first true SEM was described and developed in 1942 by Zworykin. In 1965 the Cambridge Scientific Instruments Mark I “Stereoscan” was developed as the first SEM. Resolution of 30 Ångstroms (1 Ångstrom is equal to 0.1 nm or 1×10^{10} metres) under optimal conditions is possible (EVO SEM, Carl Zeiss product literature). However, for biofilm structure the resolution is greatly reduced without initial fixation, staining, drying and metal sputter coating, which deposits a thin layer of either gold or platinum on the surface (Crawford and Burke, 2004). Electrons can penetrate uncoated biological samples, giving an image of low resolution, however, if the samples are sputter coated, the electrons are reflected to the detectors, thus giving greater resolution of the surface topography (Kämper et al., 2004). It allows straightforward transmission observations of wet samples compromising of nano-scale objects in a liquid layer. Low-vacuum technology allows imaging samples in their native state. Particularly, adapted for suspension-type samples and characterizations in materials science as well as life-science at the nano-scale (Bogner et al., 2007). SEM has been used to investigate the morphological features of supragingival plaque development using six bonded enamel block on buccal surface of canine, premolar and molar teeth (Zee, 1996), and it has also been used to study the development of dental plaque at different stages (Novaes et al., 1991), and has also been used to describe certain structural details of naturally occurring approximal plaque and to

compare them with features of the bacterial film on enamel surfaces (Newman, 1972). SEM has also been used to evaluate biofilm formation and composition on different implant materials *in vivo* (Al-Ahmad et al., 2010), as well as the characterisation of the surface chemistry, hydration, topography and roughness of a hydrophilic sandblasted and acid-etched titanium dental implant (SLActive) (Zinelis et al., 2012).

1.7.4 Confocal laser scanning microscopy (CLSM)

The application of CLSM to biofilms began in the early 1990s (Lawrence et al., 1991). Confocal microscopy in conjunction with fluorescent probes has been widely used for biofilm research. A simple and effective use of CLSM is when it is used in conjunction with freshly grown biofilms and a live/dead fluorescent stain (Baflight™). SYTO 9 and propidium iodide staining has proven superior, because it provides a clear differentiation between dead and active microorganisms without interference of background fluorescence (Decker, 2001). SYTO stains have become available to stain specific organisms within the biofilm. Most commonly utilised stains are the LIVE/DEAD® staining where SYTO 9 stains all bacterial cells (independent of cell viability), whereas charged propidium iodide penetrates dead cells due membrane damage, thus allowing the stain to be internalised within the bacterial cell and when both dyes are present, reduce SYTO 9 to fluoresce red. This allows for differentiation of live and dead cells within the biofilm. Visualisation of biofilms helps to understand structural differences and similarities that may be seen in comparison with those *in vivo*. CLSM exhibits more advantages over conventional optical microscopy due to its ability for direct non-invasive serial optical sectioning of intact and living specimens and the possibility of generating 3D images of thick transparent objects such as biological cells and tissues (Lawrence et al., 1991). It also enables the examination of biofilm cultivated on non-transparent surfaces for example minerals, metals, gels and synthetics. It also allows sagittal (xz) sectioning of biofilms (vertical thin sections) cut through the biofilm from the substratum to the exterior surface. In addition, it allows quantitative visualizations of 2D, 3D, and potentially 4D (time course) reconstructions of biofilm characteristics. This technique has been used to analyse the biofilm architecture of several bacterial species grown in continuous-flow cultures (Lawrence et al., 1991), to examine the structure of intact oral biofilms *in vitro* (Pratten et al., 2000) and *in vivo* (Auschill et al., 2001), to examine the spatial distribution of both viable and non-viable bacteria within microcosm dental plaques grown *in vitro* (Hope et al., 2002) and to assess the immediate bactericidal effect of

chlorhexidine (CHX) on biofilms (Zaura-Arite et al., 2001). In addition, structural changes and differences in the distribution of viable and non-viable bacteria associated with the change in environmental conditions can be observed (Dalwai et al., 2006). In general, CLSM offers the opportunity to visualize bacteria directly on the substrata and in the state of adherence (Hannig et al., 2007).

1.8 Treatment of peri-implantitis

Since dental implant predictability, functionality, and durability makes them an attractive option for patients and clinicians, complications can arise at any stage from patient assessment to maintenance therapy (Becker and Sennerby, 2012). As the use of dental implants continues to increase, the frequency with which clinicians will be confronted with peri-implant diseases can be expected to increase (Simonis et al., 2010). Thus, it is important to consider the treatment options available for the management of peri-implant diseases. The development of a biofilm on dental titanium implants associated with peri-implantitis may specifically include pathogens that are therapy resistant and is one of the most challenging implant complications to deal with (Simonis et al., 2010, Mombelli, 2012, Lang et al., 2011). Several factors may explain the limited clinical successful outcomes of therapy. It is likely that the instruments available for debridement around implants are not properly designed to reach the affected area. Thus, the design of implants and placement of the dental titanium implants and their superstructures might have made it difficult to maintain a plaque free and inflammation free environment around the dental titanium implants (Schwarz et al., 2011). Several treatment modalities have been proposed for the management of peri-implant diseases based on the evidence available from the treatment of periodontitis (Leonhardt et al., 1999). The treatment modalities that have been suggested to achieve this objective can be broken down into two broad categories: non-surgical and surgical (Aljateeli et al., 2012).

1.8.1 Non-surgical therapy

The current non-surgical therapeutic strategies for managing peri-implant infections still appear to be largely based on the evidence available for treating periodontitis (Mombelli and Lang, 1992). The dental community has failed to develop effective non-surgical therapeutic measures for peri-implant mucositis and peri-implantitis. This failure is partially based on the lack of sufficient scientific data on the effect of conventional anti-infective therapies on biofilms on titanium implant surface (Renvert et al., 2008). The basic and common element for treating peri-implantitis seems to be debridement of the affected surface

(implant). The surfaces of modern implants are highly micro-structured and macro-structured, which are considered favourable for osseointegration (Byrne, 2012). Such surfaces characteristics (such as threads and roughness) of an implant may facilitate initial microbial adhesion, formation of complex aggressive biofilms and may complicate debridement (Bürgers et al., 2010). Therefore, antiseptics and antibiotics have been tested for removing pathogenic biofilms (Mombelli and Lang, 1992, Lindhe et al., 2008).

1.8.1.1 Antiseptic agents

Several traditional antiseptics have been proposed for the non-surgical therapy of periodontitis as well as peri-implant mucositis and peri-implantitis. There are many chemotherapeutic agents such as chlorhexidine (CHX). Chlorhexidine gluconate (CHX; 0.2%) has been proven in many studies to be the most efficient antimicrobial solution, and is still considered by many as the gold standard (Moshrefi, 2002, Slots, 2002).

CHX is a diphenyl compound that shows a wide spectrum of antibacterial activity by altering the bacterial cell membrane, which results in leakage and cell destruction, encompassing Gram-positive and Gram-negative bacteria. CHX was shown to inhibit plaque formation and improve gingival indices around natural teeth and dental implants (Quirynen et al., 2002).

Another agent is sodium hypochlorite (NaOCl; household bleach) with its active agent undissociated hypochlorous acid (HOCl). NaOCl is a traditional disinfectant in dentistry because of its bactericidal, fungicidal, and tissue dissolving properties. HOCl is mainly used in endodontic therapy, and its proposed concentrations range from 0.5% to 5.25% (Slots, 2002, Izu et al., 2004). HOCl is effective against bacteria because of its oxidizing action and has been successfully used as a supportive antimicrobial agent in surgical peri-implantitis therapy (Slots, 2002, Izu et al., 2004).

In contrast to sodium hypochlorite, which is known for its extreme cytotoxicity, hydrogen peroxide (H_2O_2) is a relatively non-toxic agent in commonly used concentrations and shows broad antimicrobial activity and rapid bactericidal action.

Citric acid has frequently been used for the removal of bacterial endotoxin in root treatments and has also shown to exert antibacterial activity against microbial plaque deposits on periodontally diseased root surfaces. In patients with peri-implantitis, citric acid was used to detoxify plaque-infected implant areas (before regenerative treatments), and its efficacy in this respect has been shown in many *in vitro* and *in vivo* studies (Zablotsky et al., 1992).

Listerine (a combination of essential oils) was shown to have antimicrobial activity against bacteria colonizing teeth, tongue, and saliva. Listerine has successively been used under different clinical conditions, such as during post-surgical periods and in implant dentistry, because of its anti-plaque and anti-mucositis effectiveness in comparison to CHX (Cortelli et al., 2009, Mandel, 1994). Listerine's mechanism of action involves bacterial cell membrane destruction, bacterial enzymatic inhibition, and extraction of bacterial lipopolysaccharides. This bactericidal effect of essential oils, such as eucalyptol, thymol, menthol, and methyl salicylate, has been affirmed against *A. actinomycetemcomitans*, *A. viscosus*, *S. mutans*, and *S. sanguinis* (Ross et al., 1989).

Triclosan (5-chloro-2-(2, 4-dichlorophenoxy)-phenol) is effective in reducing subgingival microbiota both quantitatively and qualitatively and has served as a antimicrobial and plaque-reducing additive in many oral hygiene products, such as tooth pastes and mouth-rinses, for more than 20 years (Rosling et al., 1997a, Rosling et al., 1997b). Clinically, triclosan has been found to be effective in inhibiting dental biofilms, calculus, caries progression, and gingivitis (Arweiler et al., 2002).

A study by Bürgers et al. (2012) investigated a 60 s treatment time on oral biofilms of CHX 0.2%, H₂O₂ 3%, sodium hypochlorite 1%, citric acid 40%, Listerine cool mint (alcoholic based), and triclosan 0.3%. Sodium hypochlorite had only broad-spectrum antimicrobial effect against either *C. albicans*, *S. epidermidis*, and *S. sanguinis* on machined pure titanium substratum (median surface roughness $R_a = 0.15 \mu\text{m}$). However, sodium hypochlorite has a potentially toxic effect to both infectious agents and host cells. Also it has limited application in human infected wounds, skin, and mucosa (Slots, 2002, Spangberg et al., 1973). Other clinical studies have used adjunctive antiseptic agents including Listerine mouthrinses twice daily (Ciancio et al., 1995), chlorhexidine CHX rinsing 0.06% (Felo et al., 1997), and CHX (0.12%) rinsing plus CHX (0.12%) gel application for 30 s (Porras et al., 2002).

Ramberg et al. (2009) showed that the regular use of dentifrices containing triclosan (0.3%) may reduce the clinical signs of inflammation in the mucosa adjacent to dental implants. It has shown that the decontamination of machined discs with H₂O₂ (5 min), saturated citric acid (pH = 1, 1 min) or CHX gel (5 min) did not harm the surfaces and epithelial cells would still grow in the Ti surface. The use of 3% H₂O₂ and citric acid treated surfaces allowed better epithelial cells growth than the CHX gel treatment (Ungvári et al., 2010). Other work has shown that "CHX chips" at implant's sites resulting in a significant improvement of

periodontal parameters (probing depth-PD and bleeding on probing-BOP) at peri-implantitis sites (Machtei et al., 2012). Augthun et al. (1998) treated implants with CHX solution 0.1% for 60 s. The authors showed no damaging effect on any implant surface after application and found that the CHX 0.1% solution rinse did not remove plaque deposits on all implant surfaces (smooth, plasma sprayed implant surfaces). Another clinical study was conducted from three consecutive peri-implantitis cases treated with non-surgical debridement and subgingival CHX irrigations (Nibali and Donos, 2011). All cases were exposed for subgingival debridement. The implants were scaled with a piezoelectric device at 200 rpm (on the implant neck) and with plastic curettes on the exposed implant threads for 15 min. this was followed by subgingival irrigations with approximately 15 ml of 0.2% CHX. Patients were instructed to rinse twice a day for two weeks with CHX 0.2% after treatment. The results showed that after 12 months, the bone fill of the peri-implant infrabony defects was evident.

1.8.1.2 Antibiotic use in peri-implantitis

The use of locally delivered antibiotics in the treatment of peri-implantitis was described in the review of van Winkelhoff (2012). The theoretical advantages of locally administered antibiotics in comparison to systemically delivered antibiotics are:

- The therapy can be achieved at a high concentration in the infected site.
- The risk for side and adverse effects are reduced.
- There is no interaction with other medicines.

Mombelli et al. (2001) used tetracycline HCl polymeric fibres and applied these to partially edentulous patients with peri-implantitis lesions. The study showed that local application was effective in improving the clinical condition. This therapy reduced the mean total number of cultivable bacterial counts and significantly decreased the recovery of several periodontal pathogens (Mombelli et al., 2002). Salvi et al. (2007) used mechanical debridement in conjunction with local delivery of minocycline microspheres in the treatment of peri-implant infection. They found that after 12 months, the mean PD decreased from 5.9 mm to 4.2 mm and BOP scores reduced from 92 to 44 at sites with the deepest peri-implant.

Renvert et al. (2008) used mechanical debridement in conjunction with minocycline HCl 1 mg placed subgingivally/submucosal at implant sites and microbiota were detected by checkerboard DNA-DNA hybridization method. The authors showed a low prevalence of the target bacteria (*P. gingivalis*, *P.*

intermedia, *P. nigrescens*, *T. forsythensis*, *A. actinomycetemcomitans*, and *Treponema denticola*) with minocycline HCl treatment and the authors found moderate improvement in plaque scores.

Azithromycin® has been used in the treatment of peri-implant mucositis (Hallström et al., 2012) as an adjunct to mechanical therapy (Ericsson et al., 1996). The pharmacokinetics of Azithromycin® is characterized by a fast drug transfer from blood into intra-cellular compartments. Data have shown that Azithromycin® concentrations in gingival fluid (GCF) are higher and more sustained than in serum. The authors failed to identify microbiological advantages for the adjunct treatment with Azithromycin® in combination with debridement in cases with peri-implant mucositis. The authors showed that the use of systemic antibiotics in the treatment of peri-implant mucositis did not demonstrate better clinical results up to 3 months after treatment (Hallström et al., 2012).

Although local antibiotic therapy of peri-implantitis has a positive effect on clinical and microbiological findings, there are limitations including microbiological parameters shifting back towards pre-treatment values after 1 month of treatment, particularly in deep advanced peri-implantitis (Mombelli et al., 2001) lesions. Additional issues are that clinically, it is difficult to deliver local antibiotic therapy to the very base of deep defects (Mombelli et al., 2001). The values and needs for antibiotics in the treatment of peri-implant mucositis is questionable and must be considered in relation to the overall community risk of antibiotic resistance development. It could be concluded that non-surgical debridement of peri-implant mucositis without the adjunct use of systemic antibiotics should be the first choice of treatment (Hallström et al., 2012). The antibiotic treatment of peri-implantitis may not allow sufficient bone filling or reosseointegration in deep peri-implant bony defects. Therefore, surgical therapy may be necessary to treat peri-implant defects.

1.8.1.3 Mechanical therapy for peri-implantitis

Mechanical therapy alone proven be effective in treating bacterial infections around teeth and has been suggested as a treatment for implants (Lang et al., 2000). However, reduction of bacterial load at peri-implantitis sites by means of mechanical debridement alone remains difficult, largely due to the design of the suprastructure and the topography of the implant surface (Schär et al., 2013). Implant surface decontamination is the basic goal in the treatment of peri-implantitis. Numerous tools are available to achieve this such as use of polishing brushes, rubber polishers, Teflon, plastic, carbon or titanium curettes, and

special modified tips for ultrasonic systems and air powder flows. Studies evaluating some of these methods have shown that mechanical debridement alone with subgingival carbon fibre curettes or with the ultrasonic Vector® system showed no differences (Karring et al. 2005). Augthun et al. (1998) evaluated implants with the following treatments: Gracey curette, plastic curette, diamond polishing device, ultrasonic scaler, air powder abrasive system with sodium-hydrocarbonate solution for 60 s. They found that treatment with the diamond polishing device, ultrasonic scaler, and steel curette caused severe surface damage in all implant surfaces. However, the plastic curette and the air-powder-water abrasive system caused none to medium surface damage. The clinical study revealed differences in the efficacy of the cleaning methods and also showed that the plastic curette had a limited cleaning efficacy due to difficulties in removing plaque from the depths of the screw threads or from the plasma sprayed surfaces. The air-abrasive system on implant surface yielded completely plaque-free surfaces and revealed a high biocompatibility (Schwarz et al., 2009b). However, there are limitations in the clinical application of air powder flow (amino acid glycine or sodium bicarbonate) because of an increased risk of subcutaneous emphysema. This is a clinical condition arising from the penetration of air into causing deformity and swelling. It in the vicinity of the oral cavity this may include tissues spaces of the fascial plane (Brown et al., 1992) and may lead to visible alterations of the implant surface (Kreisler et al., 2005, Cochis et al., 2012). A study by Persson (2010) demonstrated that there was no change in the microbiota in pockets around implants with a diagnosis of peri-implantitis in dogs after treatment with hand instruments and ultrasonic device. Also they found that the trends of bacterial reduction were similar before and after 6 months of treatment. Although the results of the studies mentioned above showed an improvement in the healing of peri-implantitis lesions, a complete resolution of peri-implant mucosal inflammation was rare (Schär et al., 2013).

1.8.1.4 Laser application for treatment of peri-implant infections

As lasers can perform excellent tissue ablation with high bactericidal and detoxification effects, they have been proposed to be one of the most promising new technical modalities for the treatment of failing implants. Laser has been used as a substitute to conventional mechanical debridement (Romanos et al., 2009).

The physical properties of the laser energy and its interaction with tissues, due to reflection, scattering, transmission, and absorption, may explain why the implant surface can be decontaminated in all areas, including within the threads. The

light may induce these antibacterial effects due to its absorption by the implant and the surrounding tissues, or it may be reflected by the metal surface, causing a slight elevation in tissue temperature. The temperature changes seen during CO₂ laser irradiation have been studied extensively (Mouhyi et al., 1999, Romanos et al., 2009). Linear increases to temperatures >50°C were observed with increases in power levels and exposure times (Kreisler et al., 2002b).

The CO₂ laser has been reported to be safe and resulted in enhanced bone regeneration when utilised for decontamination of implants in the treatment of peri-implantitis. The limitations of clinical application of CO₂ laser are the increase in temperature on the implant surface and carbonisation of the adjacent bone tissue (Kreisler et al., 2002c, Schwarz et al., 2009a) and associated change at all implant surfaces. Therefore, the power output and irradiation time must be limited to avoid any unintentional thermal damage. Similar problems may arise when a diode laser is used (Kreisler et al., 2002b). The Nd:YAG (neodymium-doped yttrium aluminum garnet) laser was contraindicated for treatment of peri-implantitis because of irradiation of the implant surface and the production of morphological changes such as melting, cracks and crater formation on all titanium surfaces (Kreisler et al., 2002b). Er:YAG laser (erbium-doped yttrium aluminium garnet) has been used for the removal of subgingival calculus from periodontally diseased root surfaces without producing major thermal side effects to adjacent tissue. The Er:YAG laser has high absorption of emission wavelength at 2940 nm by water, and exhibits no thermal damage to tissue (Kreisler et al., 2002a) and its irradiation does not influence the attachment rate of osteoblasts. The Er:YAG laser was proposed as an alternative to mechanical scaling and root planning because it has the ability to remove hard deposits from the root surface. It is strong bactericidal and detoxification activity (Folwaczny et al., 2003), it is able to debride the root surface with minimal removal of tooth substance (Schwarz and Becker, 2005), its ability to ablate without producing a smear layer has the ability to remove smear layers and cementum bound endotoxin (Folwaczny et al., 2003). In addition, periodontal ligament fibroblasts show enhanced adhesion and proliferation on laser treated root surfaces. Furthermore, the laser light beam has enhanced access to grooves and concavities compared with mechanical instruments, as access is not limited by the physical size of the instrument. Er:YAG can effectively have been found to remove calculus and plaque on contaminated abutments and biofilms grown on sandblasted and acid-etched titanium surfaces (SLA) at low energy densities. *In vitro* studies showed Er:YAG laser irradiation removed *P. gingivalis* contaminated SLA implant surfaces and

resulted in similar fibroblast proliferation when compared with sterile specimens, and greater fibroblast proliferation when compared with untreated contaminated specimens (Friedmann et al., 2006). It was investigated that the mean value of residual plaque biofilm was significantly lower after treated by this laser on sandblasted and acid-etched titanium discs compared with hand instrumentation using plastic curettes and ultrasonic instrumentation treated groups. However, the formation of an oral biofilm at structured titanium surfaces interfered with the adhesion and proliferation of osteoblasts *in vitro*, and its removal using either conventional treatment procedures or Er:YAG laser was not sufficient for achievement of an acceptable biological surface (Schwarz et al., 2005).

1.8.1.5 Photodynamic therapy (PDT)

Recently, PDT has received increasing attention in dentistry (Konopka and Goslinski, 2007). PDT basically involves three nontoxic ingredients: visible harmless light; a nontoxic photosensitizer; and oxygen (Hass et al., 1997). The principle is that a photosensitizer binds to the target cells and is then activated by light of a suitable wavelength. Following activation of the photosensitizer through the application of light of a certain wavelength, singlet oxygen and other reactive oxygen species are produced. These are very toxic to the bacteria and certain cells. The bactericidal effect of photodynamic therapy can be explained by two mechanisms, DNA damage and damage to the cytoplasmic membrane of the bacteria by cytotoxic species. The latter leads to inactivation of the membrane transport system, inhibition of plasma membrane enzyme activities and lipid peroxidation (Wilson et al., 1995). For the elimination of bacteria in supragingival and subgingival plaque, antimicrobial PDT has been employed with various combinations of lasers and photosensitizing agents. Photodynamic therapy has been suggested as an alternative to chemical antimicrobial agents to eliminate subgingival species and treat periodontitis. The application of methylene blue-mediated photodynamic therapy in clinical studies using the Periowave treatment kit is as follows: methylene blue is applied directly in the dental pockets for 60 s followed by exposure to red light via a fiberoptic probe for 60 s per pocket or per tooth (10 s per site, six sites in total) (Figure 1.8).

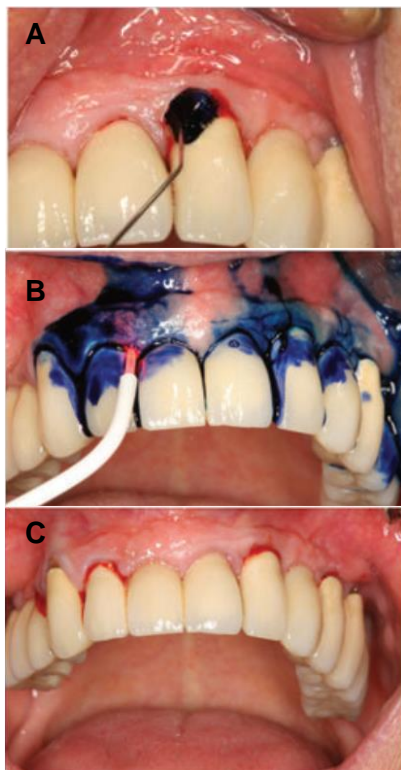


Figure 1.8. Clinical application of antimicrobial photodynamic therapy in the treatment of peri-implantitis. A. Application of the photosensitizer. The photosensitizer was placed in the peri-implant pocket. B. Irradiation with the diode laser. C. The clinical situation of therapy after 6 months. The treated site showed limited clinical improvement of peri-implant pocket and bleeding on probing occurred (Takasaki et al., 2009).

The phenothiazine dyes (toluidine blue O and methylene blue) are the major photosensitizers applied clinically in the medical field. It has been reported that methylene blue and toluidine blue O are very effective photosensitizing agents against Gram-positive and Gram-negative periodontopathic bacteria (Chan and Lai, 2003). However, Gram-negative organisms seem to be generally more resistant to PDT than Gram-positive bacteria, as a result of the differences in the outer membrane. It has been shown that toluidine blue O has a greater ability for killing Gram-positive and Gram-negative bacteria than methylene blue (Chan and Lai, 2003). For example, it has been demonstrated that *A. actinomycetemcomitans*, *P. gingivalis* and *F. nucleatum* were more susceptible to toluidine blue O than methylene blue. This is perhaps linked to the fact that toluidine blue O interacts with lipopolysaccharides more effectively than methylene blue (Chan and Lai, 2003).

PDT is an attractive treatment option as is already used in the field of periodontics (Chondros et al., 2009) and implant dentistry (Schär et al., 2013). PDT can be applied locally and PDT allows efficient bacterial elimination with high concentrations of chemical agent without producing any side effects on the host tissues, this technique could offer the rapid non-invasive topical *in vivo* application of the drug to the lesion; rapid bacterial killing after a short exposure to light; unlikely development of resistance considering the widespread generic toxicity of reactive oxygen species; and confined killing by restricting the field of

irradiation and the inherently short diffusion radius of reactive oxygen species (Sigusch et al., 2005).

Recently, antimicrobial PDT was proposed as an adjunctive method for bacterial elimination in the treatment of peri-implantitis, based on successful application in the treatment of periodontitis. Currently, there are few studies reporting the efficiency of PDT in treatment of peri-implantitis. In an *in vitro* study by Hass et al. (1997) the efficacy of antimicrobial in killing bacteria associated with peri-implantitis was examined. *A. actinomycetemcomitans*, *P. gingivalis* or *P. intermedia*, were all adhered to different surfaces (machined surface, hydroxyapatite, plasma-flame-sprayed surface, corundum-blasted and etched) and subject to PDT. This treatment completely eliminated the strains tested for all surfaces. Electron microscopic inspection of the treated surfaces revealed that combined dye/laser treatment resulted in the destruction of bacterial cells, but no damage to the titanium surface (Hass et al., 1997).

Hayek et al. (2005) compared the effects of PDT with CHX irrigation. The authors showed a significant reduction of *Prevotella* sp., *Fusobacterium* sp., and beta-haemolytic Streptococci in ligature-induced peri-implantitis in dogs. The authors also emphasised that the application of photosensitizer in a paste instead of in liquid was more favourable as it allowed easy removal after treatment. Similar antimicrobial results were also reported by Shibli et al. (2003), Hass et al. (2000) and Dortbudak et al. (2000). Indeed Hass et al. (2000) reported improvements of bone defects after 9.5 months in 21 of 24 implants studied. PDT (with mechanical debridement) has also been shown to reduce mucosal inflammation as well as minocycline microspheres (with mechanical debridement) for up to 6 months (Schär et al., 2013). The authors concluded that adjunctive PDT represents an alternative treatment modality in the non-surgical management of initial peri-implantitis. However, complete resolution of inflammation was not achieved with either of the adjunctive therapies.

Not all laboratory photodynamic therapy studies have been effective in reducing caries organisms (Haas et al., 2000). For example, methylene blue-induced photodynamic therapy was not able to reduce significantly the load of microorganisms in an *in vitro* multispecies biofilm model comprising cariogenic bacteria. Furthermore, biofilms that colonize tooth surfaces and epithelial cells lining the gingival sulcus (subgingival dental plaques) are among the most complex biofilms that exist in nature (Soukos and Goodson, 2011). In the majority of these studies, photodynamic therapy as an adjunct to scaling and root planning did not show any beneficial effects over scaling and root planning alone. Other study, have demonstrated incomplete destruction of oral pathogens

in multispecies biofilms (Müller et al., 2007, O'Neill et al., 2002) using methylene blue (Müller et al., 2007) and toluidine blue O (Qin et al., 2008). It has been suggested, in studies of model systems, that water channels can carry solutes into or out of the depths of a biofilm, but they do not guarantee access to the interior of the cell clusters (Stewart, 2003) whose diameter may range from 20 to 600 µm (Rani et al., 2005).

1.8.2 Surgical therapy

Periodontal regenerative therapy aims at complete periodontal regeneration, formation of new cementum, new periodontal ligament (PDL) and new alveolar bone. During chronic infection, bone loss persists and surgical debridement of the implant soft tissue may be required. To restore the lost bone, decontamination of implant surfaces and application of bone regeneration techniques is required (Ata-Ali et al., 2011). A recent literature review (Mombelli et al., 2012) recommended surgical access by a full-thickness flap and decontamination of implant surfaces by an appropriate debridement method, combined with systemic antibiotics and oral chlorhexidine rinses during the healing phase. Then stabilisation of the defect with a bone substitute (placement of a membrane after grafting) may be advantageous.

The evidence exists that periodontal regeneration may be induced using the principles of guided tissue regeneration (GTR). Various bone graft techniques and GBR; even in conjunction with platelet rich plasma (PRP), have been used successfully for the regeneration of lost bones in peri-implantitis. Intra-oral autogenous bone grafts are the most preferred types of grafts for GBR therapies. Other bone graft materials like demineralized freeze-dried bone and hydroxyapatite were also been used (Tomson et al., 2004). GTR is based on selective cell repopulation; the cell type that first repopulates the wound determines the nature of the regenerated tissue. A membrane covers the periodontal defect to prevent epithelial down growth and to seclude space for cells with regenerative potential to repopulate the defect site (Bosshardt and Sculean, 2009). Guided bone regeneration (GBR) is based on the same principle, creating a secluded space, in a bone environment, to regenerate bone (Hämmerle and Jung, 2003). GBR is often employed for subsequent implant installation in an originally deficient ridge (Hämmerle and Jung, 2003).

Different membranes are available, among which collagen-based membranes are mostly applied. Collagen appears to be suitable for GTR, as it is chemotactic for PDL fibroblasts, may serve as a barrier for migrating epithelial cells (Pitaru et al., 1987), and acts as a fibrillar scaffold for early vascular in growth (Blumenthal,

1993). However, membranes act mainly as physical barriers and have to be considered biologically inactive. Membranes alone are not capable of enhancing cellular events during the regeneration process. Furthermore, GBR-studies using collagen membranes showed limited bone formation (Hämmerle and Jung, 2003). Moreover, the collapse of the membrane, due to lack of mechanical stability, compromises the amount of new tissue. Therefore, as an adjunct to GTR/GBR procedures, a grafting material is placed into the defect to prevent this collapse (Hämmerle and Jung, 2003). Schwarz et al. (2008) compared BioOss® (bone substitute) and collagen membrane after 6 months, 2 years and 4 years. After 6 months they found that both materials performed equally well. After 2 and 4 years, BioOss® afforded greater benefits than collagen material alone. The difficulty of surgical manipulation is that the exposure of threads surgically will result in permanent exposure of the threads of the implant. Despite treatment and retreatment of areas affected with peri-implantitis, supporting bone may also be lost, exposing more of the surface of the implant. This is a complication in the anterior zone that leads to patient's dissatisfaction (Schwarz et al., 2008). Other measures have been designed to improve and accelerate osseous healing by increasing the bone-to-implant contact. These include the application of platelet-rich plasma (PRP). Marx et al. (1998) reported in their data on the use of PRP for promoting bone graft healing. These showed greater bone density and quality in grafts with PRP added during pre-implant augmentation. Local PRP administered during dental implant placement thus enhances bone regeneration at implant host sites in the posterior mandible during early healing (Zechner et al., 2004).

1.8.3 Cumulative interceptive supportive therapy (CIST)

Cumulative interceptive supportive treatment (CIST) is an excellent guide for the clinician to follow (Lang et al., 1997). The main goal of this approach is to diagnose peri-implant infections as early as possible to prevent explantation (extraction of dental implants) due to loss of osseointegration. The basis of this system depends on the regular recall of patient after implant placement with follow up assessment using accepted clinical periodontal parameters including:

1. The presence of plaque.
2. The bleeding tendency of the peri-implant mucosa.
3. Suppuration.
4. The presence of peri-implant pockets.
5. Radiological features of bone loss.

If the implant gives negative results for all of these above parameters, no therapy is needed. If plaque and/or an increased tendency of the peri-implant mucosal tissues to bleed is detected then the implants are mechanically cleaned (rubber cup and polishing paste used). Oral hygiene practices should be checked, and the proper plaque control technique should be instructed and reinforced (A). In the presence of pus, or if first signs of peri-implant tissue destruction is detected (pockets in the range of 4 to 5 mm and slight bone loss) regimen A should be combined with the application of a local antiseptic (B). Peri-implant pockets are then irrigated with 0.2% CHX and the patient is advised to rinse twice daily with 0.1- 0.2% CHX. If the peri-implant sulcus allows more than 5 mm of penetration of a periodontal probe then a radiograph is taken. If there is clear evidence of bone loss, then a microbiological sample is taken. Should there be evidence of anaerobic microbiota, the patient is given treatments A and B, and, in addition, is placed on systemic antimicrobial therapy (C) with an agent specifically effective against strict anaerobes (ornidazole, 1000 mg for 10 consecutive days). If the bone destruction has advanced considerably, surgical intervention to correct the tissue morphology or to apply guided bone regeneration techniques may be necessary (D). Such treatment would, however, only be given in addition to the other measures (A, B and C) (Mombelli and Lang, 1998, Lang et al., 1997, Okayasu and Wang, 2011).

1.9 Modelling dental plaque and plaque related diseases

Studying oral biofilms *in vivo* can be difficult, time consuming and constrained by ethics. Modelling such biofilms is however important for studying development and perturbation. Numerous models have been described and range from simple single species to complex microcosms.

1.9.1 Microplates

Biofilm models designed upon microplates were first described in 2001 by Guggenheim (Guggenheim et al., 2011, Guggenheim et al., 2001). Simple methods such as these are preferred to obtain results rapidly when several tests and conditions need to be addressed. It allows for the short-term exposure of biofilms to selected substances. It is a sensitive and reproducible method to verify early biofilm changes and the variation in response of different substrata. Besides simplicity of design, the media can be applied to and removed from the system virtually instantaneously. This model allows for controlled substance exposure times resembling those encountered during mouth rinsing. Moreover, exposure times during oral hygiene procedures are very short. The concentrations of mouth rinsing, inhibiting bacterial growth in the biofilm model were of the same as those required for plaque inhibition *in vivo*. This method has been used to establish microcosm biofilms for enamel demineralization and antimicrobial dose-response studies (van de Sande et al., 2011). This method has been used for the modelling of supragingival plaque biofilm for the study of plaque formation, structure and antimicrobial susceptibility (Guggenheim et al., 2001), and also used to compare the antimicrobial effects of CHX and mouth rinses available on the Swiss market (Guggenheim et al., 2011).

1.9.2 Flow cells

The flow cell model was developed by Caldwell and Lawrence (1988) and is a powerful tool for examining the early stages in biofilm formation, as it enables the observation of non-destructive biofilm development in real time (Busscher and van der Mei, 1995). It has been used for study of short-term adhesion and colonisation. The flow cells consist of a transparent chamber of fixed depth through which passes of growth medium. Figure 1.9, shows the system can be inoculated either by adding an inoculum to the medium reservoir or passing a culture through the flow cells to allow the cells to adhere before feeding with sterile medium (Busscher and van der Mei, 1995).

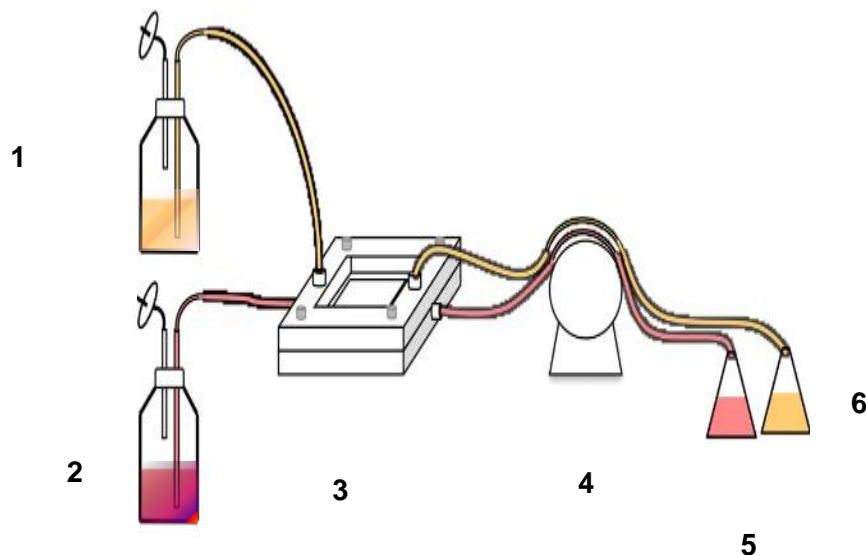


Figure 1.9. Schematic of the flow cells models; 1: saliva-supplemented medium. 2: Tissue culture medium. 3: flow cells. 4: Peristaltic pump. 5: lower chamber effluent. 6: upper chamber effluent. Reproduced and image taken from (<http://Flow+cells model source>).

1.9.3 The constant depth film fermentor (CDFF)

The CDFF was developed by Peters and Wimpenny in 1988 (Figure 1.10). The CDFF is one of the most suitable *in vitro* methods for growing reproducible biofilms that are appropriate for studying oral microbiology. The CDFF's main characteristic is that microbial growth is periodically removed to maintain constant depth. It is particular suited to studying environments like the oral cavity (Peters and Wimpenny, 1988, Wilson, 1999, Pratten et al., 2000) and has a number of advantages:

- It can operate in a septic environment by allow any mixture of medium flow and gas composition.
- It affords good reproducibly.
- It allows multiple biofilms to be produced on any given substratum.
- It allows biofilm thickness to be limited by mechanical shear forces, such as those in the oral cavity that would limit the accumulation of dental plaque.
- It can be run for unlimited periods of time.

The CDFF has been used comprehensively in a variety of applications such as:

- To investigate biofilm formation by a nine-membered community of oral bacteria (Kinniment et al., 1996a).

- To evaluate antimicrobial agents for use in clinical dentistry (Kinniment et al., 1996b).
- To determine the effect of pulsing chlorhexidine gluconate, at concentrations commonly used in mouthwashes on *Streptococcus sanguinis* biofilms and microcosm dental plaques *in vitro* (Pratten et al., 1998).
- To investigate the structure of intact oral biofilms (Pratten et al., 2000).
- Modelling oral malodour in a longitudinal study (Pratten et al., 2003).
- To develop a bacterial demineralization model (Deng and ten Cate, 2004).
- To examine biofilm structure and cell vitality in a laboratory model of subgingival plaque (Hope and Wilson, 2006)
- Modelling shifts in microbial population associated with health or disease (Dalwai et al., 2006).
- For the assessment of bacterial community structure in oral populations (Circi et al., 2010) by novel multiplex qPCR approach.



Figure 1.10. Constant depth film fermentor with power supply (Pratten, 2007).

1.10 Aims of study

The aim of this study was to generate an *in vitro* model of peri-implantitis. The success criteria for this would be:

1. To model microcosm biofilms on titanium discs in a CDFF which contained the microorganisms associated with peri-implantitis.
2. To develop a model to allow progression from health-associated bacterial community to a peri-implant mucositis-associated community and finally to a peri-implantitis-associated community.
3. To develop microscopic and molecular biology methods to characterise these communities.
4. To test whether treatment modalities are successful at perturbing the bacterial communities.
5. To use the model to test both commercially available and novel antimicrobial surfaces for the inhibition of bacterial growth or succession to a disease state.

1.11 Schematic plan of study

A brief outline of the multifaceted study is presented in (Figure 1.11). The first step of this study was to develop an *in vitro* model of peri-implantitis. The CDFF was used as an *in vitro* model and biofilm development characterised by using different culture methods (Chapter 2). Biofilms were grown on titanium discs and a model of health progressing to peri-implant mucositis (Chapter 3) was developed. This model was then modified to progress from health to peri-implant mucositis than to peri-implantitis (Chapter 4). Further characterising of this model was developed using microscopic techniques and, 16S rRNA gene cloning and sequencing methodologies (Chapter 4). Identification and quantification of bacterial number and proportions using multiplex qPCR approach was performed (Chapter 5). Novel *TaqMan* probes and primers for quantification of *Capnocytophaga* species were designed (Chapter 6). Biofilms were grown on three commercial titanium (Ti) surfaces (polished, SLA and SLActive) with a range of decontamination techniques used to clean the three infected Titanium surfaces (Chapter 7). Biofilm development was assessed on novel nano-coated antibacterial Ti surfaces (Chapter 8).

1. The constant depth film fermentor (CDFF) will be used.

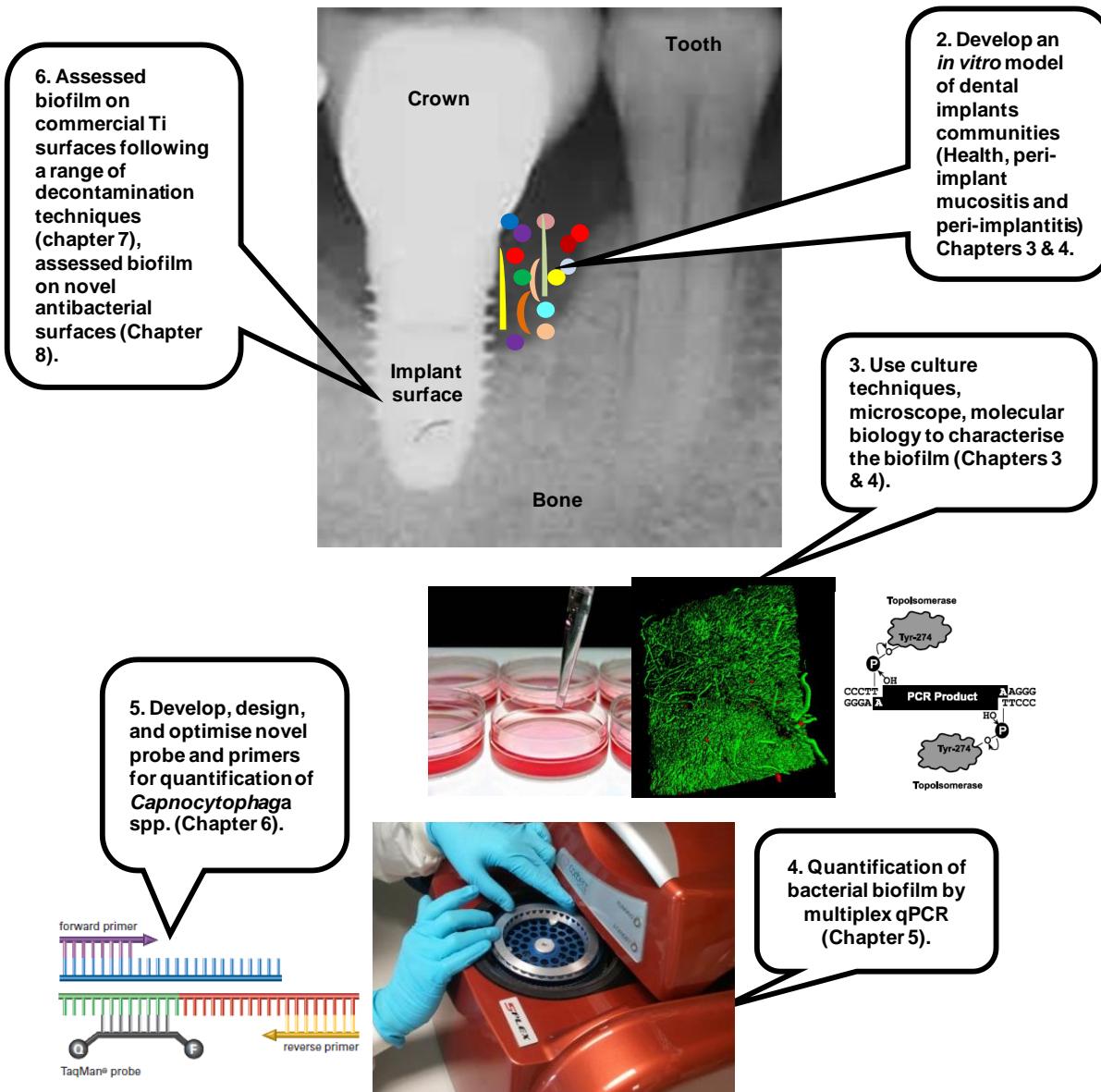


Figure 1.11. A summary schematic of the study.

Chapter 2
Materials and Methods

2.1 Growth media

A range of non-selective and selective media were used to culture bacteria from microbiological samples. The constituents for one litre of each agar are listed below. Once prepared, molten agar was poured into petri dishes.

The total anaerobic count was carried out on fastidious anaerobic agar. The agar was prepared as follows: 46.5 g of fastidious anaerobic agar powder (Lab M, Bury, UK), was added to 950 ml of deionised water and mixed thoroughly. This was then autoclaved at 121°C for 15 min, left to cool to 50-55°C in a water bath before 50 ml (5%) of defibrinated horse blood (E and O Laboratories, Bonnybridge, UK) was added.

The total aerobic count was performed on columbia blood agar. The agar was prepared as follows: 39.5 g of agar powder (Lab M) was mixed with 950 ml of deionised water. This was autoclaved at 121°C for 15 min, cooled to 50-55°C and 5% defibrinated horse blood added.

Actinomyces spp. were isolated on cadmium fluoride-acreflavin-tellurite agar (CFAT), the composition and preparation of which is described below. Trypticase soy broth (Lab M), 30 g; Agar no. 3, 12 g was mixed with 950 ml of deionised water. This was autoclaved at 121°C for 15 min, cooled to 50-55°C and 25 ml of glucose added (Sigma-Aldrich, Poole, UK), 13 mg/ml cadmium sulphate (Sigma-Aldrich), 42.5 mg/ml; sodium fluoride (Sigma-Aldrich), 1.2 mg/ml neutral acreflavin (Sigma-Aldrich), 10 mg/ml; potassium tellurite (Difco Laboratories, Oxford, UK); 0.2 g/ml of basic fuchin (Sigma-Aldrich); and 5% defibrinated horse blood added.

Gram-negative anaerobic rods were isolated on Gram-negative anaerobic agar. This was prepared by adding 46.5 g of fastidious anaerobic agar (FAA-Lab M) powder to 950 ml of deionised water and mixed thoroughly. This was autoclaved at 121°C for 15 min before being cooled to 50-55°C. Five percent defibrinated horse blood and a supplement containing 0.5 ml of a 10 mg/ml vancomycin hydrochloride (Sigma-Aldrich) solution were added.

Streptococcus spp. were isolated on mitis salivarius agar (Difco Laboratories). Ninty gram of the agar powder was added to deionised water and mixed thoroughly before being autoclaved at 121°C for 15 min. This was then cooled to 50-55°C and 1% (w/v) potassium tellurite was added aseptically.

Chapter 2: Materials and Methods

Staphylococcus spp. were isolated on mannitol salt agar (Oxoid, Hampshire, UK). This was prepared by adding 65 g of mannitol salt powder to deionised water and mixed thoroughly before being autoclaved at 121°C for 15 min. This was then cooled to 50-55°C.

Candida spp. was isolated on sabourauds dextrose agar (Oxoid, Basingstoke, UK). This was prepared by adding 41 g of the powder to deionised water and mixing thoroughly before being autoclaved at 121°C for 15 min. This was then cooled to 50-55°C.

Veillonella spp. were isolated on *Veillonella* agar (Difco Laboratories) which was prepared by adding 5 g of tryptone (Difco Laboratories), 3 g yeast extract (Oxoid) and 15 g of technical agar no.3 (Oxoid) to 950 ml of deionised water and mixing thoroughly. This was then autoclaved at 121°C for 15 min and allowed to cool to 50-55°C. Following this, 0.75 g of sodium thioglycollate (Sigma-Aldrich), 0.002 g of basic fuchin (Sigma-Aldrich), 21 ml of 60 % sodium lactate and 0.5 ml of 10 mg/ml vancomycin hydrochloride (Sigma-Aldrich) were aseptically added.

Luria Bertani (LB) agar was used for isolating and growing *E. coli* clones. It was prepared by adding 10 g of tryptone (Oxoid), 5 g yeast extract (Oxoid); 10 g NaCl and 15 g of technical agar no. 3 (Sigma-Aldrich) to 950 ml deionized water. This was mixed thoroughly, autoclaved at 121°C for 15 min and cooled to 50-55°C. Following this 1 ml of 50 µg/ml kanamycin (Sigma-Aldrich) was added.

Once cooled all of the media was poured into petri dishes in a laminar flow cabinet and allowed to set. All plates were stored at 4°C for up to 2 weeks until needed. Once inoculated, plates were incubated as appropriate either in an anaerobic atmosphere (5% Carbon dioxide, 5% Hydrogen and 90% Nitrogen) at 37°C for 4-5 days or aerobically (with the addition of 5% Carbon dioxide) at 37°C overnight.

Artificial saliva and artificial tissue fluid was prepared for the growth of microcosm plaque biofilms as follows:

To make 1 l of artificial saliva 0.5 g 'Lab-Lemco' powder (Oxoid), 1 g yeast extract (Oxoid), 2.5 g protease peptone (Oxoid), 1.25 g hog gastric mucin type III, partially purified from porcine stomach (Sigma Chemicals Co., Poole, UK), 0.18 g sodium chloride (BDH Chemicals Ltd, Poole, UK), 0.1 g calcium chloride (BDH) and 0.1 g potassium chloride (BDH) was added to deionised water. After

autoclaving at 121°C, 0.625 ml of a 40% urea (Sigma-Aldrich) solution was added.

Peri-implant sulcular fluid (PISF) was prepared as follows; 60% RPMI tissue culture medium (Sigma-Aldrich) (600 ml) was supplemented with 40% (v/v) horse serum (Sigma-Aldrich), 0.1 ml of a 5 µg/ml menadione (Sigma-Aldrich) and 1 ml of a 5 µg/ml haemin (Sigma-Aldrich).

Reduced transport fluid (RTF) was prepared according to Syed and Loesche (1972). The composition was follows: Stock solution I was made by adding 0.6 g dibasic potassium phosphate (Sigma-Aldrich) to 100 ml of deionised water followed by autoclaving. Stock solution II was made by mixing 2.5 g MgSO₄ (Sigma-Aldrich) with 100 ml of deionised water then autoclaving. Stock solution III was made by mixing 1.2 g potassium chloride (Sigma-Aldrich), 1.2 g ammonium sulphate (Sigma-Aldrich), 0.6 g monobasic potassium phosphate KH₂PO₄ (Sigma-Aldrich), 1 ml of stock solution II solution and 99 ml deionised water and autoclaved. Stock IV was made by mixing 0.8 g Sodium carbonate (Sigma-Aldrich) and 10 ml deionised water and autoclaved. To prepare 100 ml of RTF the following were mixed together 7.5 ml of Stock I with 7.5 ml of Stock III, 0.5 ml of Stock IV and 80 ml of deionised water. 5 ml of freshly made, filter sterilised 0.02 g DL-Dithiothreitol (Sigma-Aldrich) was then added to the solution.

2.2 Constant depth film fermentor set up

Briefly, the CDFF apparatus consisted of a glass vessel (18 cm in diameter, 15.0 cm depth) with stainless-steel end plates, the top one of which has ports for the entry of medium, nutrients, gas and for sampling, whereas the bottom end plate has a medium outlet (Figure 2.1). The CDFF was maintained at a constant temperature of 37°C in an incubator as shown in figure 2.2. The fermentor was sealed using silicon vacuum grease which was applied to both of the polytetrafluoroethylene (PTFE) seals, this prevented leakage of the medium and also helped to maintain the atmospheric conditions within the fermentor. The tubing was then connected to the CDFF to enable delivery of nutrients, gases and to allow the removal of waste through to an effluent reservoir. The rotating turntable holds 15 PTFE pans. Each pan contains 5 cylindrical holes (5 mm in diameter) containing PTFE plugs upon which discs of appropriate substrata, for example, commercial, coated/and or turned titanium can be held and recessed to a desired depth. The turntable in which the pans fit rotates at 3 rpm (Wilson, 1999). The speed is controlled by a 15-V DC power supply unit. The turntable

Chapter 2: Materials and Methods

rotates at a constant rate as the growth medium is pumped in via the inlets in the top plate. Attached to the top plate are two scraper blades which sweep the inocula and growth media into the recesses and once biofilms are formed prevents them from exceeding the desired depth. Silicone tubing (Fisher Scientific Ltd., UK) was attached to the inlets in the top plate and the outlet for effluent in the base plate and secured in place using cable ties. This tubing was fitted with connectors which could be attached to tubing coming from growth medium reservoirs or the inoculum, gases and also for connection to the waste medium vessel. Marprene tubing (Fisher) was also required to run through a peristaltic pump (UK) in order to maintain the desired flow rate. The whole apparatus was autoclaved at 121°C for 15 min prior to use.

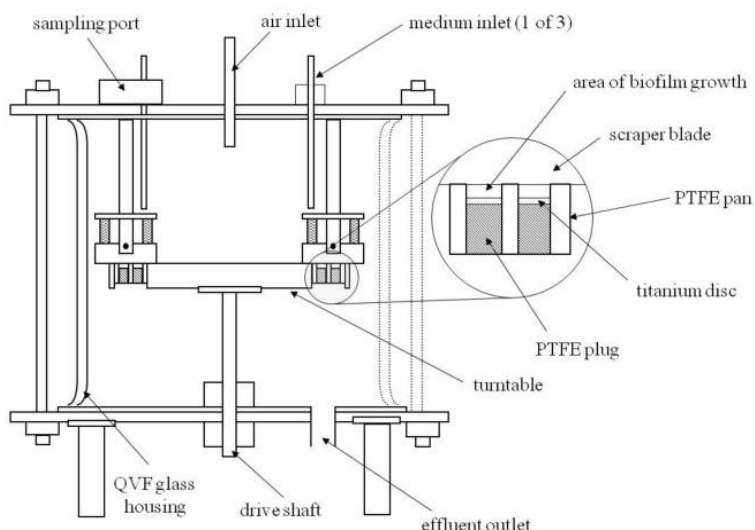


Figure 2.1. The constant depth film fermentor (CDFF): Diagram of vertical section through the fermentor (Pratten et al, 1998).



- 1. Incubator**
- 2. Filters, tubes and connectors**
- 3. Artificial saliva 500 ml**
- 4. Peri-implant sulcular fluid**
- 5. Pump**

Figure 2.2. The constant depth film fermentor (CDFF) set-up.

2.2.1 Microcosm biofilms

In order to produce microcosm biofilms to be used in the CDFF experiments, saliva was collected aseptically from ten members of the Microbial Diseases Research Department, UCL Eastman Dental Institute, who had no signs of periodontal disease (Ethical approval for the project was obtained from the UCL Ethics Committee; Project no. 1364/001). This was pooled and resuspended in 10% (v/v) glycerol and vortex mixed vigorously for 1 min to homogenize the sample. Aliquots of 1 ml were then dispensed and stored at 80°C for subsequent use for all experiments so far in 1.5 ml cryotubes.

2.2.2 *In vitro* model parameters

The biofilms were grown on moderate smooth titanium discs grade 23 (A C Service Group, Fordingbridge, UK, 5 mm in diameter and 2 mm height). Grade 23, is the higher purity version of Ti 6Al-4V. The Titanium discs were sonicated with acetone for 20 min at 50 Hz to remove adherent debris or dust then autoclaved before inserted in to sterile PTFE plugs. The discs sit on sterile PTFE plugs and are held in place by using vacuum silicone grease (Dow Corning, USA) and recessed to a depth of 600 µm. The pan was tapped down to the level of the turntable with a flat ended tool. Biofilms were removed during experiments via a port in the top plate using a flat ended tool inserted into a tapped hole in the centre of the pan.

2.2.3 Inoculation of the CDFF

A vial of stored pooled saliva (section 2.2.2) was thawed and 900 µl used to inoculate 500 ml of artificial saliva (see culture media section). This was mixed and pumped into the CDFF for 6 h at a rate 1.38 ml/min. After this time, the inoculation flask was disconnected and the CDFF fed from a medium reservoir of sterile artificial saliva. The artificial saliva was delivered via a peristaltic pump (Watson-Marlow, Falmouth, UK) at a rate of 0.5 ml/min (0.72 L/day). An aerobic atmosphere was maintained by exposure to the environment via a 0.22 µm membrane filtered air (Hepa Vent filters, Whatman, Maidstone, UK) inlet in the upper end plate. Some experiments used other gaseous environments (section 2.2.5).

2.2.4 Biofilm sampling

To sample, the turntable was stopped so as the pan wanted for sampling was directly under the sampling port. The sampling port was then swabbed with an alcohol (70% v/v) moistened swab, and opened. A sterile sampling tool was then inserted into the fermentor and screwed into the pan. The pan was removed from the CDFF was subsequently placed in a sterile universal tube and discs from each pan used for determining the bacterial composition of the biofilms. The titanium discs were aseptically removed and placed into 1 ml of reduced transport fluid (RTF) containing five autoclaved glass beads (3 mm in diameter) and then vortexed for 1 min to disrupt the biofilm. This suspension was then serially diluted up to seven 10-fold dilutions and 20 µl aliquots spread in duplicate onto appropriate media using a sterile blue plastic spreader. All plates were incubated aerobically for 48 h with 5% CO₂ except fastidious anaerobic agar, Gram-negative, *Veillonella* agar and Cadmium fluoride-acriflavin-tellurite agar plates which were incubated for 4 to 5 days in an anaerobic cabinet.

2.2.5 Conditions used for running the CDFF

Initially, to provide conditions associated with healthy dental implant, with nutrition supplied solely by saliva, an artificial saliva formulation was pumped into the CDFF at a rate of 0.5 ml/min. Subsequently, the nutrient conditions were altered by adding both artificial saliva and an artificial tissue fluid. The tissue fluid was used to mimic peri-implant sulcular fluid (PISF). This was pumped into the artificial saliva formulation at a rate of 0.5 ml/min as it flowed into the CDFF at a rate of 40 µl/min.

To provide conditions associated with peri-implant mucositis, artificial saliva was pumped into the CDFF at a rate of 0.5 ml/min. In addition, peri-implant sulcular

fluid was pumped into CDFF at a rate of 130 $\mu\text{l}/\text{min}$. This was accompanied by a switch to a more microaerophilic environment by pumping in a microaerophilic gas mixture (2% Oxygen, 3% Carbon dioxide, and 95% Nitrogen 200 bar) via a 0.22 μm membrane filtered air inlet (Hepa Vent filters) in the top plate at a rate of 200 cm^3/min .

To provide conditions associated with peri-implantitis, only PISF was pumped into the CDFF at a rate of 130 $\mu\text{l}/\text{min}$. This was accompanied to a switch to a more anaerobic environment by pumping in a CO_2 gas mixture (5% Carbon dioxide and 95% Nitrogen) via a 0.22 μm membrane filtered air inlet (Hepa Vent filters) in the top plate at a rate of 200 cm^3/min as shown in figure 2.3.

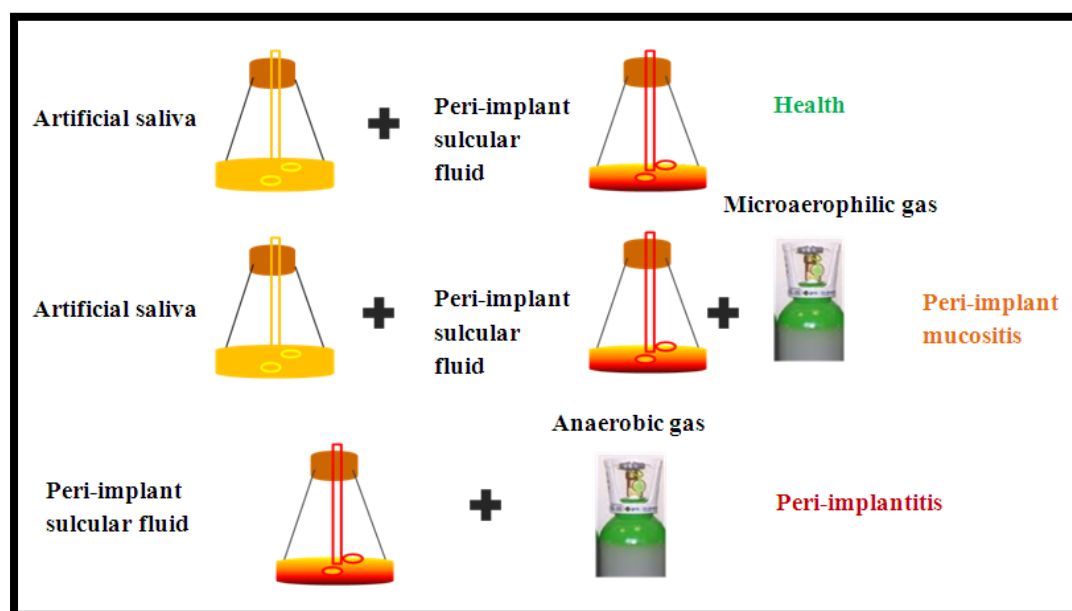


Figure 2.3. Schematic summary for development of the *in vitro* model of peri-implantitis showing the three stages of development (health, peri-implant mucositis and peri-implantitis).

2.3 Identification of cultivable species by comparative 16S rRNA gene sequencing

2.3.1 DNA extraction

A titanium disc was removed from the CDFF at six time points, 6 h, 96 h, 246 h, 438 h, 540 h and 714 h. The biofilm was suspended in 1 ml of sterile RTF containing five glass beads (3 mm in diameter) and vortexed for 1 min to create a homogenous suspension. This suspension was centrifuged for 1 min at a speed of 14600 x g. The pellet was resuspended in 50 µl phosphate buffer and subsequent DNA extraction was performed as described by (Griffiths et al., 2000). One disc from each time point was used for DNA extraction.

2.3.1.1 DNA extraction procedure

Total nucleic acid was extracted from all samples according to a previously described protocol (Griffiths et al., 2000); this method was found to be the least biased towards the extraction of nucleic acids from Gram-negative organisms. Bacterial biofilm was resuspended in 50 µl phosphate buffer. Twenty five µl of suspension and 0.2 ml of cetyltrimethylammonium bromide (CTAB) extraction buffer were added to 2 ml screw top tube containing zirconium/ silica beads 0.1 mm (Biospec Products, 454 g). To this was added 0.5 ml phenol: chloroform: isoamyl alcohol (25:24:1) and the lids were then tightened. The tubes were placed into a ribolyser bead beater (Thermo Electron Corporation, Delft, The Netherlands) and lysed for 30 s at a speed of 5.5 m/s. The lysed cells were then centrifuged at \geq 14,000 x g for 10 minutes at 4°C. The top layer of the bilayer was carefully removed and transferred to a new tube. A 0.5 ml aliquot of chloroform: isoamyl alcohol (24:1) was added and mixed well by vortexing for 6 s. The mix was centrifuged for 3 min at \geq 14,000 x g. A 0.3 ml aliquot was extracted from the top layer. The nucleic acids were precipitated by adding 2 volumes of 30% polyetheneglycol 6000 (PEG) solution and mixed well. These were left overnight at 4°C to precipitate. The preparation were then centrifuged at \geq 14,000 x g for 15 minutes. The supernatant was removed and the pellet was washed twice with 0.2 ml of ice cold 70% ethanol. This was repeated and any remaining ethanol was removed and the pellet was allowed to air-dry for 10 min at room temperature. The pellet was then resuspended in 0.1 ml Tris EDTA (TE) buffer (1.0 M Tris-HCl, pH approx. 8.0) (Sigma-Aldrich) with RNase 10 µg (Sigma-Aldrich) and incubated at room temperature. The preparation was then left on the bench for 1 hour. The DNA concentration was measured using a Nanodrop 1000

Spectrophotometer (V3.7, Thermo Fisher Scientific, USA) and by agarose gel electrophoresis section (2.3.1.3).

2.3.1.2 Polymerase chain reaction (amplifying the DNA)

PCR amplification was carried out in a reaction volume of 50 μ l consisting of 5 μ l of 10 μ M buffer, 1 μ l each of 10 mM dATP, dCTP, dGTP and dTTP (all deoxy nucleoside triphosphates from Bioline, London, UK), 2.5 μ l of 50 mM MgCl₂, 1 μ l of 100 μ M of each PCR primer (diluted 1:10) and 0.5 μ l of 2000U/ μ l Taq polymerase (Bioline) and 34 μ l of sterilized deionised water. The PCR primers used were: 27f (5' AGAGTTGATCMTGGCTCAG 3'; Sigma-Genosys) and 1492r (5' TACGGYTACCTTGTACGACTT 3'; Sigma-Genosys). The negative control was 45 μ l reaction mixed with 5 μ l of sterilized deionised water. The positive control contained 5 μ l of genomic DNA from *Escherichia coli* and the DNA template 5 μ l in 45 μ l of reaction mixture added to bring the volume to 50 μ l. PCR thermocycling was performed in a Biometra (T3000 thermal cycler, Glasgow, UK) and conditions for all samples were: (i) an initial denaturation for 5 min at 94°C, (ii) 29 amplification cycles of denaturation at 94°C for 1 min, annealing of primers at 54°C for 1 min and primer extension at 72°C for 1 min followed by (iii) a final extension step at 72°C for 5 min. The reaction products were either stored at -20°C or analysed immediately. Negative and positive controls were included in each batch of samples being analysed by PCR.

2.3.1.3 Agarose gel electrophoresis

PCR amplicons (1500 bp) were assessed by loading 5 μ l of the PCR product into wells of a 1% (w/v) agarose powder (Sigma-Aldrich) containing gel red (2 μ l/100ml) (Qiagen, Manchester, UK). Hyper ladder I marker ranging from 200-10,000 bp (Qiagen) 5 μ l was loaded into the first well. The PCR mixture 5 μ l from each sample was mixed with 2 μ l of the loading buffer and loaded into the appropriate wells of the gel. The gel was immersed in Tris-acetate EDTA buffer (Tris base 240 g, Glacial acetic acid 75.1g/ml, 100 ml 0.5 M EDTA, water to 1000 ml; Oxoid) and subjected to a voltage 100 V that led to separation of the fragments. The gel was visualised after excitation under UV transillumination by placing it in a multi-image light cabinet and the resulting image was captured using computer software programme (AlphaEaseTM, AlphaInnotech, Ringmer, UK) and stored the PCR products at -20 °C.

2.3.1.4 Purification of PCR products

PCR products were purified using the (Qiagen) purification kit. Briefly, 1 volume (45 μ l) of PCR reaction product was added to 225 μ l of Buffer PB in a QIAquick spin column placed in a 2 ml collection tube, then centrifuged at 14,000 \times g for 1 min to bind the DNA. The flow-through was discarded and 0.75 ml of diluted PE buffer (ethanol) was added into spin column to wash the DNA; this was centrifuged at 14,000 \times g for 2 minutes. The flow-through was discarded and the column centrifuged for an additional minute to remove residual ethanol. The QIAquick spin column was placed into a sterile 1.5 ml tube, 30 μ l of sterilized water was applied to the centre of the column and each tube was kept at room temperature for 1 min. The column was centrifuged at 14,000 \times g for 1 min to give 30 μ l of eluted DNA. The sample was checked by Nanodrop device (Qiagen) and run on 1% agarose gel to confirm the presence of DNA before cloning.

2.3.2 16S rRNA gene cloning

The six CDFF biofilms for each sample (6 h, 96 h, 246 h, 438 h, 540 h and 714 h) of the PCR products generated were subjected to TOPO® cloning (Invitrogen, UK) and transformation into chemically competent *E. coli* cells. Four microlitres of fresh PCR product was mixed with 1 μ l of salt solution and 1 μ l of Topo vector and made up to a volume with 6 μ l sterilized water. This was then mixed gently and incubated for 30 min at room temperature (22-23°C). The reactions were then placed on ice. The transformation was then performed by adding 2 μ l of the TOPO® cloning reaction to a 50 μ l of vial of chemically competent *E. coli* and mixed gently by thumb flushing. This was then incubated on ice for 30 min. The cells were then heat shocked for 30 sec at 42°C and immediately incubated on ice. Two hundred and fifty microlitres of super optimal broth (at room temperature) with catabolite catabolite repression (S.O.C.) medium (bacterial growth medium) was then added and the tubes horizontally in a shaker (200 rpm) at 37°C for 1 h.

2.3.2.1 Culturing

Transformed clones were plated out on to three pre-warmed LB agar plates using 3 different volumes (20, 50, and 100 μ l). After plates were warmed at 37°C, each plate spread with 40 μ l of 40 g/ml X-gal (5-bromo-4chloro-3indoyl-B-D-galactoside) and kept warm (37°C) until ready for use.

2.3.2.2 Colony counting of isolates

After overnight incubation, all LB plates for each sample (6 h, 96 h, 246 h, 438 h, 540 h and 714 h) were placed in the refrigerator (4°C) for 1 hour to intensify the potential blue colouration of the colonies. All white colonies were sampled using sterile tips and inoculated onto a new LB agar plate on a numbered grid to identify individual colonies. The newly inoculated plates were incubated overnight at 37°C and transferred to the refrigerator for storage for subsequent use.

2.3.2.3 Extraction of DNA from clones

For PCR analysis, DNA was extracted from 180 bacterial clones by a 5 min boiling procedure. Briefly, colonies were suspended in sterile nuclease free water in 1.5 µl tubes. The tubes were then boiled for 5 min. immediately after boiling; the tubes were placed on ice. This was later used as a DNA template for the PCR amplification. A positive control was prepared using *E. coli*. After subculture of an *E. coli* strain on blood agar plates, a small portion was taken with a sterile wooden toothpick from the plate and placed into 50 µl of sterile distilled water and boiled for 5 min as above. The negative control included 5 µl distilled water and 45 µl of PCR master mixer (Bioline). DNA amplifying, PCR cycling, agarose gel electrophoresis and PCR purification procedures were the same as above.

2.3.2.4 Sequencing reactions

The final step in identifying the cloned sequence was to sequence the PCR product. The DNA was sequenced and aligned by Sanger technique at the UCL Cancer Institute and Wolfson Institute for Biomedical Research. The 16S rRNA PCR products were partially sequenced using primer 357F of 2-5 pmoles/µl (59-CTCCTACGGGAGGCAGCAG-39; Lane, 1991) and the ca. 1500 bp sequences submitted to the Ribosomal Database Project RDP (<http://rdp.cme.msu.edu/index.jsp>) for identification. Further analysis was performed and compared using Blast (<http://ncbi/Blast/>) in order to find the closest match with the 16S rRNA gene. More than 98% identity in the 16S rRNA gene sequence was the criterion used to identify bacteria at the species level.

2.4 Quantitative PCR analysis of biofilm samples

2.4.1 Preparation of DNA for standard curve generation

Depending on the specific target of the primers used for each PCR assay a standard curve of bacterial genomic DNA from a known number of bacterial cells was created. One swab from a plate of each organism was suspended in 1 ml of RTF. The viable bacterial numbers in this culture was than enumerated by serial dilution and plating on fastidious anaerobic media. In order to produce standard

curves for the enumeration of organisms, DNA was used in the optimisation reactions from the following reference strains: *Fusobacterium nucleatum* (NCTC 10562), *Lactobacillus casei* (ATCC 334), *Veillonella dispar* (NCTC 11831), *Neisseria subflava* (DSM 17610), *Actinomyces naeslundii* (DSM 17233), *Prevotella intermedia* (DSM 20706), *Streptococcus sanguinis* (NCTC 02863) and *Streptococcus mutans* (ATCC 700610).

Total nucleic acid was extracted from all samples according to the protocol of Griffiths and colleagues (2000) using a bead-beating phenol: chloroform: isoamyl alcohol (25:24:1) extraction followed by 30% PEG 6000 precipitation and 70% ethanol wash (section 2.3.1.1).

2.4.2 QPCR assay set up

The three triplex qPCR assays were performed using 2 µl of extracted DNA to enumerate eight oral taxa as well as the total number of organisms. All reactions were run in triplicate in a final volume of 25 µl. Sensimix Probe (Bioline) qPCR mastermix was used and the Rotor-gene 6500 (Qiagen) cycler using the green, yellow and red channels for data collection. Each reaction contained the previously described concentrations of the oligonucleotides. The reaction conditions were performed as specified by the manufacturer with the annealing/extension temperature ranging from 60°C to 64°C. Species specific primers and dual-labelled fluorogenic probes were designed for all organisms using 16S rRNA gene sequences. It was essential to have enough points to generate a standard curve containing at least six 10-fold dilutions of reference DNA for each sample with at least three replicate wells to ensure the accuracy. It was also essential to have control wells which contained no template to ensure purity of all the reagents used.

2.4.3 PCR conditions

The standard PCR conditions for qPCR were an initial step of 95°C for 10 min, followed by 40 cycles of 95°C for 15 s, x°C for 60 s (x= 60°C for FLV & SSU, x= 64°C for NAP) (Circi et al., 2010).

2.4.4 Analysis of qPCR results

The amount of fluorescence detected by the qPCR machine as the reaction proceeded was plotted as an amplification plot using the Rotor gene 6000 (Qiagen). From this plot, a threshold line was set as the level of detection where the fluorescence intensity exceeded any back ground fluorescence. This line was

within the exponential phase of detection. The point at which the fluorescence detected in a particular sample crossed this line was the cycle threshold (C_t). This value was important in calculating the amount of bacterial DNA in sample.

2.4.5 Standard curve

To generate a standard curve from DNA extracted from known quantities of bacterial cells, this C_t number was plotted against the log number of bacteria. By grouping replicate samples together, the rotor gene 6000 (Qiagen) software automatically calculated the mean and the standard deviations so it was possible to immediately see the reproducibility between replicate samples.

2.5 Biofilm imaging

2.5.1 Confocal laser scanning microscopy (CLSM)

2.5.1.1 Sample preparation

Biofilm samples from the CDFF were usually flat and could be mounted and stained with relative ease. The titanium discs supporting the biofilms were placed in a 5 cm (diameter) tissue culture wells, with flat bases, and held in place by silicon vacuum grease. 1 μ l of each of the components A and B of *BacLight*TM Live/Dead viability stain (Molecular Probes, Invitrogen) was added to 5 ml of RTF. Five ml of this solution was carefully added to the biofilm in the wells and incubated in the dark for 15 min. The biofilms were examined with a Radiance 3000 confocal Laser scan head (Bio-Rad, Jena, Germany) in conjugation with a BX51 stereomicroscope (Olympus, Southhall, UK), equipped with a x40 water immersion lens which was used to visualise the naturally hydrated state of biofilms. The scan area was resolution 1024x1024 pixels. The size of field of view range 74.50, 119.9 to 215 Microns. The resulting collection of confocal optical sections was merged by BioRad (Bio-Rad) Lasersharp software as stacks of images.

2.5.1.2 Image analysis

All images were analysed by Image J software (rsb.info.nih.gov/ij). Three-dimensional images were created from the live (green) and dead (red) colour channels using the 3D project tool of Image J and then combined to create a single RGB (red-green-blue) stack using RGB merge. This allowed the spatial visualization of live and dead bacteria within the biofilm structure. The CLSM was calibrated on 500 speed/step1micron/1024 resolution/1-2.5 zoom /(x-y) level.

Chapter 3
**Development of an *in vitro* biofilm model of health and peri-implant
mucositis**

3.1 Introduction

The oral cavity represents a fluid system in which the microbiota present in saliva may colonize teeth and any artificial surfaces following the deposition of glycoprotein containing pellicle. Bacterial biofilms accumulate in specific ecological niches which provide the optimal ecological conditions for colonisation, such as at periodontal pockets, tonsils, and the crypts and folds of the tongue. Biofilms will form on all surfaces in this fluid system including fixed and removable prostheses, and implants.

Oral implants are hard non-shedding surfaces anchored in the jawbone and penetrating the mucosa. A few minutes after implant installation, single bacterial cells attach to the pellicle layer. Over time, these colonies mature and form a complex microbiota (Mombelli, 1998). Findings from clinical and experimental studies have shown that the formation of a submucosal biofilm plays an essential role in the initiation and spread of inflammation and eventually, leads to the loss of marginal bone (Lindhe et al., 1992, Lang et al., 1993).

Peri-implantitis is a bacterially induced inflammatory reaction that results in the loss of supporting bone around an implant, which may eventually leads to loss of the implant fixture (implant failure) (Lindhe and Meyle, 2008).

The weakness of dental implants comes from the lack of direct attachment between the dental implant and the mucosa which may facilitate migration of bacteria along the implant surface and increase the risk of peri-implantitis and implant failure (Meffert, 1988, Mombelli and Lang, 1998, Esposito et al., 1998, Hardt et al., 2002).

Peri-implant tissues are susceptible to bacterial infections in a similar manner to periodontal infections (Fürst et al., 2007). Although the main source of nutrients for many microbial inhabitants of the oral cavity is from saliva and the diet (Wilson, 1999), there are a number of other nutrient sources, for example, microbes adhering to mucosal surfaces, which may obtain their nutrients directly from the products secreted and excreted by the cells to which they are attached. Furthermore, microbes colonising the gingival crevice are likely to obtain many of their nutrients from gingival crevicular fluid (GCF) rather than from saliva (Loesche, 1968). Since GCF originates from plasma, its chemical composition is thought to mirror that of blood (Ficara et al., 1975). Adonogianaki et al. (1995), found no differences in PISF and GCF in healthy and inflamed sites, and concluded that the inflammatory and immune responses were similar around the tooth and implant. Furthermore, Apse et al. (1989) reported that the volume of GCF did not differ between implant sites and natural teeth, and the features of

Chapter 3: Development of an *in vitro* model of health and peri-implant mucositis

inflammation were similar. The flow rate of GCF at healthy sites is thought to be in the region of 0.3 µl per tooth per hour. It is reported that the flow rate increases during inflammation of the gingival margin by up to 30 fold (Goodson, 2003, Utto, 2003). Flow rates of GCF and PISF have been shown to be similar around teeth and implants, respectively (Adonogianaki et al., 1995).

Well-maintained titanium implants usually harbour low amounts of plaque and little marginal inflammation. Supragingival and subgingival plaque at successful implant sites seems to resemble the microbiota associated with gingival health. However, an increased proportion of putative periodontal pathogens have been documented at implant sites of dentate patients as compared to edentulous individuals, suggesting that the periodontal pocket serves as a reservoir for colonization of titanium implants (Quirynen and Listgarten, 1990, Mombelli and Mericske-Stern, 1990, Becker et al., 1990). Furthermore, peri-implantitis lesions are associated with the presence of subgingival plaque which contains a large diversity of Gram-negative anaerobic rods, fusiform bacteria, motile and curved rods and spirochetes (Mombelli et al., 1987). The lesions are well vascularised and contain a large amount of densely packed inflammatory cells such as neutrophils, macrophages, lymphocytes and plasma cells and frequently the contaminated dental implants are surrounded by 'crater-like' bone defects (Lindhe et al., 1992, Leonhardt et al., 1992).

There are several limitations when analyzing the natural extent of inflammation around dental implants, these may often hinder access for adequate clinical examination. Experiments on the probing depths show that with deep peri-implant bone pockets, the pocket is not always accessible to its full depth. Therefore, probing of peri-implant pockets may fail to reach the very deep areas of the bone pocket. As a result, the species at the base of the pocket cannot be sampled and may remain undetected (Apse et al., 1991). Additionally, implants have a more complex anatomy that impairs adequate probe measurements (Máximo et al., 2009). Practical and ethical issues arise when carrying out clinical studies in patients and the historical dogma that probing around implants should be avoided (Gould et al., 1981). There is therefore a need to develop *in vitro* models to help in the fundamental understanding of the microbiology associated with peri-implantitis. One of the most suitable *in vitro* methods of growing reproducible biofilms for modelling dental plaque is the constant depth film fermenter (CDFF) developed by Peters and Wimpenny (1988). This model originally used a plaque inoculum and reached a steady state after 4 days (Kinniment et al., 1996). The CDFF model has been used to study the structure

Chapter 3: Development of an *in vitro* model of health and peri-implant mucositis

and spatial distribution of viable and non-viable supragingival plaque bacteria (Pratten et al., 2000) and bacterial shifts associated with health and disease (Dalwai et al., 2006). The aim of this part of the study was to develop an *in vitro* model for evaluating the bacterial populations associated with healthy dental implants progressing to peri-implant mucositis assessed by bacterial culture and CLSM.

3.2 Materials & Methods

The constituents for the microbiological culture media used are described in chapter 2. The CDFF was set up was as described in section 2.2.1, Microcosm biofilms were generated as described in section 2.2.2 and the *in vitro* model parameters were as described in section 2.2.3.

3.2.1 Inoculation of the CDFF

A vial of frozen pooled saliva was thawed and 900 μ l used to inoculate 500 ml of artificial saliva, this was mixed and pumped into the CDFF at a rate 1.38 ml/min for 6 h. Serial dilutions of the remaining 100 μ l of pooled saliva were carried out and plated out on selective and non-selective culture media. All plates were incubated under appropriate conditions.

3.2.2 Changes in environmental parameters from a healthy implant and progressing to peri-implant mucositis

Experiment 1: In this study, microcosm biofilms were grown on titanium (Ti) discs, and artificial saliva was used as the sole nutrient source. Biofilms were grown for 348 h (17 days) and sampled throughout the period (8 sampling points). Samples were removed and grown on selective and non-selective culture media (and incubated under appropriate conditions) to assess the number of CFU per ml and structural biofilm analysis was carried out using CLSM.

Experiment 2: The reproducibility of the model was assessed by repeating experiment 1. Biofilms were grown for 360 h (15 days) and sampled throughout this period (7 sampling points).

Experiment 3: To model peri-implant mucositis, the environmental progression from a healthy dental implant to an implant with peri-implant mucositis the environmental conditions in this experiment were altered. Microcosm biofilms were grown for 438 h and sampled throughout this period (15 sampling points). For the first 7 days, the biofilms were grown with artificial saliva at a rate of 0.5 ml/min plus, PISF introduced at a rate of 40 μ l/min. After 222 h, peri-implant sulcular fluid was added at a rate of 130 μ l/min and a microaerophilic gaseous mixture was supplied at a rate 200 ml/min. Samples were taken at set times and bacteria and fungi cultured from these on selective and non-selective culture

Chapter 3: Development of an *in vitro* model of health and peri-implant mucositis

media to assess the number of CFU/ml. Structural analysis of biofilms was performed using CLSM at set time points.

3.2.3 Structural analysis of biofilms using CLSM

Analysis of the biofilm structure was performed by CLSM throughout this part of study. One titanium disc was examined under the CLSM at each time point for experiment 1 and experiment 3. The CLSM was carried out as described in 2.5.1.2.

3.3 Results

3.3.1 Inoculum analysis

The microbial community present in the pooled saliva, used as the inoculum for the CDFF, was analysed using selective and non-selective culture media. The numbers of each of the bacterial groups analysed are shown in Table 3.1. In experiment 1, the anaerobic microorganisms and streptococci dominated with over ca. 10^7 cfu per ml recovered. In experiment 2, the most numerous were again, anaerobic species with slightly fewer aerobic microorganisms (ca. 10^7 cfu/ml). In experiment 3, the most numerous were aerobic microbial species (ca. 10^7 cfu/ml), with fewer anaerobic species (ca. 10^6 cfu/ml).

Table 3.1. Composition of pooled saliva (inoculum) on selective and non-selective culture media for three experiments. Mean and \pm standard deviation of ($n = 2$).

Bacteria species	(CFU/ml) Mean \pm SD Exp.1	(CFU/ml) Mean \pm SD Exp.2	(CFU/ml) Mean \pm SD Exp.3
Anaerobic spp.	$3.5 \times 10^7 \pm 7 \times 10^4$	$5.98 \times 10^7 \pm 1.34 \times 10^5$	$5.75 \times 10^6 \pm 11.3 \times 10^5$
Aerobic spp.	$2.5 \times 10^6 \pm 14.1 \times 10^4$	$2 \times 10^7 \pm 7 \times 10^3$	$1.30 \times 10^7 \pm 1.4 \times 10^4$
Gram-negative anaerobic spp.	$2.5 \times 10^6 \pm 14.1 \times 10^4$	$6 \times 10^6 \pm 0$	$1.25 \times 10^6 \pm 0$
Streptococcus spp.	$2.78 \times 10^7 \pm 7.7 \times 10^4$	$1.38 \times 10^6 \pm 2.8 \times 10^4$	$3.75 \times 10^6 \pm 2.1 \times 10^4$
Actinomyces spp.	$8 \times 10^6 \pm 5.6 \times 10^4$	$6 \times 10^6 \pm 2.8 \times 10^4$	$1.25 \times 10^6 \pm 2.8 \times 10^3$

3.3.2 Culture analysis

Experiment 1: The microcosm biofilms were grown on titanium (Ti) discs and artificial saliva was used as a nutrient source. In this study, microcosm biofilms were grown for 348 h and sampled 8 times, at 6 h, 24 h, 48 h, 72 h, 96 h, 168 h, 192 h, and 348 h. Figure 3.1, shows biofilm growth over time on Ti discs (mean of 2 discs) as assessed by culture on selective and non-selective culture media. The total number of bacteria in the biofilm increased overtime from inoculation at 6 h to around 96 h, with slight exception to this exhibited by *Actinomyces* species and Gram-negative anaerobic species which initially decreased in numbers at early sampling points to ca. 10^3 . CFU counts for all groups analysed increased by approximately 1 \log_{10} at 192 h (ca. 10^9) and reduced again to a level similar (ca. 10^7 – ca. 10^8) to the previous sampling point (168 h).

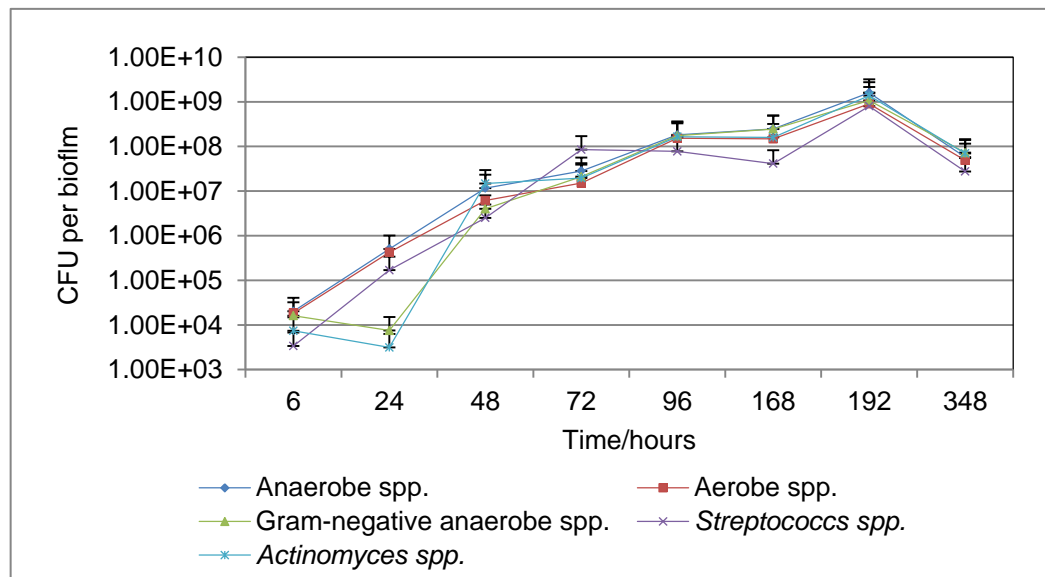


Figure 3.1. Composition of biofilms (viable count data from 5 different media) sampled from the CDFF at different time points (6 h – 348 h). Error bars represent standard deviations ($n = 2$).

Experiment 2: To check the reproducibility of the system, experiment 1 was repeated. Microcosm biofilms were grown for 360 h (15 days) and sampled throughout this period at 6 h, 24 h, 48 h, 72 h, 96 h, 168 h, and 360 h (Figure 3.2). Samples from three (Ti) discs were grown on selective and non-selective culture media. The total number of bacteria in the biofilm increased overtime from the inoculation at 6 h until around 96 h. Following this, the numbers seemed to stabilise from 72 h until the final sampling point at 360 h. The *Actinomyces*

species were present in fewer numbers at most points but recovered to 2.88×10^7 CFU/ml at 360 h.

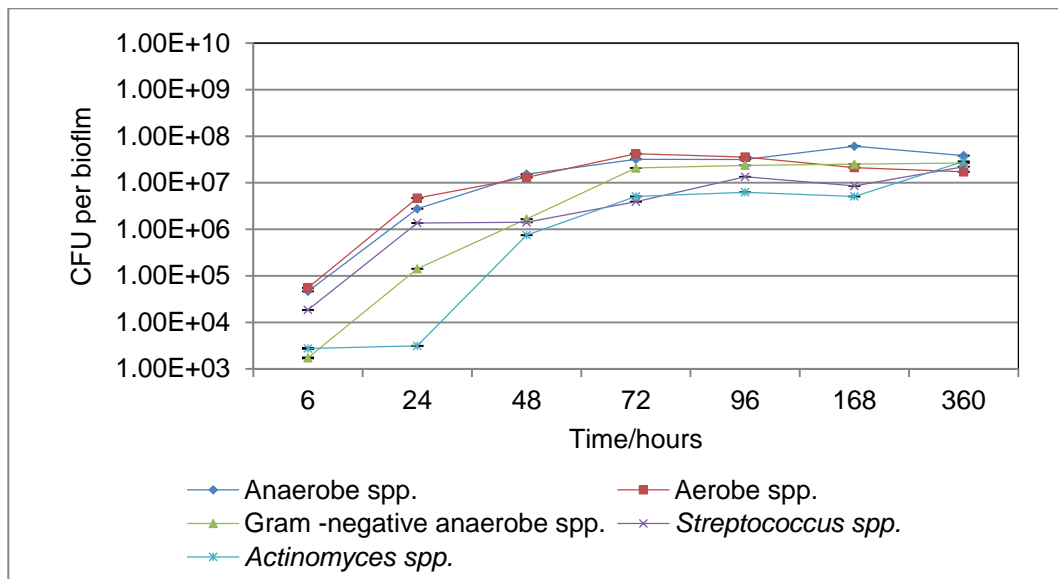


Figure 3.2. Composition of biofilms (viable count data from 5 different media) sampled from the CDFF at different time points (6 h – 360 h). Error bars represent standard deviation ($n = 3$).

Comparing experiments 1 and 2, the total numbers of bacteria in the biofilms increased overtime from inoculation at 6 h to 96 h. There was a difference between both experiments in particular at 96 h (ca 10^8 vs. 10^7 Exp. 1 and Exp. 2, respectively) and overall, numbers were lower in experiment 2.

Experiment 3: Microcosm biofilms were grown for 438 h and sampled at 6 h, 24 h, 48 h, 72 h, 96 h, 192 h, 216 h, 222 h, 246 h, 270 h, 342 h, 366 h, 390 h, 414 h, and 438 h. For the first 7 days, the biofilms were grown with artificial saliva introduced at a rate of 0.5 ml/min plus a peri-implant sulcular fluid (PISF) was added at a rate of 40 μ l/min and after this, peri-implant sulcular fluid was added at a rate of 130 μ l/min and microaerophilic atmosphere gas mixture, at a rate of 200 ml/min, was supplied.

The viable count data generated from the samples is shown in Figure 3.3. Samples from two (Ti) discs were grown on selective and non-selective culture media. The total number of bacteria in the biofilm increased over time from inoculation until 96 h. All groups of bacteria that were cultured seemed to broadly follow this pattern. *Candida* numbers increased at 192 h and reduced in numbers at 270 h, but recovered somewhat at 366 h later time points. Following the change to the peri-implant mucositis conditions, the numbers of anaerobic and

Chapter 3: Development of an *in vitro* model of health and peri-implant mucositis

aerobic bacteria increased. *Streptococcus* species numbers initially reduced in populations at 270 h but recovered again at 366 h.

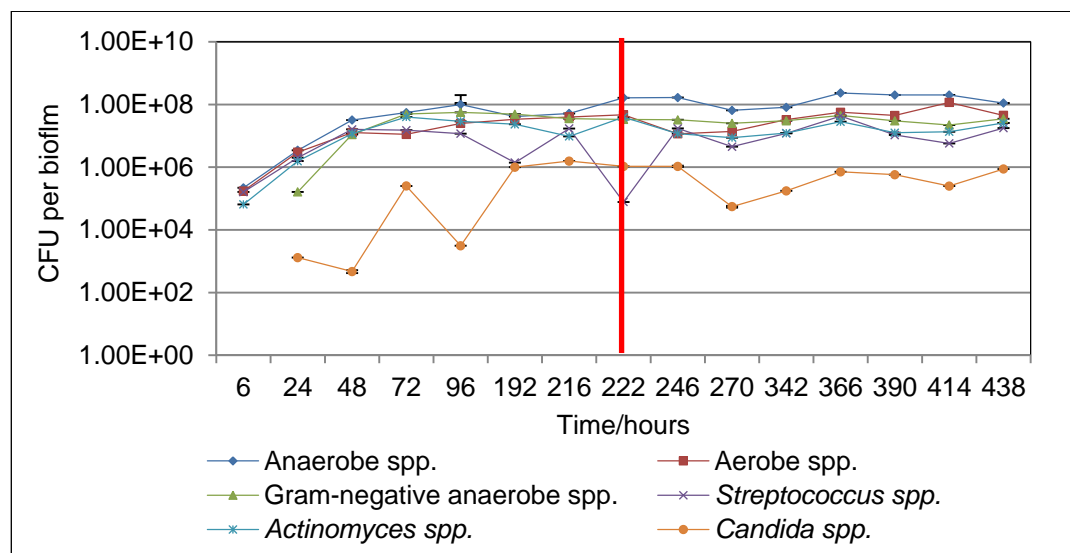


Figure 3.3. Composition of biofilms (viable count data from 5 different media) sampled from the CDFF at different time points (6 h – 438 h). Red vertical line represent time of introduction of microaerophilic gas mixture and increased flow rate of peri-implant sulcular fluid at 222 h. Error bars represent standard deviation ($n = 2$).

3.3.3 Structural analysis of biofilms using CLSM data

Confocal laser scanning microscopy images were obtained throughout this study.

Experiment 1: During modelling of healthy dental implant conditions, different structural features could be observed (Figure 3.4). After 6 h, the early biofilm covered only parts of the Ti surface. It was low in morphotypic diversity; the cells observed all appeared to be coccoid and very few rods were observed. In addition to the high numbers of cocci, the surfaces became completely covered with biofilm over time and by 72 h the biofilm showed opening void like structures.

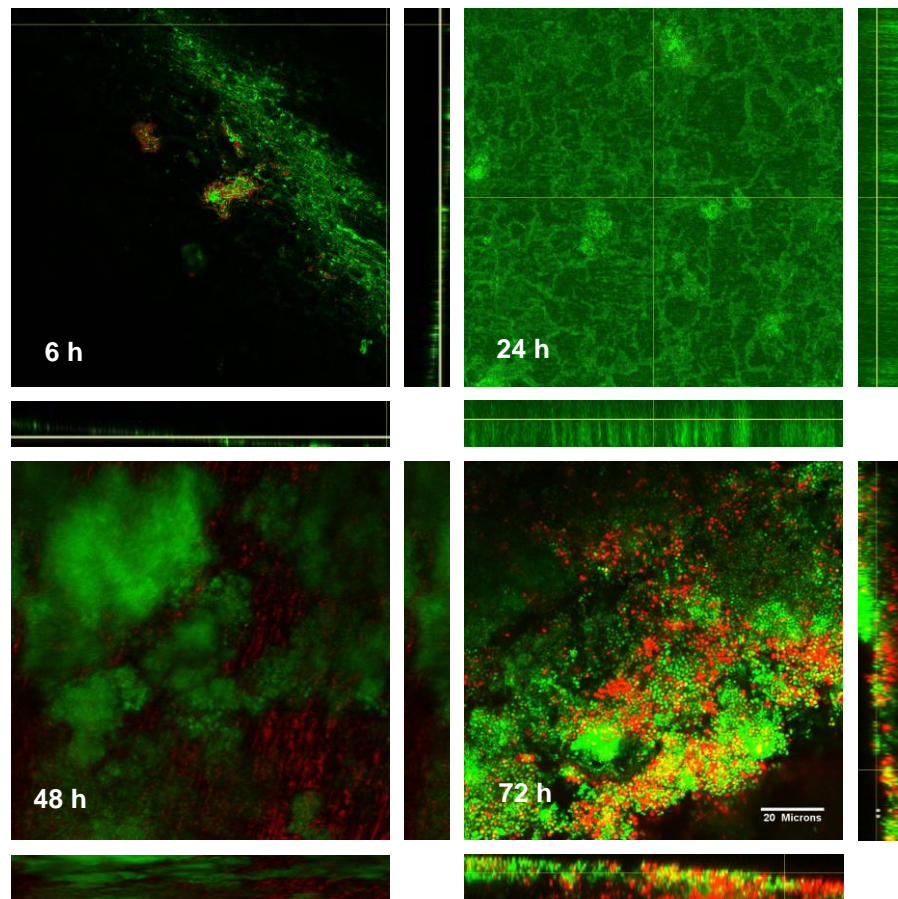


Figure 3.4. Images were taken through the z axis within the biofilm, vertical panels are xy voxels and horizontal panels are xz voxel. CLSM images along the z plane of microcosm biofilms were grown for 348 h. At 6 h, the young biofilm is characterised by the presence of viable and non-viable chains (rods and cocci). Scale bar (20 μ m).

Chapter 3: Development of an *in vitro* model of health and peri-implant mucositis

At 96 h, the titanium surface was covered completely with rods and large numbers of fusiform bacteria, as shown in Figure 3.5. Once the surface was covered, the biofilm appeared to expand to form closely packed microcolonies at 168 h and 192 h. At 348 h, the biofilm formed a dense mat with a large spectrum of cell morphotypes, ranging from coccoid to small rods and filaments with the formation of columnar microcolonies with their long axis perpendicular to the surface.

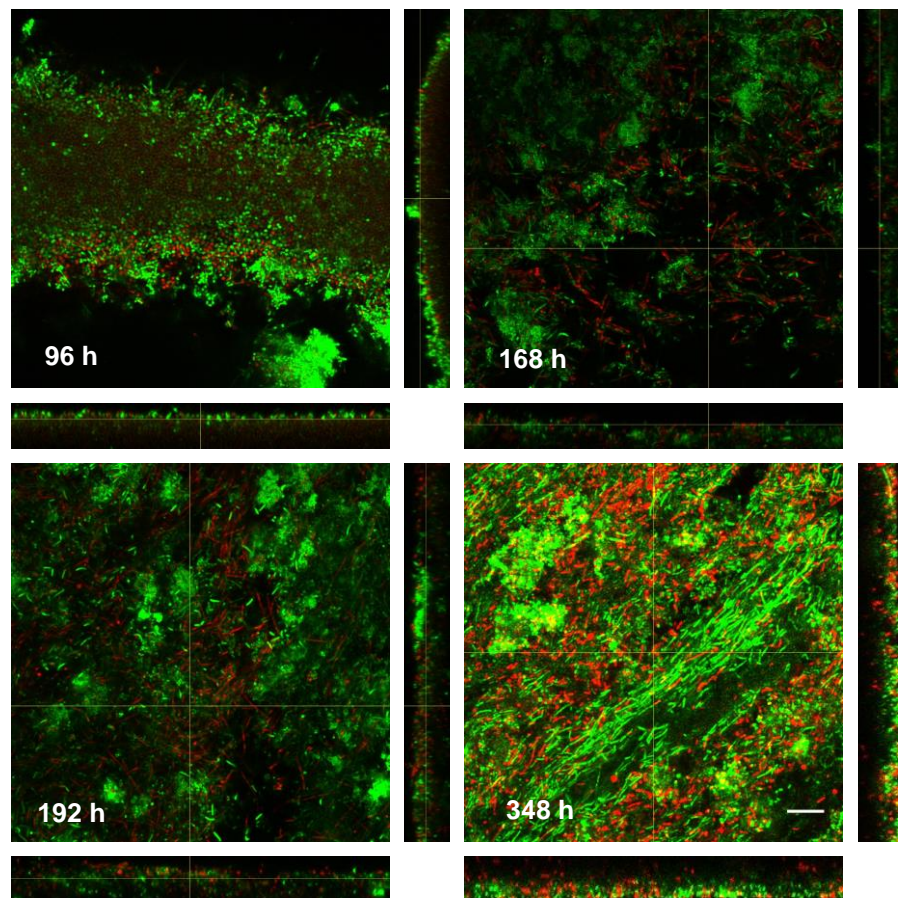


Figure 3.5. Images were taken through the z axis within the biofilm, vertical panels are xy voxels and horizontal panels are xz voxel. CLSM images were characterised by the presence of extensive numbers of filaments or 'fusiform-shaped' bacteria covering the Ti surface. Few rod or coccal shaped bacteria were evident beneath and those present appeared non-viable cells (red channel). Scale bar (20 μ m).

Experiment 3: These biofilms appeared to be denser with voids and fewer numbers of non-viable cells at 96 h (Figure 3.6). At 192 h, the biofilms were observed to be covering a large area of substratum with viable and non-viable coccoid bacteria in particular, at the centre of the image with few filamentous bacteria. After 222 h, with an increased flow of peri-implant sulcular fluid (PISF) associated with a change in the environment from an aerobic to microaerophilic atmosphere, fusiform bacteria began to proliferate and form micro-colonies that were closely packed (at 246 h). At 342 h, non-viable cells were observed with a large spectrum of viable cells (cocci, small rods and filaments).

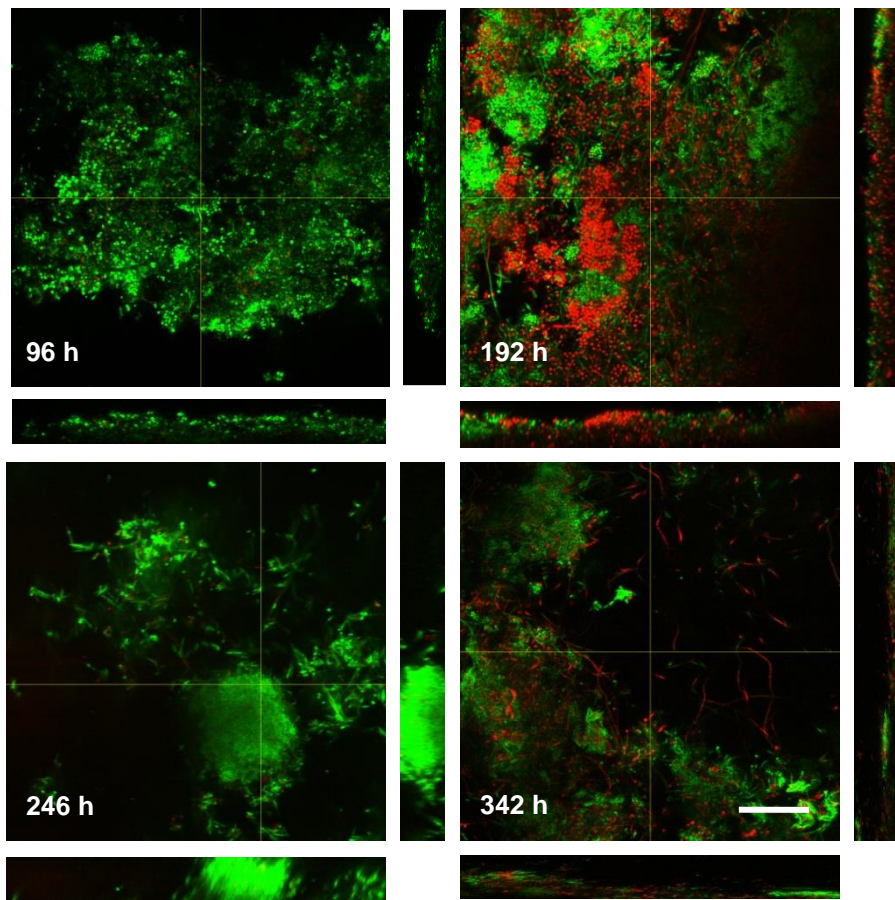


Figure 3.6. Images were taken through the z axis within the biofilm, vertical panels are xy voxels and horizontal panels are xz voxel. CLSM images were characterised by the presence of fusiform shapes which covered the Ti surface, with few rod or coccoid shaped bacteria being evident beneath these cells, and when present were non-viable (red channel) cells. Scale bar (20 μ m).

Chapter 3: Development of an *in vitro* model of health and peri-implant mucositis

At 366 h, viable and non-viable chains of bacteria were observed (Figure 3.7). At 414 h, the presence of different morphotypes (rods, cocci, filaments) with open void structures (non-stained black areas in the biofilm section) was evident. The large areas of non-viable bacteria observed at 414 h were replaced by mostly viable bacterial cells at 438 h.

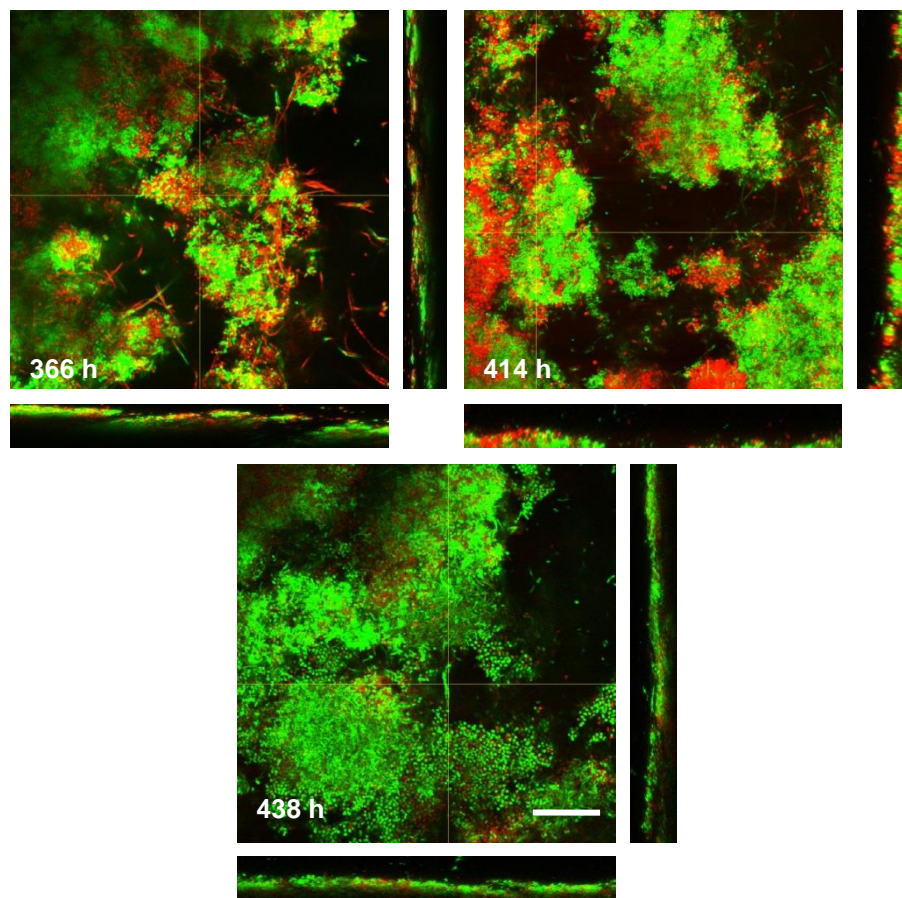


Figure 3.7. Images were taken through the z axis within the biofilm, vertical panels are xy voxels and horizontal panels are xz voxel. CLSM images showing microcosm biofilm grown under microaerophilic environment with increased flow of PISF represented by 366 h, 414 h and 438 h. Scale bar (20 μ m).

3.3.4 Biofilm thickness analysis

The thickness of one biofilm of each experiment 1 and 3 was measured at each sampling point and calculated using Image J software.

Experiment 1: After 6 h the depth of the biofilm was 1 μm , approximately 1 cell thick increasing to ca. 19 μm at 348 h. (Figure 3.8).

Experiment 3: For the first 7 days, the biofilms were growth using artificial saliva and PISF as sources of nutrients. After 6 h the depth of the biofilm was 1 μm . The depth of biofilm at 96 h was ca. 29 μm then reduced to ca. 26 μm at 192 h. After 222 h with an increased PISF flow, the biofilm depth reduced to ca. 20 μm (Figure 3.8). The biofilm in this experiment was a lot deeper than experiment 1 at comparable measurement points for example at 96 h in experiment 1 it was ca. 18 μm while in experiment 3 it was ca. 29 μm .

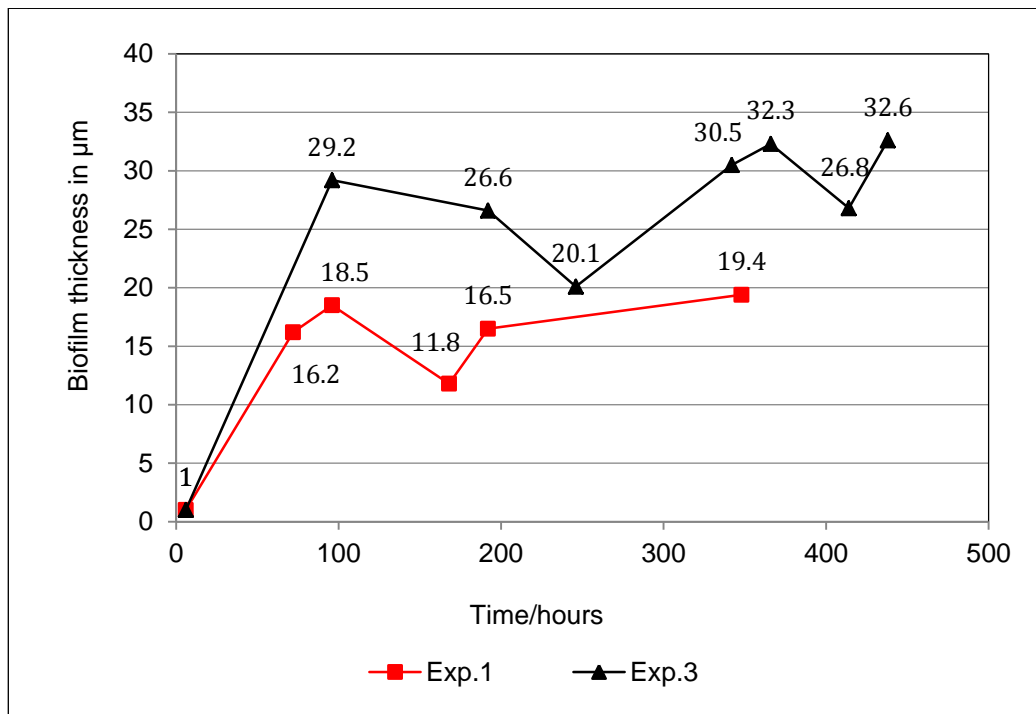


Figure 3.8. The thickness of biofilm at different time points in μm . At 222 h, a change in the environment to a microaerophilic atmosphere was initiated with increased introduction of PISF for experiment 3.

3.4 Discussion

Plaque mediated diseases are a result of a shift in the balance of the resident microbiota due to responses in local environmental changes (Marsh, 2003). The disease process that causes peri-implantitis is similar to the pathological process that occurs around natural teeth during gingivitis and periodontitis (Silverstein et al., 1994, Subramani et al., 2009). The aim of this part of study was to produce biofilms that mimicked those associated with healthy dental implant conditions and peri-implant mucositis conditions. *In vitro* biofilms were grown using a CDFF on titanium disc surfaces. A natural biofilm can often be complex and non-reproducible (Kinniment et al., 1996) thus, the aim was to grow microcosm biofilms in various environments and make an effort to maintain good reproducibility. The parameters used in this study were based on those of (Dalwai et al., 2006). The CDFF is particularly suited to studies of biofilms of oral bacteria because it provides an environment similar to the oral cavity. A CDFF was used for the study of peri-implantitis for several reasons; it provides a reproducible manner of formation of biofilms overtime. It is a widely used and an accepted tool for simulating *in vivo* situation; it provides an environment similar to that found in the oral cavity. It is a sophisticated apparatus that can generate large numbers of biofilms. It has been used previously for the study of bacterial perturbation (Wilson, 1999), to successfully model supragingival dental plaque (Wilson et al., 1995) and modelling population shifts associated with health or disease (Dalwai et al., 2006). Furthermore, the removal of surfaces of the biofilms by the scraper blades mimics the continuous removal of the outermost layers of the dental plaque owing the shear forces present in the oral cavity (Lamfon et al., 2003). Furthermore, the used of saliva in all experiments had several advantages; it generated a biofilm that consisted of many complex and original organisms. Use of saliva also leads to the possibility in other studies to examine plaque behaviour, ecology, and pathology and for the testing of potential clinical interventions (Sissons et al., 1991).

The nutrients which are available at the site of an implant in both health and disease are complex and dynamic. For modelling healthy dental implants, the main source of nutrients of biofilms growing above the gingival margin is saliva, in contrast, for biofilms growing subgingivally, the main source of nutrients is gingival crevicular fluid (GCF) (Wilson, 1999). Artificial saliva based on the formulation of Russell and Coulter (1975) was used throughout the experiments. A key feature of this formulation is the inclusion of hog gastric mucin (HGM), which functions not only as a major source of nutrients for oral bacterial

Chapter 3: Development of an *in vitro* model of health and peri-implant mucositis

communities (Bradshaw et al., 1989), but also covers the surfaces of the substratum to form a conditioning film.

For modelling peri-implant mucositis a changing nutrient regime was needed. The flow rates of peri-implant sulcular fluid used in the experiments were determined based on data from a number of papers. The gingival crevicular fluid flow rate, the amount of GCF produced *in vivo* per day is only a few millilitres, which would be impracticable to reproduce *in vitro* (Wilson, 1999). For example, gingivitis subjects have GCF flow rates of 0.087 $\mu\text{l}/\text{min}$, whereas moderate periodontal pockets have a flow rate of 0.4 $\mu\text{l}/\text{min}$ (Goodson, 2003, Uitto, 2003). Many factors are known to influence the flow rate of gingival crevicular fluid, and many studies have shown a correlation between the severity of gingival inflammation and gingival crevicular fluid flow rates. Furthermore, the results of these studies imply that alveolar bone resorption, in addition to gingival inflammation may be factors that influence GCF flow rates (Cimasoni, 1983). It has been shown that the amount of crevicular fluid around osseointegrated dental implants is similar to that around teeth in the same individual (Apse et al., 1989). The results of this imply, that to grow the biofilm on these titanium discs it was necessary to supplement the medium with GCF in addition to artificial saliva. The artificial medium, mimicking sulcus fluid, used in this study consisted of both Roswell Park Memorial Institute medium (RPMI) and horse serum. RPMI is used to culture eukaryotic cells in tissue culture. Horse serum has been previously demonstrated to be suitable for the growth and maintenance of a pathogenic subgingival microbiota (Curtis et al., 1988). Haemin and menadione were added to the nutrient medium to simulate the effect of bleeding which is known to occur with inflammatory periodontal diseases (Loesche et al., 1983) and peri-implantitis (Berglundh et al., 2011). These two complex nutrients were added together to the CDFF: artificial saliva and crevicular fluid via one port. The combination of these constituents with their differing, but crucial nutrient properties was thought to produce a good representation of the nutrient milieu found around unsuccessful dental implants. The data from these studies was used to calculate the flow rate in healthy dental implants of 40 $\mu\text{l}/\text{min}$ and in peri-implant mucositis one of 130 $\mu\text{l}/\text{min}$. These rates were used in this study.

Despite the access of air to the oral cavity, there are few strict aerobic microorganisms within the plaque community (Wilson, 1999), as atmospheric air (O_2) does not penetrate far into the biofilm due to diffusion issues and facultative taxa utilising it preferentially. The current model system was therefore maintained with appropriately low oxygen levels (2%). The majority of oral

bacteria are anaerobic or species whose growth is optimum under CO₂-enriched conditions, such as streptococci (Loesche et al., 1983) or capnophilic microorganisms requiring CO₂. As a result, a 5% gas mix of CO₂ in nitrogen has been frequently used in the past (Bradshaw et al., 1997). Microaerophilic gas composed of 2% O₂, 3% CO₂ and 95% nitrogen was therefore introduced into the CDFF in experiment 3.

The microbial community present in the pooled saliva used as the inoculum for the CDFF was analysed. Very low variation was observed in bacterial numbers between the three pooled saliva samples which were profiled. The first CDFF experiment modelled a healthy dental implant microcosm. The culturable microbiota was shown to increase in number to a limit at 96 h then plateaued at 162 h. This growth was probably limited by environmental pressures such as nutrient limitation or toxic metabolites. Indeed, the total aerobic and anaerobic viable count was very similar. In experiment 2 here there were broad similarities in how the biofilms developed during both experiments as revealed by viable counts. The experiment showed an unexpected 'spike' in bacterial numbers at approximately 192 h which then reduced. There was a difference between both experiments in particular at 96 h (ca. 10⁸ vs. ca. 10⁷ Exp. 1 and Exp. 2, respectively). Following this, the numbers seemed to stabilise are shown in Figure 3.1 and Figure 3.2.

For experiment 3, a healthy implant progressing to peri-implant mucositis was modelled by increasing PISF (40 µl/min increased to 130 µl/min) and changing to microaerophilic conditions (2% O₂, 3% CO₂, 95 % nitrogen). The viable count data progressed as expected and early time points were similar to experiment one and experiment two. Following the change to the peri-implant mucositis the number of anaerobes increased in populations and the number of aerobes and streptococci reduced at later time points. The anaerobic bacteria were the dominant component throughout. This was perhaps expected as the biofilm gradually developed so the metabolism of pioneer species created conditions suitable for the colonization by bacteria with more demanding atmospheric requirements. Oxygen is consumed by the aerobic and facultatively anaerobic species and replaced with carbon dioxide and other gases generated as end products of microbial metabolism. The lowering of oxygen tension favours the growth of obligate anaerobes species. Additional nutrient sources also become available due to metabolism of the pioneer species and the complex molecules in the PISF. These would be expected to alter the composition of microbiota and alter the total viable count.

Chapter 3: Development of an *in vitro* model of health and peri-implant mucositis

Confocal laser scanning microscopy is a useful method allowing the structure of dental plaque to be analysed without disruption. The biofilms obtained were not homogenous in structure, but presented a highly heterogeneous architecture in terms of distribution of cells and fluid filled space. Biofilms on other surfaces such as enamel have previously produced the same structure (Nyvad et al., 1989). The biofilm obtained from experiment 1 appeared to contain large areas of voids and few bacteria at 6 h. The numbers of viable cells increased at 48 h with greater distribution of cells. Following 72 h, the dense biofilm completely covered the substratum. Later, the biofilm contained a mat of fusiform-like bacteria and few cocci at 168 h. At 348 h, the biofilm completely covered with highly organised, dense morphotypes (cocci, rods, filaments) bacteria. The results of this study are in accordance with Scarano et al. (2004) who reported high numbers of bacteria adhered to titanium surface after 24 h of exposure *in vivo*. In experiment 3, the biofilm contained a dense structure of viable bacteria by 96 h. At 192 h the biofilm contain mixture of viable bacteria and non-viable bacteria. After a shift in the environmental conditions to favour peri-implant mucositis, the fusiform like organisms were observed at 246 h, and were denser at 438 h. These findings were in agreement with the previous study of Nyvad and Fejerskov (1989) who reported that if plaque was allowed to accumulate undisturbed then a shift of bacteria occurred after 7 days from coccoid to anaerobic rods and filaments by 14 days. Also the structure of the biofilms seemed to follow the progression reported in a previous study (Pratten et al., 2000) in which low nutrition biofilms had an open structure, but biofilms culture under high nutrient conditions, such as those with saliva or GCF, would be expected to have greater density in terms of their structure. The variation in biofilm thickness values is depicted in Figure 3.8. The biofilm thickness was between ca. 16 μm at 72 h and ca. 19 μm at 96 h. After 72 h, the thickness of the biofilm thickness was not seen to vary significantly. Under conditions emulating peri-implant mucositis (experiment 3) the biofilm depth increased to ca. 30 μm in a mature biofilm (96 h - 438 h). This was probably due to the introduction of additional nutrients PISF (40 $\mu\text{l}/\text{min}$ increased to 130 $\mu\text{l}/\text{min}$) which may have provided the community with more carbon, nitrogen etc, thus facilitating a more dense, deeper biofilm. It has been suggested that the biofilm structure and composition are linked to substrate nutrients or nutrient concentration. A high nutrient environment like artificial saliva and artificial crevicular fluid might be expected to produce a biofilm of high density rather than one more open structure. In addition, biofilms of more than 4 old days may produce a different

structure than early biofilms. The results of this study were in accordance with Al-Ahmad et al. (2010), where biofilm thickness were shown to be between 19.78 μm and 36.73 μm after 3 days and between 26.11 μm and 32.43 μm after 5 days *in vivo*.

3.5 Conclusion

The results of this part of the study have shown that the culture data did not reveal changes in the bacterial community given that the CLSM data suggested large differences in the structure, morphotypes present and thickness of the biofilms. To understand this further, it was decided to analyse the biofilms by independent cultural techniques.

Chapter 4
**Development of an *in vitro* microcosm model to simulate a healthy dental
implant, peri-implant mucositis and peri-implantitis**

4.1 Introduction

The Sixth European Workshop in Periodontics held in 2008, defined peri-implant diseases as follows: peri-implant mucositis is the presence of inflammation of the peri-implant mucosa without signs of loss of bone support, while peri-implantitis, in addition to inflammation of the mucosa, is characterized by a loss of bone support (Lindhe et al., 2008). Peri-implantitis is mediated by the microbiota within the plaque biofilm on the dental implant surface (Mombelli et al., 2011).

Microbiological studies in healthy peri-implant tissues have demonstrated the presence of large proportions *S. mitis*, *S. sanguinis* and *S. oralis* with a low proportion of anaerobic species, a small number of Gram-negative species, and a low detection of periodontopathogenic bacteria (Heuer et al., 2007). However, there is also contrary literature showing low numbers of anaerobic Gram-negative bacilli in some healthy implants sites (Shibli et al., 2008, Zitzmann and Berglundh, 2008, Quirynen et al., 2002).

Peri-implant infections consist of a microbiota very similar to that found in periodontal disease, and species such as *P. nigrescens*, *C. rectus* and *A. actinomycetemcomitans* are common (Shibli et al., 2008). An imbalance between the bacterial challenge and host response (Esposito et al., 1998, Berglundh et al., 2002) results in changes in the soft and hard tissues. These changes in the composition of the local microbiota are characterized by an increase in pocket depth and bone loss (Quirynen et al., 2002). These changes include:

- an increased total bacterial load (Shibli et al., 2008),
- an increase in the proportion of *A. actinomycetemcomitans*, *Fusobacterium* species, *P. intermedia* and *P. gingivalis*,
- a decrease in the proportion of all cocci,
- an increase in the proportion of motile organisms and spirochetes (Quirynen et al., 2002).

The oral cavity provides a habitat in which the resident microbiota is able to form a wide variety of biofilms. After the placement of titanium implants, the rapid colonization of bacteria has been observed at the peri-implant sulcus (van Winkelhoff et al., 2000). Although there is a large diversity of species associated with peri-implantitis (Kumar et al., 2012), not all species can be detected using traditional culture techniques. It has been estimated that less than 2% of all bacteria can be cultured using artificial media (Pratten et al., 2003) and unculturable taxa probably exist in all multispecies communities. To overcome the potential shortfall of traditional culture used in the previous chapter, a

molecular biology technique was used here. From the literature review it was seen that there are studies that have used 16S rRNA cloning and sequencing to identify the bacterial diversity of peri-implantitis biofilms. For example, Koyanagi et al. (2010, 2013) analysed samples from the deepest lesion of peri-implantitis by 16S rRNA gene cloning and sequencing and found that *Eubacterium* spp., *Fusobacterium* spp. and *Streptococcus* spp. had the major predominance at peri-implantitis. Moreover, in this study a wide variety of unculturable and unrecognized bacteria were found around diseased implants. These authors (2010) also concluded that the biofilm in peri-implantitis had a more complex microbiota than that in periodontitis. Hence, there is a possibility, that unexpected bacteria not related to periodontitis could be involved in inflammation around peri-implant tissues.

In this part of study, the aim was to:

1. Develop an *in vitro* model using microcosm biofilm associated with healthy dental implant which can be progressed to mimic peri-implant mucositis and peri-implantitis.
2. Characterise the changes in three communities developed in this model using selective and non-selective culture techniques.
3. Characterise biofilm structure, thickness and spatial distribution of viable and non-viable cells using confocal laser scanning microscopy (CLSM).
4. Characterise the richness of the three communities using 16S rRNA gene cloning and comparative sequencing.

4.2 Materials & Methods

4.2.1 Culture media

The constituents for each medium used are described in chapter 2. Growth media is described in section 2.1, constant depth film fermentor set up is described in section 2.2.1, microcosm biofilms were generated as described in section 2.2.2 and the *in vitro* model parameters are described in section 2.2.3.

4.2.2 Inoculation of the CDFF

Whole human saliva was used as an inoculum; this was mixed and pumped into the CDFF. The nutrient source used was artificial saliva and artificial tissue fluid (PISF). The compositions of artificial saliva used is described in chapter 2, section 2.2.3.

4.2.3 Production of the biofilm

Titanium discs were placed into a constant depth film fermentor which was operated at 37°C. After the inoculum was disconnected, the CDFF (Exp. 4 and Exp. 5) was fed from a reservoir of sterile artificial saliva using a peristaltic pump at a flow rate 0.5 ml/min.

- Peri-implant sulcular fluid was pumped into the CDFF at a flow rate 40 µl/min to simulate healthy conditions.
- Peri-implant sulcular fluid was pumped into the CDFF at a flow rate 130 µl/min as well as a microaerophilic gas mixture to simulate peri-implant mucositis.
- Peri-implant sulcular fluid was pumped into the CDFF at a flow rate 130 µl/min as well as an anaerobic gas mixture to simulate peri-implantitis conditions.

The sampling pans were aseptically removed from the CDFF at different time points:

- Under healthy conditions at 6 h, 48 h, 96 h and 216h.
- Under peri-implant mucositis at 222 h, 246 h, 366 h, 390 h, 438 h and 510 h.
- Under peri-implantitis conditions at 516 h, 540 h, 588 h, 612 h and 714 h.

4.2.4 Culture methods

In order to maintain the populations present in pooled saliva. Serial dilutions of 100 µl pooled saliva were plated out on mitis salivarius agar (Difco), blood agar (LABM), fastidious anaerobic agar (Oxoid), cadmium fluoride-acreflavin-tellurite agar, mannitol salt agar plates (Oxoid), sabouraud's dextrose agar plates and, Gram-negative anaerobic agar (Oxoid) for both experiments. A *Veillonella* spp. agar plate was used for experiment 5 only. Serial dilutions were carried out on each type of culture medium and 20 µl (in duplicate) was spread on each plate. Plates were incubated in an anaerobic atmosphere (5% carbon dioxide, 5% hydrogen and 90% nitrogen) at 37°C for 4-5 days, except mitis salivarius agar plates, mannitol salt agar plates, sabouraud's dextrose agar plates and blood agar plates where were incubated aerobically (plus 5% carbon dioxide) at 37°C for 48 hours.

4.2.5 Confocal laser scanning microscopy, viability mapping and image analysis

CLSM was carried throughout this study period on biofilms grown on Ti discs. The CLSM images were acquired with a water immersion objective lens (x 40) and image were obtained with a zoom factor of 1 to 2.5, and a field resolution of 1024 x 1024 µm. CLSM image were obtained from a total 3 – 7 randomly selected sites per disc. To measure the distribution of viable and non-viable bacteria within the depth of the biofilm, fluorescence intensity profiles were also obtained using image J analysis software and orthogonal views. To create an orthogonal view, image stacks, comprising of both red and green channels were merged together then re-combined as a single RGB. To measure the thickness of biofilms, the “free hand” tool on Image J toolbar was used to manually draw on xz – voxel and yz - voxel sections mean measurement.

4.2.6 16S rRNA gene cloning and sequencing

DNA was isolated and purified at six time points: 6 h, 96 h, 246 h, 438 h, 540 h and 714h. One disc from each time point was used for DNA extraction. The pellet was resuspended in 50 µl phosphate buffer and subsequent DNA extraction was performed as described in section 2.3.1. PCR amplification, produced isolation, purification, cloning and sequencing was then carried out. All sequencing was performed at (The Wolfson Institute for Biomedical Research, UCL. The 16S rRNA PCR products were partially sequenced using primer 357F (59-CTCCTACGGGAGGCAGCAG-39; Lane, 1991) and the sequences checked using the Chromas LITE program, submitted to the Ribosomal Database Project

Chapter 4: Development of an *in vitro* microcosm model

RDP (<http://rdp.cme.msu.edu/index.jsp>) and identified using blast. Further analysis was performed in order to find the closest match with the 16S rRNA gene. More than 98% sequence identity in the 16S rRNA gene sequence database was the criterion used to identify bacteria at to the species level.

4.3 Results

4.3.1 Culture analysis

The composition of the salivary inoculum was assessed using selective and non-selective culture media for specific species detection and for total bacteria enumeration in experiment one and experiment two. The culture data of pooled saliva was populated by a range of species as shown in table 4.1.

Experiment 4: the salivary inoculum had high numbers of Gram-negative anaerobes (ca. 10^6 CFU/ml), anaerobes (ca. 10^5 CFU/ml), aerobes (ca. 10^5 CFU/ml) and streptococci (ca. 10^5 CFU/ml).

Experiment 5: this study was a repeat experiment; the inoculum had high numbers of aerobes (ca. 10^7 CFU/ml), anaerobes (ca. 10^7 CFU/ml), streptococci (ca. 10^6 CFU/ml), Gram-negative anaerobes (ca. 10^6 CFU/ml) and *Actinomyces* spp. (ca. 10^6 CFU/ml).

Table 4.1. Composition of pooled saliva (inoculum) on selective and non-selective culture media. Error bars represent standard deviation ($n = 2$).

Bacteria species	Mean \pm SD Exp. 4	Mean \pm SD Exp. 5
Anaerobe spp.	$2.4 \times 10^5 \pm 0$	$1 \times 10^7 \pm 2.33 \times 10^5$
Aerobe spp.	$2 \times 10^5 \pm 5.6 \times 10^2$	$1.08 \times 10^7 \pm 1.06 \times 10^5$
Gram-negative anaerobe spp.	$2.4 \times 10^6 \pm 3.11 \times 10^4$	$1.78 \times 10^6 \pm 5.16 \times 10^4$
Streptococcus spp.	$1.70 \times 10^5 \pm 1.13 \times 10^3$	$2.85 \times 10^6 \pm 2.40 \times 10^4$
Actinomyces spp.	$2.51 \times 10^4 \pm 0$	$1.65 \times 10^6 \pm 1.98 \times 10^4$
Candida spp.	$2.5 \times 10^4 \pm 1.27 \times 10^3$	$6.75 \times 10^5 \pm 7.78 \times 10^3$
Staphylococcus spp.	$1.4 \times 10^4 \pm 1.41 \times 10^2$	$5.07 \times 10^2 \pm 3.54 \times 10^1$
Veillonella spp.	-	$7 \times 10^5 \pm 1.2 \times 10^4$

4.3.1.1 Aerobe and anaerobe viable counts

For both experiments 4 and 5, microcosm biofilms were grown for 714 h and sampled 15 times throughout this period. The viable counts obtained for both aerobes and anaerobes (Figure 4.1) showed a rapid increase from ca. 10^5 CFU/ml to ca. 10^7 CFU/ml at 48 h and fluctuated around this number for the duration of the experiment.

4.3.1.2 Selective media

For both experiments 4 and 5, similar patterns of growth were observed for the microorganisms assessed. Briefly, the total viable counts increased from the time of inoculation until 72 h. this was evident for each bacterial group (Figures 4, 2 and 4.3). Following the change to peri-implantitis a reduction in all bacterial numbers occurred, followed by a gradual increase in the levels of Gram-negative anaerobic bacteria (Figure 4.2).

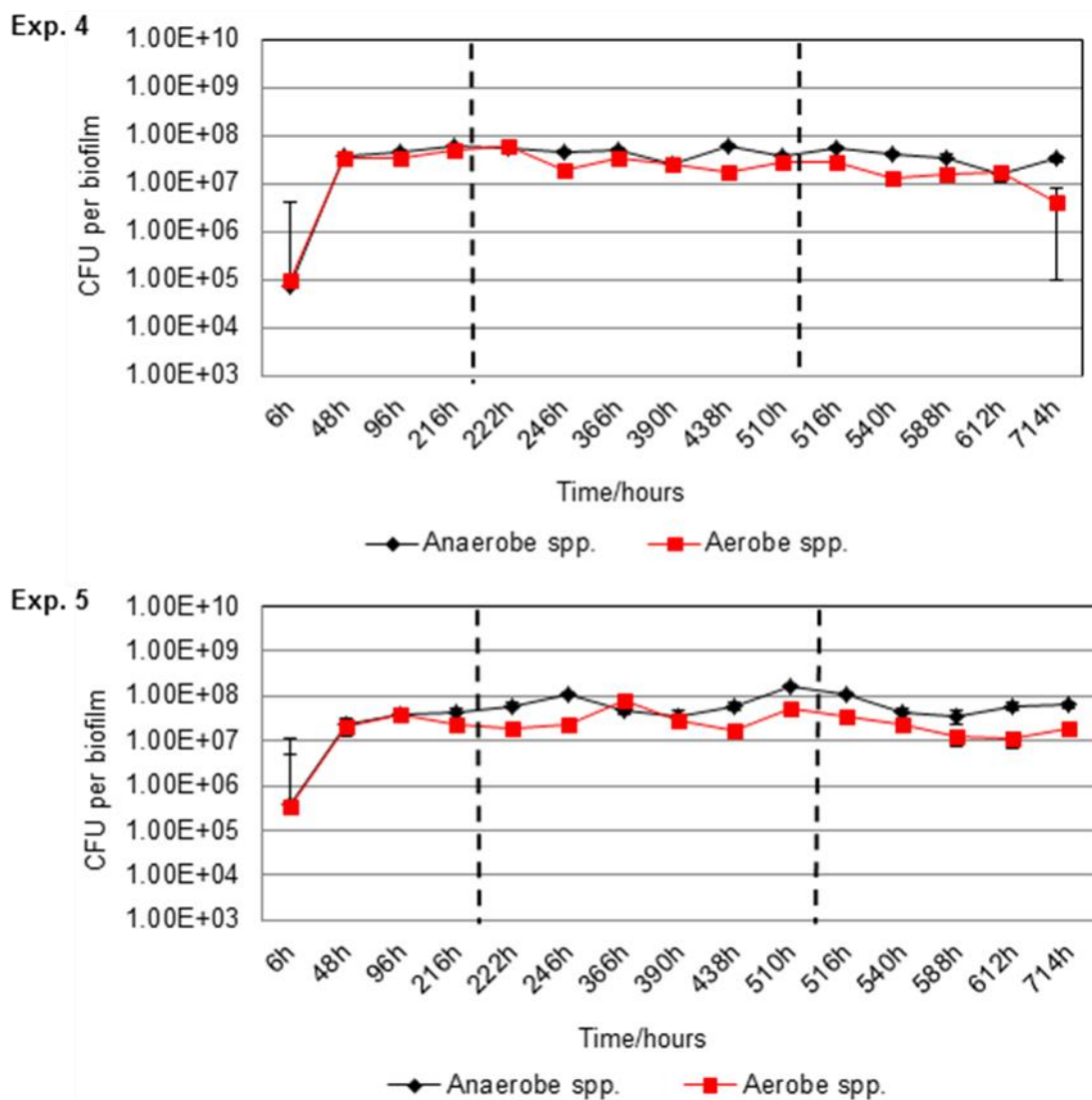


Figure 4.1. Viable counts of aerobic and anaerobic spp. of microcosm biofilm under health, peri-implant mucositis and peri-implantitis conditions. First black dash line represents the switch over to microaerophilic gas mixture and increased flow of PISF, second black dash line represents switch over to an anaerobic gas mixture and PISF only. Error bars represent standard deviation ($n = 4$). Graphs show data from experiments 4 and 5.

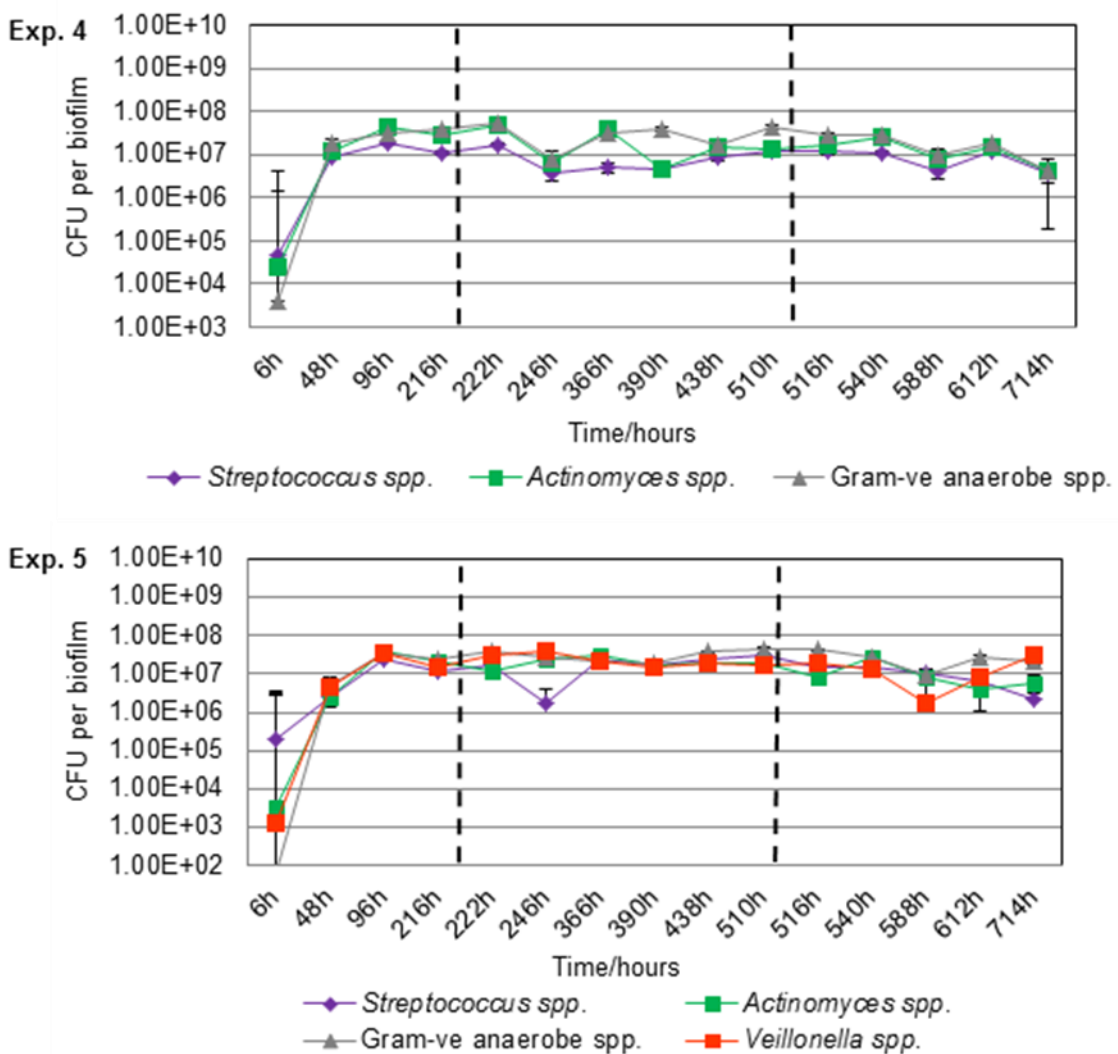


Figure 4.2. Viable counts of *Streptococcus* spp., *Actinomyces* spp., Gram negative anaerobe spp. and *Veillonella* spp. of microcosm biofilm under health, peri-implant mucositis and peri-implantitis conditions. First black vertical dash line represents the switch over to microaerophilic gas mixture and increased flow of PISF, second black dash line represents switch over anaerobic gas mixture and PISF only. Error bars represent standard deviation ($n = 4$). Graphs represent combined data from experiments 4 and 5.

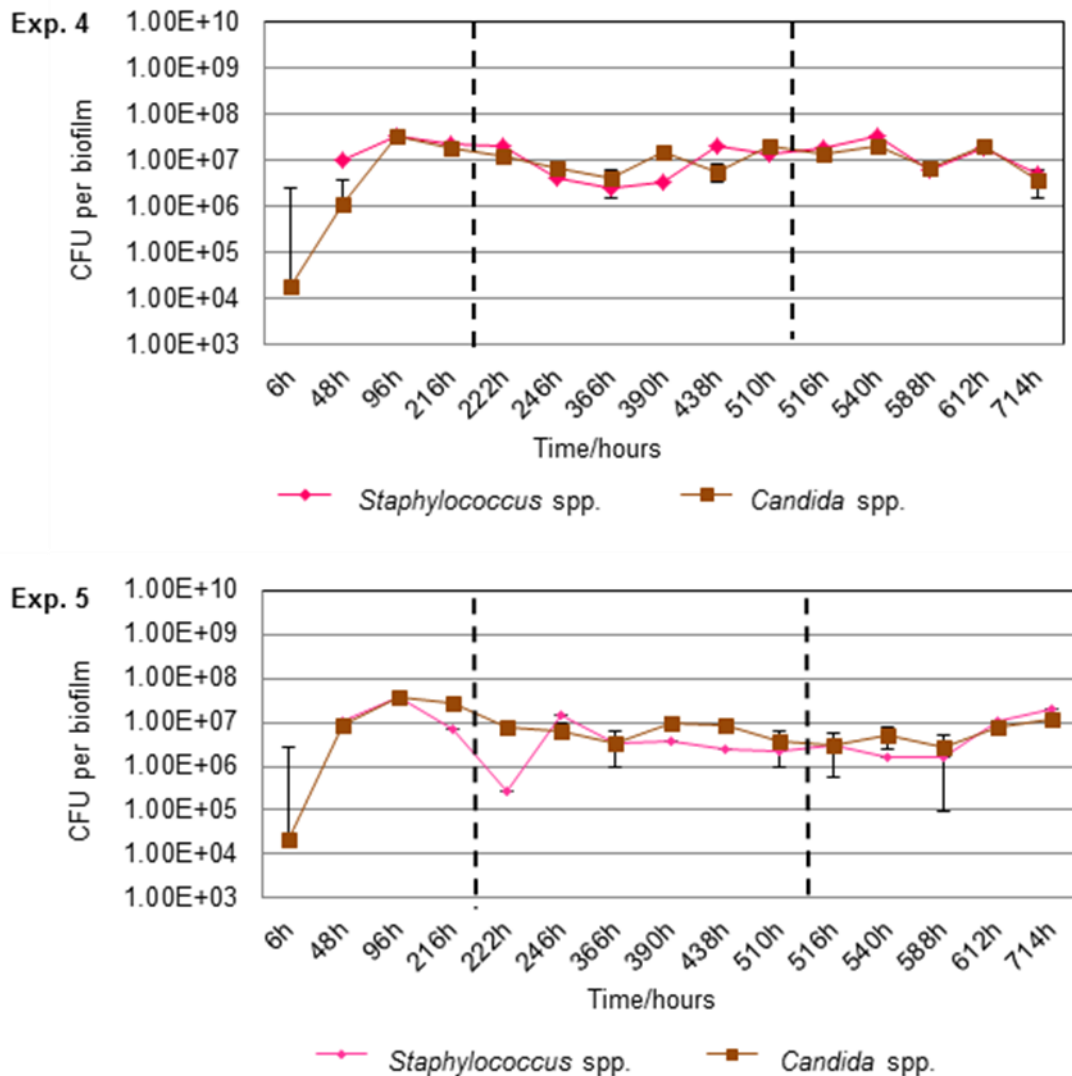


Figure 4.3. Viable counts of *Candida* spp. and *Staphylococcus* spp. from microcosm biofilms under health, peri-implant mucositis and peri-implantitis conditions. First vertical black dash line represents the switch over to microaerophilic gas mixture and increased flow of PISF, second black dash line represents switch over anaerobic gas mixture and PISF only. Error bars represent standard deviation ($n = 4$). Graphs represent combined data from experiments 4 and 5.

4.3.2 Structural analysis of biofilm using CLSM

4.3.2.1 CLSM and image analysis of experiment CDFF 4 and 5

CLSM imaging was carried throughout the two experiments. Representative images from health, peri-implant mucositis and peri-implantitis are shown in figures 4.4 to 4.12.

Under health conditions: for the first 96 h, the “early” biofilm consisted of both viable and non-viable cells with an open structure (Figure 4.4).

Under peri-implant mucositis conditions: at 246 h, the biofilm appeared to be denser but still showed an open structure (Figure 4.5). At 366 h, there was a reduction in the number of viable cells. Numerous cell morphotypes were also present (rods, cocci, filaments) (Figure 4.6). At 390 h in experiment 5 the biofilm was characterised by a high density of viable and non-viable cells and numerous different cell morphotypes (Figure 4.7). At 438 h, images showed a mature biofilm characterised by predominately filamentous organisms and rods in chains, some of these organisms were surrounded by cocci (Figure 4.8) with an abundance of viable rods and non-viable filaments in both experiments.

Under peri-implantitis conditions: the biofilm structure showed almost complete titanium surface coverage with areas of multilayers of microorganisms at 540 h (Figure 4.9). At 588 h, the biofilm showed an abundance of viable rods and non-viable filaments (Figure 4.10). At 612 h the biofilm showed an abundance of both viable and non-viable rods and filaments (4.11). At 714 h, the biofilm showed numerous morphotypes of cells (cocci, rods, filaments and fusiform bacteria) (Figure 4.12). When biofilms were examined in the z-plane (x–y), parallel sections showed circular areas of densely packed bacteria, representing “chimneys” of multilayered complex microcolonies. However, the central part of these protruding microcolonies varied with regard to their composition. These included cocci (Figure 4.4) or rod-shaped (Figure 4.7), fusiform (Figure 4.11) and filamentous bacteria (Figure 4.12).

4.3.2.1.1 Health conditions

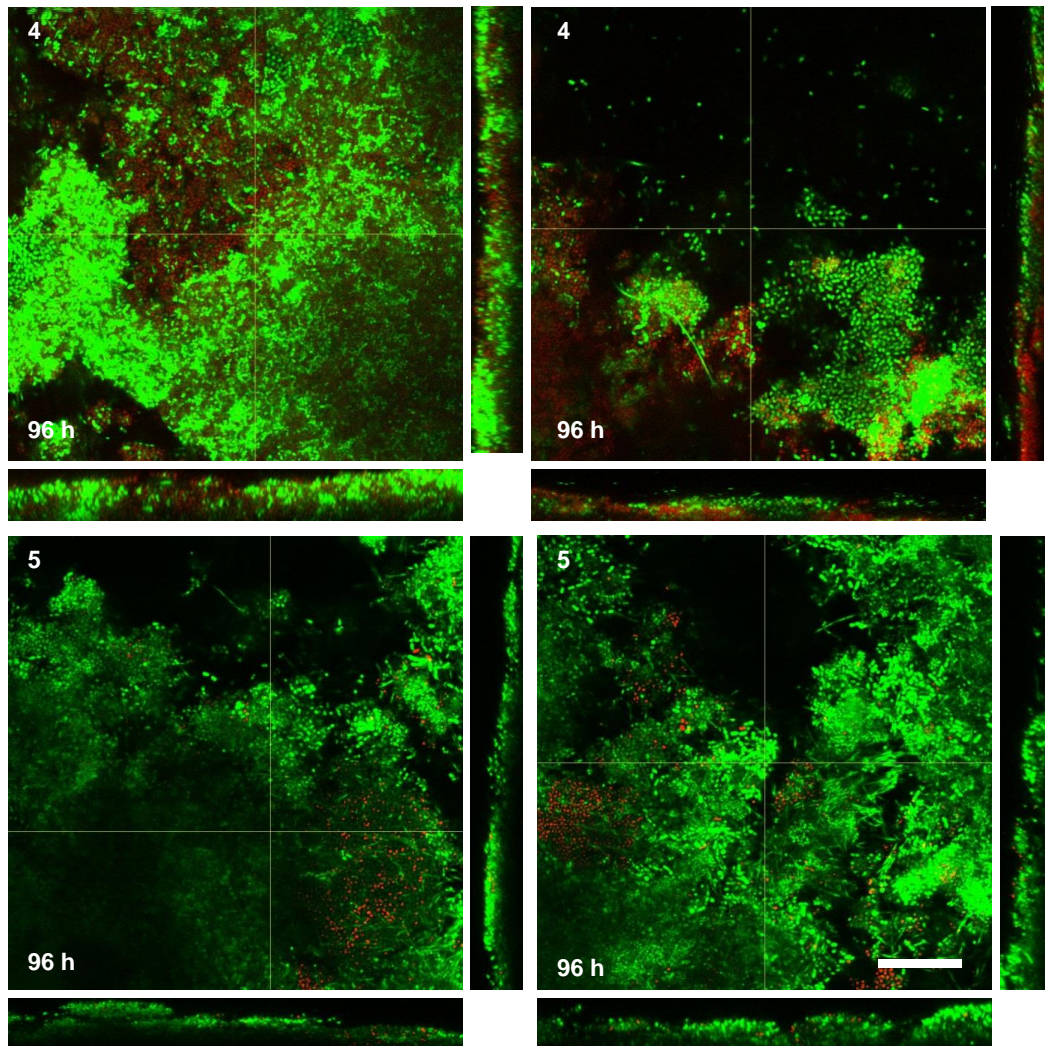


Figure 4.4. Representative CLSM images of healthy dental implant biofilms sampled at 96 h with x, y and z planes presented. Scale bar (20 μ m).

4.3.2.1.2 Peri-implant mucositis conditions

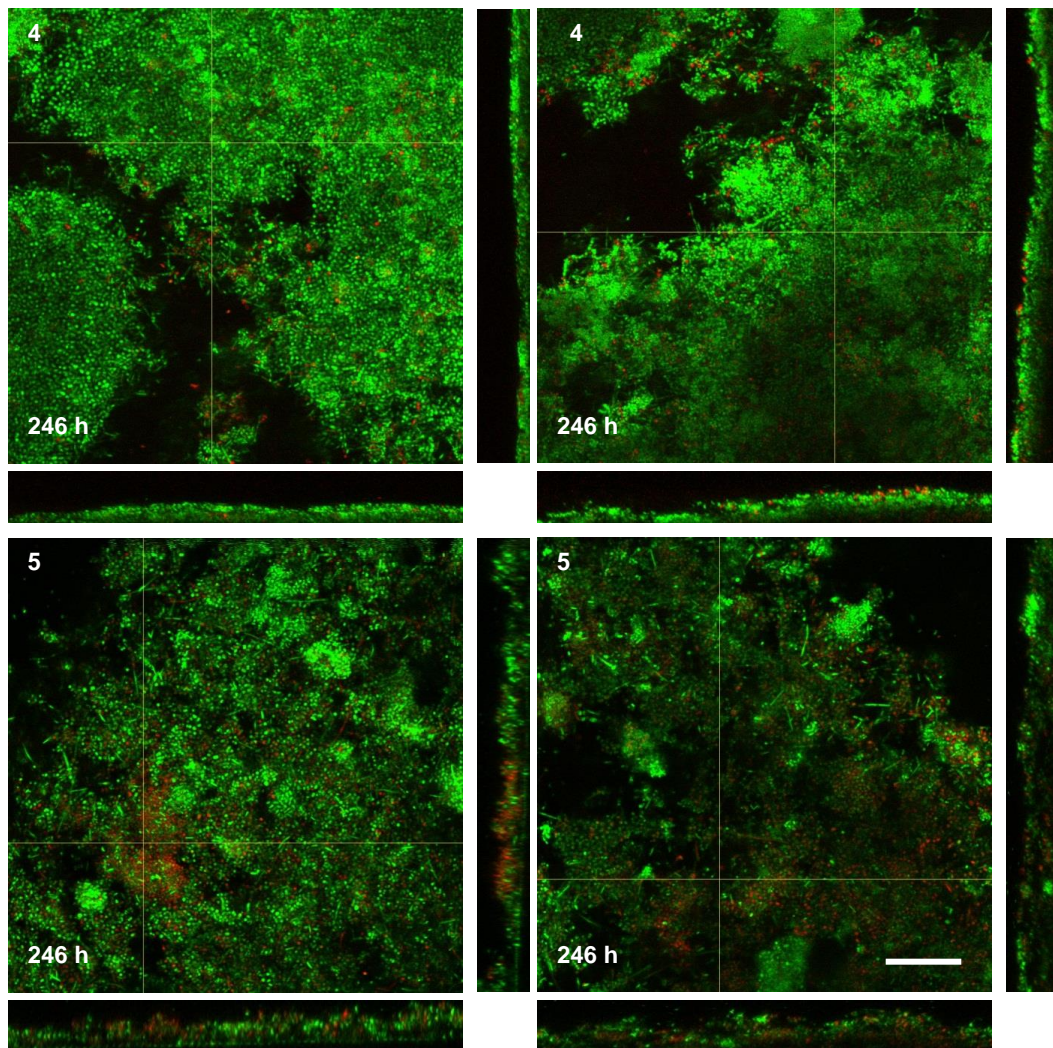


Figure 4.5. Representative CLSM images of peri-implant mucositis biofilms sampled at 246 h with x, y and z planes presented. Scale bar (20 μ m).

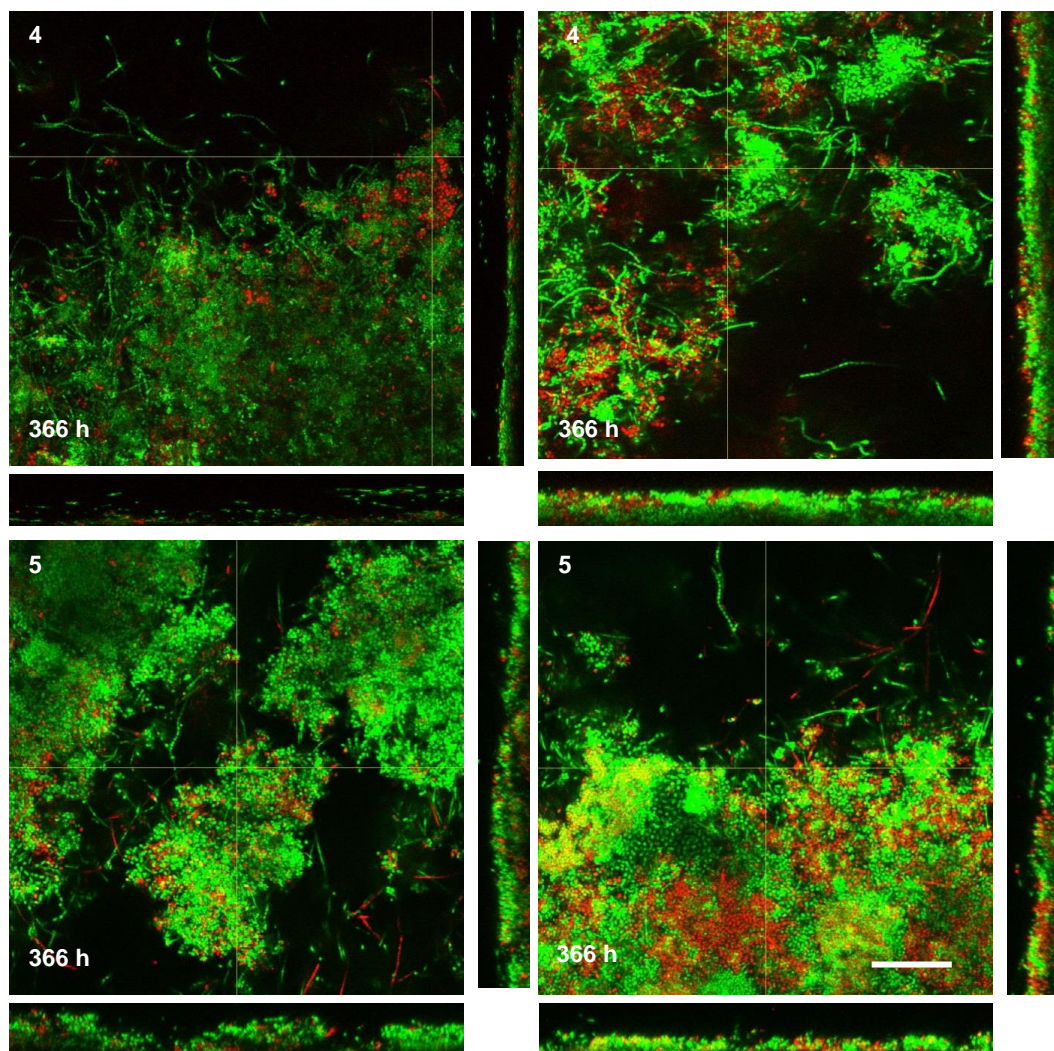


Figure 4.6. Representative CLSM images of peri-implant mucositis biofilms sampled at 366 h with x, y and z planes. Scale bar (20 μ m).

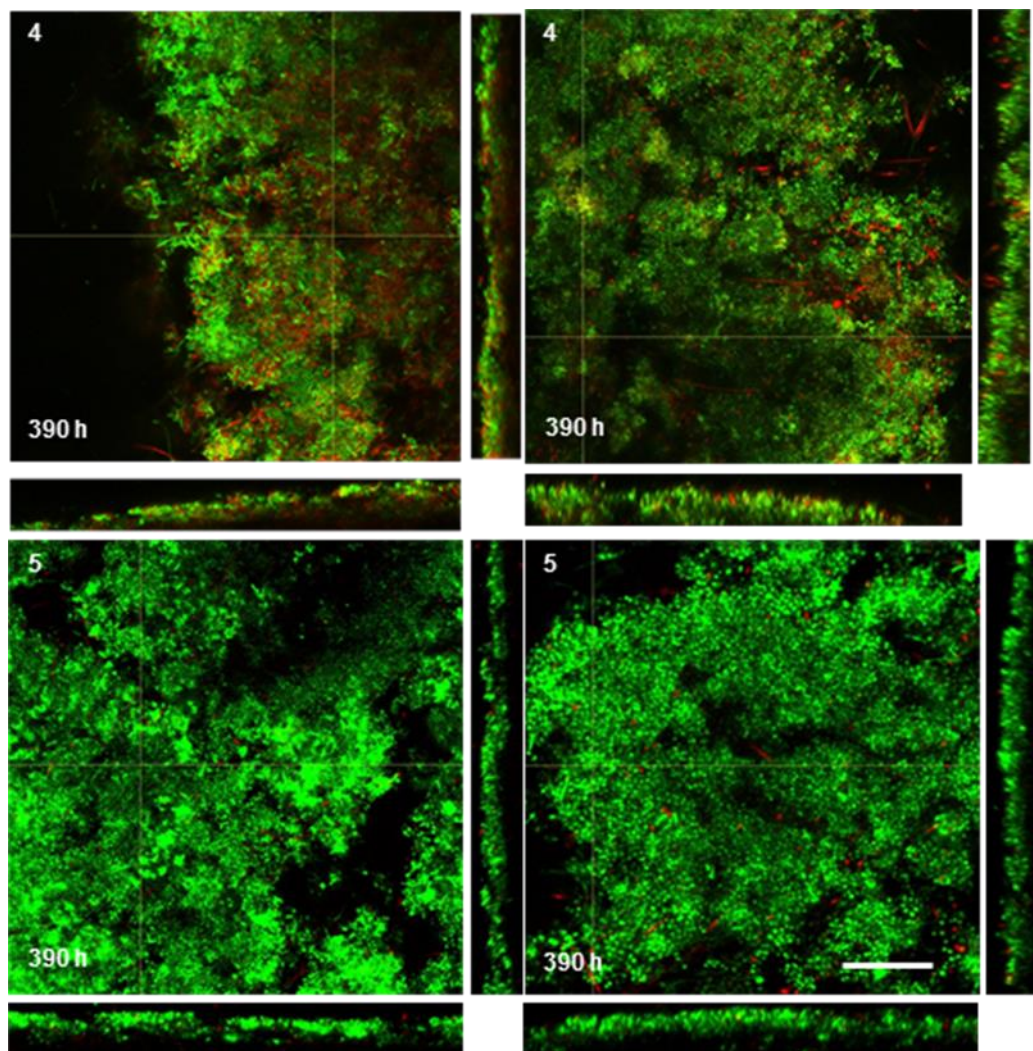


Figure 4.7. Representative CLSM images of peri-implant mucositis biofilms sampled at 390 h with x, y and z planes presented. Scale bar (20 μ m).

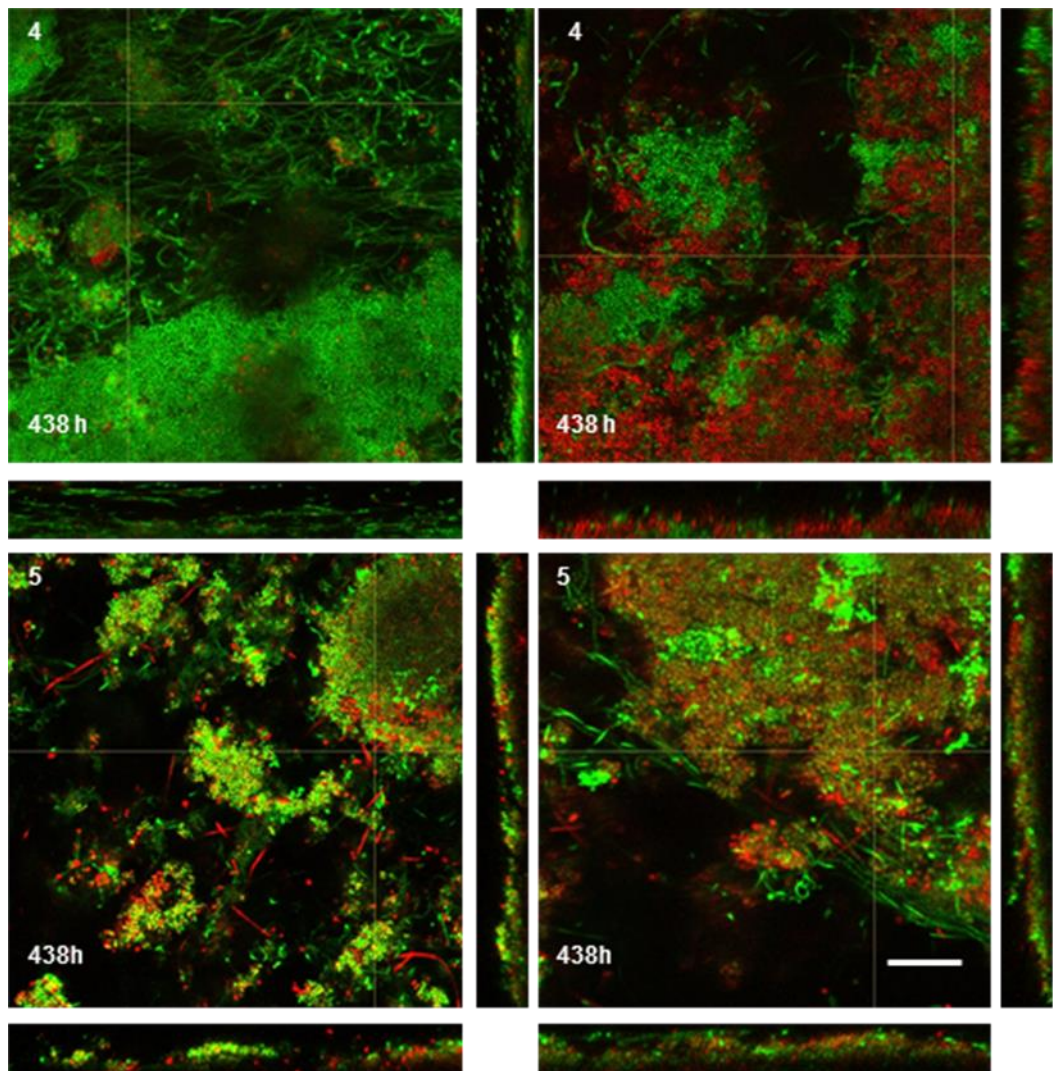


Figure 4.8. Representative CLSM images of peri-implant mucositis biofilms sampled at 438 h with x, y and z planes presented. Scale bar (20 μ m).

4.3.2.1.3 Peri-implantitis conditions

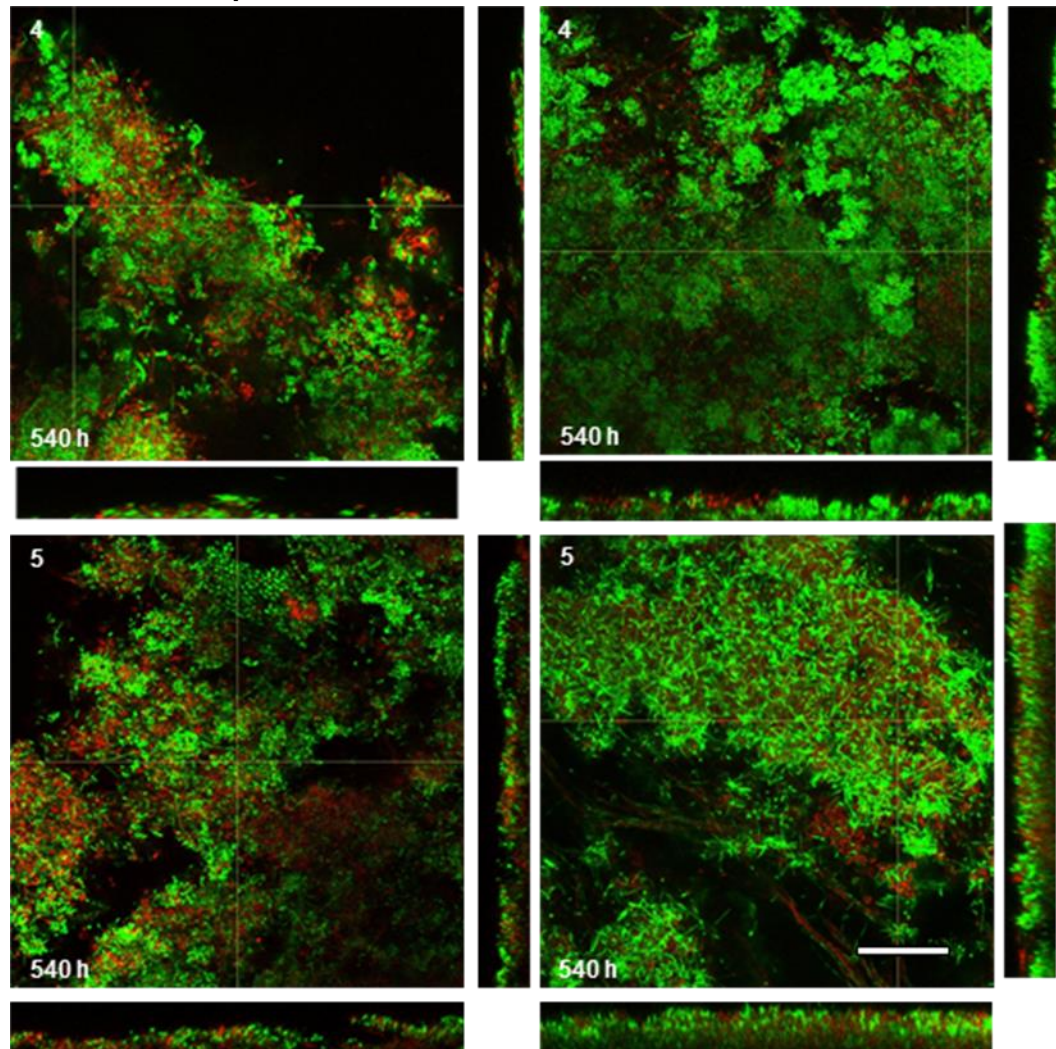


Figure 4.9. Representative CLSM images of peri-implantitis biofilms sampled at 540 h with x, y and z planes presented. Scale bar (20 μ m).

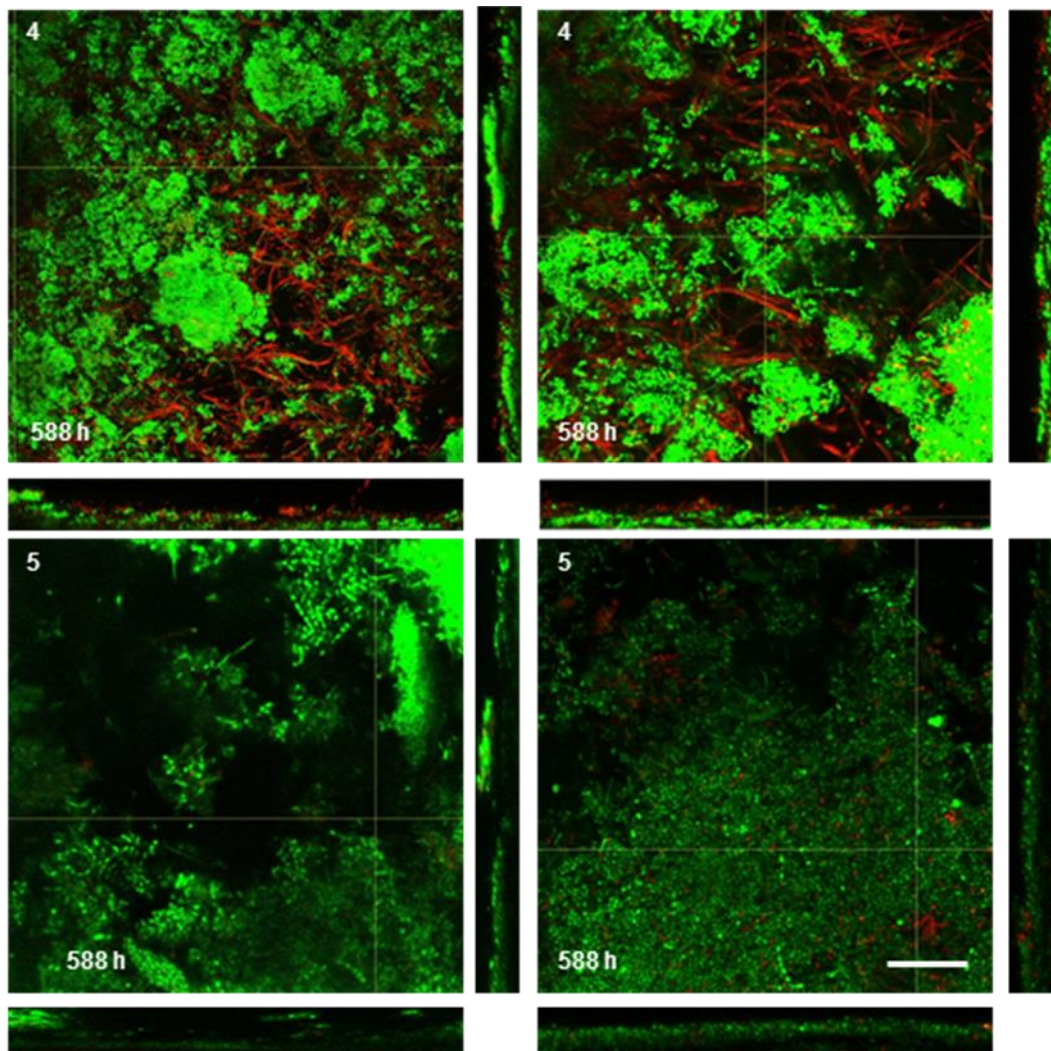


Figure 4.10. Representative CLSM images of peri-implantitis biofilms sampled at 588 h with x, y and z planes presented. Scale bar (20 μ m).

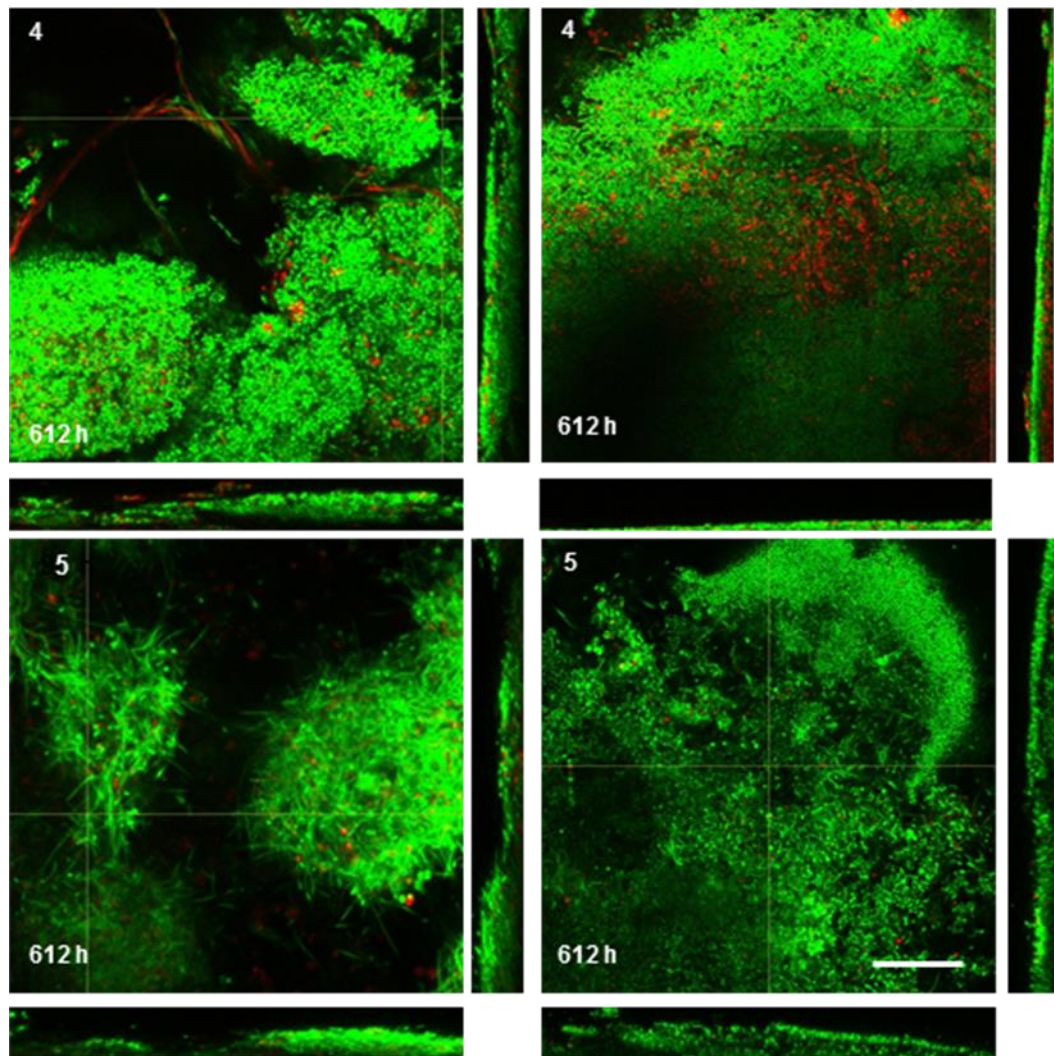


Figure 4.11. Representative CLSM images of peri-implantitis biofilms sampled at 612 h with x, y and z planes presented. Scale bar (20 μ m).

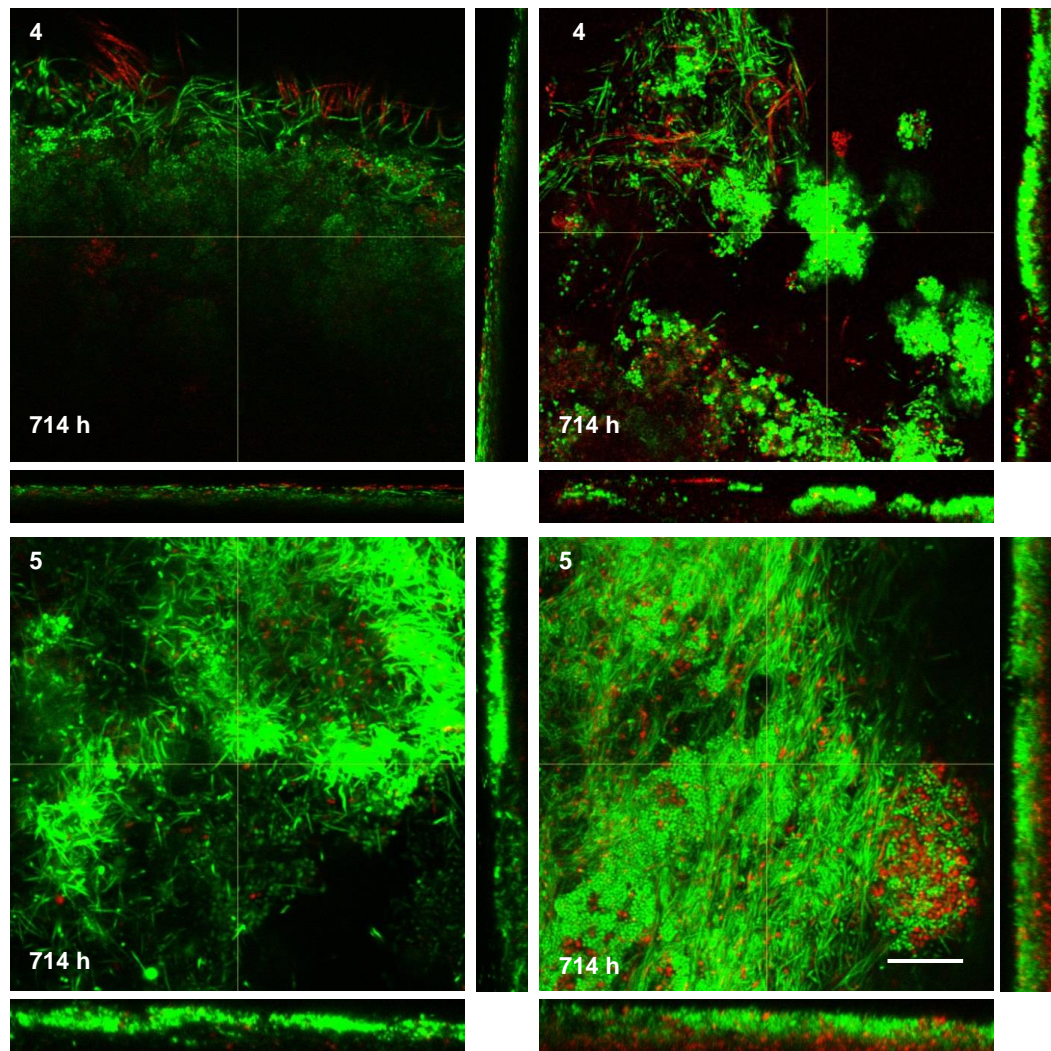


Figure 4.12. Representative CLSM images of peri-implantitis biofilms sampled at 714 h with x, y and z planes presented. Scale bar (20 μ m).

4.3.2.2 Viability mapping

The fluorescent intensity profiles from both the green and red channels, for image stacks were calculated using Image J software. The data were analysed through open image and the relative intensity (fluorescence) values were obtained for each channel for both experiments 4 and 5.

Under health conditions:

In experiment 4, CLSM analysis of a 96 h biofilm (health) was performed (Figure 4.13). It can be seen that the viable bacteria were dominant in the peripheral portion (slice 53) and declined in numbers on progression through the biofilm to slice 79 (Ti surface). This can also be observed in a subjective manner in figure 4.16. CLSM analysis of a 96 h biofilm from experiment 5 is also shown in figure 4.13. The viable bacteria were dominant throughout (maximum at slice 54) declining on progression through the biofilm down to slice 80. The red channel was extremely low in experiment 5 (96 h) compared to that of experiment 4 (ca. 0% vs. up to ca. 15%). This may be as a result of analysing a randomly selected single specific biofilm column.

Under peri-implant mucositis conditions:

In experiment 4, CLSM analysis of a 246 h biofilm (peri-implant mucositis) was performed and the results are presented in figure 4.13, it can be seen that viable bacteria were dominant in the peripheral portion (slice 29) and declined on progression through the biofilm down to slice 51 (Ti surface). This can also be observed in a subjective manner in figure 4.17. CLSM analysis of a 246 h biofilm from experiment 5 is also presented in figure 4.17. Here, the viable bacteria were dominant throughout (maximum at slice 32) declining on progression through the biofilm down to slice 53. The red channel was low in experiment two (246 h) compared to that of experiment one (ca. 15% vs. up to ca. 20%).

In experiment 4, CLSM analysis of a 366 h biofilm (peri-implant mucositis) was performed and is presented in figure 4.13. It can be seen that the viable bacteria were dominant in the peripheral portion (slice 75) and declined on progression through the biofilm to slice 97 (Ti surface). The same observation can be made in a subjective manner in figure 4.18. CLSM analysis of a 366 h biofilm from experiment 5 is also illustrated in figure 4.18. Here, the viable bacteria were dominant throughout (maximum at slice 24) declining on progression through the biofilm to slice 55. This again can also be seen in a subjective manner in figure

4.18. The red channel was low in experiment 5 (366 h) compared to that of experiment 4 (ca. 12% vs. up to ca. 19%).

In experiment 5, only CLSM analysis of a 390 h biofilm (peri-implant mucositis) was performed and in figure 4.13. Viable bacteria were dominant in the peripheral portion (slice 25) and declined on progression through the biofilm down to slice 84 (Ti surface). This can also be seen in a subjective manner in figure 4.19. The red channel was low in (ca. 9%).

CLSM analysis of a 438 h biofilm (peri-implant mucositis) is shown in figure 4.14 for experiment 4, with viable bacteria being dominant in the peripheral portion (slice 62) and declining through the biofilm to slice 82 (Ti surface). This can also be observed in a subjective manner in figure 4.20. CLSM analysis of a 438 h biofilm from experiment 5 (Figure 4.14), shows that the viable bacteria were dominant throughout (maximum at slice 67) but declined on progression through the biofilm down to slice 96. The red channel was low in experiment two (438 h) compared to that of experiment one (ca. 1% vs. up to ca. 25%).

Under peri-implantitis conditions:

Analysis of CLSM fluorescence relative to biofilm depth for 540 h biofilms (peri-implantitis) is presented for experiments 4 and 5 in figure 4.14 and 4.21. In both cases, viable bacteria were dominant in the peripheral portion (slice 83; experiment 4, slice 33; experiment 5). The amount of viable fluorescence then declines with increasing biofilm depth. Similar findings were evident for later time points (588 h, 612 h and 714 h), with viable cells again predominating, but declining as the depth of the biofilm increased (Figures 4.22 - 4.24).

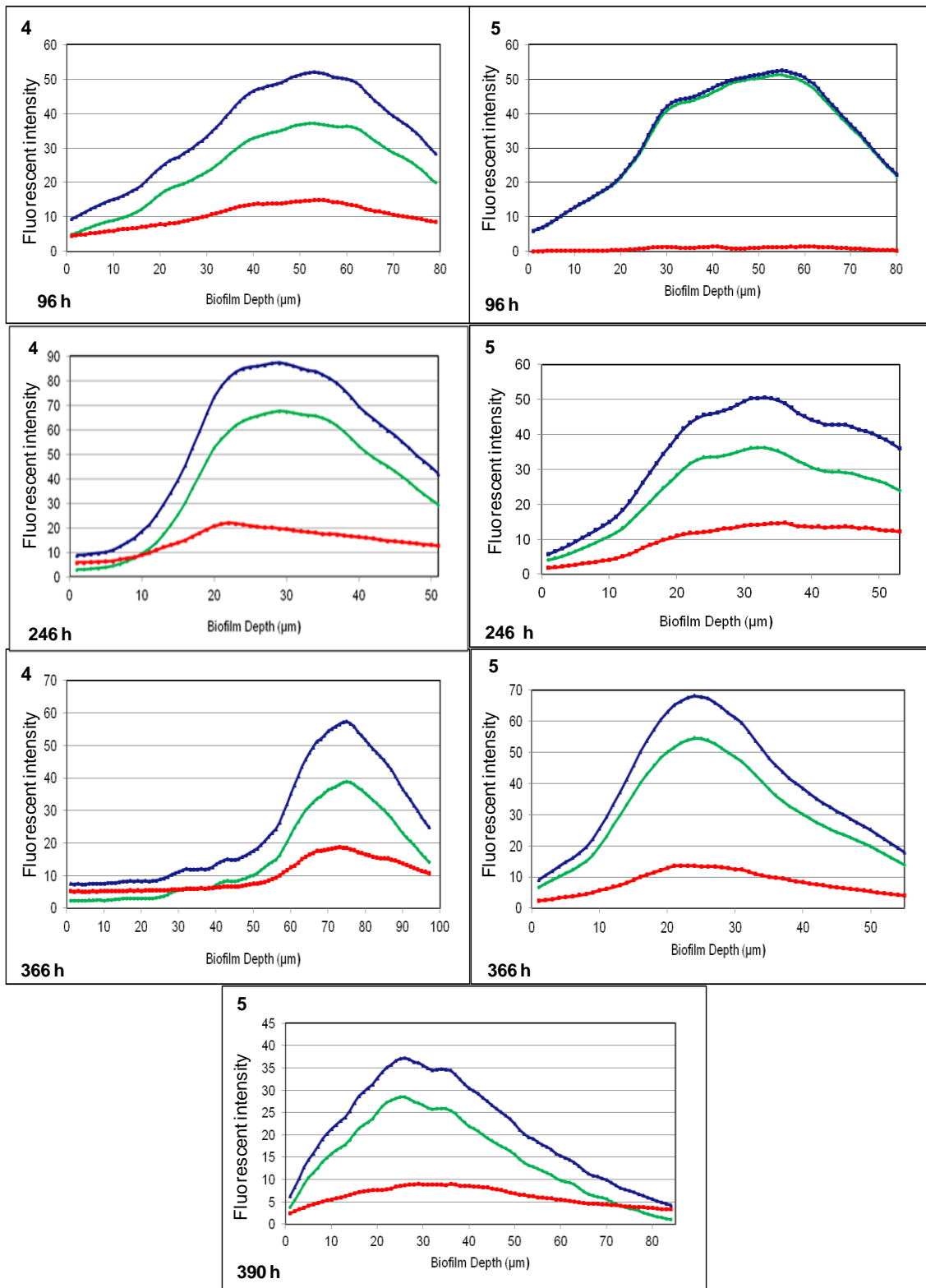


Figure 4.13. Fluorescent image intensity, blue line represents the total biomass intensity while the green and red lines represent the viable and non-viable channels from the CLSM stacks images; under health condition at 96 h, under peri-implant mucositis at 246 h, 366 h and 390 h. 4 and 5 represent individual experiments.

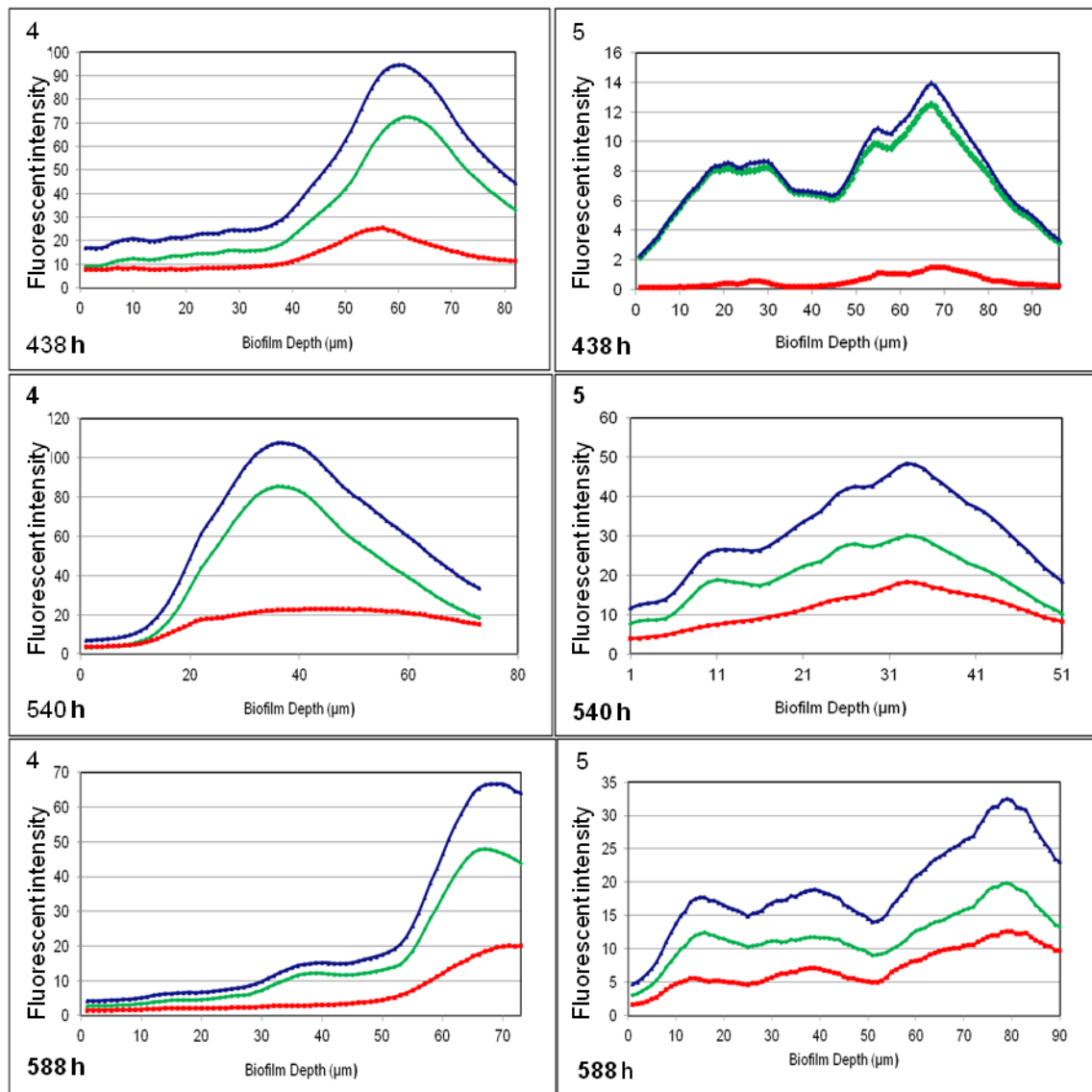


Figure 4.14. Fluorescent image intensity, blue line represents the total biomass intensity while the green and red lines represent the viable and non-viable channels from the CLSM stacks images; under peri-implant mucositis at 438 h and under peri-implantitis at 540 h, 588 h. 4 and 5 represent individual experiments.

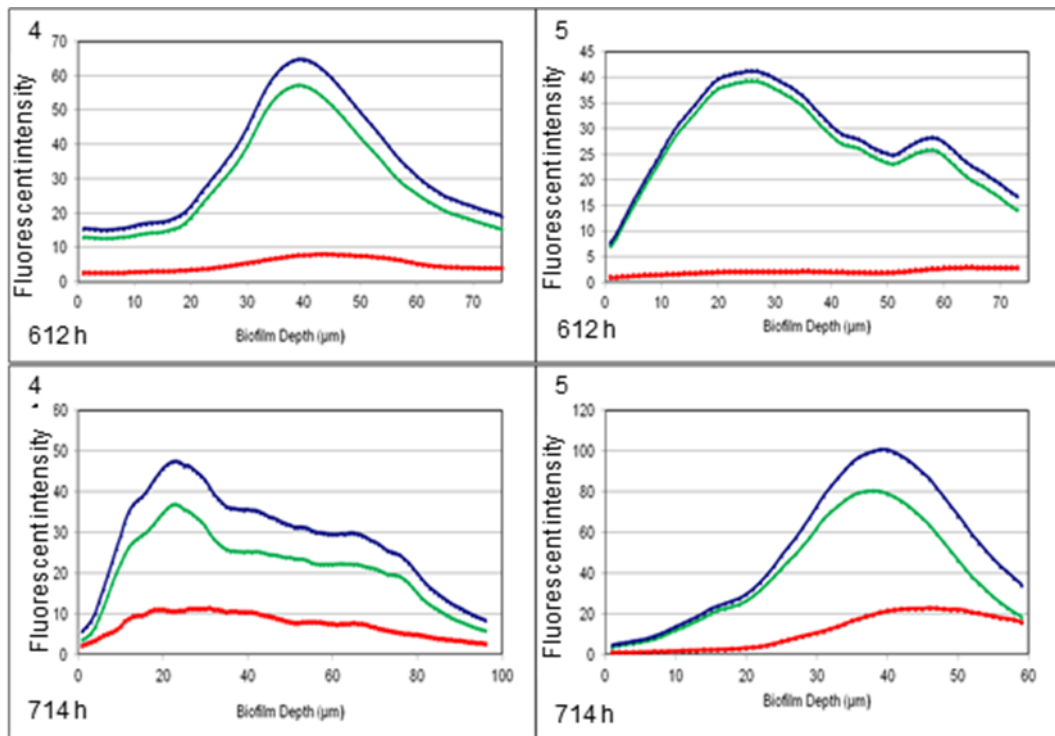


Figure 4.15. Fluorescent image intensity, blue line represents the total biomass intensity while the green and red lines represent the viable and non-viable channels from the CLSM stacks images; under peri-implantitis at 612 h and 714 h. 4 and 5 represent individual experiments.

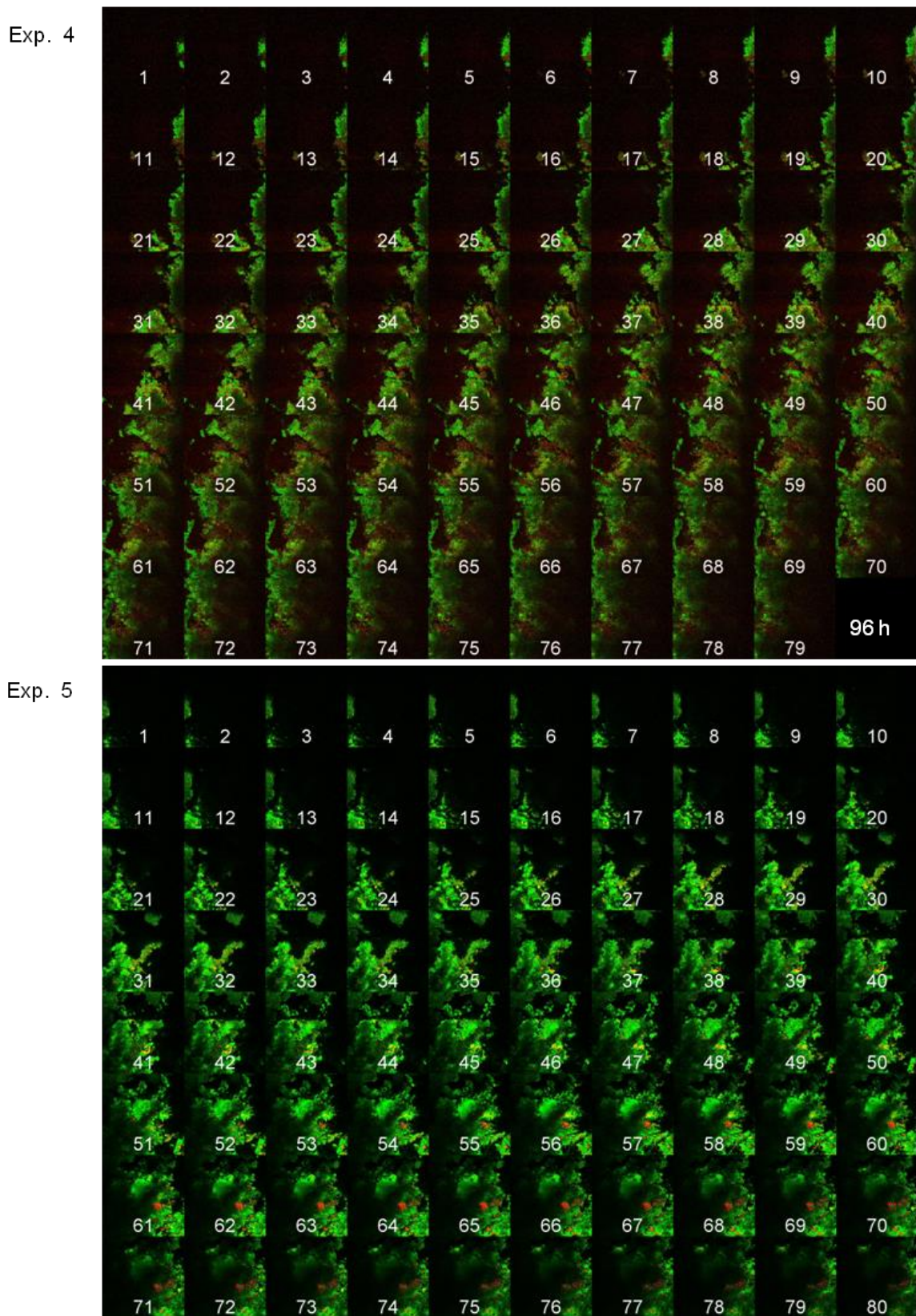


Figure 4.16. Individual optical sections of biofilms sampled at 96 h from both experiments 4 and 5. Numbering is from 1 at the apex in 1 μm increments until the titanium surface is reached.

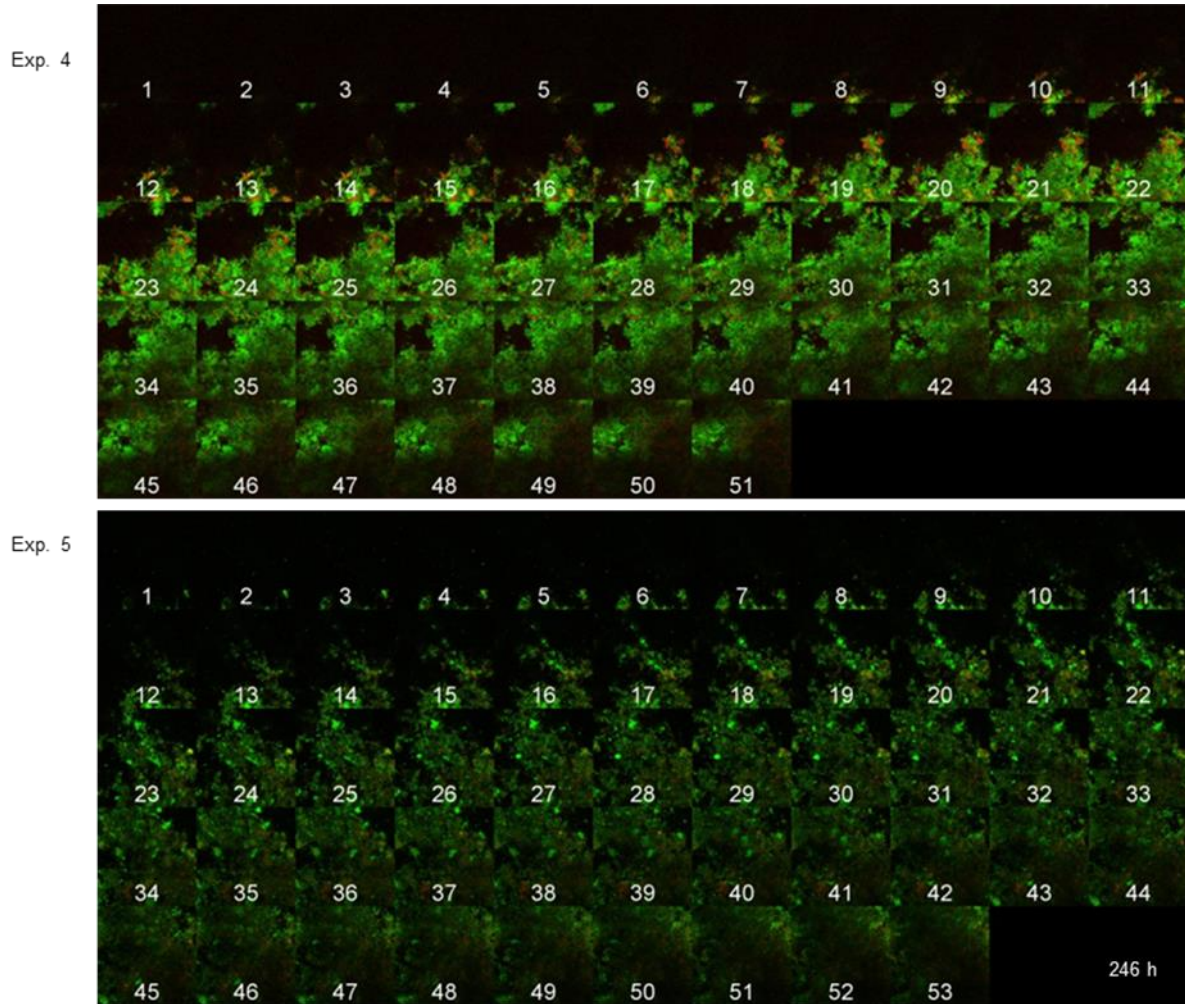


Figure 4.17. Individual optical sections of biofilms sampled at 246 h for both experiments 4 and 5. Numbering is from 1 at the apex in 1 μm increments until the titanium surface is reached.

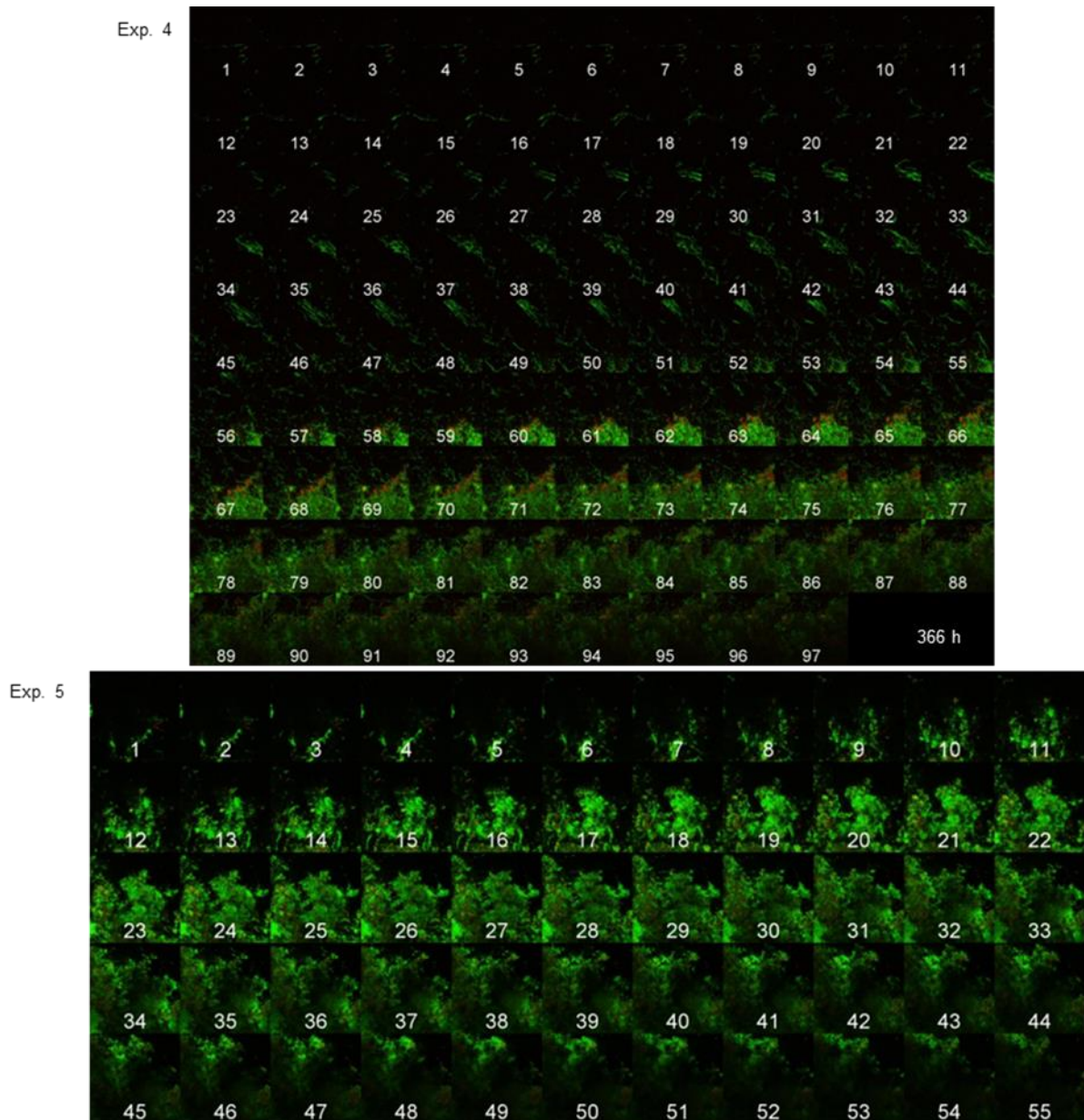


Figure 4.18. Individual optical sections of biofilms sampled at 366 h for both experiments 4 and 5. Numbering is from 1 at the apex in 1 μm increments until the titanium surface is reached.

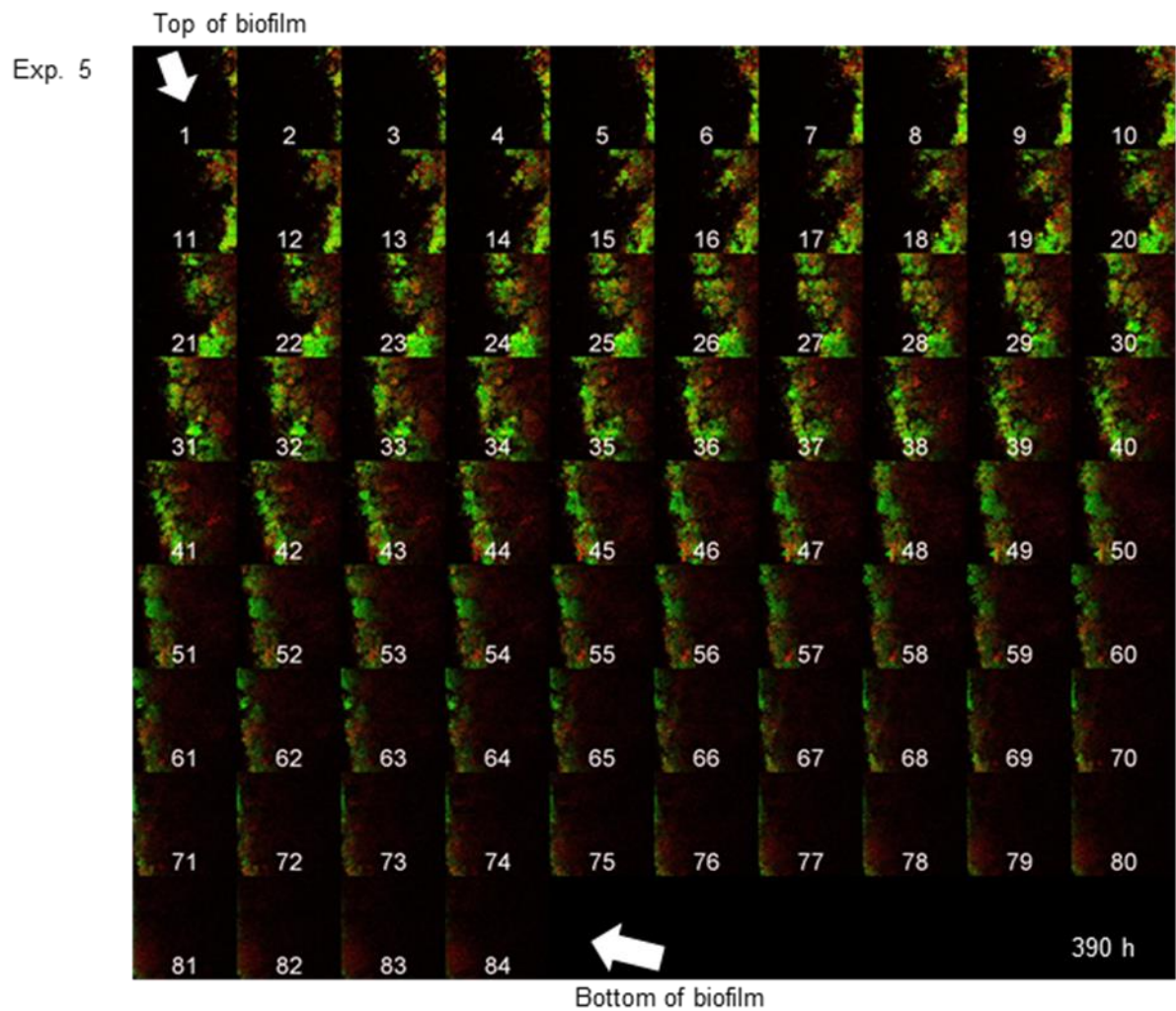


Figure 4.19. Individual optical sections of biofilms sampled at 390 h from experiments 5. Numbering is from 1 at the apex in 1 μm increments until the titanium surface is reached.

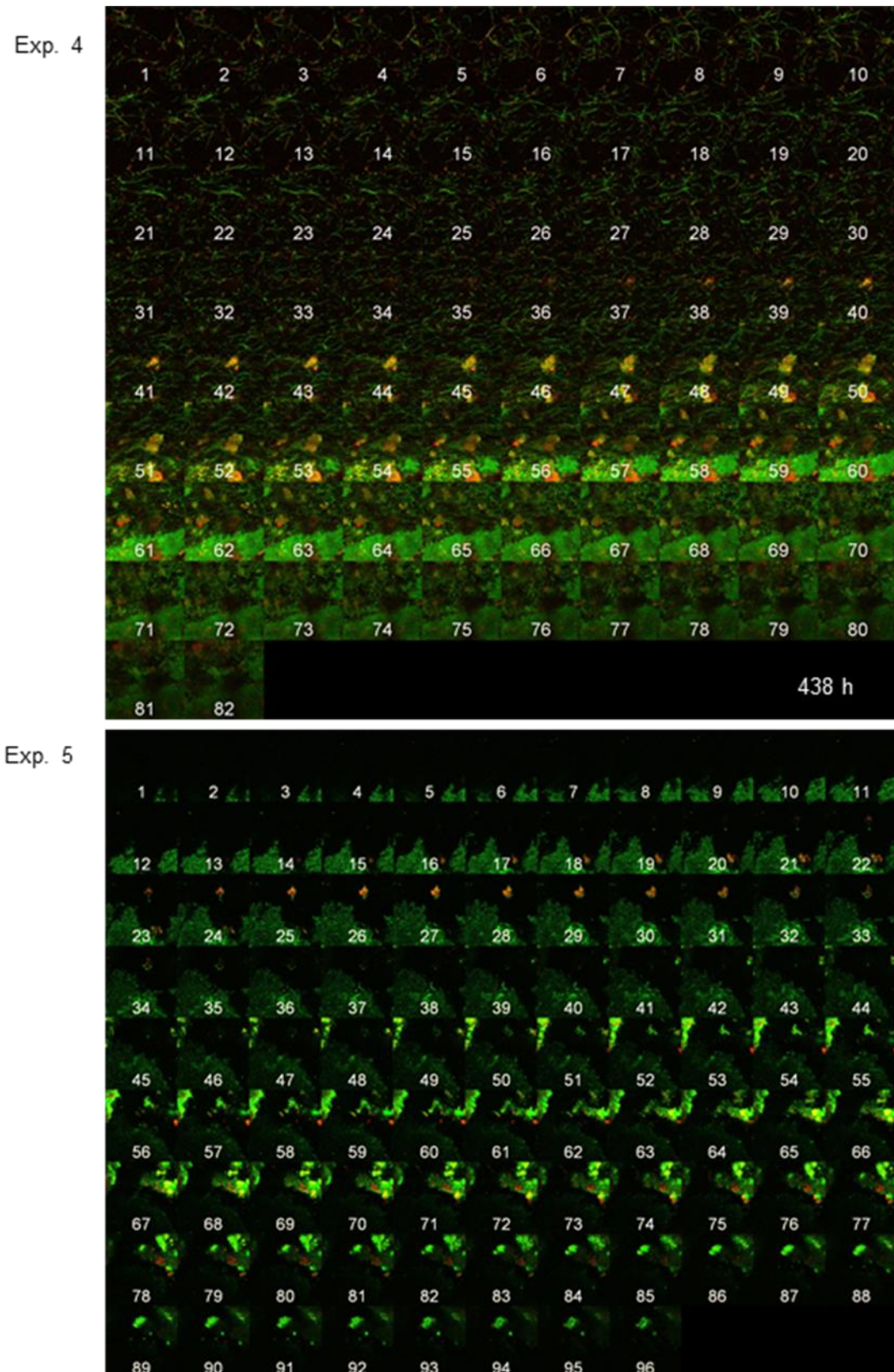


Figure 4.20. Individual optical sections of biofilms sampled at 438 h from both experiments 4 and 5. Numbering is from 1 at the apex in 1 μm increments until the titanium surface is reached.

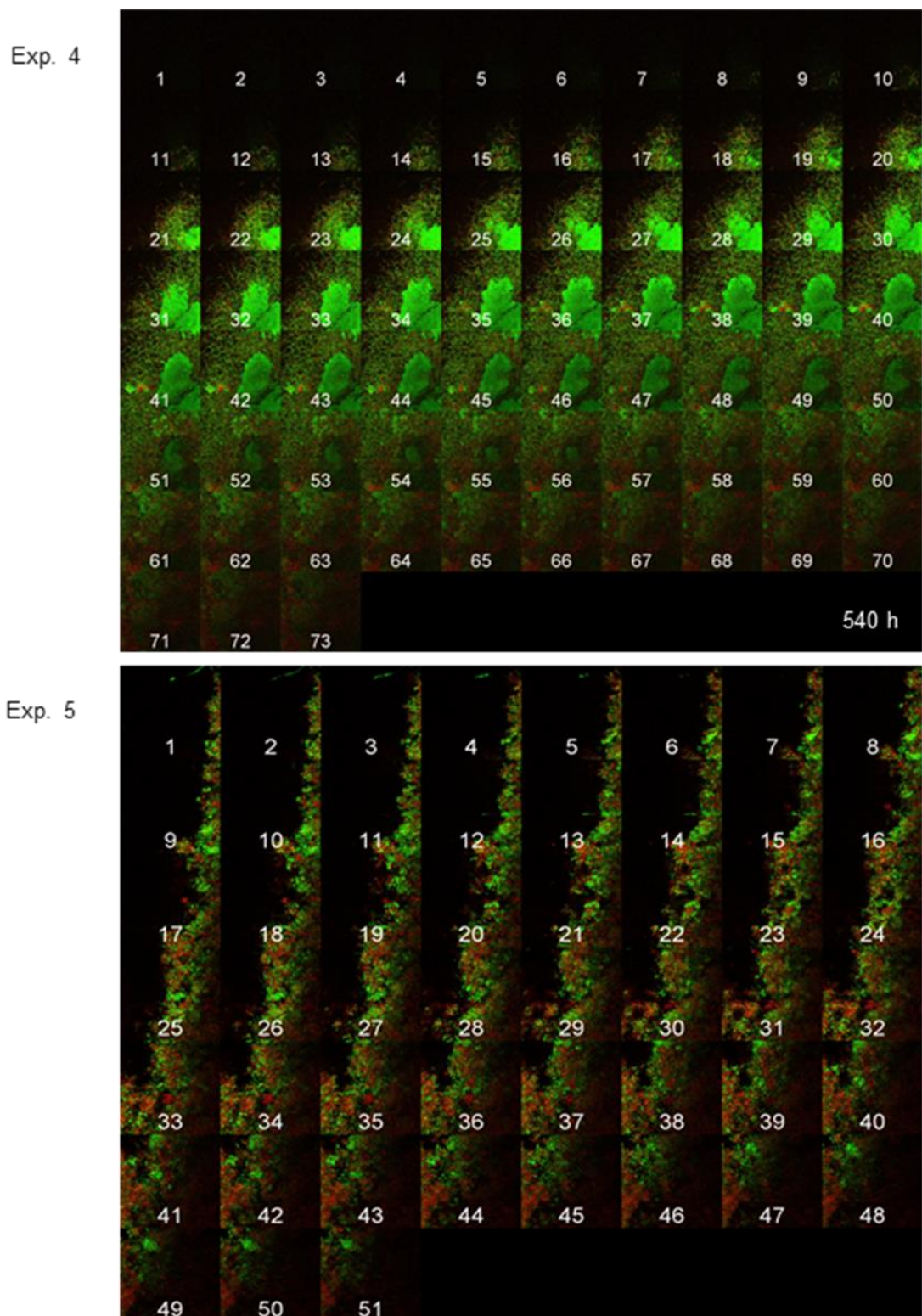


Figure 4.21. Individual optical sections of biofilms sampled at 540 h from both experiments 4 and 5. Numbering is from 1 at the apex in 1 μm increments until the titanium surface is reached.

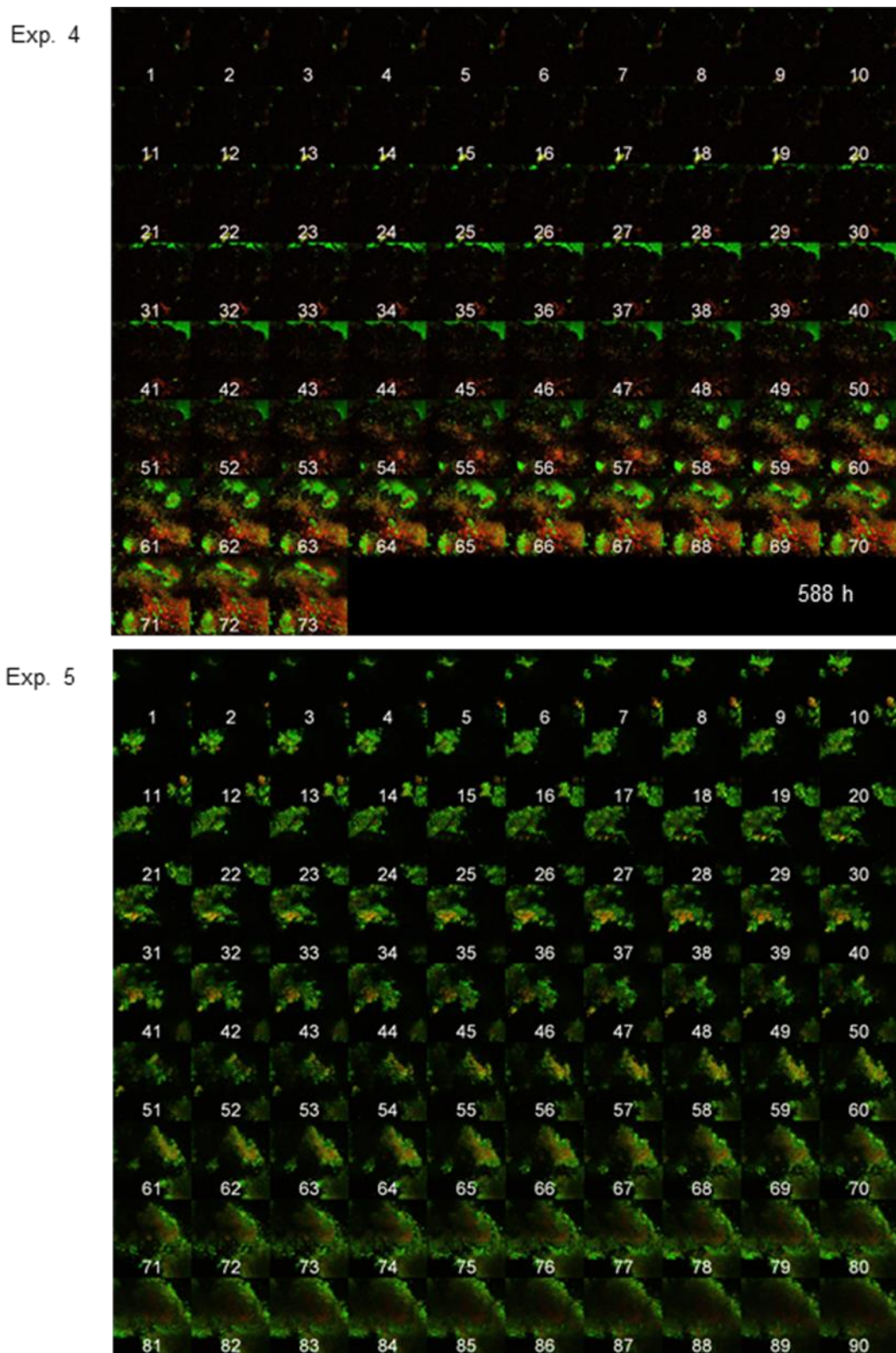
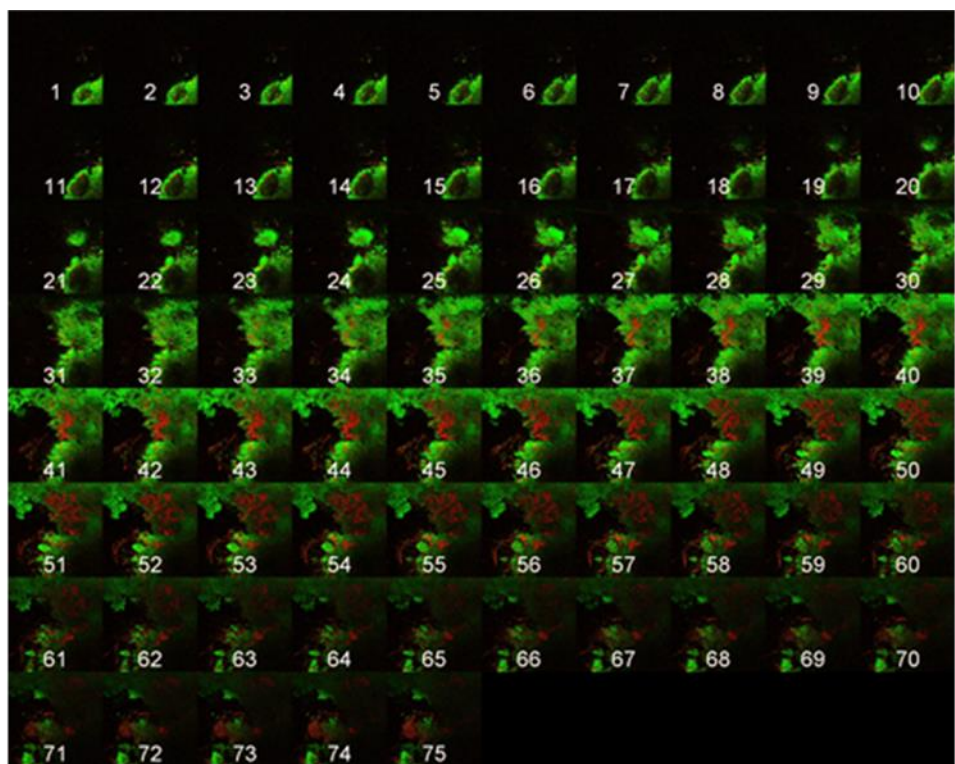


Figure 4.22. Individual optical sections of biofilms sampled at 588 h from both experiments 4 and 5. Numbering is from 1 at the apex in 1 μm increments until the titanium surface is reached.

Exp. 4

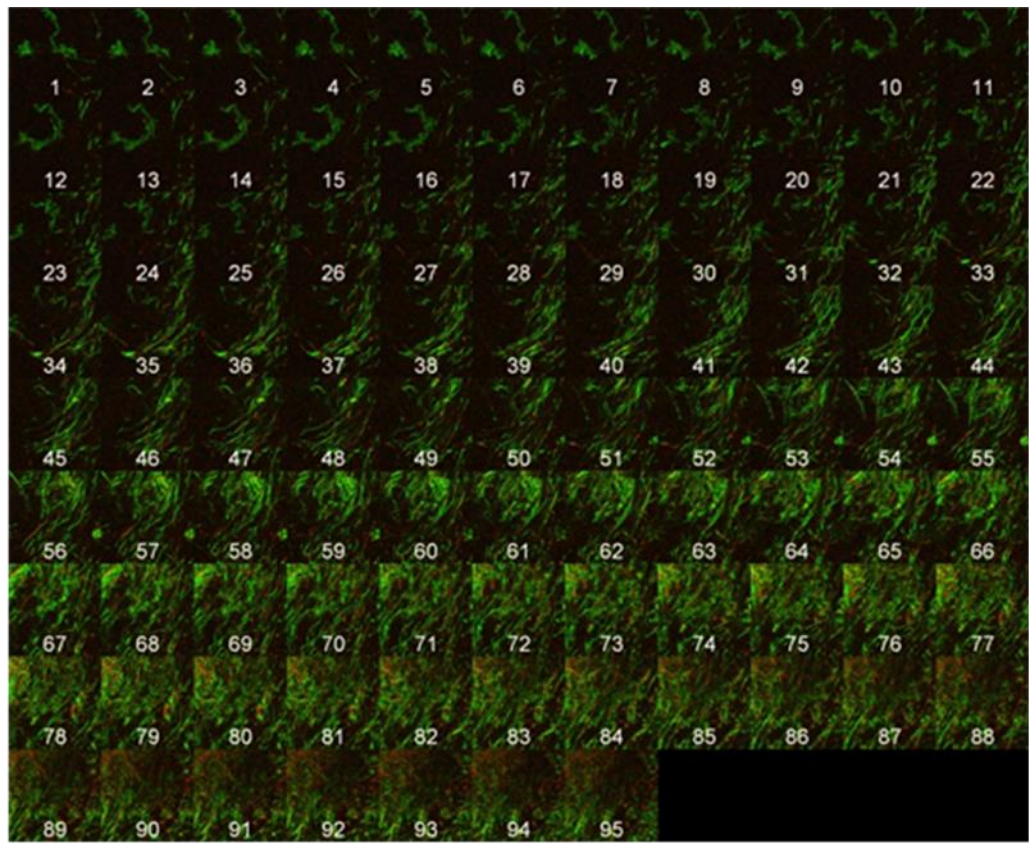


Exp. 5



Figure 4.23. Individual optical sections of biofilms sampled at 612 h from both experiments 4 and 5. Numbering is from 1 at the apex in 1 μm increments until the titanium surface is reached.

Exp. 4



Exp. 5

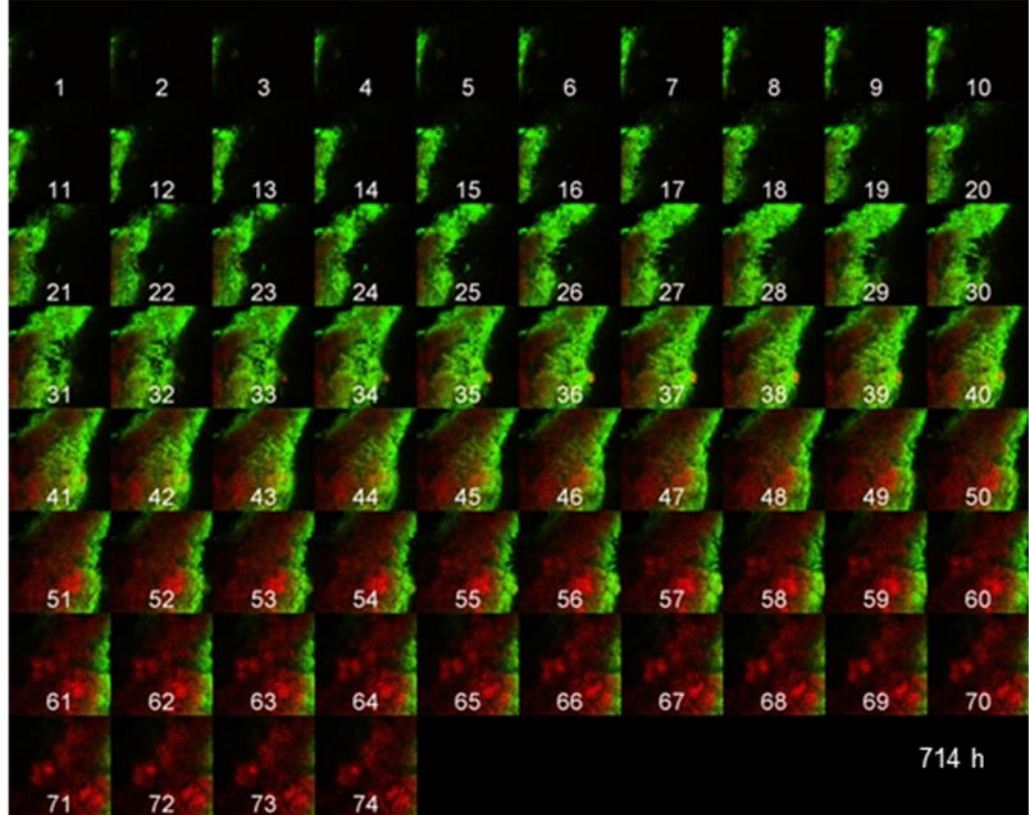


Figure 4.24. Individual optical sections of biofilms sampled at 714 h from both experiments 4 and 5. Numbering is from 1 at the apex in 1 μm increments until the titanium surface is reached.

4.3.3 Biofilm thickness

The thickness of the biofilm at each sampling point was calculated from the orthogonal view using Image J software (Figure 4.25). Under healthy conditions, experiment 4 at 6 h, the biofilm thickness was (ca. 1 μm) increasing at 96 h to ca. 51 μm . Under peri-implant mucositis, the biofilm thickness seems to drop slightly to ca. 30 μm at 246 h when a change of atmosphere and increased peri-implant sulcular fluid flow occurs. At 366 h, the biofilm thickness increased to ca. 38 μm then remained constant to ca. 31 μm at 438 h. Under peri-implantitis conditions, the biofilm thickness fluctuated between ca. 41 μm and ca. 36 μm at 540 h and 588 h, respectively. At 612 h, the biofilm thickness increased slightly to ca. 42 μm and remained constant at 714 h. In experiment 5, the biofilm thickness under health conditions at 6 h, was ca. 1 μm and increased at 96 h to ca. 34 μm . Under peri-implant mucositis conditions, the biofilm thickness reduced slightly to ca. 29 μm at 246 h. Under peri-implantitis conditions, the biofilm thickness was constant at 540 h (ca. 25 μm) and at 588 h, it reduced to ca. 21 μm . At 612 h, the biofilm thickness increased to ca. 31 μm then decreased slightly at 714 h to ca. 28 μm .

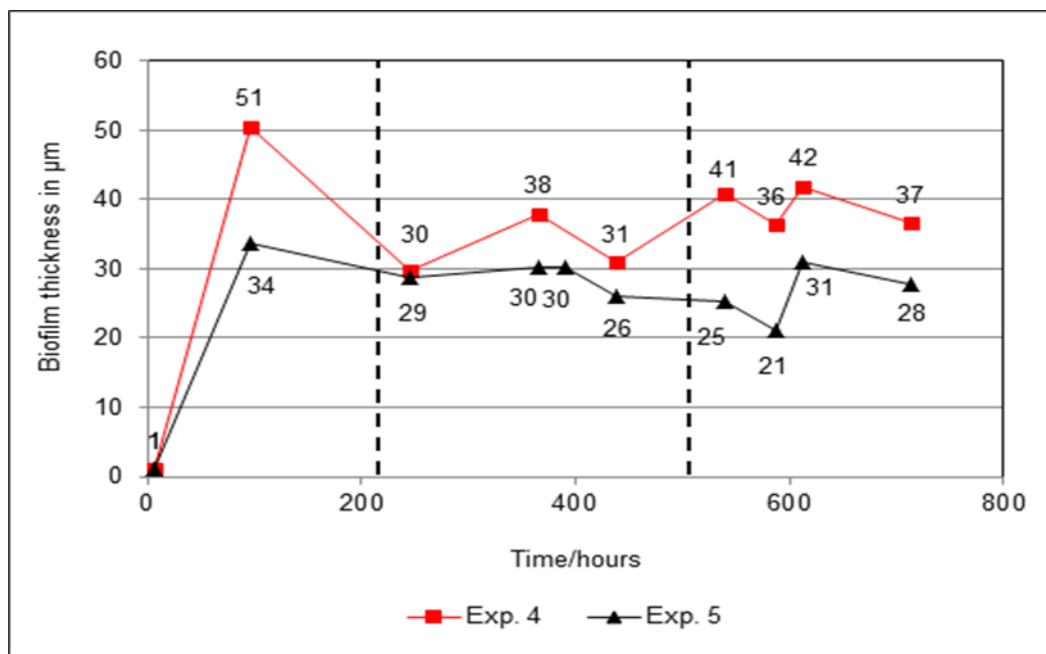


Figure 4.25. Changes in biofilm thickness (μm) over time. First black dash line represents the switch over to microaerophilic gas mixture, second black dash line represents switch over anaerobic gas mixture.

4.3.4 Comparisons between experiment 4 and experiment 5

The CFU per biofilm data for both runs is presented in Table 4.2 along with the means of these data.

Comparison between health and peri-implant mucositis conditions

There was a reduction difference in *Candida* spp. counts between health (96 h and 216 h) and peri-implant mucositis (390 h and 438 h) conditions. There was no difference observed in the counts of anaerobic spp., aerobic spp., Gram-negative anaerobic spp., *Actinomyces* spp., *Streptococcus* spp. and *Staphylococcus* spp. between these above conditions at the same time points. *Veillonella* spp. was not present in experiment 5 therefore it could not be compared.

Comparison between health and peri-implantitis conditions

There was a reduction difference in *Actinomyces* spp. counts between health (96 h and 216 h) and peri-implantitis (612 h and 714 h) conditions. There was also a difference of *Candida* spp. counts between health (96 h and 216 h) and peri-implantitis (612 h and 714 h). There was no difference in the counts of anaerobic spp., aerobic spp., Gram-negative anaerobic spp., *Streptococcus* spp. and *Staphylococcus* spp. between these above conditions at the same time points.

Comparison between peri-implant mucositis and peri-implantitis conditions there was no difference observed in the colony counts on selective and non-selective media for these two conditions at 390 h, 438 h and at 612 h, 714 h.

Table 4.2. The mean CFU/ml data of biofilm generated in experiment 4 and experiment 5 under healthy, peri-implant mucositis and peri-implantitis conditions.

Bacteria species	Health 96 h & 216 h			Peri-implant mucositis 390 h & 438 h			Peri-implantitis 612 h & 714 h		
	Exp. 4 Total	Exp. 5 Total	Mean	Exp. 4 Total	Exp. 5 Total	Mean	Exp. 4 Total	Exp. 5 Total	Mean
Aerobe spp.	8.25E+07	5.86E+07	7.06E+07	4.08E+07	4.41E+07	4.24E+07	2.08E+07	2.90E+07	2.49E+07
Anaerobe spp.	1.04E+08	8.06E+07	9.25E+07	8.33E+07	9.63E+07	8.98E+07	4.76E+07	1.21E+08	8.44E+07
Streptococcus spp.	2.98E+07	3.63E+07	3.30E+07	1.31E+07	4.05E+07	2.68E+07	1.59E+07	9.03E+06	1.25E+07
Actinomyces spp.	6.89E+07	6.03E+07	6.46E+07	1.97E+07	3.70E+07	2.84E+07	1.98E+07	1.01E+07	1.49E+07
Gram-ve anaerobe spp.	7.05E+07	6.06E+07	6.56E+07	5.78E+07	5.81E+07	4.54E+07	2.20E+07	4.73E+07	3.06E+07
Candida spp.	5.21E+07	6.54E+07	5.88E+07	2.03E+07	1.84E+07	1.93E+07	2.47E+07	2.00E+07	2.24E+07
Staphylococcus spp.	5.66E+07	4.40E+07	5.03E+07	2.28E+07	6.14E+06	1.45E+07	2.24E+07	3.04E+07	2.64E+07

4.3.5 16S rRNA gene PCR, gene cloning and sequencing

Biofilms from 6 time points were analysed by 16S rRNA gene cloning and comparative sequencing. A total of 30 random clones from each transformation for each time point were sequenced and identified, the results are shown in Table 4.3.

Health conditions (6 h and 96 h)

The artificial saliva and PISF medium with aerobic condition resulted in dominant populations mainly of *Streptococcus mitis* group (22/60) and *Neisseria* species (14/60), followed by the *S. salivarius* group (8/60). There was a 40:20 split with respect to Gram-positive and Gram-negative taxa.

Peri-implant mucositis conditions (246 h to 438 h)

The increased flow of PISF and microaerophilic gas mixture into the system resulting resulted in a predominance of *Streptococcus* spp. (15/60), *Neisseria* spp. (9/60) and *Capnocytophaga* spp. (7/60) with low numbers of *Abiotrophia defectiva*, *Gemella haemolysans*, *Granulicatella para-adiacens*, *Eikenella corrodens*, *Fusobacterium nucleatum*, and *Fusobacterium periodonticum*. *Veillonella parvula* and TM7 were also detected. The ratio of Gram-positive and Gram-negative taxa decreased to a 26:34 split.

Peri-implantitis conditions (540 h to 714 h)

Obligate and facultative anaerobic Gram-negative bacteria dominated (42/60) including *Capnocytophaga* spp. (16/60) and *Veillonella* spp. (14/60) together with a few examples of *Parvimonas micra*, *Peptococcus* sp. and *Neisseria* spp. The ratio of Gram-positive and Gram-negative taxa further decreased to an 18:42 split.

Chapter 4: Development of an *in vitro* microcosm model

Species (Health) 6 h and 96 h	No. of Clones	Species (Peri-implant mucositis) 246 h and 438 h	No. of Clones	Species (Peri-implantitis) 540 h and 714 h	No. of Clones
<i>Enterococcus hirae</i>	1	<i>Abiotrophia defectiva</i>	1	<i>Abiotrophia defectiva</i>	1
<i>Gemella sanguinis</i>	1	<i>Gemella haemolysans</i>	2	<i>Gemella haemolysans</i>	2
<i>Granulicatella paraadiacens</i>	1	<i>Granulicatella para-adiacens</i>	1	<i>Granulicatella para-adiacens</i>	1
<i>Mycobacterium chelona</i>	2	<i>Parvimonas micra</i>	6	<i>Parvimonas micra</i>	2
<i>Mycobacterium</i> sp.	1	<i>Peptococcus</i> sp.	1	<i>Peptococcus</i> sp.	2
<i>Rothia mucilaginosa</i>	4	<i>Streptococcus anginosus</i> group	1	<i>Streptococcus mitis</i> group	9
<i>Streptococcus mitis</i> group	22	<i>Streptococcus mitis</i> group	13	Uncultured <i>Streptococcus</i> group	1
<i>Streptococcus salivarius</i> group	8	<i>Streptococcus sineses</i>	1	Total Gram-positive	18
Total Gram- positive	40	Total Gram-positive	26	<i>Capnocytophaga ochracea</i>	1
<i>Klebsiella pneumonia</i>	4	<i>Capnocytophaga leadbetteri</i>	2	<i>Capnocytophaga sputigena</i>	14
<i>Moraxella osloensis</i>	1	<i>Capnocytophaga ochracea</i>	2	<i>Klebsiella pneumoniae</i>	1
<i>Neisseria</i> sp.	10	<i>Capnocytophaga sputigena</i>	3	<i>Leptotrichia</i> sp.	2
<i>Neisseria perflava</i>	3	<i>Eikenella corrodens</i>	1	<i>Neisseria mucosa</i>	1
<i>Neisseria mucosa</i>	1	<i>Fusobacterium nucleatum</i>	2	<i>Neisseria subflava</i>	1
Uncultured <i>Enterobacterium</i>	1	<i>Fusobacterium periodonticum</i>	1	<i>Neisseria</i> sp.	1
Total Gram- negative	20	<i>Klebsiella pneumoniae</i>	2	Uncultured <i>Neisseria</i> sp.	3
		<i>Neisseria</i> spp.	9	<i>Escherichia coli</i>	3
		<i>Leptotrichia</i> sp.	5	Uncultured <i>Veillonella</i>	1
		<i>Veillonella parvula</i>	3	<i>Veillonella dispar</i>	2
		<i>Veillonella</i> sp.	1	<i>Veillonella parvula</i>	10
		<i>Vibrio</i> sp.	1	<i>Veillonella</i> sp.	1
		TM7	1	Total Gram- negative	42
		Total Gram- negative	34		

Table 4.3. Taxa detected by using 16S rRNA gene cloning and sequencing from microcosm biofilms grown on titanium surfaces in a CDFF at different time points 6 h and 96 h representing health, 246 h and 438 h representing peri-implant mucositis and, 540 h and 714 h representing peri-implantitis. Green shading refers to organisms commonly classified from the literature as being associated with healthy dental implants. Yellow shading refers to organisms associated with peri-implant mucositis and red shading refers to dominant organisms associated with peri-implantitis. Blue shading refers to organisms not normally associated with the resident oral microbiota.

4.4 Discussion

Peri-implant infections (peri-implant mucositis and peri-implantitis) are caused by a biofilm covering the dental implant surface and crown (Ata-Ali et al., 2011). In the previous chapter, an *in vitro* method was developed to generate a dental plaque biofilm associated with healthy dental implants progressing to peri-implant mucositis conditions in a manner similar to the *in vivo* situation. In this chapter, the model was further developed to include peri-implantitis conditions. From an ecological standpoint, this model was designed to reflect the changes in a community as a result of environmental changes (nutritionally and atmospherically). The microcosm biofilms were characterised by traditional culture and CLSM microscopy as well as molecular biology techniques. The gaseous environment mixtures in the CDFF were used to represent those conditions encountered when the lesion is above or below the gingival margin. The results presented in this chapter represent the analysis of biofilms generated within the CDFF for 29 days in two independent experiments.

4.4.1 Culture analysis

The microbiological characterisation of the saliva inoculum and the CDFF biofilms was based on the use of a variety of agar media. There was variation in the starting inoculum for experiments 4 and 5. Furthermore, it was a slight concern that higher numbers and Gram-negative anaerobe spp. was evident compared with total anaerobes (Experiment 4). The reason for this remains unclear but could relate to the effectiveness of the agars employed. However, the total microbial counts increased from 216 h and then reached a steady state with minor fluctuations. This growth profile appeared to be constant for each target group of microbes. This was also apparent using of the selective media which encourage the growth of specific genera or microbiota that may be part of the oral consortium.

In terms of progression from healthy implant conditions to those of peri-implant mucositis conditions, significant changes in *Candida* species occurred. Changes were also evident in *Actinomyces* spp. levels as the transition from the healthy condition to peri-implantitis conditions occurred. No other changes in microbial groups were seen between peri-implant mucositis and peri-implantitis conditions. To ascertain the reproducibility the model the similarity between both experiments was confirmed by viable counts. The total counts of *Actinomyces* spp., *Streptococcus* spp., anaerobes spp. and aerobes spp. increased during the hours 96 h, 246 h, 438 h and 540 hours. There was slight decrease observed in

the prevalence of *Candida* spp. between health and peri-implant mucositis (Table 4.1). There was no difference observed in the counts of bacteria on other selective and non-selective media.

There was reduction in the levels of *Actinomyces* spp. between health and peri-implantitis conditions (Table 4.1). There were no differences encountered between peri-implant mucositis and peri-implantitis conditions. This small variation in both experiments could be attributed to the metabolic activity of some bacteria present in microcosm provides lifestyles suitable for the growth of oxygen intolerant bacteria (Bradshaw et al., 1996). Overall, few differences between the numbers of target bacteria and fungi across the disease conditions were seen. This may reflect the ability of the biofilm community to alter metabolic pathways with the changing conditions. However, more detailed characterisation using CLSM and molecular techniques, showed changes were occurring at the biofilm structure, genera and species level.

4.4.2 Characterisation of biofilm architecture

Several methods have been used to view the microstructure of biofilms including light microscopy, transmission electron microscopy, scanning electron microscopy (SEM) and confocal laser scanning microscopy (CLSM). Traditional light microscopy has been used only in the early stages of colonisation and plaque development, while electron microscopy usually requires dehydration of biofilm specimen, which may cause disruptive shrinkage and the loss of biofilm matrix (Pratten et al., 2000). However, by using CLSM, to optically section the biofilm without disruption, a different kind of analysis can be performed. For example the differences in intensity profiles can be used to profile the biofilm and, with detailed analysis, yield information about the viability in protruding surface structures. Image stack data can also be combined to give a projection through the biofilm showing all optical sections.

In general, fluorescence microscopy approaches offer the opportunity to visualize bacteria directly on substrata and in the state of adherence (Hannig et al., 2007). The CLSM has been used with vital fluorescent stains to determine the structure of natural, heterogeneous nature of intact undisturbed microcosm biofilms (Wood et al., 2000). Under healthy conditions, after 96 h, the immature biofilm was found to be low in morphotypic diversity, as the cells all appeared to be coccoid in nature. However, the biofilms appeared to contain stacks and fluid-filled spaces and were highly heterogeneous in their architecture. These findings agreed with previous *in vitro* electron microscopy studies of developing dental

plaque (Takeuchi and Yamamoto, 2001). In addition to the prevalence of coccoid cells that have been reported as the principal components of dental plaque, after 6 h the titanium surface were covered by colonies of dividing bacteria that initially spread laterally along the increasing surface. Small numbers of rod-shaped and filamentous bacteria were also evident which has also been reported previously by Nyvad and Kilian (1987). Once the surface is fully covered, proliferating bacteria are reported to grow to form columnar microbial colonies that are closely packed and compete for space and nutrients with neighboring colonies in dental plaque (Listgarten, 1976). Under peri-implant mucositis, after approximately 1 week the filamentous bacteria began to penetrate the coccoid bacteria from the surface, gradually replacing the coccoid microbiota and finally leading to a predominantly filamentous microbiota. This has also been reported previously on a covered surface by Listgarten (1994). Non-viable bacteria then became more widely distributed through out the biofilm, this process appeared to continue for approximately 2 - 3 weeks.

In general, an increase in nutrient supply such as the provision of PISF and artificial saliva leads to the formation of a dense biofilm, mostly due to an increase in production of extracellular polysaccharide (EPS) by the oral microbiota (Pratten et al., 2000). The increased EPS provides another source of nutrients and plays an important key role in biofilm architecture by providing points of attachment for new species. The structure of the biofilms seemed to follow the progression reported by a previous study (Pratten et al., 2000) in which low nutrition biofilms had an open structure but in biofilms in a high nutrient environment like saliva/PISF might be expected to produce high-density biofilm.

Columnar colonies subsequently disappeared and were replaced by a dense mat of filamentous bacteria under peri-implantitis conditions at 612 h and 714 h. These biofilms developed as a result of a higher flow rate of nutrients and an anaerobic atmosphere. The biofilm associated with the anaerobic atmosphere revealed dense embedded clusters of long filaments on titanium disc surfaces.

The present study also showed that the cell viability increased from the upper surface of the biofilm and then decreased towards the titanium surface (substratum) at 96 h under health conditions. After the increased flow of peri-implant sulcular fluid at 246 h, 366 h, 390 h (experiment two only) and 438 h, the fluorescence intensity of viable cells demonstrated maximum fluorescence intensity in the deeper layer. The non-viable bacteria appeared to form a more significant portion and were visible in the uppermost region. Such distribution of

viable and non-viable cells also been reported previously in laboratory grown biofilms (Dalwai et al., 2006, Hope and Wilson, 2002). At 540 h, 588 h, 612 h and 714 h, the viable bacteria proportions decreased from the titanium surface and then increased towards the biofilm upper surface; the non-viable fluorescence demonstrated maximum intensity closer to the titanium surface under peri-implantitis and anaerobic atmosphere.

Biofilm thickness was not uniform. Hence, the structure of biofilm can range from the relatively featureless, flat type to one consisting of a more complex organisation involving tower like stacks consisting of microbes enclosed in an extracellular matrix separated by water channels (Dige et al., 2007). Under healthy conditions at 96 h in experiment 4, the biofilm thickness was greatest and then fluctuated slightly under peri-implant mucositis at 366 h (38 μm) and increased again in peri-implantitis (ca. 41 μm) at 540 h. In experiment 5, the biofilm thickness was 34 μm at 96 h. The biofilm thickness then fluctuated between ca. 29 μm at 246 h, to ca. 27 μm at 714 h. This variability in biofilm thickness between both experiments highlights the heterogeneity of (Figs 4.4 & 4.6) (Dige et al., 2007). This study data is agreed with cultural technique viable counts represented with high viable counts at 96 h and fluctuated slightly until 714 h. The results of CLSM images have useful in mapping the *in vitro* distribution of viable bacteria (Auschill et al., 2001) and revealing similar channels to those seen with *in vivo* plaque samples (Wood et al., 2000).

However, the culture data and the CLSM data did not agree in terms of detecting community changes associated with environmental changes. The CLSM data highlighted difference in biofilm structure and cell morphology in the biofilms which was not apparent from the bacterial culture. These differences may be due to the possibility that a large proportion of the community was unculturable on the media that was used.

4.4.3 Characterisation of biofilm using comparative 16S rRNA gene cloning and sequencing

The limited shift of microbiota from health to mucositis to peri-implantitis was unexpected and the change of conditions was expected to alter the microbial population to a far greater extent. An explanation for this could be that some taxa increased in number and others decreased but these were not cultured, forming part of the unculturable proportion of the community.

A large proportion of the bacterial community are unculturable either because of incorrect nutrition supplied in the growth media or as a result of living in a biofilm

in a stressful environment (viable but unculturable). To further understand this, it was decided to analyse the biofilms by molecular microbiological techniques to establish the diversity of the species in the biofilm communities.

The molecular biology technique negates the bias involved with culturing bacteria and relies on detecting the bacterial DNA in the sample to identify the bacterial species. 16S rRNA gene cloning and comparative sequencing was carried out to see if the community changed with altered environment. Six biofilms were selected for analysis: at early health at 6 h and late health at 96 h sampling points, peri-implant mucositis (early at 246 h) and late at 438 h sampling points, and induction of peri-implantitis early at 540 h and late 714 h sampling points. The healthy biofilms were dominated by a range of oral streptococci such as *Streptococcus mitis* and *Streptococcus salivarius* groups. These species are frequently detected in healthy dental implant biofilms (Lee and Wang, 2010, Lee et al., 1999, Mombelli et al., 1988). These data, particularly with regards to Gram-positive facultative bacteria and Gram-negative bacteria which were recovered mainly by independent culture technique and data from other studies support our findings (Rams et al., 1984, Sanz et al., 1990).

Other molecular biology techniques have been used to characterise peri-implantitis e.g. Checkerboard DNA-DNA hybridization. This was previously employed to study the microbiota associated with dental implant infections and showed that *Parvimonas micra* were positively associated with peri-implantitis (Al-Radha et al., 2012). Máximo et al. (2009) detected *S. sanguinis*, *S. gordonii*, *P. intermedia*, *V. parvula* at elevated levels in peri-implant mucositis. In infected dental implants, Newman and Flemming (1988) reported an increased incidence of *Capnocytophaga* spp. A further study by Alcoforado et al. (1991) reported pathogenic bacteria such as *P. micra*, *Fusobacterium* spp. and *P. intermedia* associated with infected dental implant. The same author reported significant numbers of enteric rods and *Capnocytophaga* spp. Augthun and Conrads (1997) detected *N. mucosa*, *C. ochracea* and *Fusobacterium* spp. at elevated levels in peri-implantitis while *E. corrodens* was identified with less frequency. Other clinical studies found that the microbiota associated with peri-implantitis was more diverse than that of the healthy implants including *F. nucleatum* and *Granulicatella adiacens* (Koyanagi et al., 2010, Koyanagi et al., 2013, Kumar et al., 2012). The result of this present study showed that some *Streptococcus* spp., *Neisseria*, *V. dispar*, *Capnocytophaga* spp. and *F. nucleatum* were identified in peri-implantitis. Differences at species level were observed between the three states, and some as yet unreported bacteria from this environment were also

detected, such as TM7 and *Vibrio* spp. (Al-Radha et al., 2012). Surprisingly little is thus far known about the microbiological differences between peri-implant mucositis and peri-implantitis which may signify that in most cases, the disease evolves gradually from mucositis to peri-implantitis. There is no evidence for the existence of one or a limited number of specific pathogens for peri-implantitis (Mombelli and Décailliet, 2011). The presence of these principal periodontal pathogens in the disease model was evidence that the model may be reflecting the clinical situation. These data support the CLSM data in that different morphologies taxa were present at these different time points. The data indicate that peri-implant communities differ in health, peri-implant mucositis and peri-implantitis and several species; including previously unsuspected and unknown organisms are unique to these niches. Furthermore, peri-implantitis appears to be a heterogeneous infection, which is dominated by Gram-negative bacteria as identified by pyrosequencing techniques (Kumar et al., 2012).

4.5 Conclusions

The results of this investigation have shown that it is possible to produce an *in vitro* model of microcosm biofilms growing on titanium discs. The study has shown that using an *in vitro* model it is possible to create peri-implantitis biofilms grown under conditions similar to those which would exist *in vivo*. The data confirmed that the biofilms were reproducible between independent CDFF experiments and within the two experiments. Furthermore, the CDFF allowed the study of the events that cause the microbiota to progress from a “commensal” to a pathogenic community. 16S rRNA analysis was used successfully to explore the diversity of this biofilm community, avoiding the need for lengthy cultural procedures. The sequencing methodology provided a more representative picture than was previously possible by culture. The CLSM analysis supports the sequencing data in that high numbers of long rods that may be *Capnocytophaga* spp. were present in the biofilm. Furthermore, viability profiling including both viable and non-viable data, has also revealed more information, which could be used to quantify the penetration effects of antibacterial and oral disinfectant agents. The identification of the organisms causing the infectious process remains a goal both to understand the disease process and to provide effective antimicrobial and supportive treatment of infected dental implants.

Chapter 5

Characterization of microcosm biofilm associated with healthy, peri-implant mucositis and peri-implantitis conditions using multiplex qPCR

5.1 Introduction

Numerous methods of microbial detection and quantification have been developed, mainly driven by the need to detect putative pathogens. These include, in the first instance, direct microscopy (van-Leeuwenhoek, 1674) and several hundred years later, bacterial culture. Indeed, cultural-based methods have until recently been the main method for detecting and enumerating pathogens and indeed microbial communities. However, there are some drawbacks to these, including the facts that they are:

- time consuming
- labour intensive
- do not take account of fastidious taxa
- do not take account of viable but non culturable taxa

This approach may not therefore reflect the true composition of a mixed bacterial community and enumerating bacteria may also produce erroneous results (Dymock et al., 1996).

Polymerase chain reaction (PCR) has become a powerful tool due to its speed, sensitivity, simplicity and specificity (Rodu, 1990). It has been used successfully in clinical microbiology to detect slow growing microorganisms or organisms that are difficult to culture (Nadkarni et al., 2002). However, it is difficult to accurately quantify the number of bacteria by conventional PCR because the reaction is evaluated after gene amplification is completed. In addition the quantification of PCR products can be affected by contamination, interfering substances and unequal amounts of collected samples. Also it is difficult to use for routine diagnosis because of the additionally required time for handling and post PCR analysis such as gel electrophoresis and radioactive hybridization (Nadkarni et al., 2002, Suzuki et al., 2004, Dewhirst et al., 2010).

In recent years, quantitative PCR (qPCR) methods have revolutionised the investigation of bacterial communities and infections (Suzuki et al., 2004). The qPCR is a convenient technique that enables detection of absolute numbers of bacteria when used in combination with data derived from available accurate standards and sample size (Price et al., 2007). However, this method does not provide evidence of pathogen viability and bacterial activity since the probes, and or primers, detect DNA originating from living or dead bacteria. qPCR provides high sensitivity and specificity and it offers a faster detection time and increased accuracy compared with traditional methods. qPCR is

Chapter 5: Characterization of microcosm biofilm using multiplex qPCR

attractive because of its ease of use, relatively low cost in terms of laboratory manpower, rapid turnaround time, and potential to be fully automated. When used with species-specific primers, qPCR can also provide a precise and sensitive method for more accurate quantitation of individual species as well as quantification of total bacteria (using universal primers), and is therefore a useful tool for studies on the aetiology of peri-implantitis (D'Ercole et al., 2008). Furthermore, a large number of samples can be accurately measured at one time (Morikawa et al., 2008, Rupf et al., 2011). These methods are now being employed in the study of microbial communities involved in both oral health and disease (Dalwai et al., 2007, Ledder et al., 2007, Keijser et al., 2008, Cric et al., 2010, Sakamoto et al., 2005).

The early development of biofilms on implant surfaces has been found to be similar to that on natural teeth and on other restorative materials placed in the oral cavity (Subramani et al., 2009). Studies dealing with the microbiota associated with infected implants indicated that the presence of more complex, multiple species community existed and was analogous to those in periodontal lesion (Mombelli et al., 2011). A close association was demonstrated between peri-implantitis and several microorganisms associated with periodontitis including: *Porphyromonas gingivalis*, *Fusobacterium* spp., *Parvimonas micra*, *Actinomyces israelii*, *Prevotella* spp., *Tannerella forsythia*, *Aggregatibacter actinomycetemcomitans*, *Treponema denticola*, *Campylobacter rectus*, *Capnocytophaga* sp. and *Eikenella corrodens* (Sanz et al., 1990, Becker et al., 1990, Rosenberg et al., 1991, Alcoforado et al., 1991, Mombelli et al., 1992, Kalykakis et al., 1996, Augthun and Conrads, 1997, Keller et al., 1998, Leonhardt et al., 1995, Persson et al., 1996, Leonhardt et al., 1999, Barboza et al., 2002, Mombelli, 2002, Buchmann et al., 2003, Botero et al., 2005, Persson et al., 2006, Shibli et al., 2008, Máximo et al., 2008, Máximo et al., 2009, Emrani et al., 2009, Tabanella et al., 2009, Persson et al., 2010). However, microorganisms not primarily associated with periodontitis such as *Staphylococcus* spp., *Pseudomonas* spp. and enterics such as *Escherichia coli*, *Helicobacter pylori* and yeast such as *Candida* spp. have also been isolated (Rams et al., 1991, Rams et al., 1990, Leonhardt et al., 2003, Persson et al., 2010).

In previous chapters, an *in vitro* peri-implantitis model was developed which allows modelling of three conditions health, peri-implant mucositis and peri-implantitis.

Chapter 5: Characterization of microcosm biofilm using multiplex qPCR

The aim of the current study was to use three triplex qPCR assays designed and optimized previously by Ceric et al. (2010), to determine the numbers (and proportion) of eight orally important taxa including: *Fusobacterium nucleatum*, *Lactobacillus casei*, *Veillonella dispar*, *Neisseria subflava*, *Actinomyces naeslundii*, *Prevotella intermedia*, *Streptococcus sanguinis* and *Streptococcus mutans*. Some of these taxa are associated with gingivitis (Zee, 1996, Zee et al., 1996) and therefore, the aim was to determine their presence and amount in mucositis/peri-implantitis associated communities. Others are health associated and were used to report on health associated microbiota (Kumar et al., 2006). In addition to these, quantification of the total number of bacteria present was also evaluated. This would allow for the calculation of the proportion of each species within the community and allow comparison between the three conditions.

5.2 Materials & Methods

5.2.1 Preparation of DNA for standard curve generation

Depending on the specific target of the primers used for each PCR assay, a standard curve of bacterial genomic DNA from a known number of bacterial cells was created. One swab from a plate of each organism was suspended in 1 ml of RTF. The colony forming units in this culture were then enumerated by serial dilution and plating on fastidious anaerobic agar. Total nucleic acids were extracted from all samples according to the protocol of (Griffiths et al., 2000) (chapter 2, section 2.3.1.1.). In order to produce standard curves for the enumeration of microorganisms, purified DNA was used in the optimisation reactions from the following reference strains: *Fusobacterium nucleatum* (NCTC 10562), *Lactobacillus casei* (ATCC 334), *Veillonella dispar* (NCTC 11831), *Neisseria subflava* (DSM 17610), *Actinomyces naeslundii* (DSM 17233), *Prevotella intermedia* (DSM 20706), *Streptococcus sanguinis* (NCTC 02863) and *Streptococcus mutans* (ATCC 700610).

5.2.2 Quantitative PCR analysis of biofilm samples

One disc containing a biofilm from two CDFF experiments described previously in chapter 4 was used; this resulted in 15 sampling points from each of the two experiments. The samples used were from 6 h, 48 h, 96 h, 216h, 222 h, 246 h, 366 h, 390 h, 438 h, 510 h, 516 h, 540 h, 588 h, 612 h and 714 h biofilms.

Three triplex qPCR assays were designed to enumerate three organisms associated with gingivitis (*F. nucleatum*, *A. naeslundii*, *P. intermedia*); three organisms associated with oral health (*S. sanguinis*, *V. dispar*, *N. subflava*); and two organisms strongly implicated in dental caries (*S. mutans*, *L. casei*). A universal primers and probe was used to quantify the total number of cells.

5.2.3 Oligonucleotide primers and TaqMan probes

The specific primers and specific probes used for detection and quantification of microorganisms listed (Ciric et al., 2010) are shown in table 5.1. The dual labeled fluorogenic probes were single stranded oligonucleotides labeled with two different dyes. Reporter dyes included 6FAM, HEX and Cy5 and were located at the 5' end. The no fluorescent quenching molecule (black hole Quencher, BHQ™) was located at the 3' end (Livak et al., 1995). The length of amplicon for all assays was approximately 100 bp except for the universal amplicon which was approximately 450 bp (Table 1.5).

Chapter 5: Characterization of microcosm biofilm using multiplex qPCR

Table 5.1. Primers and probes used in the three triplex qPCR arrays. The triplex were composed of *F. nucleatum*, *L. casei* and *V. dispar* (FLV); *N. subflava*, *A. naeslundii* and *P. intermedia* (NAP); and *S. sanguinis*, *S. mutans* and universal (SSU) with few modifications to the assays previously reported (Ciric et al., 2010).

Assay	Organism	Sequence	Concentration (nM)	Annealing/extension temperature
FLV	<i>F. nucleatum</i>	F 5'-ACAATCCGAACTAAGAATAGTTTC-3' R 5'-GTCATCATGCCCTTACG-3' P 5'-6FAM-TCC[-A]CCT[-C][A][C]GG[+C]TTT-BHQ1-3'	900 900 50	113 bp
	<i>L. casei</i>	F 5'-AGAGTTGATCTGGCTCAG-3' R 5'-ACTCGTCCATGTTGAATCTC-3' P 5'-HEX-CGA[-T]CA[-T]CA[-A]CG[-A]G[-A]A[-C]TCG-BHQ1-3'	50 900 50	111 bp
	<i>V. dispar</i>	F 5'-CTAACATGGAGTTAATAGACGGAA-3' R 5'-CAGCTACGATCCGAACCTGAG-3' P 5'-Cy5-AGC[-A]A[-C]CCGA[-G]AA[-C][A]CT-BHQ2-3'	300 50 50	84 bp
	<i>N. subflava</i>	F 5'-AACGTATTACCGCAGTATG-3' R 5'-TGAGGCAATCTCACAAAC-3' P 5'-HEX-TGAC[-C][T][+G]CG[-A]TT[-A]CTAGCG-BHQ1-3'	900 300 100	110 bp
	<i>A. naeslundii</i>	F 5'-GAGCACGCCGCTCTGTA-3' R 5'-ACCTGCCGCCCTCGAA-3' P 5'-6FAM-CCTCGTCGCCACGGTGGTCA-BHQ1-3'	900 900 300	128 bp
	<i>P. intermedia</i>	F 5'-GCCTAACACCGATGTTGTC-3' R 5'-CGCACCAACAAAGCTATCAG-3' P 5'-Cy5-CA[-T][+C]CC[-A]TCC[-T]CC[-A]CC-BHQ2-3'	300 900 300	95 bp
SSU	<i>S. sanguinis</i>	F 5'-GTGTCATCAATTCCAGAAAAG-3' R 5'-ATTGGCTGATGTGGAGTC-3' P 5'-HEX-AGA[-T]GA[-C]CA[-C]CA[-C]CGT-BHQ1-3'	900 900 50	104 bp
	<i>S. mutans</i>	F 5'-TCACAGAAAAGACAAAGTTAC-3' R 5'-AACTACTAACCAAGGCCAAC-3' P 5'-Cy5-TA[-G]CC[-G]C[-A]GC[-A]TCA[-A]TG-BHQ2-3'	900 300 300	138 bp
	universal	F 5'-TCTTACGGGAGGCAGCAGT-3' R 5'-GGACTACCAGGGTATCTAATCCTGTT-3' P 5'-6FAM-CGTATTACCGCGGCTGCTGGCAC-BHQ1-3'	900 300 100	450 bp

5.2.4 QPCR assay

The universal primers and probe sets used were based on the original Lane sequences (Lane, 1991), as shown in Table 5.1.

All reactions were run in triplicate in a final volume of 25 µl. Sensimix Probe (Bioline) qPCR mastermix was used, together with the Rotor-gene 6500 (Qiagen) cycler using the green, yellow and red channels for data collection. Each reaction contained the concentration of the oligonucleotides as shown in Table 5.1.

The reaction conditions were performed as specified by the manufacturer with the annealing/extension temperature ranging from 60°C to 64°C. Data collection took place during the annealing/extension step. Species-specific primers and dual-labelled fluorogenic probes were designed for all organisms using 16S rRNA gene sequences. In order to produce standard curves for the enumeration of organisms, DNA extractions were performed on organisms that had been enumerated using viable counts making it possible to relate numbers of cells to volumes of DNA. DNA used in the optimisation reactions and for the running of standards was obtained from the reference strains. A

Chapter 5: Characterization of microcosm biofilm using multiplex qPCR

mixture of DNA from different strains was used for the reference and standard DNA in the universal assay. Standard curves consisting of eight 10-fold dilutions of reference DNA were run in triplex assays. The detection limit for each of the single taxon was accepted as 20 cells, as determined by Cricic et al. (2011).

5.2.5 Statistical analysis

Bonferroni test analysis was used to test whether changes in the numbers of individual taxa under the three growth conditions were significant (significant level when $P < 0.05$ and $P < 0.01$).

5.3 Results

5.3.1 Standard curve

Analysis of the standard curve can provide important information about the assay. The assays were initially validated from a serial dilution of high quality template. Each concentration was amplified in triplicate to determine reproducibility. The standard curve was constructed from a measure of threshold cycle (C_t) against log template quantity as shown in figure 5.1. The efficiency of the reaction was shown as being close to 100%. Reproducibility of the replicate reactions reflected assay stability, with R^2 values of 0.98 or above being indicative of a reliable or stable assay.

An optimised assay resulted in a standard curve with a slope between -3.2 and -3.5 as shown in figure 5.2. Reactions efficiencies were found to be 0.99 for *F. nucleatum*; *L. casei* 0.99; *V. dispar* 0.97; *N. subflava* 0.99; *A. naeslundii* 0.99; *P. intermedia* 0.96; *S. sanguinis* 0.99; *S. mutans* 0.94; and 0.92 for the universal.

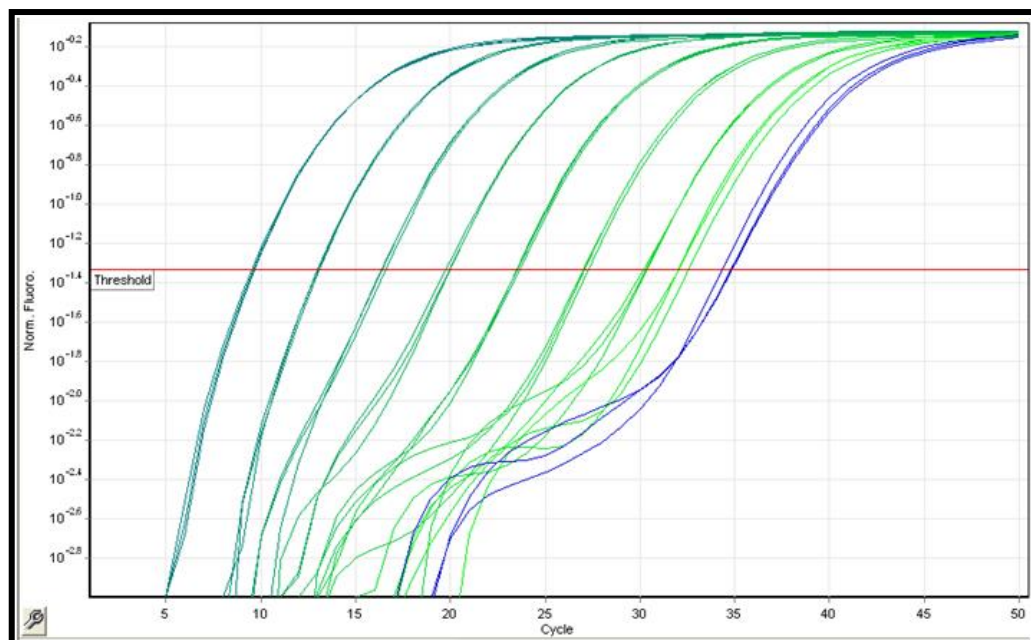


Figure 5.1. The standard curve of *L. casei* generated from a plot C_t against log concentration for eight 10-fold serial dilutions.

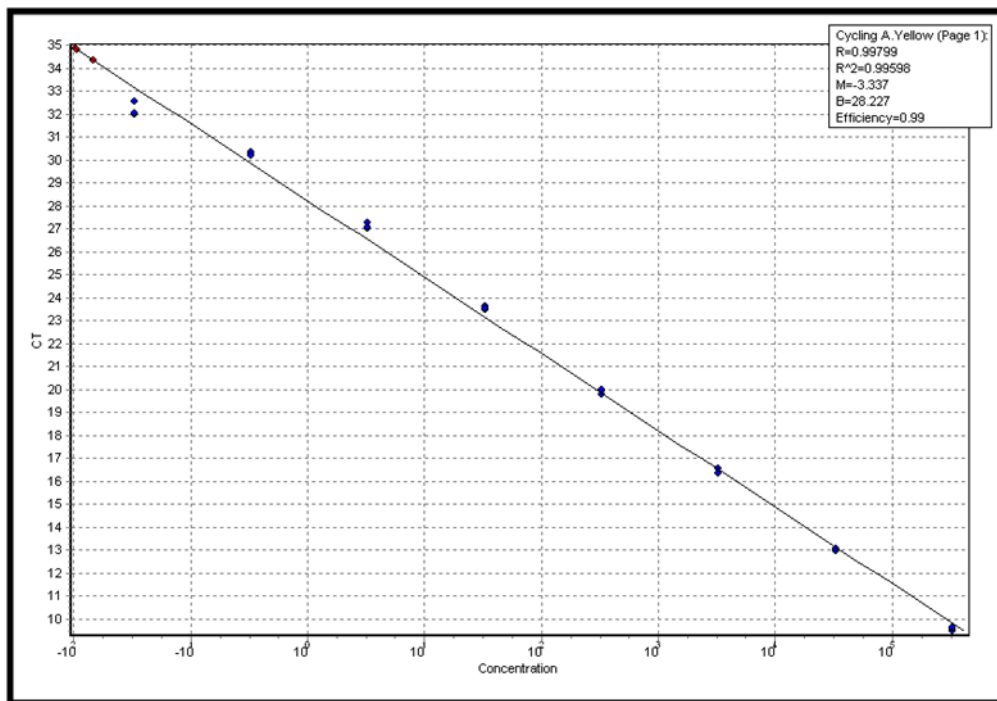


Figure 5.2. The linear slope of *L. casei*, with a slope of -3.337 and an R^2 of 0.99 for triplicate samples replicated three times.

5.3.2 Quantification of bacteria by qPCR

The total number of bacteria in each sample was quantified using universal probes and primers for the 16S rRNA gene. Following this, the number and proportion of each of the target species was investigated at each time point throughout the CDFF experiment (health, peri-implant mucositis and peri-implantitis). The results of this are shown in figures 5.3 – 5.10.

5.3.2.1 Detection of *Fusobacterium nucleatum*

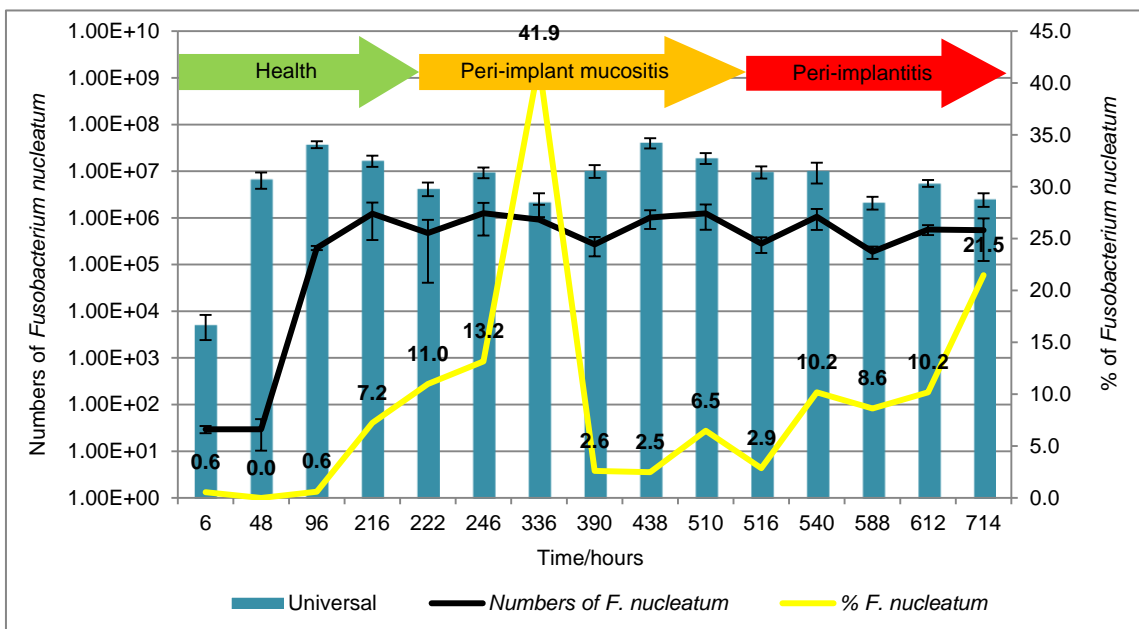


Figure 5.3. Total counts of bacteria obtained by qPCR represented by blue bars. Numbers of *F. nucleatum* obtained by qPCR are represented by the black line. The proportion of *F. nucleatum* is represented by the yellow line with data points labelled. At 222 h the environment was changed to a microaerophilic atmosphere with increased introduction of PISF. At 516 h, the change of environment to anaerobic atmosphere. *F. nucleatum* error bars represent standard deviation ($n = 6$). Universal error bars represent standard deviation ($n = 9$).

5.3.2.2 Detection of *Lactobacillus casei*

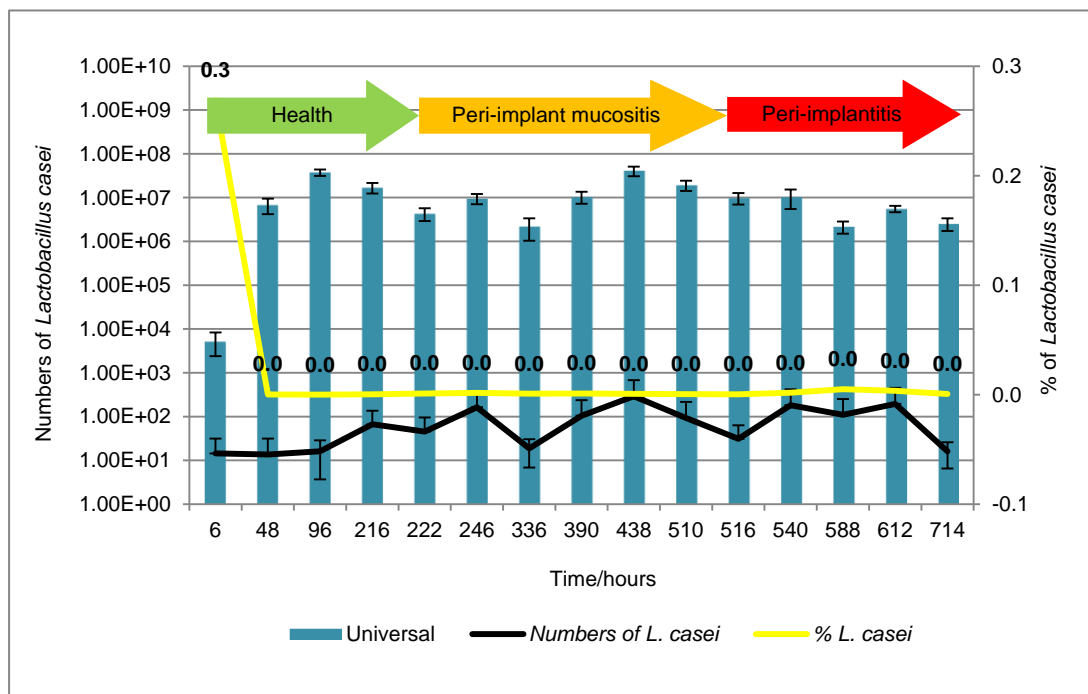


Figure 5.4. Total counts of bacteria obtained by qPCR represented by blue bars. Numbers of *L. casei* obtained by qPCR are represented by the black line. The proportions of *L. casei* are represented by the yellow line with data points labelled. At 222 h the environment was changed to a microaerophilic atmosphere with increased introduction of PISF. At 516 h, the change of environment to anaerobic atmosphere. *L. casei* error bars represent standard deviation ($n = 6$). Universal error bars represent standard deviation ($n = 9$).

5.3.2.3 Detection of *Veillonella dispar*

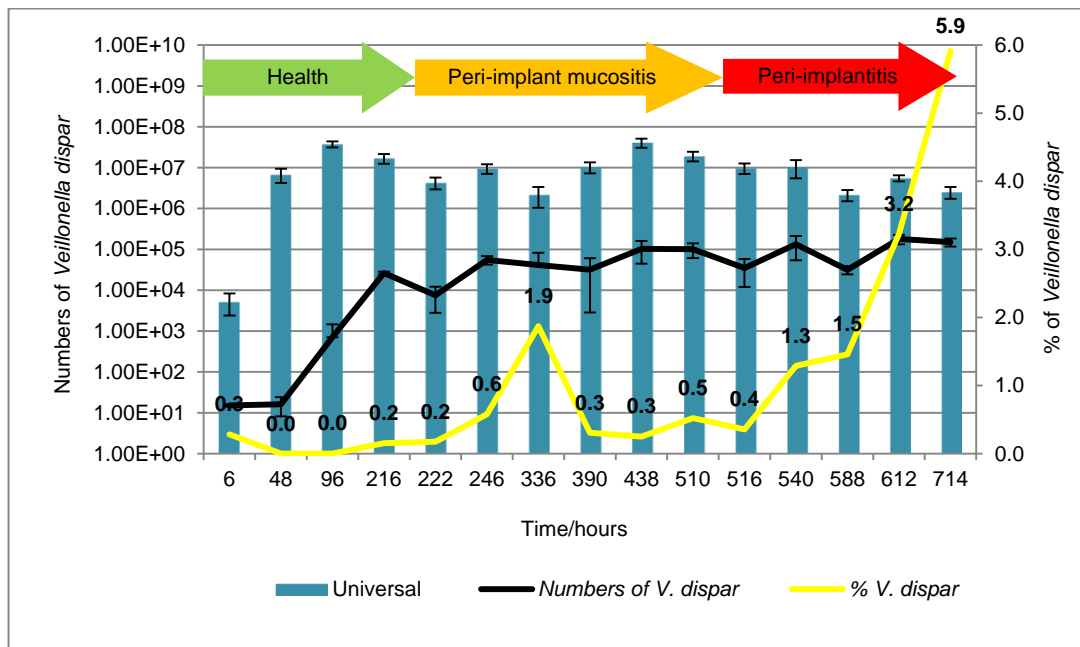


Figure 5.5. Total counts of bacteria obtained by qPCR represented by blue bars. Numbers of *V. dispar* obtained by qPCR are represented by the black line. The proportions of *V. dispar* are represented by the yellow line with data points labelled. At 222 h the environment was changed to a microaerophilic atmosphere with increased introduction of PISF. At 516 h, the change of environment to anaerobic atmosphere. *V. dispar* error bars represent standard deviation ($n = 6$). Universal error bars represent standard deviation ($n = 9$).

5.3.2.4 Detection of *Neisseria subflava*

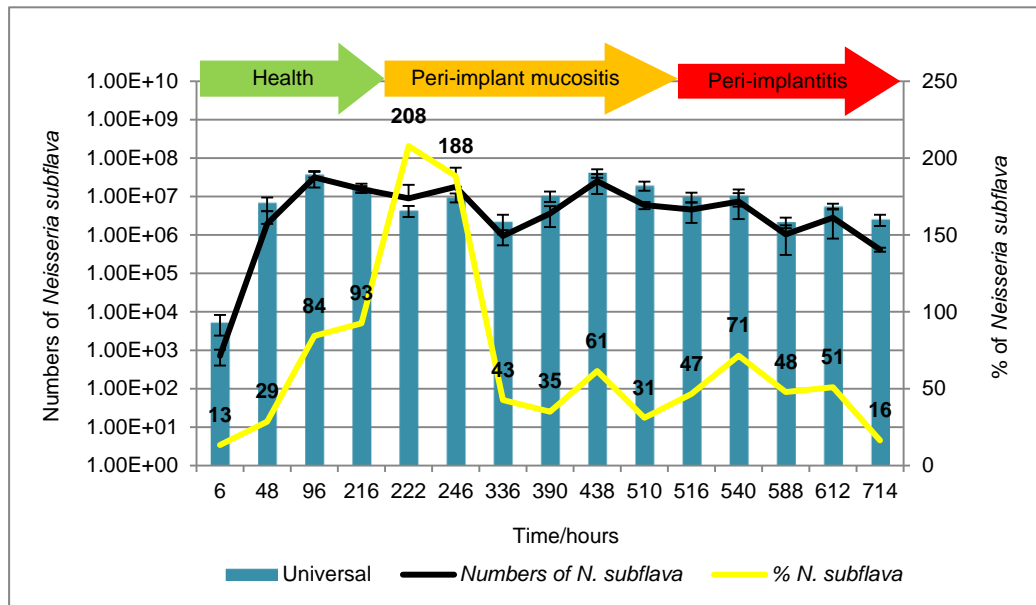


Figure 5.6. Total counts of bacteria obtained by qPCR represented by blue bars. Numbers of *N. subflava* obtained by qPCR are represented by the black line. The proportions of *N. subflava* are represented by the yellow line with data points labelled. At 222 h the environment was changed to a microaerophilic atmosphere with increased introduction of PISF. At 516 h, the change of environment to anaerobic atmosphere. *N. subflava* error bars represent standard deviation ($n = 6$). Universal error bars represent standard deviation ($n = 9$).

5.3.2.5 Detection of *Actinomyces naeslundii*

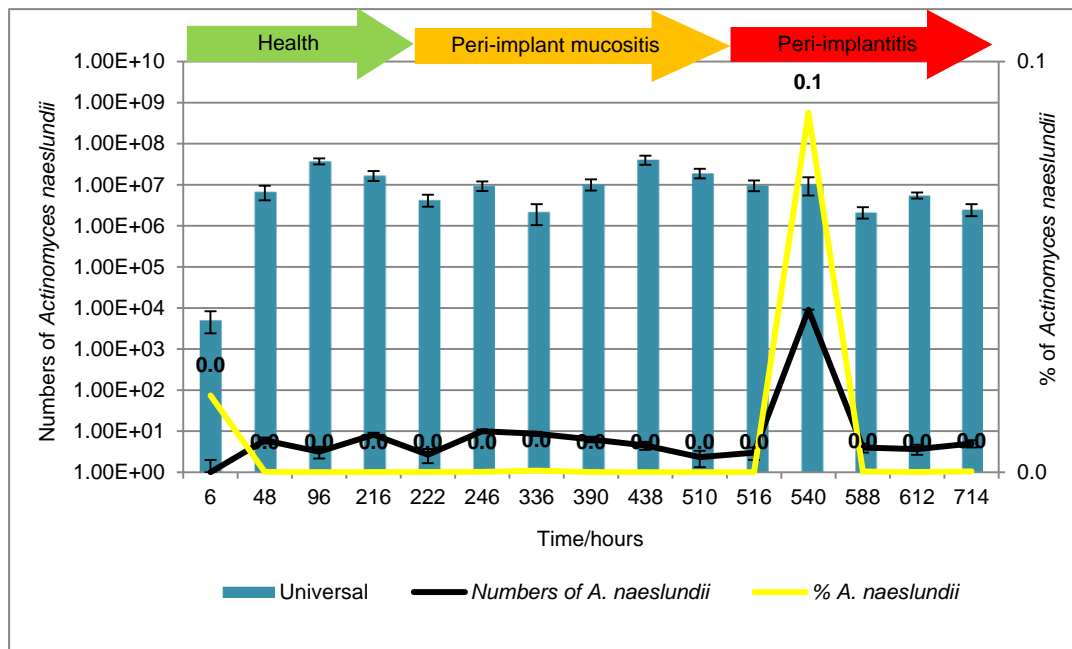


Figure 5.7. Total counts of bacteria obtained by qPCR represented by blue bars. Numbers of *A. naeslundii* obtained by qPCR are represented by the black line. The proportions of *A. naeslundii* are represented by the yellow line with data points labelled. At 222 h the environment was changed to a microaerophilic atmosphere with increased introduction of PISF. At 516 h, the change of environment to anaerobic atmosphere. *A. naeslundii* error bars represent standard deviation ($n = 6$). Universal error bars represent standard deviation ($n = 9$).

5.3.2.6 Detection of *Prevotella intermedia*

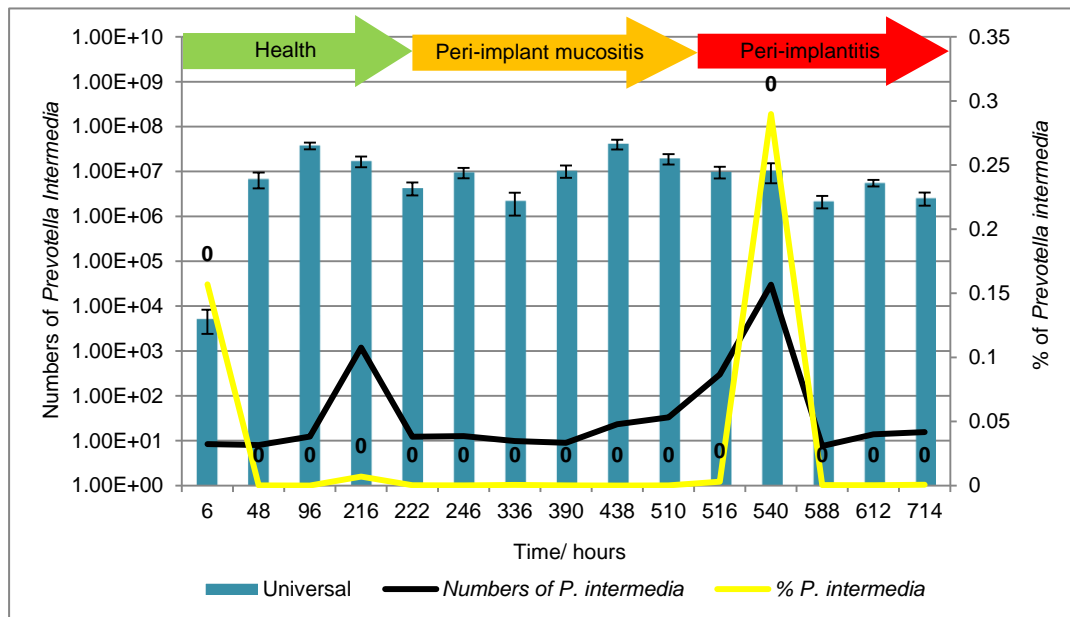


Figure 5.8. Total counts of bacteria obtained by qPCR represented by blue bars. Numbers of *P. intermedia* obtained by qPCR are represented by the black line. The proportions of *P. intermedia* are represented by the yellow line with data points labelled. At 222 h the environment was changed to a microaerophilic atmosphere with increased introduction of PISF. At 516 h, the change of environment to anaerobic atmosphere. *P. intermedia* error bars represent standard deviation ($n = 6$). Universal error bars represent standard deviation ($n = 9$).

5.3.2.7 Detection of *Streptococcus sanguinis*

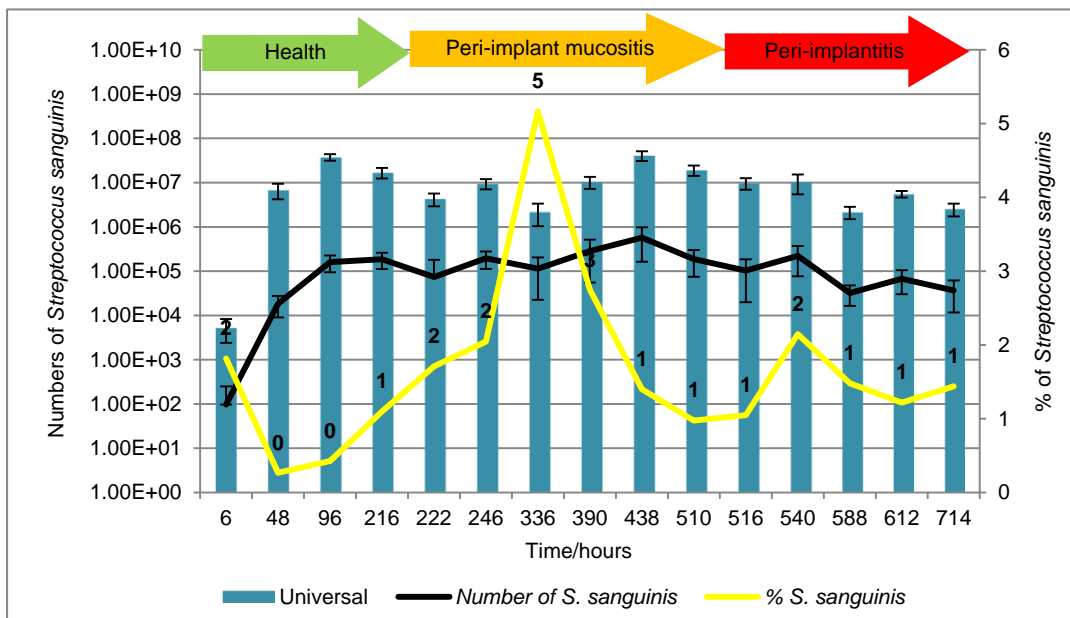


Figure 5.9. Total counts of bacteria obtained by qPCR represented by blue bars. Numbers of *S. sanguinis* obtained by qPCR are represented by the black line. The proportions of *S. sanguinis* are represented by the yellow line with data points labelled. At 222 h the environment was changed to a microaerophilic atmosphere with increased introduction of PISF. At 516 h, the change of environment to anaerobic atmosphere. *S. sanguinis* error bars represent standard deviation ($n = 9$). Universal error bars represent standard deviation ($n = 9$).

5.3.2.8 Detection of *Streptococcus mutans*

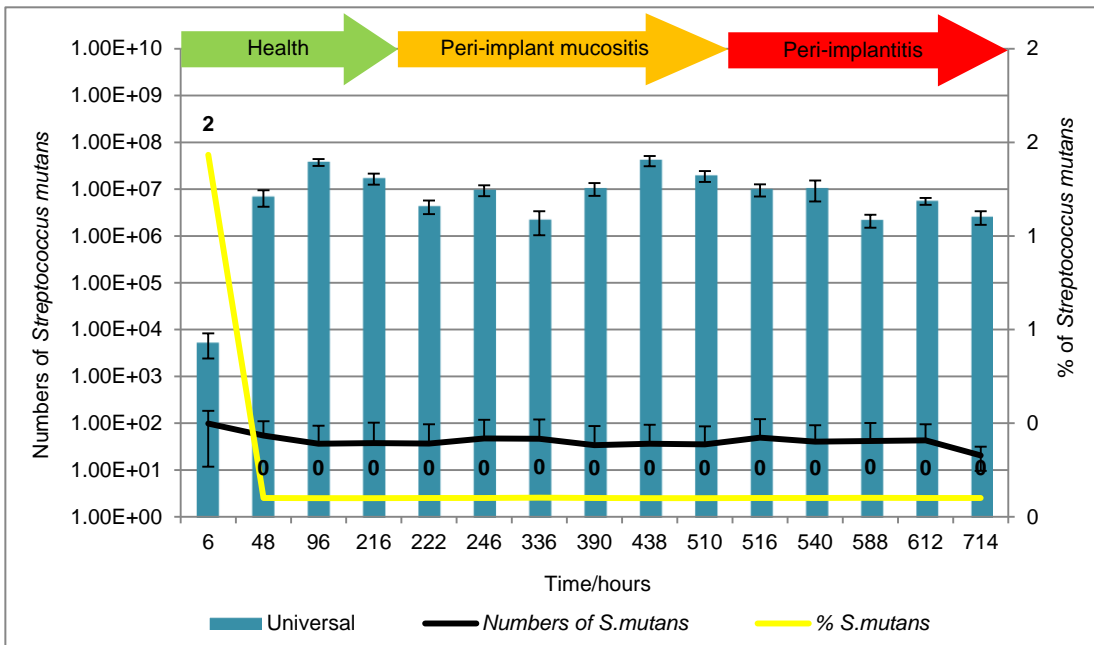


Figure 5.10. Total counts of bacteria obtained by qPCR represented by blue bars. Numbers of *S. mutans* obtained by qPCR are represented by the black line. The proportions of *S. mutans* are represented by the yellow line with data points labelled. At 222 h the environment was changed to a microaerophilic atmosphere with increased introduction of PISF. At 516 h, the change of environment to anaerobic atmosphere. *S. mutans* error bars represent standard deviation ($n = 9$). Universal error bars represent standard deviation ($n = 9$).

5.3.3 CDFF peri-implant biofilm communities

The data regarding the numbers of individual taxa were analysed and the total number of organisms present over the experiment is shown in tables 5.2, 5.3 and 5.4. Based on all the amplified taxa, the highest number of bacteria detected was 4.09×10^7 at 438 h, and the lowest number was 5.35×10^3 at 6 h.

Health communities: The most numerous bacteria were *N. subflava* (ca. 10^7 at 96 h – ca. 10^7 at 216 h), followed by *F. nucleatum* (ca. 10^5 at 96 h – ca. 10^6 at 216 h), *S. sanguinis* (ca. 10^5 at 96 h – ca. 10^5 at 216 h), *V. dispar* (ca. 10^2 at 96 h – ca. 10^4 at 216 h), *P. intermedia* (1.19×10^3 at 216 h), whilst *L. casei*, *S. mutans* and *A. naeslundii* were below the detection limit (< 20) as shown in table 5.2.

Peri-implant mucositis communities:

There was little change in total numbers of organisms present over time, the numbers increased from around 10^6 at the start of the experiment to around 10^7 cells per disc up to 222 hours and remained at this level throughout the experiment. The numbers of *L. casei*, *P. intermedia* and *A. naeslundii* were very low throughout the experiments. Other taxa increased after changing the environment conditions between 246 h and 438 h. For example, *N. subflava* (from 1.8 to 2.5×10^7), *F. nucleatum* (from 1.26×10^6 - 1.02×10^6), *V. dispar* (from ca. 10^4 to ca. 10^5), and *S. sanguinis* increased by 1 \log_{10} (ca. 10^5). *Streptococcus mutans* was detected in low levels at all the time points as shown in table 5.3.

Peri-implantitis communities:

The total number of organisms remained broadly steady over the duration of the experiment. The numbers of *L. casei* and *S. mutans* were at similar levels throughout the experiments. However, the numbers of *V. dispar* only increased by 1 \log_{10} throughout the experiment (from ca. 10^4 to ca. 10^5), numbers of *F. nucleatum*, *N. subflava* and *S. sanguinis* deceased by around 1 \log_{10} (ca. 10^6 , ca. 10^5 , ca. 10^4 , respectively). *Prevotella intermedia* and *A. naeslundii* were below the detection limit throughout, as shown in table 5.4.

Comparison of taxa numbers between communities: Statistical analysis using Bonferroni test showed there was a significant difference in the levels of *S. sanguinis* between health and peri-implant mucositis conditions ($P < 0.01$). There

Chapter 5: Characterization of microcosm biofilm using multiplex qPCR

was a significant difference in the numbers of *F. nucleatum*, *V. dispar*, *N. Subflava* between health and peri-implantitis conditions ($P < 0.01$). There was also a significant difference in the levels of *F. nucleatum*, *V. dispar*, *N. subflava* and *S. sanguis* between peri-implant mucositis and peri-implantitis conditions ($P < 0.01$).

Table 5.2. Numbers of each of the taxa investigated in microcosm biofilms samples under health conditions. \pm represents standard deviation.

Health	6 h	48 h	96 h	216 h
<i>F. nucleatum</i> <i>n</i> = 6	2.95×10^1 $\pm 5.09 \times 10$	2.95×10^1 $\pm 1.29 \times 10^1$	2.27×10^5 $\pm 2.34 \times 10^4$	1.23×10^6 $\pm 8.93 \times 10^5$
<i>L. casei</i> <i>n</i> = 6	Below the detection limit	Below the detection limit	Below the detection limit	6.65×10^1 $\pm 7 \times 10^1$
<i>V. dispar</i> <i>n</i> = 6	Below the detection limit	Below the detection limit	7.06×10^2 $\pm 7.63 \times 10^2$	2.63×10^4 $\pm 2.16 \times 10^3$
<i>N. subflava</i> <i>n</i> = 6	7.17×10^2 $\pm 3.17 \times 10^2$	1.94×10^6 $\pm 2.22 \times 10^6$	3.17×10^7 $\pm 1.46 \times 10^7$	1.57×10^7 $\pm 2.91 \times 10^6$
<i>A. naeslundii</i> <i>n</i> = 6	Below the detection limit			
<i>P. intermedia</i> <i>n</i> = 6	Below the detection limit	Below the detection limit	Below the detection limit	1.19×10^3 $\pm 1.27 \times 10^3$
<i>S. sanguinis</i> <i>n</i> = 9	9.73×10^1 $\pm 1.52 \times 10^2$	1.83×10^4 $\pm 9.27 \times 10^3$	1.60×10^5 $\pm 6.57 \times 10^4$	1.87×10^5 $\pm 7.64 \times 10^4$
<i>S. mutans</i> <i>n</i> = 9	9.82×10^1 $\pm 8.64 \times 10^1$	5.46×10^1 $\pm 5.6 \times 10^1$	3.66×10^1 $\pm 5.15 \times 10^1$	3.77×10^1 $\pm 6.52 \times 10^1$
Universal <i>n</i> = 9	5.35×10^3 $\pm 2.95 \times 10^3$	6.81×10^6 $\pm 2.62 \times 10^6$	3.75×10^7 $\pm 6.32 \times 10^6$	1.70×10^7 $\pm 4.56 \times 10^6$

Table 5.3. Numbers of each of the taxa investigated in microcosm biofilms samples under peri-implant mucositis conditions.
 ± represents standard deviation.

Peri-implant mucositis	222 h	246 h	336 h	390 h	438 h	510 h
<i>F. nucleatum</i>	4.73×10^5 ± 4.33×10^5	1.26×10^6 ± 8.38×10^5	9.22×10^5 ± 9.85×10^5	2.69×10^5 ± 1.2×10^5	1.02×10^6 ± 4.39×10^5	1.25×10^6 ± 6.94×10^5
<i>L. casei</i>	4.52×10^1 ± 5.07×10^1	1.63×10^2 ± 2.07×10^2	Below the detection limit	1.04×10^2 ± 1.32×10^2	2.92×10^2 ± 3.86×10^2	9.3×10^1 ± 1.23×10^2
<i>V. dispar</i>	7.51×10^3 ± 4.72×10^3	5.53×10^4 ± 1.29×10^4	4.12×10^4 ± 4.13×10^4	3.18×10^4 ± 2.9×10^4	1.02×10^5 ± 5.79×10^4	1.01×10^5 ± 3.97×10^4
<i>N. subflava</i>	8.97×10^6 ± 1.13×10^7	1.8×10^7 ± 3.83×10^7	9.39×10^5 ± 4.01×10^5	3.63×10^6 ± 2.02×10^6	2.51×10^7 ± 1.34×10^7	5.99×10^6 ± 1.27×10^6
<i>A. naeslundii</i>	Below the detection limit					
<i>P. intermedia</i>	Below the detection limit	Below the detection limit	Below the detection limit	Below the detection limit	2.33×10^1 ± 1.3×10^1	3.32×10^1 ± 9.22×10^0
<i>S. sanguinis</i>	7.37×10^4 ± 1.07×10^5	1.95×10^5 ± 8.26×10^4	1.14×10^5 ± 9.11×10^4	2.85×10^5 ± 2.3×10^5	5.72×10^5 ± 4.09×10^5	1.88×10^5 ± 1.13×10^5
<i>S. mutans</i>	3.68×10^1 ± 5.79×10^1	4.73×10^1 ± 7.08×10^1	4.64×10^1 ± 7.36×10^1	3.39×10^1 ± 5.32×10^1	3.66×10^1 ± 5.61×10^1	3.53×10^1 ± 5.04×10^1
Universal	4.31×10^6 ± 1.39×10^6	9.55×10^6 ± 2.5×10^6	2.2×10^7 ± 1.16×10^6	1.04×10^7 ± 3.16×10^6	4.09×10^7 ± 1.02×10^7	1.93×10^7 ± 5.07×10^6

Table 5.4. Numbers of each of the taxa investigated in microcosm biofilms samples under peri-implantitis conditions. \pm represents standard deviation.

Peri-implantitis	516 h	540 h	588 h	612 h	714 h
<i>F. nucleatum</i>	2.81×10^5 $\pm 1.04 \times 10^5$	1.05×10^6 $\pm 5.02 \times 10^5$	5.87×10^5 $\pm 5.49 \times 10^4$	5.65×10^5 $\pm 1.35 \times 10^5$	5.47×10^5 $\pm 4.28 \times 10^5$
<i>L. casei</i>	3.1×10^1 $\pm 3.21 \times 10^1$	1.83×10^2 $\pm 2.38 \times 10^2$	1.1×10^2 $\pm 1.41 \times 10^2$	1.95×10^2 $\pm 2.57 \times 10^2$	1.62×10^1 $\pm 9.66 \times 10$
<i>V. dispar</i>	3.5×10^4 $\pm 2.30 \times 10^4$	1.34×10^5 $\pm 7.96 \times 10^4$	3.17×10^4 $\pm 7.3 \times 10^3$	1.79×10^5 $\pm 4.65 \times 10^4$	1.51×10^5 $\pm 3.39 \times 10^4$
<i>N. subflava</i>	4.57×10^6 $\pm 2.51 \times 10^6$	7.41×10^6 $\pm 4.82 \times 10^6$	1.04×10^6 $\pm 7.37 \times 10^5$	2.83×10^6 $\pm 2.02 \times 10^6$	4.16×10^5 $\pm 5.01 \times 10^4$
<i>A. naeslundii</i>	Below the detection limit	9.07×10^3 $\pm 1.28 \times 10^4$	Below the detection limit	Below the detection limit	Below the detection limit
<i>P. intermedia</i>	2.99×10^2 $\pm 2.52 \times 10^2$	3×10^4 $\pm 3.29 \times 10^4$	Below the detection limit	Below the detection limit	Below the detection limit
<i>S. sanguinis</i>	1.03×10^5 $\pm 8.3 \times 10^4$	2.23×10^5 $\pm 1.46 \times 10^5$	3.21×10^4 $\pm 1.57 \times 10^4$	6.76×10^4 $\pm 3.75 \times 10^4$	3.67×10^4 $\pm 2.5 \times 10^4$
<i>S. mutans</i>	4.93×10^1 $\pm 7.24 \times 10^1$	4.04×10^1 $\pm 5.03 \times 10^1$	4.16×10^1 $\pm 5.99 \times 10^1$	4.29×10^1 $\pm 5.17 \times 10^1$	2.06×10^1 $\pm 1.1 \times 10^1$
Universal	9.81×10^6 $\pm 2.85 \times 10^6$	1.04×10^7 $\pm 4.9 \times 10^6$	2.17×10^6 $\pm 6.69 \times 10^5$	5.55×10^6 $\pm 9.34 \times 10^5$	2.55×10^6 $\pm 8.25 \times 10^5$

5.4 Discussion

Microcosm plaque biofilms grown in the CDFF on titanium (Ti) discs had previously been characterized by direct amplification and cloning of 16S rRNA genes (see chapter 4 section 4.3.6). The species detected by cloning, included *Streptococcus* spp. and *Neisseria* spp. under health conditions, but these changed to *Neisseria* spp., *F. nucleatum*, *Veillonella* spp. and *Capnocytophaga* spp. under peri-implant mucositis. Further changes occurred under peri-implantitis conditions when *Capnocytophaga* spp. and *Veillonella* spp. were also detected. Although this provided insight into the community, there was no way of quantifying the numbers of these species. Therefore, to characterize these changes further, a quantitative PCR method for specific species was chosen.

The triplex qPCR method was designed to enumerate eight microorganisms; whilst a universal probe served to enumerate all microorganisms and allow for the calculation of the proportions of each taxon within the total community (Circic et al., 2010). To create higher specificity and efficiency in multiplex reactions, locked nucleic acid (LNA) was used. LNA is nucleic acid that contains a 2'-O, 4'-C methylene bridge (Circic et al., 2010). All assays contained locked nucleic acid except for the assay of *A. naeslundii* and the universal standard dual-labelled fluorogenic probes (see table 5.1).

In this study, all reactions efficiencies were found to be $\geq 97\%$, with the exception of the universal assays, where the efficiency was 92%. The reason for the lower efficiency of the universal assay could be due to the length of the amplicons (Circic et al., 2010), which was approximately 450 bp in comparison to the other amplicons which were approximately 100 bp.

The bacterial community found in saliva was dominated by *V. dispar*, *N. subflava*, *F. nucleatum*, *A. naeslundii*, and *S. sanguinis*. These taxa have been observed in previous culture independent studies and are associated with healthy dental plaque biofilms (Kumar et al., 2006). Two studies have shown that the dominant phyla in saliva were Firmicutes, Bacterioidetes, Proteobacteria, Actinobacteria, and Fusobacteria by culture independent methods (Price et al., 2007, Keijser et al., 2008). The triplex qPCR method had previously shown similar a similar picture: the Firmicutes were the dominant organisms, followed by Proteobacteria, Fusobacteria, Actinobacteria, and Bacterioidetes (Circic et al., 2010).

Neisseria subflava is a bacterial species that is amongst one of the earliest colonisers, and are generally aerobic although their growth is stimulated by CO₂ and retarded under anaerobic conditions. In this present study, differences in the proportions of *N. subflava* were seen between health and peri-implantitis conditions and also between peri-implant mucositis and peri-implantitis conditions (P < 0.01). Numbers of *N. subflava* were significantly higher in numbers at 96 h under health conditions and reduced under peri-implant mucositis after 336 h, recovering slightly under peri-implantitis conditions.

Streptococcus sanguinis counts were 1.57×10^7 ($\pm 2.91 \times 10^6$) at 216 h, and these numbers remained similar under peri-implant mucositis (438 h) at 1.88×10^5 ($\pm 1.13 \times 10^5$). The streptococci possess adherence and metabolic capacities that enable them to colonize a wide structure of oral cavity sites (Nobbs et al., 2009). It can be hypothesised that the growth of the pioneer community (such as *S. sanguinis* and others) altered the environment in a number of ways. These may include oxygen utilisation, the production of reducing compounds, and the excretion of metabolic end-products.

Veillonella dispar is able to coaggregate with a variety of oral bacteria including species belonging to the genera *Streptococcus*, *Fusobacterium*, *Neisseria* and *Actinomyces* (Bradshaw et al., 1996). *Veillonella dispar* levels were shown to be significantly different between health and peri-implantitis and between peri-implant mucositis and peri-implantitis (P < 0.01).

Some of the taxa investigated were only detected at low levels, including *P. intermedia*, *L. casei*, *S. mutans*, and *A. naeslundii*. *Actinomyces naeslundii* is known to be one of the early colonizers in the formation of dental plaque (Mombelli, 1987). It is likely that the environmental conditions within the CDFF experiments were not optimal for these taxa.

Streptococcus mutans was detected at very low levels from microcosm plaque samples (Tables 5.2-5.4), representing a very small proportion (less than ca 0.1%) of the total bacteria detected. Heuer et al. (2012) reported the absence of *S. mutans* around the abutment of dental implants using culture independent methods. The lack of glucose or sucrose could be the cause for the low detection of rates of these organisms (Circi et al., 2010). *Prevotella intermedia* are more commonly isolated from dental plaque after the development of peri-implant disease (Mombelli et al., 1995). Serum is a constituent of gingival crevicular fluid (PISF) and has been shown to enhance the growth of *Prevotella* spp. and *P. gingivalis* (ter Steeg et al., 1987). *Prevotella intermedia* is an oral pathogen and

that is not usually found in high proportions in healthy oral environments. The proportions of *P. intermedia* at all time points in this study were very low. This finding is not in agreement with others who found high levels of *P. intermedia* associated with failing implants (Becker et al., 1991, Rosenberg et al., 1991, Augthun and Conrads, 1997, Mombelli, 2002, Leonhardt et al., 1995).

Fusobacterium nucleatum numbers increased slightly once environmental conditions mimicking peri-implant mucositis occurred. The proportion of *F. nucleatum* increased at 336 h then reduced and recovered again at 714 h. There was a significant difference in the levels of *F. nucleatum* between health and peri-implantitis and between peri-implant mucositis and peri-implantitis conditions. This may be due to the introduction of the large proteinaceous nutrients (e.g., amino acids and oligonucleotide peptides) present in PISF which could be exploited by this species. For protein-derived nutrients, *F. nucleatum* is often associated with peri-implantitis and is frequently cultivated from the surfaces of dental implants which have lost osseointegration (Mombelli, 1987). *Fusobacterium nucleatum* is considered an important organism in the formation of dental plaque and acts as a bridging organism between primary and late colonisers (Bradshaw and Marsh, 1999).

Lactobacillus casei was detected in low proportions, which was in agreement with the previous data of cloning and comparative sequencing (chapter 4). Also, dental implants associated with either with health or diseases do not usually harbour *L. casei* (Kumar et al., 2012, Al-Radha et al., 2012). Furthermore, whilst *L. casei* are commonly isolated from the oral cavity they usually only compromise less than 1% of the total cultivable microorganisms (Marsh, 2010).

The species found in consistently high numbers from the beginning of all of the experiments were *N. subflava*, *S. sanguinis*, and *V. dispar*. All of these species have been shown to be early colonizers during the formation of dental plaque as well as being among the most abundant taxa in the oral microbiota (Marsh, 2003, Zaura et al., 2009, Keijser et al., 2008). The prevalence of *Actinomyces* spp., *Lactobacillus* spp., *Prevotella* spp., and *F. nucleatum* is known to increase during inflammation of gingiva at the expense of *Streptococcus* spp. (Syed and Loesche, 1978, Moore and Moore, 1994). In the current study, the numbers of *F. nucleatum* increased over time under peri-implant mucositis and peri-implantitis conditions and *S. sanguinis* numbers declined after an initial peak coinciding with the *F. nucleatum* increase (Tables 5.3, 5.4).

5.6 Conclusions

The qPCR findings were in agreement with 16S rRNA gene cloning and sequence data generated in chapter 4. The multi-triplex qPCR method allowed for the quick and efficient targeted analysis of the microbial community structure present in health and disease conditions associated with dental implants. Indeed, using qPCR it was possible to differentiate between the taxa in health and peri-implantitis and between peri-implant mucositis and peri-implantitis conditions. The use of qPCR to assess the species numbers of these populations allows particular organisms to be assessed more accurately than they can be by cultural analysis.

As the most abundant microbiota determined using comparative 16S rRNA gene cloning and sequencing was *Capnocytophaga* species, it was deemed to be beneficial to develop a probe and specific primers for quantifying of *Capnocytophaga* from three dental implant conditions biofilms. This research will be discussed in the next chapter.

Chapter 6
Design and evaluation of a quantitative PCR assay for the detection of
***Capnocytophaga* spp.**

6.1 Introduction

Many facultative anaerobic species have been implicated in peri-implantitis (Mombelli, 1987, Bower, 1996). Of these, several studies have reported the isolation of *Capnocytophaga* spp. from peri-implantitis sites (Sanz et al., 1990, Mombelli, 1987, Apse et al., 1989, Augthun and Conrads, 1997, Fardal et al., 1999, Renvert et al., 2007). The genus *Capnocytophaga*, first proposed by Leadbetter et al. (1979) consists of five species: *C. gingivalis*, *C. ochracea*, *C. sputigena*, *C. granulosa*, and *C. haemolytica*, all of which can be isolated from the human oral cavity (Ciantar et al., 2001a). Another species, *Capnocytophaga cynodegmi*, is also present in the normal flora. Both can cause wound infections in humans after animal bite, *C canimorsus* being associated with more severe infections (Brenner et al., 1989).

They comprise a group of capnophilic/facultative anaerobic Gram-negative, fusiform rods. *Capnocytophaga* spp. manifest various features particularly their ability to adhere and co-aggregate with other bacteria, an important feature in biofilm formation. As well as being associated with peri-implantitis. Salvi et al. (2008) also showed that *Capnocytophaga sputigena* could be isolated from healthy implants. As stated by Socransky and Haffajee (1992), it is vital for pathogens to be present at the inception of periodontal diseases, however, the development of disease will not take place as long as the species does not exceed the threshold for the host. Indeed, It has been established that the mean number of target bacteria and others were involved in infection is higher in infected implants compared with healthy areas (van Winkelhoff and Wolf, 2000). Importantly, most of the periodontal microbiota can be found in healthy individuals, although in smaller numbers and lower proportions (Ximénez-Fyvie et al., 2000).

Recently, the TaqMan qPCR technique has been used as described in detail in Chapter 5 (Suzuki et al., 2004). This method allows the detection and quantification of specific nucleic acid sequences. It offers a sensitive, efficient, and reliable approach to quantitation. The specificity and sensitivity of qPCR allows it to be used to amplify and quantify targeted DNA from any DNA source. Using the TaqMan system, it is easy to establish the total number of bacterial cells present in samples directly, without culturing, and is useful for detecting species that are difficult to grow in culture (D'Ercole et al., 2008). Furthermore, qPCR results can be obtained in 6-8 hours from sampling compared with up to 14 days by culture (Suzuki et al., 2004). qPCR has been used for the

identification of *P. gingivalis* (Boutaga et al., 2003, Sakamoto et al., 2002), *A. actinomycetemcomitans* (Sakamoto et al., 2001, Jervøe-Storm et al., 2005), *T. denticola* (Sakamoto et al., 2001, Asai et al., 2002, Yoshida et al., 2004) and *T. forsythensis* (Jervøe-Storm et al., 2005), *P. intermedia*, *F. nucleatum*, *P. gingivalis* and *T. forsythensis* (Jervøe-Storm et al., 2005). In previous chapters, the microbial components of the biofilm community have been observed by CLSM, cultured on nutrient agars and detected and identified by 16S rRNA gene cloning and sequencing. The 16S rRNA gene cloning presented in Chapter 4 showed that *Capnocytophaga* spp. seemed to increase under peri-implantitis conditions. Therefore, the main goal of this chapter was to develop a specific TaqMan qPCR assay for detection, identification and quantification of *Capnocytophaga* spp. from microcosm biofilms on titanium surfaces at different ages representing health and disease conditions. This work is the first to develop, design and optimise a specific probe and primers for quantification of *Capnocytophaga* species.

6.2 Materials and Methods

6.2.1 Evaluation of qPCR primers

6.2.1.1 Bacterial strains and culture conditions

Capnocytophaga ochracea ATCC 33596 (MLC 23/38) was used as the test microorganisms in this study. The bacterial strain was grown on fastidious anaerobic agar (Lab M) with 5% defibrinated horse blood (E and O Laboratories, Bonnybridge, UK) for 3 to 4 days at 37°C under anaerobic conditions. In addition, the following closely and more distantly related reference strains were used as negative controls: *Fusobacterium nucleatum* (NCTC 10562), *Lactobacillus casei* (ATCC 334), *Veillonella dispar* (NCTC 11831), *Neisseria subflava* (DSM 17610), *Actinomyces naeslundii* (DSM 17233), *Prevotella intermedia* (DSM 20706), *Streptococcus sanguinis* (NCTC 02863), *Streptococcus mutans* (ATCC 700610), *Porphyromonas gingivalis* (DSM 20709), *Tannerella forsythia* (ATCC 43037) and *Aggregatibacterium actinomycetemcomitans* (ATCC 33384).

6.2.1.2 Design of oligonucleotide primers

The 16S rRNA gene sequences of the oral *Capnocytophaga* species were retrieved from the Ribosomal data base (<http://rdp.cme.msu.edu/>). These sequences were aligned using Clustal w2 (<http://www.ebi.ac.uk/Tools/msa/clustalw2/program>). Clustal format files were aligned using a portion of the 16S rRNA gene containing the amplicon for *Capnocytophaga* species. A 100% sequence identity was observed for all 8 species. On the basis of the sequence alignments of specific regions from different strains, a conserved sequence region for each bacterium was selected for designing the PCR primers using primer 3 version 4.0 (<http://frodo.wi.mit.edu/primer3/>). Confirmation of the primer specificity was performed by blast (www.ncbi.nlm.nih.gov/blast) while probe specificity to the region of interest was confirmed using probe check (<http://131.130.66.200/cgi-bin/probecheck/probecheck.pl>; figures 6.1, 6.2 and table 6.1).

The 6-carboxyfluorescein (6-FAM) molecule was located at the 5' end of the probe and the no fluorescent quenching molecule (black hole Quencher, BHQ™) was located at the 3' end (Livak et al., 1995). The primers listed in table 6.1 were tested for their signalling specificity for their target using conventional PCR using SYBR Green I (section 6.2.1.4). The sequence for primers and probe was employed with locked nucleic acid with their final concentrations as shown in table 6.2. These primers were specific when assessed by conventional PCR and

Chapter 6: Design novel specificTaqMan probe and primers

with TaqMan probe using qPCR using TaqMan probe. Analysis of the melting curves showed no production of non-specific products which would interfere with obtaining accurate results (Tables 6.2; figures 6.1 to 6.4).

Table 6.1. Lists of primers based on 16S rRNA gene sequence were designed in this study for detection and quantification of *Capnocytophaga* species.

Primer	Length	Sequence 5'- 3'	bp	T _m °C
Forward	23	GGAATCATTGGGTTAAAGGGTC	143	65.1
Reverse	22	GCATTTCACCGCTACACTACAC		63.4
Forward	21	GACTGCCTTATGGGTTGTAAA	147	59.2
Reverse	18	GATAACGCTCGCATCCTC		59
Forward	20	GCTGGAATCGCTAGTAATCG	188	61.3
Reverse	18	ACGGCTAGGTTGTTACGA		58.3
Forward	24	ATAGCGAAGGCATATTACTAACAA	142	59.7
Reverse	21	TAGCCACTCAGATTACTCCAA		59

Table 6.2. Sequences of primers and probe were used with final concentration.

Primers	Sequence 5'- 3'	nM	bp	T _m °C
Forward	CTCCTACGGGAGGCAGCAG	300 nM	224	67.3
Reverse	ATCATTGGGTTAAAGGG	900 nM		56.3
Probe	6FAM AAGG[+G]AA[+G]AA[+T]AA[+G]GG[+C]TBHQ1	200 nM		

Chapter 6: Design novel specificTaqMan probe and primers

CTCTCTACGGGAGGCAGCAG	
Cochracea	GGATGTCCCCCACACTGGTACTGAGATAACGGACAGACTCTACGGAGGCAGCAGTGAG 349
Csputigena	GGATGTCCCCCACACTGGTACTGAGATAACGGACAGACTCTACGGAGGCAGCAGTGAG 349
Cleabetteri	GGATATCCCCCACACTGGTACTGAGATAACGGACAGACTCTACGGAGGCAGCAGTGAG 323
Chaemolytica	GGATGTCCCCCACACTGGTACTGAGATAACGGACAGACTCTACGGAGGCAGCAGTGAG 264
Ccynodegmi	GGATGTCCCCCACACTGGTACTGAGACACGGACAGACTCTACGGAGGCAGCAGTGAG 319
Canimorsus	GGAGGTCCCCCACACTGGTACTGAGACACGGACAGACTCTACGGAGGCAGCAGTGAG 311
Cgingivalis	GGAGATCCCCCACACTGGTACTGAGACACGGACAGACTCTACGGAGGCAGCAGTGAG 347
Cgranulosa	GGAGATCCCCCACACTGGTACTGAGACACGGACAGACTCTACGGAGGCAGCAGTGAG 300

Cochracea	GAATATTGGACAATGGTCGGAAGACTGATCCAGCCATGCCCGGTGCAAGGATGACTGCC-T 408
Csputigena	GAATATTGGACAATGGTCGGAAGACTGATCCAGCCATGCCCGGTGCAAGGATGAGGTC-C 408
Cleabetteri	GAATATTGGACAATGGTCGGAAGACTGATCCAGCCATGCCCGGTGCAAGGAAAGACGGCC-T 382
Chaemolytica	GAATATTGGTCAATGGTCGGAAGACTGAAACAGCCATGCCCGGTGCAAGGATGACCGGCC-T 323
Ccynodegmi	GAATATTGGACAATGGTCGGAAGACTGATCCAGCCATGCCCGGTGCAAGGATGACCGGCC-T 378
Canimorsus	GAATATTGGACAATGGTCGGAAGACTGATCCAGCCATGCCCGGTGCAAGGATGACCGGCC-T 370
Cgingivalis	GAATATTGGTCAATGGTCGGAAGACTGAAACAGCCATGCCCGGTGCAAGGAAATGCC-T 406
Cgranulosa	GAATATTGGTCAATGGTCGGAAGACTGAAACAGCCATGCCCGGTGCAAGGAAATGCC-T 359
***** TAAGG[-G]AA[-G]AA[-T]AA[-G]GG[-C]T *****	
Cochracea	TAT-GGGTTGTAACACTGCTTTGTAAGGAAAGATAAGGGTACGGCTAGTTGATGACG 467
Csputigena	TAT-GGGTTGTAACACTGCTTTGTAAGGAAAGATAAGGGTACGGTACTCTGATGACG 467
Cleabetteri	TAT-GGGTTGTAACACTGCTTTGCAAGGGAAAGATAAGGACTACGAGTAGTTGATGACG 441
Chaemolytica	TAT-GGGTTGTAACACTGCTTTGATGGGAAGATAAGGGTACGGTACTCTGATGACG 382
Ccynodegmi	TAT-GGGTTGTAACACTGCTTTGATGGGAAGATAAGGTCTACGGTGTAGATTGATGACG 437
Canimorsus	TAT-GGGTTGTAACACTGCTTTATACAGGAAAGATAAGGTCTACGGTGTAGATTGATGACG 429
Cgingivalis	TAT-GGGTTGTAACACTGCTTTATGGGAAGATAAGGTGTACGGTGTACATTGATGACG 465
Cgranulosa	TAT-GGGTTGTAACACTGCTTTATGGGAAGATAAGGACTACGGTGTACGGTGTACATTGATGACG 418

Cochracea	GTACCTTACGAAATAAGCATCGCTAACCTCGTGCAGCAGCCCGGTAAACGGAGGATG 527
Csputigena	GTACCTTACGAAATAAGCATCGCTAACCTCGTGCAGCAGCCCGGTAAACGGAGGATG 527
Cleabetteri	GTACTCTCGGAATAAGCATCGCTAACCTCGTGCAGCAGCCCGGTAAACGGAGGATG 501
Chaemolytica	GTACTATGAAATAAGCATCGCTAACCTCGTGCAGCAGCCCGGTAAACGGAGGATG 442
Ccynodegmi	GTACCATACGAAATAAGCATCGCTAACCTCGTGCAGCAGCCCGGTAAACGGAGGATG 497
Canimorsus	GTACTATGAAATAAGCATCGCTAACCTCGTGCAGCAGCCCGGTAAACGGAGGATG 489
Cgingivalis	GTACCATATGAAATAAGCATCGCTAACCTCGTGCAGCAGCCCGGTAAACGGAGGATG 525
Cgranulosa	GTACCATATGAAATAAGCATCGCTAACCTCGTGCAGCAGCCCGGTAAACGGAGGATG 478
***** ATCATGGGTTAAAGGG *****	
Cochracea	CGAGCOTTATCCCGAATCATGGGTTAAAGGCTCGTAGGCCGGCTAATAAGTCAGGG 587
Csputigena	CGAGCOTTATCCCGAATCATGGGTTAAAGGCTCGTAGGCCGGCTGATAAGTCAGGG 587
Cleabetteri	CGAGCOTTATCCCGAATCATGGGTTAAAGGCTCGTAGGCCGGCTAATAAGTCAGGG 561
Chaemolytica	CGAGCOTTATCCCGAATCATGGGTTAAAGGCTCGTAGGCCGGCTATTAAGTCAGGG 502
Ccynodegmi	CGAGCOTTATCCCGAATCATGGGTTAAAGGCTCGTAGGCCGGCTATTAAGTCAGGG 557
Canimorsus	CGAGCOTTATCCCGAATCATGGGTTAAAGGCTCGTAGGCCGGCTTATAAGTCAGGG 549
Cgingivalis	CGAGCOTTATCCCGAATCATGGGTTAAAGGCTCGTAGGCCGGCTTATAAGTCAGGG 585
Cgranulosa	CGAGCOTTATCCCGAATCATGGGTTAAAGGCTCGTAGGCCGGCTTATAAGTCAGGG 538

Figure 6.1. Regions used as target for *Capnocytophaga* species. The primers and TaqMan probe based on alignment of the 16S rRNA gene sequence. The black forward primer position 357F (Lane, 1991) and red text is the reverse primer position. Blue text is the dual labelled probe position; [] represents locked nucleic acid bases; *** represents identical aligned sequences.

Chapter 6: Design novel specific TaqMan probe and primers

	CTCTACGGGGAGGCAAGCAG	350
Smutans	TGATCGGCCACACTGGGACTGAGACACGGCCAGACTCTACGGGAGGCAGCAGTAGGGA	350
Ssanguinis	TGATCGGCCACACTGGGACTGAGACACGGCCAGACTCTACGGGAGGCAGCAGTAGGGA	356
Lsalivarius	TGATCGGCCACATTGGACTGAGACACGGCCAGACTCTACGGGAGGCAGCAATAGGGA	347
Vdispar	TGAACGGCCACATTGGGACTGAGACACGGCCAGACTCTACGGGAGGCAGCAGTAGGGA	305
Fnucleatum	TGATCGGCCACAGGGGACTGAGACACGGCCAGACTCTACGGGAGGCNGCTGGGA	268
Anaeslundii	TGGACGGTACACTGGGACTGAGACACGGCCAGACTCTACGGGAGGCAGCAGTAGGGA	366
Nsubflava	TGATCGGCCACACTGGGACTGAGACACGGCCAGACTCTACGGGAGGCAGCAGTAGGGA	294
Cochracea	ATGTCCTCCCACACTGGTACTGAGACACGGCCAGACTCTACGGGAGGCAGCAGTAGGGA	351
Cgingivalis	AGATCCCCCACACTGGTACTGAGACACGGGACAGACTCTACGGGAGGCAGCAGTAGGGA	349
Pgingivalis	TTATCCCCCACACTGGTACTGAGACACGGGACAGACTCTACGGGAGGCAGCAGTAGGGA	341
Tforsythensis	AGGTCCCCCACACTGGTACTGAGACACGGGACAGACTCTACGGGAGGCAGCAGTAGGGA	365
Pintermedia	AGGTCCCCCACATTGGAACTGAGACACGGTCAAACCTCTACGGGAGGCAGCAGTAGGGA	335
* * * * *		
Smutans	TC--GGATCGAAAGCTCTGTTGAAAGTCAGAACGTTGTGAGAGTTGAAAGTTCACAC	465
Ssanguinis	TC--GGATCGAAAGCTCTGTTGAAAGAGAAGAACGGGTGTGAGAGTTGAAAGTTCACAC	471
Lsalivarius	TC--AGATCATAAAACCTGTTGTTAGAAAAAAACACGAGTGAAGAGTCAACTGTTACATC	462
Vdispar	TC--GGGTTGTAAAGCTCTGTTAATCGGGACGAA-AGGCCTTCTGGAAATAGTTAGAAG	419
Fnucleatum	TC--GGAATGTAAAGTGTCTTCAGTTGGGAGAA-----ACAAA-----	363
Anaeslundii	TC--GGGTTGTAAACCTCTTCGCCAGTGAAG-----CAGGCCTGCTCGTTGTG	472
Nsubflava	TC--GGGTTGTAAAGGACTTTGTCAGGGAAAGAAAAGGA-TAGGTTAAATACCCCTGTC	407
Cochracea	TAT-GGGTTGTAAACTGCTTTGTAAGGGAAAGAATAAG--GGCTACCGCTAGTTGA--	462
Cgingivalis	TAT-GGGTTGTAAACTGCTTTGATAGGGAAAGAATAAG--GTGTACGTGTAATTGATG--	460
Pgingivalis	TAA-GGATGTAAACTCTTTATACGGGAATAACGGG--CGATACGAGTATTGAT--	452
Tforsythensis	TAT-GGGTTGTAAACTCTTTACAGGGGAAATAATG--AGATACGTGTAATTGAT--	476
Pintermedia	TAT-GGGTTGTAAACTGCTTTGTTGGGGATAAGCG--GGCACGTGTGCCCYTT--	447
* * * * *		
TAAGG[+GJAA[-GJAA[+TJAA[+GGG[+CJ]		
Smutans	AGT-----GACGGTAGCTTACAGAAAGGGACGGCTAACTACGTGCCAGCAGCC	514
Ssanguinis	TGT-----GACGGTAGCTTACAGAAAGGGACGGCTAACTACGTGCCAGCAGCC	520
Lsalivarius	TAT-----GACGGTAGCTAACCAACAAGTCACGGCTAACTACGTGCCAGCAGCC	511
Vdispar	GATT-----GACGGTACCGAATAGAAAGCCACGGCTAACTACGTGCCAGCAGCC	469
Fnucleatum	-----TGACGGTACCAACAGAAGAAGTGAACGGCTAATAACGTGCCAGCAGCC	410
Anaeslundii	GGTGGGT-----TGACGGTAGCTGGATAAGAAGCCCGGGCTAACTACGTGCCAGCAGCC	526
Nsubflava	-----TGA-----TGACGGTACCTGAAATAAGCAGCCGGCTAACTACGTGCCAGCAGCC	457
Cochracea	-----TGACGGTACCTTACGAAATAAGCATCGGCTAACTCCGTGCCAGCAGCC	509
Cgingivalis	-----TGACGGTACCATATGAATAAGCATCGGCTAACTCCGTGCCAGCAGCC	507
Pgingivalis	-----TGAATGTACCGTAAGAATAAGCATCGGCTAACTCCGTGCCAGCAGCC	499
Tforsythensis	-----TGCATGTACCTGTGATAAAGCATCGGCTAACTCCGTGCCAGCAGCC	523
Pintermedia	-----TGCATTTACCTTCGAATAAGGACGGCTAATTCCGTGCCAGCAGCC	494
* * * * *		
ATCATTTGGGTTAAAGGG		
Smutans	GCGGTAAACGTAGGTCCCAGCGTTGTCGGATTATTGGGCTAAAGGGAGCAGGC	574
Ssanguinis	GCGGTAAACGTAGGTCCCAGCGTTGTCGGATTATTGGGCTAAAGCGAGCAGGC	580
Lsalivarius	GCGGTAAACGTAGGTCCCAGCGTTGTCGGATTATTGGGCTAAAGGGAAACGCAGGC	571
Vdispar	GCGGTAAACGTAGGTCCCAGCGTTGTCGGATTATTGGGCTAAAGCGCGCAGGC	529
Fnucleatum	GCGGTAAACGTAGGTCCCAGCGTTGTCGGATTATTGGGCTAAAGCGCGCAGGC	470
Anaeslundii	GCGGTAAACGTAGGTCCCAGCGTTGTCGGATTATTGGGCTAAAGAGCTCGTAGGC	586
Nsubflava	GCGGTAAACGTAGGTCCCAGCGTTGTCGGATTATTGGGCTAAAGAGCTCGTAGGC	517
Cochracea	GCGGTAAACGTAGGTCCCAGCGTTGTCGGATTATTGGGCTAAAGGCGCAGAGC	569
Cgingivalis	GCGGTAAACGTAGGTCCCAGCGTTGTCGGATTATTGGGCTAAAGGCGCAGAGC	567
Pgingivalis	GCGGTAAACGTAGGTCCCAGCGTTGTCGGATTATTGGGCTAAAGGCGCAGAGC	559
Tforsythensis	GCGGTAAACGTAGGTCCCAGCGTTGTCGGATTATTGGGCTAAAGGCGCAGAGC	583
Pintermedia	GCGGTAAACGTAGGTCCCAGCGTTGTCGGATTATTGGGCTAAAGGCGCAGAGC	554
* * * * *		

Figure 6.2. Signature sequences for the closely and more distantly related reference strains were aligned by Clustal W2 program. The black forward primer position 357F (Lane, 1991) and red text is the reverse primer position. Blue text is the dual labelled probe position; [] represents locked nucleic acid bases; *** represents identical aligned sequences.

6.2.1.3 Genomic DNA extraction

Genomic DNA from pure cultures was extracted using the method described by Griffiths et al. (2000) Chapter 2.

6.2.1.4 Optimization of qPCR amplification

The specificity of potential primers for their desired target was assessed using conventional PCR against the oral species previously described (6.2.1.1). PCR amplification was carried out in a reaction volume of 50 μ l containing 5 μ l of buffer, 1 μ l each of 10 mM dATP, dCTP, dGTP and dTTP (all deoxynucleoside triphosphates from Bioline, London, UK), 2.5 μ l of 50 mM MgCl₂, 1 μ l/100 μ M each PCR primer (1:10 diluted) and 0.5 μ l of 2000 U/ μ l Taq polymerase (Bioline) and 34 μ l of sterilised water. The negative control was 45 μ l of reaction mix with the template replaced by 5 μ l of sterilised deionised water. PCR thermocycling was performed using a Biometra T3000 thermal cycler (Biometra) conditions for all samples were: (i) an initial denaturation for 5 min at 94°C, (ii) 29 amplification cycles of denaturation at 94°C for 1 min, annealing of primers at 60°C for 1 min and primer extension at 72°C for 1 min followed by (iii) a final extension step at 72°C for 5 min.

The reaction products were assessed by loading 5 μ l of the PCR product into the wells of a 1% (w/v) agarose gel containing gel red (2 μ l/100 ml). A Five μ l of hyper ladder I marker was loaded into the first well. Five μ l of the PCR reaction mixture from each was mixed with 2 μ l of the loading buffer and loaded into the appropriate wells of the gel. The gel was immersed in Tris-acetate EDTA buffer (Oxoid) and subjected to 100 V that led to separation of the fragments. The gel was visualised after excitation under UV transillumination (Ringmer, UK) by placing it in a multiimage light cabinet, resulting image was captured by a computer software programme (AlphaEaseTM, AlphaInnotech, Ringmer, UK) to confirm that only one product of the appropriate length was obtained.

Primers concentrations and annealing temperatures optimised by conventional PCR. The tested primer concentration was tested 100 nM, 300 nM and 900 nM. The primer annealing temperatures were tested were 54°C, 58°C and 60°C. The TaqMan probe concentration was assessed by qPCR at 100 nM, 200 nM, 300 nM, and 900 nM. Subsequently the reactions were optimized for qPCR assays. The probe annealing temperature was tested at 60°C, 61°C, 62°C, 63°C and

64°C using Rotor-gene 6500 (Qiagen) cycler with green channel for data collection. The qPCR was performed in triplicate. Negative control reaction (NTC) mixtures contained molecular sterile-filter H₂O instead of template DNA.

6.2.1.5 Real time PCR assays and melting curve

qPCR was performed in a final volume of 10 μ l containing PCR SensiMix (SensiMix probe™, Bioline), for SYBR Green probe (Sigma, SYBR Green JumpStartTaq™ Ready Mix™)/or for TaqMan probe (Sigma), forward primer and reverse primer (Sigma), DNA template, and molecular H₂O (Sigma). The composition of the reaction is shown in table 6.3. Quantitative PCR reactions were carried out using the Rotor-gene 6500 (Qiagen) cycler and using the green channel for data collection.

Table 6.3. qPCR assays reactions for single tube and 5 tubes.

qPCR Mastermix	Volume to add for single tube 10 μ l	Volume to add for 5 qPCR tubes
PCR SensiMix™ Probe	5 μ l	25 μ l
Primer forward (300 nM)	0.3 μ l	1.5 μ l
Reverse primer (900 nM)	0.9 μ l	4.5 μ l
Water (H ₂ O)	3.4 μ l	17 μ l
DNA template	0.2 μ l	1 μ l
TaqMan or SYBR Green (200 nM)	0.2 μ l	1 μ l

6.2.1.6 Melting curve cycling conditions

The contents of each reaction were labeled and replicate samples grouped together using the software. It was necessary to include the dissociation curve (melting curve) to check the production of non-specific products when using SYBR Green probe (Invitrogen). The melting curve was used to obtain the melting temperature (T_m) of the target nucleic acid sequence. The standard PCR conditions used for SYBR Green probe cycling were an initial cycle of activation at 95°C for 10 min, followed by 40 cycles of denaturation at 95°C for 15 s, then annealing/extension at 60°C for 15 s, followed by a final cycle at 72°C for 15 s. Melting curves were plated between 50°C and 99°C.

6.2.1.7 TaqMan probe assay for qPCR data collection

The TaqMan probe (Sigma) sequence was designed to quantify *Capnocytophaga* species. The qPCR cycling conditions were an initial cycle of activation at 95°C for 10 min, followed by 40 cycles of denaturation at 95°C for 15 s, then annealing/extension at 64°C for 60 s.

6.2.1.8 Standard curve for *Capnocytophaga* species

Colonies from an agar plate of *C. ochracea* was suspended in 1 ml of sterile RTF. Bacteria were enumerated by plating serial dilutions in phosphate buffer saline on fastidious anaerobic agar with 5% defibrinated horse blood and incubating for 5 days at 37°C under anaerobic conditions. In order to produce standard curves for the enumeration of organisms, DNA extraction was performed and by using viable count (CFU/ml), the numbers of cells were related to amounts of DNA. Standard curves consisting of six 10-fold dilutions of reference DNA were run in triplicate on a Rotor-gene 6500 cycler using the green channel for data collection.

6.2.1.9 Reproducibility and Reliability

To assess the reproducibility of the TaqMan PCR assay. Six ten fold serial dilutions of target bacteria were amplified in three separate runs under the same conditions. The reliability of the qPCR was evaluated by three amplifications of the same dilution range in a single run.

6.2.1.10 Quantitative PCR analysis of biofilm samples

One disc of each CDFF experiment (biofilms from two experimental runs used) from the previous chapter was used, resulting in 15 samples (6 h, 48 h, 96 h, 216h, 222 h, 246 h, 366 h, 396 h, 438 h, 510 h, 516 h, 540 h, 588 h, 612 h and 714 h). The biofilms were centrifuged for 1 min (14600 × g). These had previously been stored at -80°C. These were thawed and DNA extracted as previously (Chapter 2).

6.3 Results

6.3.1 Agarose gel electrophoresis of PCR products

The specificity of potential primers for their desired target was assessed using conventional PCR against the oral test species. The gel was visualised after excitation under UV transillumination by placing it in a multiimage light cabinet and the resulting image was captured by a computer software programme (AlphaEase™) to confirm that only one product (red arrow) of the appropriate length size was obtained as shown in figure 6.3.

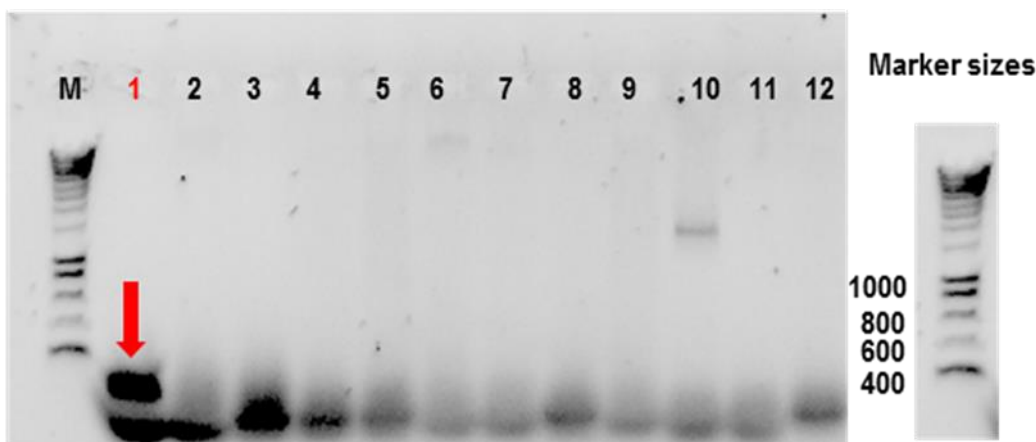


Figure 6.3. Gel electrophoresis image of *C. ochracea* PCR products. Expected size by: 224 bp, 1 by: *C. ochracea* (red arrow). 2 by: *F. nucleatum*, 3 by: *L. casei*, 4 by: *V. dispar*, 5 by: *N. subflava*, 6 by: *A. naeslundii*, 7 by: *P. intermedia*, 8 by: *S. sanguinis*, 9 by: *S. mutans*, 10 by: *P. gingivalis*, 11 by: *T. forsythia*, and 12 by: *A. actinomycetemcomitans* and M by: Hyperladder I.

6.3.2 Melting curve

There was no production of primer dimers or non-specific products using SYBR Green assays (Figure 6.4). The data showed the lowest C_t value with the highest fluorescent signal (red colour) triplicate samples and negative control samples (blue colour) at 60°C annealing temperature.

The specific TaqMan probe with the primers for *Capnocytophaga ochracea* were found to be specific for their desired target, efficient and amplification specific cleavage resulted in a bright, clean and reliable amplification plots (Figure 6.5).

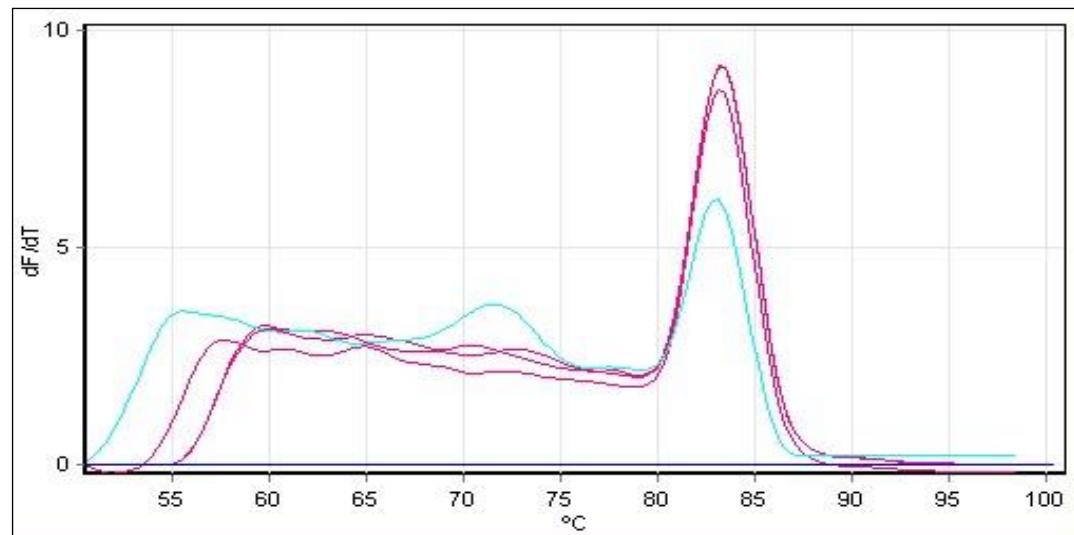


Figure 6.4. A SYBR Green melt curve demonstrating the target amplicons have a T_m of around 84°C. The y axis represents the derivative of fluorescence changes and the x axis represents the temperature (°C).

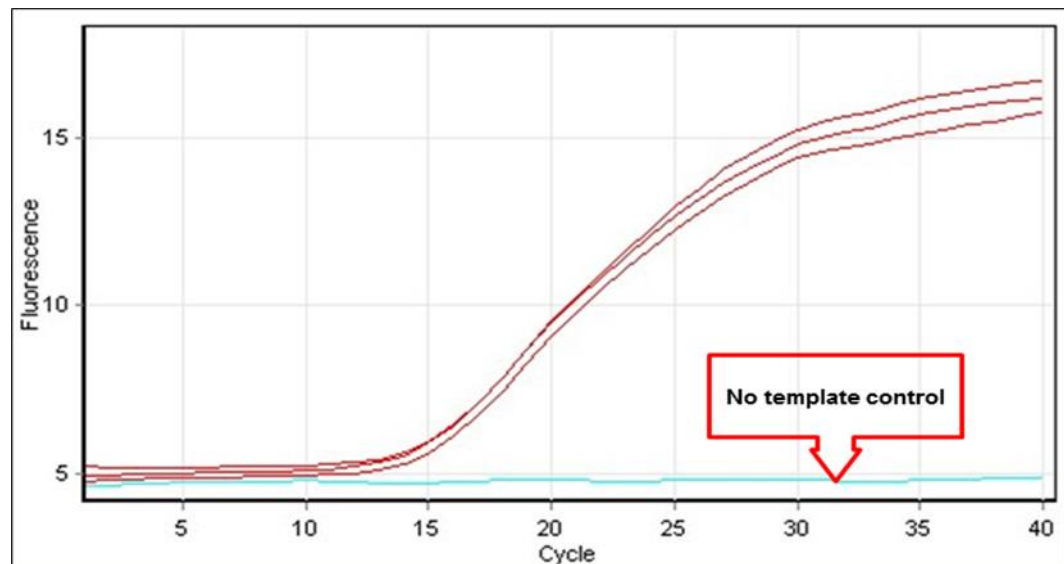


Figure 6.5. *C. ochracea* amplification plot determined by qPCR using primers set and TaqMan probe shows the optimal probe concentration given the lowest C_t value with the highest fluorescent signal (red colour) triplicate samples and negative control samples (blue colour) at 60°C annealing temperature.

6.3.3 Specificity of primers and TaqMan probe

The primers (Table 6.2) were tested and optimised for their specificity with the other reference strains and the analysis was carried out by qPCR.

Figure 6.6, shows there is some cross reactivity with *V. dispar*, *F. nucleatum* and *P. gingivalis* at 60°C. When the melting temperature was raised to 63°C the cross reactivity was reduced and only *F. nucleatum* was amplified (Figure 6.7). No cross reactivity was apparent when the temperature was further increase to 64°C (Figure 6.8).

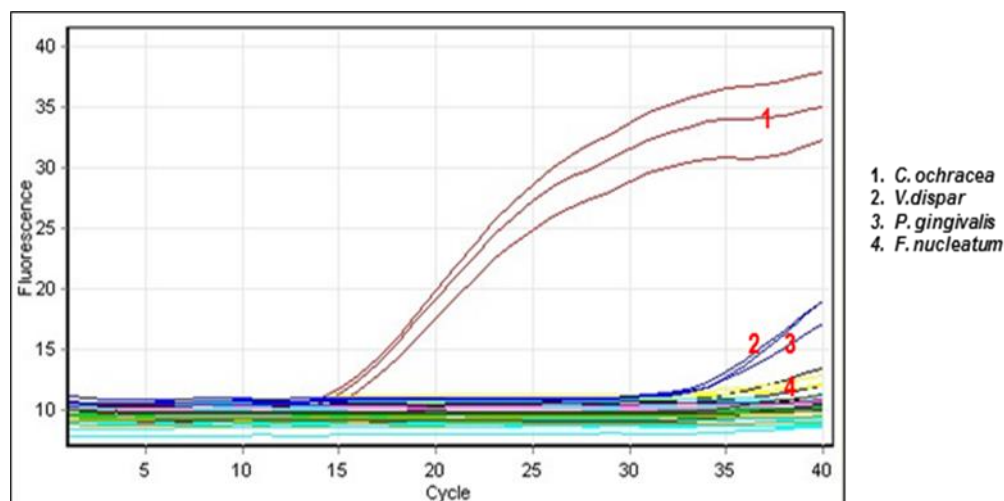


Figure 6.6. The amplicon of *C. ochracea* (red colour) is specific at 60°C against all strains mentioned in section 6.2.1.1 except *V. dispar* (blue colour), *F. nucleatum* (yellow colour) and *P. gingivalis* (black colour).

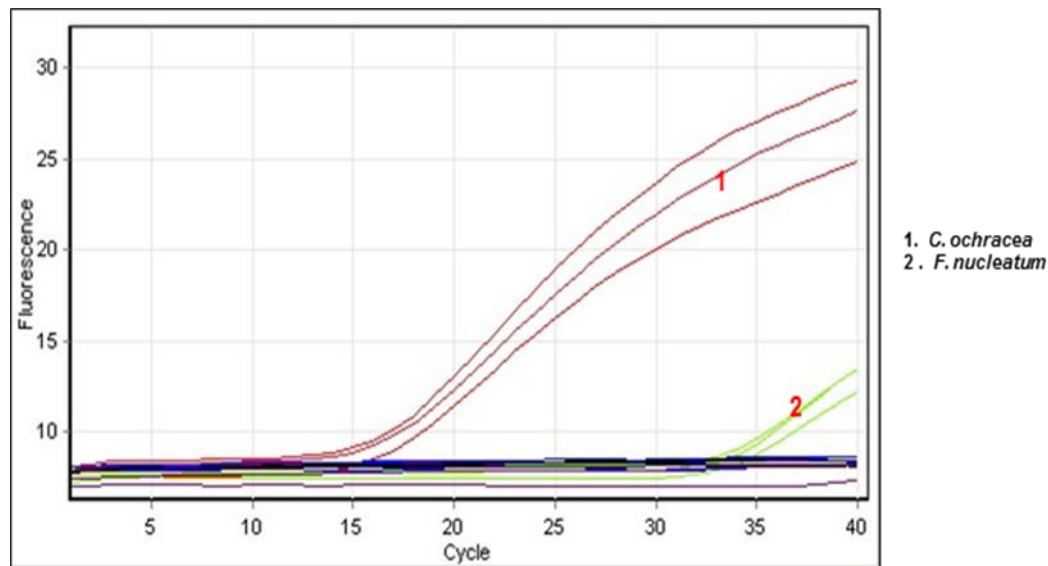


Figure 6.7. The amplicon of *C. ochracea* is specific at 63°C against all strains except *F. nucleatum* (green colour).

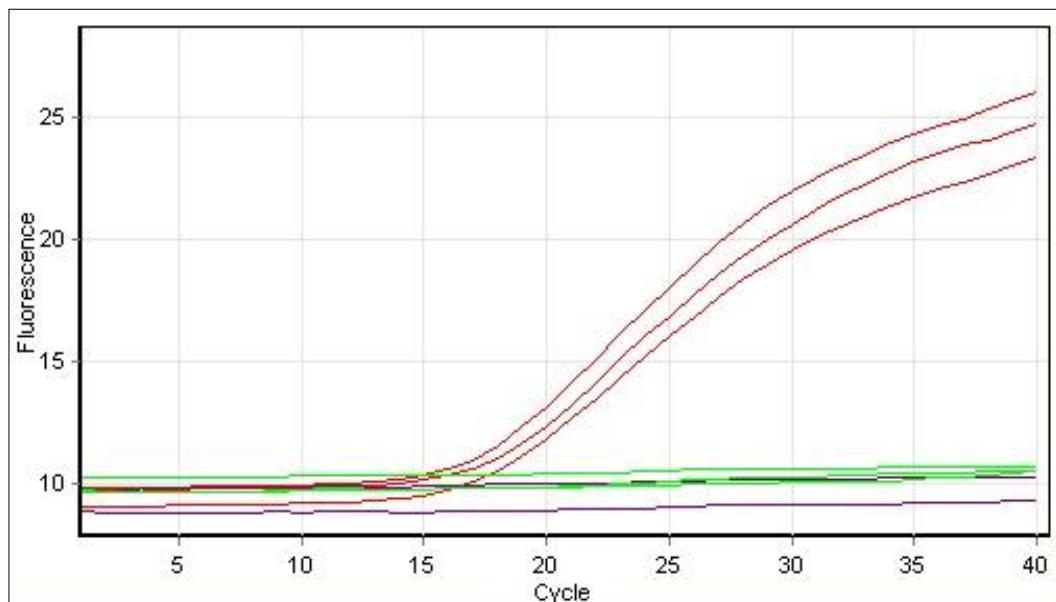


Figure 6.8. The Amplicon is specific for *C. ochracea* at 64°C against all strains.

6.3.4 Standard curve

In order to measure assay efficiency the relative C_t value for subsequent dilutions of *Capnocytophaga* DNA was plotted and the R^2 and slope calculated. A measure of whether the standard curve was accurate or not was a distance of approximately 3.3 cycles for the cycle threshold between each ten folds dilution and an R^2 value above 0.98. Each point represents an amount of *Capnocytophaga* DNA corresponding to the C_t value. The relation coefficient of straight line was $R^2 = 0.99139$ which is indicated a reliable or stable assay with a slope equal -3.649 and Assay efficiency equal 88% (Figure 6.9).

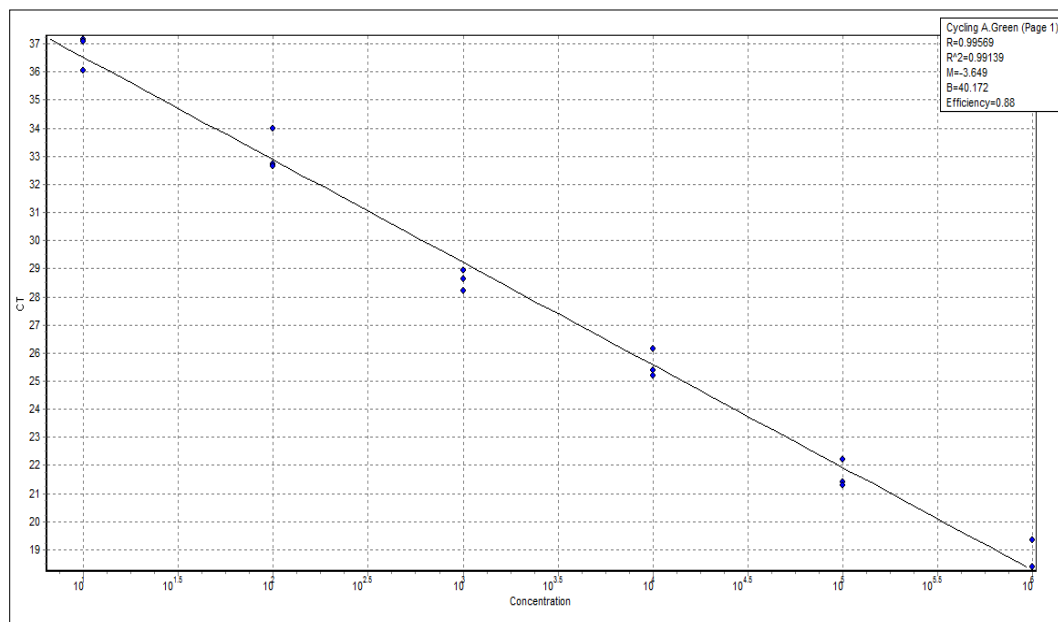


Figure 6.9. The standard curve is linear from 10^1 to 10^6 copies of *C. ochracea*.

6.3.5 Quantification of *Capnocytophaga* species

Total bacterial were quantified using universal probes and primers for the 16S rRNA region as mentioned previously in chapter 5. The *Capnocytophaga* spp. numbers were quantified in biofilm samples from a number of time points from the *in vitro* peri-implantitis model section 6.2.1.10. At 222 h, the change of environment to microaerophilic atmosphere with increased introduction of PISF. At 516 h, the change of environment to anaerobic atmosphere (Figure 6.10).

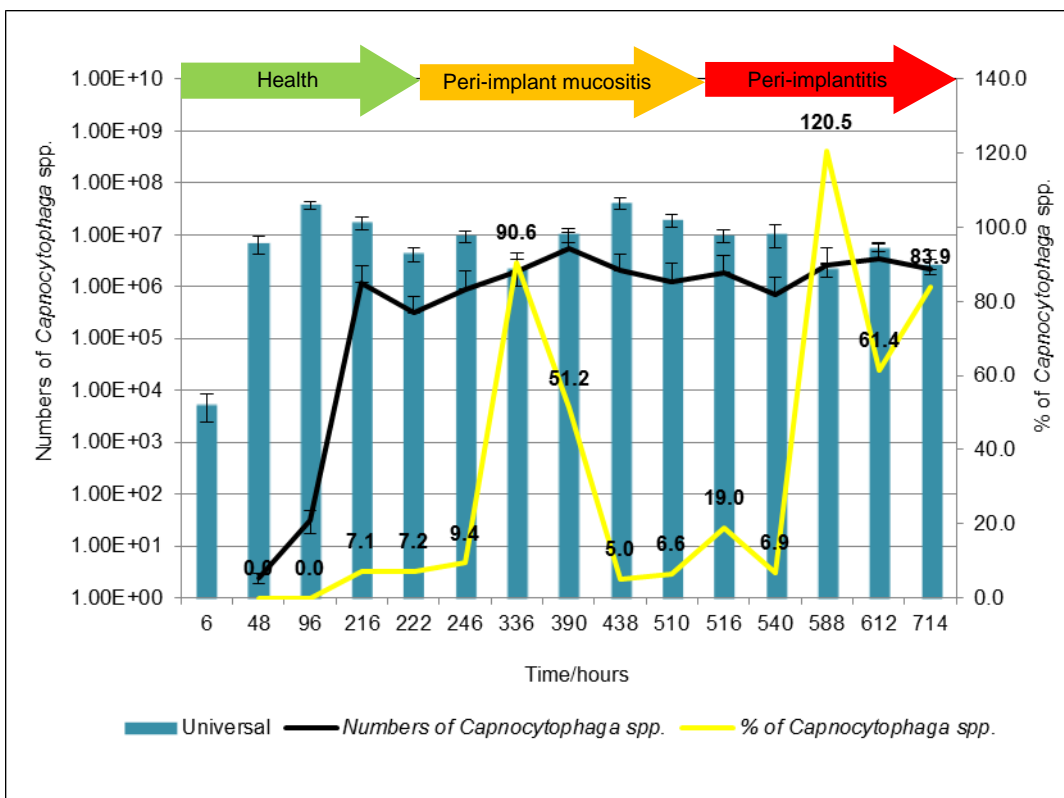


Figure 6.10. Total numbers of bacteria determined by qPCR represented by blue bars. Numbers of *Capnocytophaga* spp. obtained by qPCR are represented by the black line. The proportions of *Capnocytophaga* spp. are represented by the yellow line with data labelled. *Capnocytophaga* spp. error bars represents standard deviation ($n = 6$). Universal error bars represent standard deviation ($n = 9$).

6.3.6 CDFF peri-implant biofilm communities

The number of *Capnocytophaga* were analysed by qPCR over the course of a CDFF experiment. The detection limit was reported to be 20 cells (Ciric et al., 2011). The number of organisms detected by qPCR was lower under conditions emulating health. Indeed, *Capnocytophaga* spp. were not detected until 216 h, at which point they represented ca 7.06% of total bacteria. When the conditions were altered to emulate peri-implant mucositis, *Capnocytophaga* spp. represented between 5% and 10% with a “spike” at 366 h at 90.6% (Figure 6.10).

The number of *Capnocytophaga* were found to be higher in condition of peri-implant mucositis at 390 h and 438 h than under health conditions (Table 6.4). When the conditions were altered again to emulate peri-implantitis and indeed steady state was attained, the proportion of *Capnocytophaga* spp. represented ca. 83.9% a high proportion of the species present.

Table 6.4. The mean value of *Capnocytophaga* species investigated by qPCR of microcosm biofilms grown in the CDFF under health, peri-implant mucositis and peri-implantitis conditions, \pm standard deviation ($n = 6$).

Health		Peri-implant mucositis		Peri-implantitis	
Time	Mean \pm SD	Time	Mean \pm SD	Time	Mean \pm SD
6 h	0	222 h	3.09×10^5 $\pm 3.37 \times 10^5$	516 h	1.86×10^6 $\pm 2.21 \times 10^6$
48 h	2.37×10^1 $\pm 5.31 \times 10^1$	246 h	8.97×10^5 $\pm 1.08 \times 10^6$	540 h	7.15×10^5 $\pm 7.69 \times 10^5$
96 h	3.21×10^1 $\pm 1.52 \times 10^1$	336 h	1.99×10^6 $\pm 2.56 \times 10^6$	588 h	2.62×10^6 $\pm 2.91 \times 10^6$
216 h	1.20×10^6 $\pm 1.30 \times 10^6$	390 h	5.32×10^6 $\pm 5.82 \times 10^6$	612 h	3.41×10^6 $\pm 3.69 \times 10^6$
		438 h	2.05×10^6 $\pm 2.28 \times 10^6$	714 h	2.14×10^6 $\pm 2.89 \times 10^6$
		510 h	1.27×10^6 $\pm 1.54 \times 10^6$		

6.4 Discussion

Per-implantitis is clinically observed as an inflammatory condition of the supporting structures of dental implants that leads to progressive degradation of bone tissue and subsequent loss of implants (Mombelli and Décaillat, 2011). The microbiota associated with peri-implantitis is varied (Augthun and Conrads, 1997, Koyanagi et al., 2010, Koyanagi et al., 2013) and include *Capnocytophaga* spp., which play an important role in the onset of periodontal disease (Ciantar et al., 2001b). Recently, qPCR techniques have been developed for providing better detection for oral pathogens (Boutaga et al., 2007) and qPCR assays are powerful and convenient tools that allow quantification and identification in a single assay (Suzuki et al., 2004).

One of the most abundant groups of bacteria identified by 16S rRNA gene cloning and sequencing in biofilms grown under peri-implantitis conditions were *Capnocytophaga* species (Chapter 4). Therefore, due to the interest in this species, primers were developed for use in Taqman qPCR assays. A crucial aspect of qPCR is the design and testing of primers and probes based on the nucleotide sequence of the target organism. To be successful, qPCR assays depend on the relative concentration of primers, the probe concentration, PCR buffer concentration, probe design (with locked nucleic acids bases), cycling temperatures and amounts of DNA template.

Chapter 5 utilised existing primer sets developed at the Eastman Dental Institute (Circic et al., 2011) for a wide variety of organisms. These allowed the study of absolute numbers and changes in proportions of specific species in oral biofilms in an *in vitro* model before and after their exposure to the anti-plaque agent, chlorhexidine (Zaura et al., 2011, Circic et al., 2011).

In this part of study two strategies were employed. Firstly, to design specific primers for *Capnocytophaga* spp. that did not cross-react with sequences from non-target organisms. It is difficult to identify specific nucleotide sequences or to distinguish the 16S rRNA genes of closely related species. In fact, the microorganisms in dental plaque are characterised by a number of closely related species (Spratt, 2004). Furthermore, identification of these organisms by culture and by PCR is difficult due to a high degree of genetic and phylogenetic similarity with other species (Pratten et al., 2003). For example, *F. nucleatum* is genetically very closely related to *C. ochracea*, which show cross reactivity with other taxa including: *V. dispar* and *P. gingivalis*

16S rDNA of bacterial sequences were aligned and regions of homogeneity within the genus were identified. Once these were identified oligonucleotide primers and the probe set targeting 16S signature sequences were designed using primer software v.4.0. These were then tested in silica by comparing against the sequences within 16S rDNA databases using a similarity search program to see if they cross-reacted with other taxa. The primers listed, on Table 6.1, were designed for the target microorganisms. The specificity of the primers for the target sequence was determined against target strains and with other references showed that some of primers pairs had cross reactivity. Therefore, an alternative forward (357 F Lane, 1991) primer and reverse primer was suggested by Dr David Spratt (data not published, previously designed for endpoint PCR detection of *Capnocytophaga* species). These primers were specific when assessed by conventional PCR and with a probe for qPCR. Analysis of the melting curve showed no production of non-specific products which would interfere with the results. The standard curve efficiency was found to be < 90%. The reason for the low efficiency of the assay could be due to the length of the amplicons (Ciric et al., 2010); this was approximately 224 bp, based on the 16S rRNA gene.

At each cycle, the accumulation of PCR products was detected by monitoring the increase in fluorescence of the reporter dye, and double stranded DNA binding SYBR green. After the PCR, melting curve results showed no production of primer dimers or non-specific products and the specific probe showed no cross reaction at 64°C. All the reactions were analysed using the Rotor-gene 6500 cycler (Qiagen). Furthermore, their specificity was thoroughly tested by both conventional PCR (Figure 6.4) and qPCR, demonstrating the suitability for detection of target microorganism (Figures 6.5 - 6.8).

Capnocytophaga spp. were detected in the samples at a number of time points and became a significant part of the microbiota at later time points under peri-implantitis conditions. The most significant observation from this study was that the results of the qPCR confirmed the trend observed by 16S ribosome RNA gene cloning and sequencing at same sampling points (Chapter 4). A greater proportion of *Capnocytophaga* spp. were identified under peri-implant mucositis conditions at 246 h and 438 h, where *Capnocytophaga* spp. accounted for ca. 12%. Under peri-implantitis conditions, *Capnocytophaga* spp. accounted for ca. 27% at 450 h and 714 h using cloning and sequencing (Chapter 4). The

proportion of these species was very low at 6 h, 48 h and 96 h under health condition and this would be expected, as *Capnocytophagae* spp. are generally undetectable in the health community with streptococci etc. dominating early oral biofilms (Marsh, 2010). It can be postulated that under health conditions the numbers of *Capnocytophaga* spp. were below the detection limit i.e. less than 20. Once disease conditions were implemented, the numbers increased, probably as a result of the altered environmental conditions at 246 h and 438 h. In terms of the changes in the communities associated with environmental conditions emulating health and disease, the proportion of *Capnocytophaga* species was shown to be different between peri-implant mucositis and peri-implantitis, This present study confirmed the trend observed by 16S ribosome RNA gene cloning and sequencing and results were also supported by CLSM data which showed large numbers of *Capnocytophaga* like rods in biofilms grown under peri-implantitis conditions (Chapter 4).

6.5 Conclusion

A primary aim of the CDFF for assessing the dental plaque associated with peri-implantitis was to test antimicrobial agents for their efficacies against the buildup of plaque. The use of qPCR to assess the *Capnocytophaga* spp. and other taxa in communities perturbed by in antimicrobials will allow the fast and accurate assessment of the effects of these compounds on the population. It was shown that qPCR primer design for specific taxa is achievable in the context of a project such as this and has allowed analysis of complex communities. It also allows the primer set to be used in any *in vitro* or indeed *ex-vivo* samples for detection and quantification of *Capnocytophaga* species. Furthermore, these data give credibility to the ecological plaque hypothesis. It has been shown that the number of bacteria of a specific species is able to increase from below detectable levels (reported here to be less than 20) to become predominant species under disease conditions in a closed environmental situation.

Chapter 7

An *in vitro* assessment of antibacterial treatment strategies, which are currently available against peri-implantitis biofilms

7.1 Introduction

In previous chapters, an array of methods was employed for targeted identification of microorganisms associated with healthy peri-implants, peri-implant mucositis and peri-implant disease using an *in vitro* model. These techniques showed that the *in vitro* model of peri-implantitis which has been developed appears to be a valid simulation of the dynamic bacterial biofilm which exists on dental implant surfaces. The ultimate aim of developing such a reproducible and realistic model of these conditions was to utilise the model to determine the efficiency of current and novel decontamination therapies.

The accumulation of bacterial biofilms has been defined as a primary etiological factor for the development and progression of peri-implant infections (Mombelli et al., 2012). Changes in the microbial composition of plaque such as an increase in Gram-negative anaerobic bacteria can lead to peri-implantitis (Mombelli and Décailliet, 2011). The imbalance between microbial load and host defence may then lead to implant infection, which in turn results in the loss of the supporting bone and ultimately, loss of dental implants (Heitz-Mayfield, 2008, Scarano et al., 2004). In addition to streptococci, the fusobacteria and especially *Fusobacterium nucleatum* are known to play a significant role in plaque development as they are able to co-adhere to many oral microorganisms. Renvert et al. (2007) reported that *Neisseria mucosa*, *F. nucleatum* and *Capnocytophaga* spp. predominantly occurred within implant submucosal sites. In the development of peri-implantitis infections, the roughness of the implant surface plays an important role in the formation of biofilms. Albrektsson and Wennerberg (2004), defined smooth surfaces as having an average roughness (S_a) value of $< 0.5 \mu\text{m}$, minimally rough surfaces having an S_a of $0.5 - 1 \mu\text{m}$, moderately rough surfaces having an S_a $1 - 2 \mu\text{m}$ and rough surfaces having an $S_a > 2 \mu\text{m}$.

Rough surfaces of crowns, implant abutments, or prostheses bases accumulate and harbour significantly more plaque biofilms than smooth surfaces. Polished implant surfaces have shown less plaque accumulation than sand-blasted and acid-etched implant surfaces (Schwarz et al., 2006). A review by Renvert et al. (2011) confirmed this finding and they concluded that implants with rough surfaces were more likely to lead to peri-implantitis. It has been reported by Quirynen and Bollen (1995) that up to 25 times more bacteria adhere to rough surfaces than smooth ones. This is because rough surfaces provide niches that protect bacteria from host defences and routine oral hygiene treatments (Quirynen et al., 2002).

Chapter 7: An *in vitro* assessment of antibacterial treatment strategies

The removal of biological contamination from structured implant surfaces is difficult to achieve. As with periodontal diseases, various therapies have been proposed to reduce the number of pathogenic species and improve clinical parameters of peri-implant diseases (Klinge et al., 2002, Roos-Jansåker et al., 2003, Mombelli et al., 2001). Indeed, several methods have been applied to remove supra and subgingival plaque biofilm for implant disinfection (Schwarz et al., 2005). These methods include use of polishing brushes, rubber polishers, teflon, plastic, carbon or titanium curettes, special modified tips for ultrasonic systems, and air powder flows (Augthun et al., 1998, Fox et al., 1990), burnishing with cotton pellet soaked in water, citric acid, or using air powdered abrasives. A potential disadvantage of conventional ultrasonic systems might be related to the working tip which may cause loss of osseointegration at advanced defect sites (Braun et al., 2005). Furthermore, all surfaces treated with ultrasonic systems showed conspicuous surface damage (Schwarz et al., 2004).

Air powder flow can be associated with an increased risk of emphysema on clinical application and damage to the implant micro-topography (Schwarz et al., 2009). Persson et al. (2001) reported a lack of re-osseointegration at implants sites receiving surface decontamination using either abrasive pumice with a rotating tooth brush or cotton pellets soaked in sterile saline in an animal model. Instrumentation with metal curettes can remove the edge of irregularities but often damage machined titanium surfaces resulting in scratches and modification of the surfaces (Rühling et al., 1994).

Citric acid can be effective in inhibiting multispecies biofilms. However, acid chemotherapeutic agents have an irritating effect if applied in contact with gingival tissues for prolonged periods. Valenza et al. (1987) have shown that application of citric acid to the gingiva with periodontal disease for 5 and 10 min caused diffuse edema with cytologic alterations. Other *in vitro* studies determined that bacterial lipopolysaccharides can be removed from structured implant surfaces following application of citric acid, tetracycline HCL, CHX, hydrogen peroxide, chloramines-T, sterile sodium solution, modified ultrasonic systems or air powder flows (Kreisler et al., 2005). In this context, there is the potential risk of damage to the implant micro-topography following application of these chemicals (Kreisler et al., 2005). Other agents such as hydrogen peroxide are also harmful to the cell membrane integrity and cause irreparable biological damage (Braun et al., 2005). Using an animal model, Kim et al. (2012) found that contaminated implants swabbed with saline showed increased bone regeneration on fresh sockets compared to contaminated implants swabbed with

Chapter 7: An *in vitro* assessment of antibacterial treatment strategies

10% of H₂O₂ where inflammation who observed around the implants and less osseointegration.

Besides the mechanical removal of biofilms, lasers have been introduced as a potential alternative in reducing pathogen levels on implant surfaces. For example, solid state lasers such as Er:YAG lasers have been considered promising therapies for peri-implant disinfection (Kreisler et al., 2002). However, a different approach again is the use of lasers as a potential therapeutic method for decontamination of implants (photodynamic therapy; PDT). PDT employs a non toxic dye, termed a photosensitizer, and low intensity visible light (660-905 nm). PDT has the potential to be important in several clinical applications such as disinfection of root canals, periodontal pockets, and carious lesions. In the periodontal field, PDT has shown efficiency in the treatment of periodontitis and peri-implantitis in animal models and clinical trials (Dörtnedel et al., 2001). PDT offers the advantages in that the photosensitizer can be targeted to its cell or tissue and illumination can be spatially directed to the lesion. It has been reported that bacterial killing by the photochemical reaction is mainly caused by damage to the bacterial cytoplasmic membrane, leading to DNA damage (Konopka and Goslinski, 2007). The results of a number of *in vitro* studies have demonstrated the effective and efficient use of PDT for periodontal and peri-implant diseases (Takasaki et al., 2009). However, sufficient clinical and microbiological data that support the effect of PDT for non-surgical periodontal treatment has not been demonstrated.

Finally, antimicrobial substances, as well as local or systemic antibiotics can be applied as adjunctive measures the treatment of peri-implant infections. CHX is still considered a “gold standard” among oral antimicrobial agents. Chlorhexidine is a broad spectrum antimicrobial that is active against a wide range of Gram-positive and Gram-negative supragingival and subgingival plaque bacteria and fungi (Lee et al., 2005). The mode of action of CHX is by causing damage to the microbial cell membrane, leading to cytoplasmic leakage. The agent is frequently employed as a rinsing solution (0.1 - 0.2%). Nevertheless, several studies have demonstrated that this compound may have an adverse effect on oral tissues. For example, direct application of CHX during regenerative treatment of peri-implantitis leads to toxic effects on gingival fibroblasts, osteoblasts and endothelial cells; thus inhibiting the early healing phase of peri-implantitis (Giannelli et al., 2008).

Different treatments of titanium surface can modify the implant microstructural properties that in turn are able to affect bone formation processes. According to

Chapter 7: An *in vitro* assessment of antibacterial treatment strategies

Renvert et al. (2009), re-osseointegration is defined as the formation of new bone on to a previously biofilm contaminated implant surfaces, and this is the aim of treating peri-implantitis. Cooper et al. (1999), concluded that an increase in surface roughness of titanium implants improved bone integration, and surface roughness is known to have positive impact on the bone to implant contact (Shalabi et al., 2006). In contrast to the surface of natural teeth, surfaces of modern implants are highly micro-structured and macro-structured to improve osseointegration. However, as previously discussed rough surfaces facilitate initial microbial adhesion and formation of complex biofilms, and make sufficient debridement of implant surfaces very difficult. Furthermore, effective periodontal debridement of pathogenic biofilms on rough titanium implant surfaces is nearly impossible to achieve in daily practice because of the textured surface and the screw-shaped design of the implants. All the previously described therapies have shown efficiency in decontamination, but have failed in their ability to also restore biocompatibility (Schwarz et al., 2012). This work is the first to assess the effects of specific treatments on *in vitro* biofilms cultured under conditions of peri-implant mucositis and peri-implantitis.

7.1.1 Objectives

This study evaluated the efficiency of current and novel treatment modalities for the elimination of biofilms on different titanium surfaces using an *in vitro* model of peri-implantitis.

The CDFF *in vitro* model of peri-implant infection was used to investigate:

- a.** The viable numbers of facultative anaerobes, Gram-negative anaerobes, *Staphylococcus* spp. and *Candida* spp., remaining on three different titanium surfaces (polished, SLA and SLActive) following a range of decontamination regimes.
- b.** The remaining biofilm on titanium discs post-treatment. This was analysed using CLSM and Baflight™ viability staining and the biofilm thickness was also determined.
- c.** The surface biocompatibility, which was analysed by culture of MG-63 cells (osteosarcoma cell line) on three different titanium surfaces; polished SLA and SLActive following a range of decontamination regimes.
- d.** Cell morphology following a range of decontamination regimes was analysed by scanning electron microscopy (SEM).

7.2 Materials and Methods

7.2.1 Commercial titanium (Ti) discs

Standard Ti discs were provided by the Straumann Company (Basel, Switzerland). These discs were 5 mm in diameter and 0.1 mm thick, and exhibited three different surface characteristics polished, Sand blasting acid etching (SLA) and Sand blasting acid etching active (SLActive). For the polished surface, discs with surface roughness of 0.2 μm were used with an arithmetic mean surface roughness R_a value of < 0.5 μm , this polished surface was considered smooth. SLA (sand blasted, large grit, acid etched) has a moderately rough surface, with an R_a equal to 1.75 μm . The SLA surface is produced by a large grit sand-blasting process with corundum particles that leads to a macroroughness on the titanium surface. This is followed by treating with a strong acid-etching bath with a mixture of HCl/H₂SO₄ at elevated temperature for several minutes.

This process produces fine micropits superimposed on the rough blasted surface; the chemical composition of SLA surface structure is titanium oxide. SLActive (a surface modification of SLA with the same surface roughness) is manufactured by rinsing the titanium surface after the etching procedure under nitrogen (N₂) protection and continuous storage in an isotonic sodium chloride (NaCl) solution. This modification results in a hydroxylated/hydrated and highly hydrophilic surface (Rupp et al., 2002).

7.2.2 Microcosm biofilms

Aliquots of 1 ml of pooled saliva were dispensed into 1.5 ml cryotubes and stored at -80°C for subsequent use (Chapter 2). The CDFF microcosm biofilms were grown and evaluated at two time points:

366 h representing a peri-implant mucositis associated biofilm.

612 h representing a peri-implantitis associated biofilm.

7.2.3 Medium and Inoculum

The medium used in the CDFF was artificial saliva with a composition identical to that previously described (Chapter 2, Section 2.1). This consisted of mucin containing artificial saliva and peri-implant sulcular fluids (used to provide nutrients present in tissue exudates, which are major component of peri-implant sulcular fluid)

7.2.4 CDFF set up

A CDFF was used as described previously in Chapter 2, Section 2.2.1. The CDFF containing its pans was autoclaved at 121°C for 15 min and discs were then added aseptically to the pans through the sampling port (Figure 7.1). Sample discs were carefully placed on to five plugs with a pair of sterile titanium tweezers without touching the surfaces. During all experiments, the CDFF was maintained at a constant temperature of 37°C. A vial of 900 µl of stored pooled saliva was thawed and used to inoculate 500 ml of artificial saliva. This was mixed and pumped into the CDFF for 6 h at a flow rate of 1.38 ml/min. The inoculation flask was then disconnected and the CDFF was fed from a medium reservoir of sterile artificial saliva. The artificial saliva was circulated via a peristaltic pump at a flow rate of 0.72 l day⁻¹ which was representative of the daily salivary flow rate (Pratten et al., 1998).

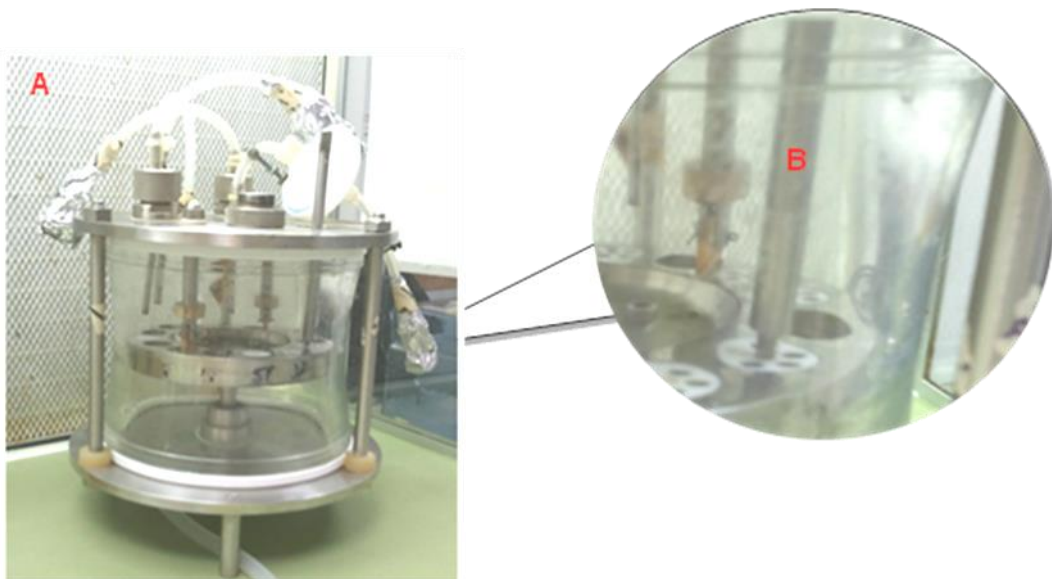


Figure 7.1. The CDFF containing pans were autoclaved at 121°C for 15 min. A. The Ti discs were added aseptically to the pans through the sampling port with a flat-ended tool inside a flow cabinet. B. The pan was tapped down to the level of the turntable with a flat-ended tool.

7.2.5 *In vitro* model parameters

The titanium discs were placed on PTFE plugs and held in place using vacuum silicone grease. The discs were recessed to a depth of 600 µm using sterile titanium tweezer without touching the top of the disc surfaces. The pan was tapped down to the level of the turntable with a flat-ended tool. Biofilms were removed during experiments via a port in the top plate using a flat-ended tool inserted into a tapped hole in the centre of the film pan. Extracted biofilms were subjected to various analyses (Figure 7.1).

7.2.6 Conditions used for running the CDFF

Conditions associated with healthy dental implants, peri-implant mucositis and peri-implantitis were generated as previously described (Chapter 2, section 2.2.5).

7.2.7 Titanium surface decontamination

Each of the discs removed from the CDFF was allocated to a specific treatment including an untreated control group. In the treatment group, discs were subjected to non-mechanical, mechanical or both non-mechanical and mechanical decontamination measures. The non-mechanical decontamination therapy was the application of reduced transport fluid, 0.2% chlorhexidine mouthwash or photodynamic therapy (PDT). The mechanical decontamination group consisted of titanium brush (TiBrush) supplied by Straumann® and combined use of titanium brush and photodynamic therapy (TB + PDT).

7.2.7.1 Non-mechanical cleaning

7.2.7.1.1 Reduced transport fluid (control untreated biofilms)

In the control group, the disc was left completely immersed in reduced transport fluid for 60 s. Once removed, the disc was then immersed in post treatment reduced transport fluid for serial dilution.

7.2.7.1.2 Chlorhexidine

For this study, the chlorhexidine used was Corsodyl (Chlorhexidine Digluconate 0.2% w/v; GlaxoSmithKline, Brentford, UK). The discs were completely submerged for 60 s in 1 ml of chlorhexidine. Following treatment, the discs were dipped into post-treatment in RTF to remove excess chlorhexidine. The chlorhexidine concentration was chosen as this was the concentration employed

in the standard clinical procedure to manage peri-implantitis patient's protocol for management of patients with peri-implantitis (Salvi et al, 2007; Bürgers, 2012).

7.2.7.1.3 Photodynamic therapy (PDT)

The photosensitiser used was 3, 7-Bis (dimethyl-amino) phenazathionium chloride trihydrate (methylene blue) (Sigma) at a concentration of 0.005% (w/v). This was prepared in sterile water and kept in the dark at room temperature. Methylene blue (0.5 ml – 1.0 ml) was then added to the disc and left *in situ* for 60 s prior to irradiation.

7.2.7.1.3.1 Light Source

A pulsed diode soft laser (Periowave™, Figure 7.2) with a wavelength of 660 - 675 nm and a power output of 13.68 J/cm² for 60 s, was used for all the irradiation experiments. The power output was measured using a TPM-300 thermopile power meter (Genetic-*eo*, Québec, Canada). A uniform light distribution was emitted from the tip of the laser at a fixed distance of 1 cm from the disc. Static irradiation for the entire disc was completed in 60 s. The methylene blue was then removed.



Figure 7.2. Periowave photodisinfection system.

7.2.7.2 Mechanical cleaning

7.2.7.2.1 Titanium brush (TB)

The titanium coated brush (Figure 7.3) manufactured by Straumann, has a shank of approximately 10 mm in length and the end bristle was fitted to a slow speed NSK Contra angle handpiece (ERI 6i 16:1).

The hand piece was attached to the portable NSK Mio Coreless Micromotor System (120V). Mechanical decontamination was carried out at the selected speed at 300 rpm for 60 s. To avoid contact on the surface of interest, the disc was placed into a sterile petri dish and held with sterilize titanium tweezer from their edges to prevent movement during decontamination process. During brushing, the plate was filled with approximately 5 ml of RTF, to allow the surface of the disc to be irrigated continuously to emulate the irrigation with clinical conditions. (Note: one TiBrush was used to decontaminate two discs and then discarded).

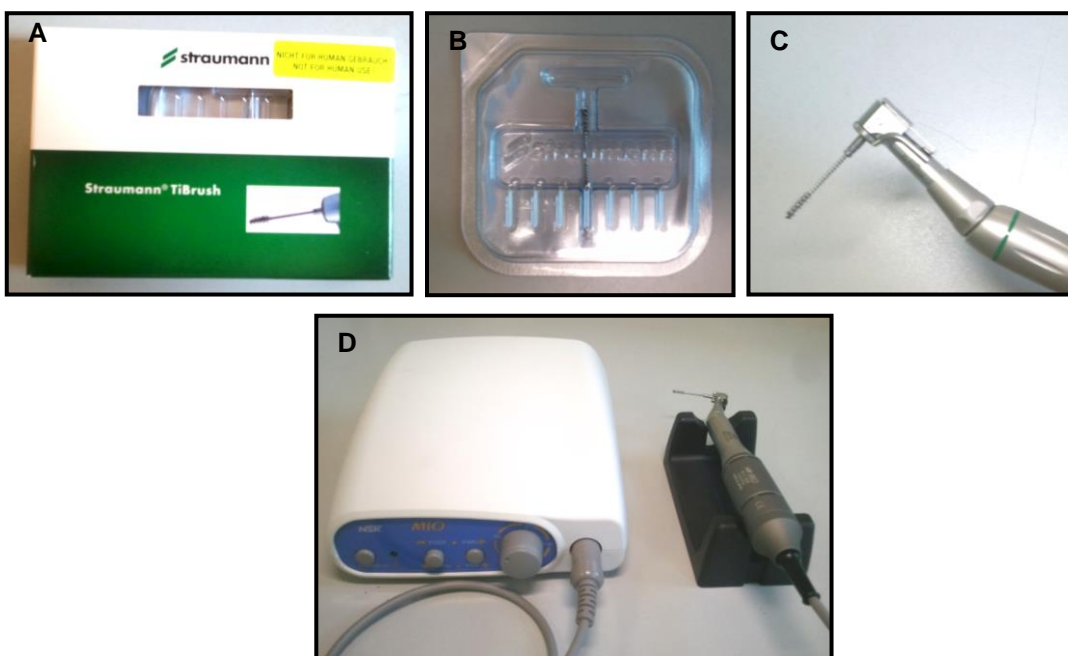


Figure 7.3. A. The Straumann TiBrush; B. The titanium brush (manufactured by Straumann); C. Slow speed NSK Contra angle handpiece (ERI 6i 16:1); D. Portable NSK Mio Coreless Micromotor System (120V).

7.2.7.2.2 Combination of titanium brush followed by photodynamic therapy (TiBrush + PDT)

Similar to the methods described above, a combination technique was applied, which first used the Straumann titanium brush for 60 s to disrupt and remove the biofilm, followed by PDT for 60 s. The methylene blue was removed by repeatedly dipping into RTF to ensure removal of the photosensitiser.

7.2.8 Biofilm sampling

Biofilms sampling have been described previously (chapter 2 section 2.2.4) and these were employed with minor modification. The titanium discs were aseptically removed and subjected to the appropriate decontamination method (or placed in 1 ml RTF in the case of the control). The biofilm was then removed from the discs by vortex mixing with glass beads (5 beads of 3 mm diameter per disc) for 1 min. The recovered biofilm suspension was then serially diluted up to 10^7 fold and 20 aliquots were spread in duplicate onto appropriate media to give viable counts. The biofilm microorganisms were cultured on fastidious anaerobic agar culture media, Gram-negative anaerobe culture media, mannitol salt culture media for isolation of *Staphylococcus* spp. and Sabourauds dextrose culture media for isolation of *Candida* species. All plates were incubated aerobically for 48 h with 5% CO₂, except fastidious anaerobic agar and Gram-negative anaerobic agar which were incubated for 4 to 5 days under anaerobic conditions. Following appropriate incubation, the colonies were counted (CFU/biofilm) and used to calculate the viable counts (CFU/biofilm) of different species.

7.2.9 Confocal laser scanning microscope

The structure of CDFF biofilm has previously been studied using confocal laser scanning microscopy (CLSM). The current research used CLSM to analyse those biofilms grown under peri-implantitis conditions. The aim of this study was to contribute to the limited knowledge of biofilm structures following treatment therapies. For microscopy observations, discs harbouring biofilms were carefully held with sterilize forceps and processed. Each biofilm was subsequently immersed in 5 ml solution of RTF with *Baclight*™ viability staining and stored in a dark place, covered with foil for 15 min. Each biofilm was analysed by Image J in combination with Image analysis software for investigation of microbial biofilms. The cell counting function was used to measure total bacterial biomass and the distribution of the green (live) channel and red (dead) channel in one image.

Other colours such as cream colour were considered as dead or dying (Chávez de Paz, 2009).

7.2.10 Biocompatibility test

An Alamar blue assay was used to assess metabolic activity of the MG-63 cells. Alamar blue is a dye that is used to assess the metabolic activity of MG-63 cells by functioning as an oxidation-reduction indicator. Alamar Blue dye is reduced from blue to a pink fluorescence by live cells. The oxidation-reduction process is based on the detection of the level of oxidation. The level of fluorescence was monitored at 530 nm excitation and 590 nm emission wavelength.

7.2.10.1 Standard curve of MG-63 cells

The cell media were first removed and 900 μ l of fresh culture media was added to each well of a 24-well plate containing MG-63 cells. One well devoid of MG-63 cells served as a control. Subsequently, a 100 μ l of Alamar blue was added to each well and incubated for exactly 4 h in incubator at 37°C. After 4 h incubation, 2 \times 100 μ l were taken from each well and transferred to a black 96 h well plate. The fluorescence was measured immediately (Luminoskan Ascent Microplates Reader, Labsystems, UK) at 530 nm excitation wavelength and 590 nm emission wavelength using software Ascent version 2.4.

7.2.10.2 MG-63 cells on decontamination surfaces

Once the surface decontamination had been performed, discs from both test and control groups were irradiated with UV (254 nm wavelength; 230 V, 50 Hz) for 30 min per side prior to cell culture. MG-63 cells were cultured and maintained in 75 cm² flask in 500 ml of Dulbecco's modified Eagle medium (DMEM; Gibco, Paisley, UK) containing 10% fetal bovine serum (FBS; Gibco), 1% penicillin-streptomycin, at 37°C in 5% CO₂ incubator. The medium was changed every 48 h – 72 h. The cells were washed with phosphate-buffered saline (PBS; Gibco) and detached with trypsin-EDTA solution (0.25% trypsin-EDTA; Gibco) at 37°C for 2 min. Once trypsinised, the cells were counted using a coulter-counter via haemocytometer using trypan blue. The MG-63 cells were then seeded onto the discs in a 48-wells plate, at a concentration of 2500 cells/disc and incubated for 4 h at 37 °C. The culture medium was added to ensure that the final volume of each well was 200 μ l and the preparation was incubated at 37°C. The MG-63 cells were incubated and aliquots harvested at different time periods (day 1, 4

Chapter 7: An *in vitro* assessment of antibacterial treatment strategies

and 7) for the Alamar blue assay as shown in figure 7.4 and figure 7.5. All subsequent experiments were performed in duplicate.

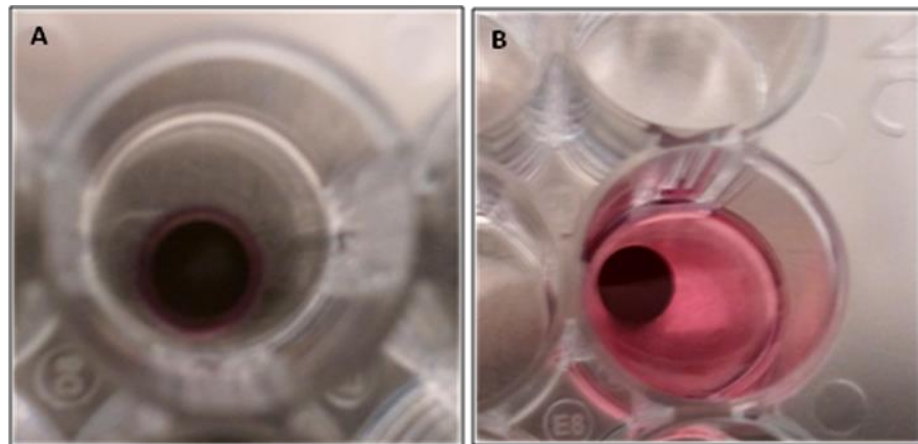


Figure 7.4. A. MG-63 cells were placed onto a disc; B. 200 µl of culture medium was added after 4 h of incubation of MG-63 cells.

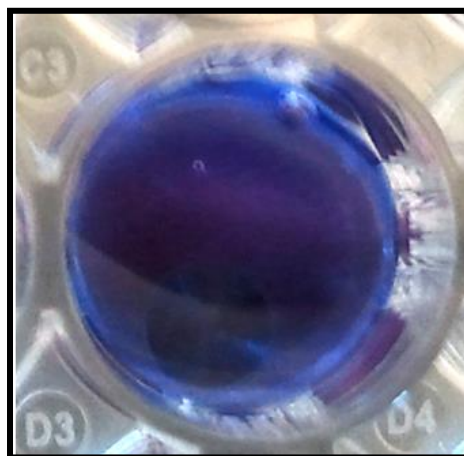


Figure 7.5. 20 µl of Alamar blue was added into the medium and incubated for 4 h prior to fluoroscan assay.

7.2.10.3 Fluoroscan assay

After 24 h, the 48 well plates were removed from the incubator. To each well, 20 μ l of Alamar blue was added to the medium giving a final concentration of 10% v/v). After incubation for 4 h at 37°C, 100 μ l of medium was removed and the optical densities of each sample were read at 530 nm (excitation wavelength) and 590 nm (emission wavelength) on a micro-plate reader (Fluoroscan II). Fluorescence was measured in arbitrary fluorescent units. A control using just MG-63 cells and Alamar blue was also prepared. The same steps were repeated for data collection on day 4 and day 7. Once the samples for the reading were collected, the medium in each experimental well (containing the disc) and control well was changed. The existing medium was removed and replaced with 200 μ l of medium. The plate was then returned to the incubator until the next sampling point. For the control group, the same protocol was applied, except that the surfaces had not previously been inoculated with biofilm. Sterile discs were placed in the well plate, exposed under the UV radiation as described previously prior to cell culture (Figure 7.6).

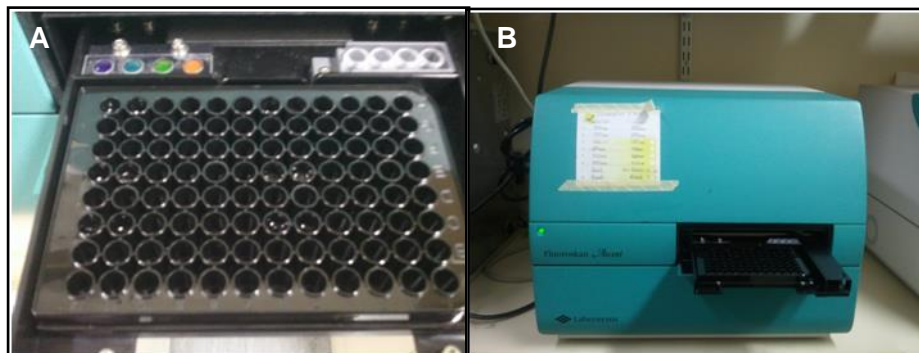


Figure 7.6. A. 100 μ l of sample (medium and Alamar blue) was removed and placed into each well of 96 wells. B. The optical densities of each sample were read at 530 nm (excitation) and 590 nm (emission) on a micro-plate reader (Fluoroscan II).

7.2.10.4 Scanning electron microscopy (SEM)

SEM was used to investigate osteoblast morphology in the presence of biofilm (control), sterilised discs and those 'decontaminated' by the three specific approaches. Analysis by field emission scanning electron microscopy (FE-SEM) for the discs cultured under conditions of peri-implantitis was performed.

These discs were fixed with 4% paraformaldehyde in 0.1 M phosphate buffer (pH 7.4) and stored at - 4°C for 1 week. They were dehydrated for 10 mins in a graded series 50%, 70%, 90% and twice in 100 % of ethanol, treated with

Chapter 7: An *in vitro* assessment of antibacterial treatment strategies

isoamyl acetate for 1 min, and then sputter-coated with gold and the surface and cellular morphology was observed. Images of the discs with and without biofilm following the various decontamination regimes were obtained both without biofilm and with biofilm and following decontamination regimes.

7.3 Results

7.3.1 Cultural analysis

Culture-based analysis of the inoculum showed the total number of microorganisms for the targeted groups were ca. 10^7 CFU/ml (Gram-negative anaerobic bacteria), ca. 10^6 CFU/ml (*Candida*) and ca. 10^2 CFU/ml (staphylococci) (Table 7.1).

Table 7.1. The mean \pm standard deviation of CFU/ml ($n = 4$) of the salivary inoculum.

Bacteria species	Mean (CFU/ml) \pm SD
Anaerobe spp.	$1.85 \times 10^7 \pm 3.19 \times 10^6$
Gram-negative anaerobe spp.	$8 \times 10^6 \pm 7.60 \times 10^6$
<i>Candida</i> spp.	$3.31 \times 10^6 \pm 9.90 \times 10^5$
<i>Staphylococcus</i> spp.	$3.75 \times 10^2 \pm 2.50 \times 10^2$

7.3.2 Substratum

7.3.2.1 Peri-implant mucositis conditions

The biofilm CFU/ml data revealed some differences between treatments and between biofilms when grown on the three different surfaces. The culture data for the various decontamination regimes with error bars representing the standard deviation for 366 h peri-implant mucositis microcosm are shown in figures 7.7, 7.8 and 7.9.

Polished Surface (Fig 7.7)

Compared with the control, reduced numbers of anaerobic bacteria and *Candida* were evident when the combined technique, PDT or CHX treatments were used. There was reduction of anaerobe spp., *Candida* spp. between control and TiBrush. There was reduction of Gram-negative anaerobe spp. between control and combined techniques, and CHX. There was reduction of *Staphylococcus* spp. between control and all decontamination regimes. From these data it is shown that CHX and combined technique (TiBrush and PDT) were the most efficient decontamination regimes.

SLA Surface (Fig 7.8)

Compared with control surfaces, there was a reduction in the total number of anaerobic bacteria, Gram-negative anaerobic bacteria, and *Candida* on surfaces treated with the combined technique, Tibrush and PDT. There was reduction of *Staphylococcus* spp. between control and TiBrush, PDT. Compared with the control, there was a reduction in the number of staphylococci when surfaces were treated with CHX. From these data it was shown that the TiBrush was the most efficient decontamination regime.

SLActive Surface (Fig 7.9)

Compared with control surfaces, reduction in the numbers of anaerobic bacteria, Gram-negative anaerobic bacteria, *Candida* and staphylococci occurred following application of the combined technique, TiBrush and PDT. A reduction in the number of staphylococci, *Candida*, anaerobic bacteria and Gram-negative anaerobic bacteria was also evident when surfaces were treated with CHX. From these data it was shown that a combined technique (TiBrush and PDT), TiBrush and PDT were the most efficient decontamination regimes.

Significant differences were found between biofilms when grown on the three different surfaces under peri-implant mucositis at 336 h.

On all surfaces, a reduction in the number of CFU/ml of anaerobe bacteria was observed between the polished surface and both the SLA surface and SLActive surface. Lower numbers of Gram-negative anaerobic bacteria were evident on polished surfaces compared with both SLA and SLActive surfaces. There were no differences between *Candida* spp. and *Staphylococcus* spp. numbers on all three surfaces.

Overall, these data show that the lowest number of microorganisms in mature biofilms (366 h) occurred on polished surfaces, with comparably higher numbers present on the SLA and SLActive surfaces.

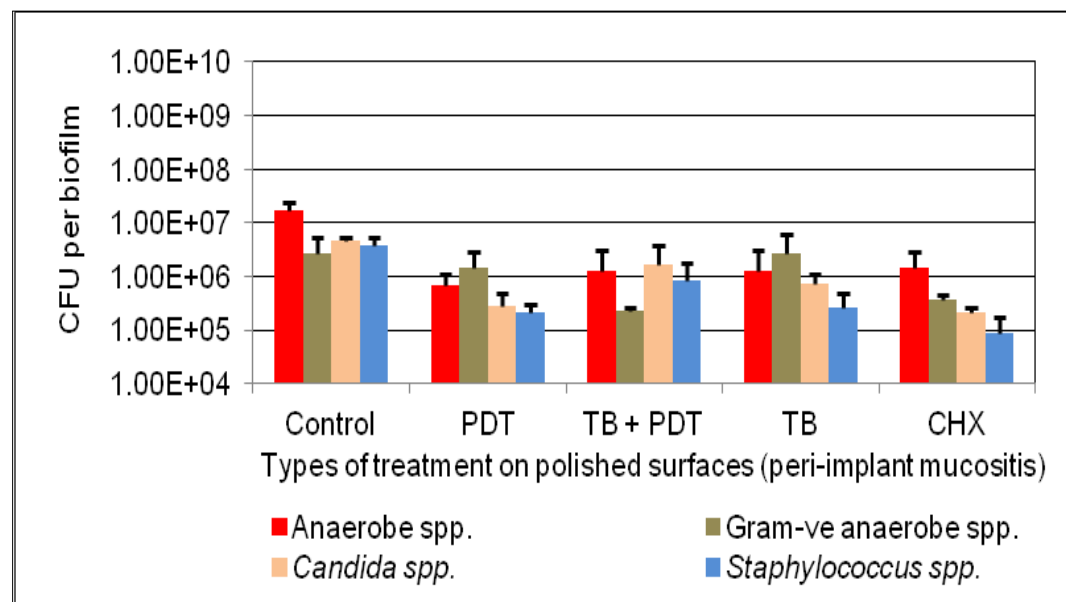


Figure 7.7. The composition of the biofilm microorganisms (CFU/ml) after decontamination techniques on polished titanium surfaces under peri-implant mucositis conditions. Error bars represent standard deviation ($n = 4$).

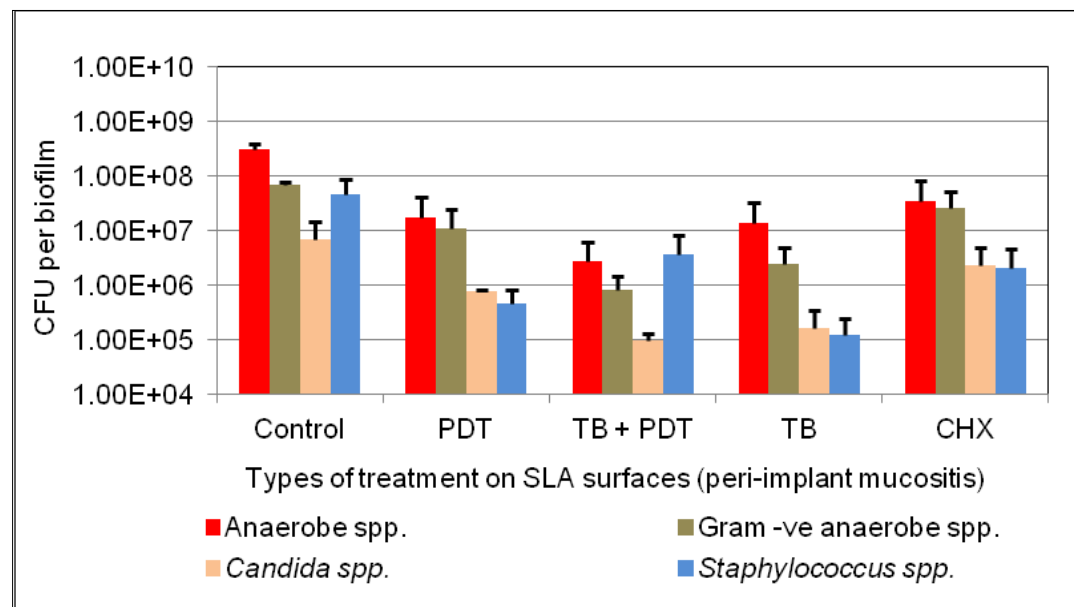


Figure 7.8. The composition of the biofilm microorganisms (CFU/ml) after decontamination techniques on SLA titanium surfaces under peri-implant mucositis conditions. Error bars represent standard deviation ($n = 4$).

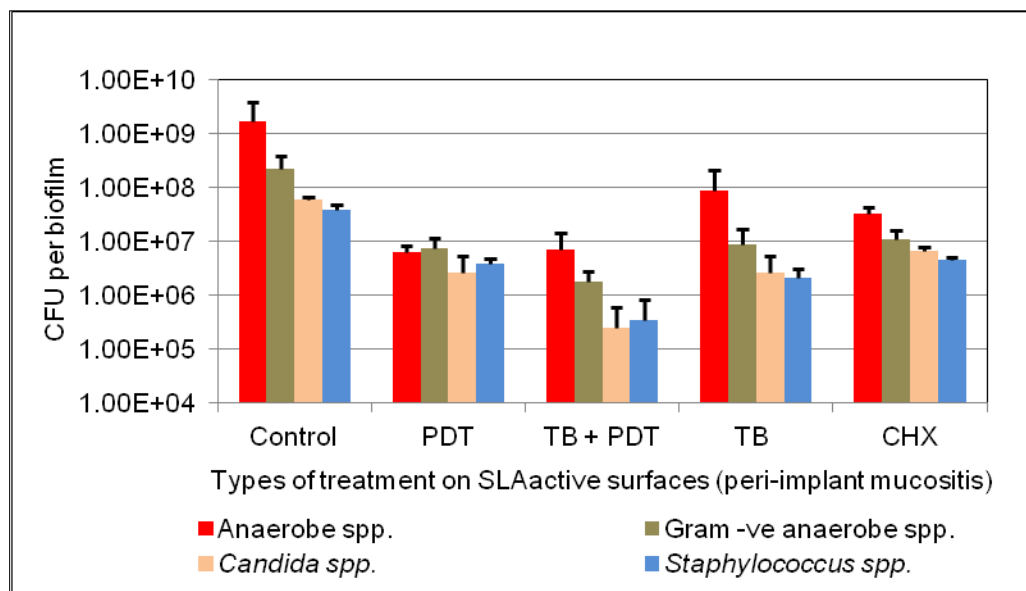


Figure 7.9. The composition of the biofilm microorganisms (CFU/ml) after decontamination techniques on SLActive titanium surfaces under peri-implant mucositis conditions. Error bars represent standard deviation ($n = 4$).

7.3.2.2 Peri-implantitis conditions

Analysis of the biofilm CFU data revealed some significant differences between treatments and between biofilms between biofilms cultured on the three different surfaces. The culture data (CFU/biofilm) for the various decontamination regimes with error bars representing the standard deviation for 612 h peri-implantitis microcosm (Figures 7.10, 7.11 and 7.12).

Polished Surface (Fig 7.10)

Compared with the control surfaces, treatment with the TiBrush, combined technique or PDT resulted in reduced numbers of anaerobic bacteria, Gram-negative anaerobic bacteria, *Candida* and staphylococci. In addition, compared with the control, a reduction in the number of these same groups of microorganisms was evident following CHX treatment. From these data, the TiBrush was deemed as the most efficient decontamination regime.

SLA Surface (Fig 7.11)

There was reduction in the number of anaerobe spp., Gram-negative anaerobe spp., *Candida* spp., *Staphylococcus* spp. between control and combined techniques, PDT, TiBrush and CHX. From these data, the combined technique (TiBrush and PDT) was the most efficient decontamination regime.

SLActive Surface (Fig 7.12)

Lower numbers of anaerobic bacteria, Gram-negative anaerobic bacteria, *Candida* and staphylococci were evident on the SLActive surfaces after use of the combined technique (TiBrush and PDT) or TiBrush compared with the control.

The difference in microbial numbers was found between biofilms cultured on the three different surfaces under peri-implantitis conditions at 612 h. comparing the levels of microorganisms for the untreated control surfaces, it was apparent that the numbers of anaerobic bacteria were lower on the polished surface compared with the SLActive surface. No other differences were evident between surfaces.

Overall, these data show that polished surfaces were different from SLActive surfaces, whilst no difference was evident between SLA and SLActive surfaces. Also, polished surfaces were not different from SLA surfaces.

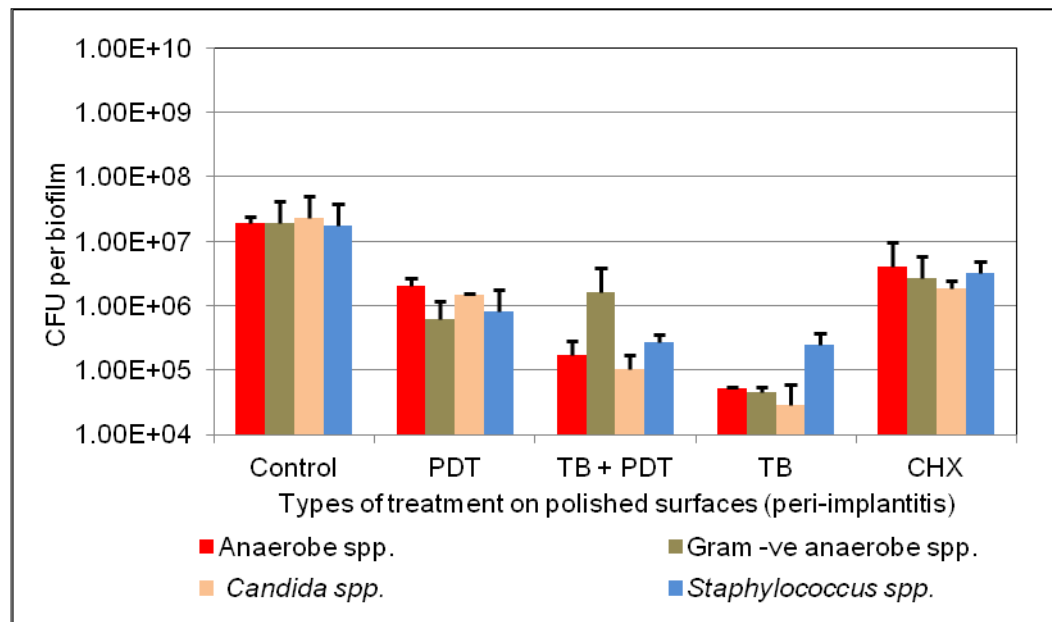


Figure 7.10. The total counts of biofilm microorganisms (CFU/ml) after decontamination techniques on polished titanium surfaces under peri-implantitis conditions. Error bars represent standard deviation ($n = 4$).

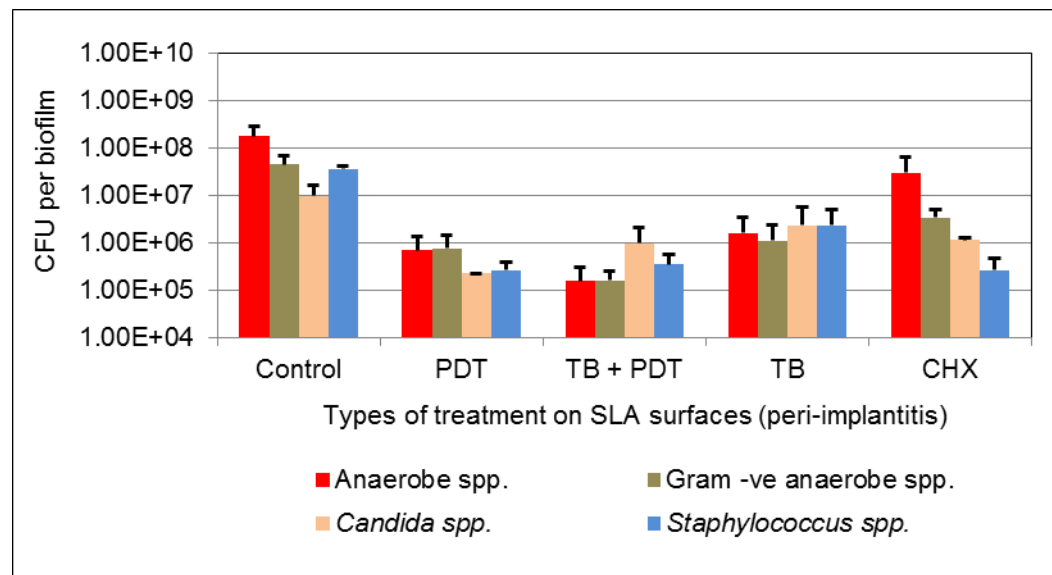


Figure 7.11. The total counts of biofilm microorganisms (CFU/ml) after decontamination techniques on SLA surfaces under peri-implantitis conditions. Error bars represent standard deviation ($n = 4$).

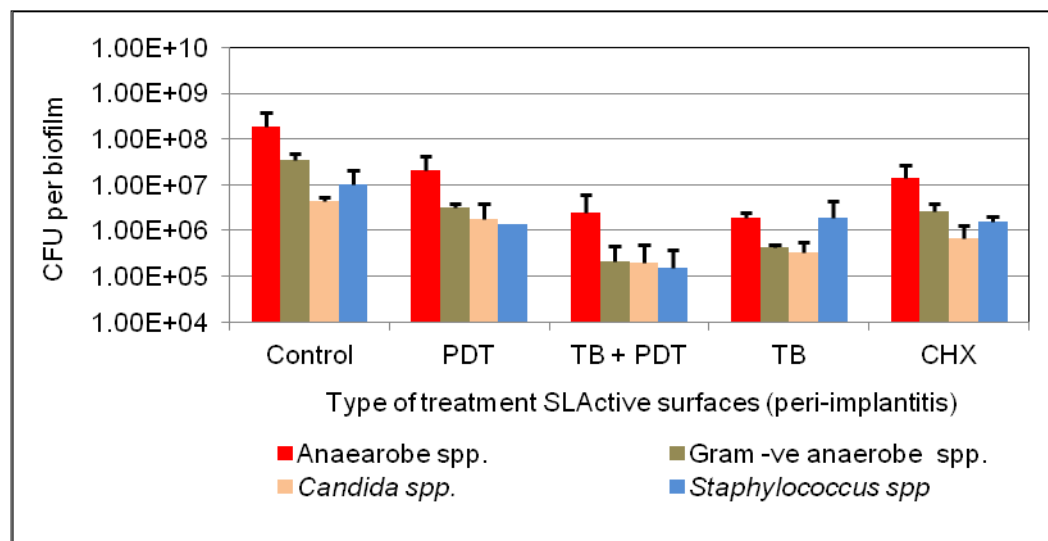


Figure 7.12. The total counts of biofilm microorganisms (CFU/ml) after decontamination techniques on SLActive surfaces under peri-implantitis conditions. Error bars represent standard deviation ($n = 4$).

7.3.3 Biofilm analysis using CLSM

Biofilms grown on polished, SLA and SLActive surfaces were analysed by Image J in combination with an investigation of total biomass (a volume/area of fluorescence) were analysed using the Bioimage-L software package. The cell counting function was used for measuring live (Green), dead (Red) or cream coloured (cells were assumed to be dying).

The CLSM imaging results for the control untreated biofilms (RTF) are shown in figure 7.13: The total biomass of the 3 surfaces ranged between ca. 22,000 μm^3 for the polished surface and was higher for the other two surfaces (ca. 27,000 μm^3). The CLSM images of the biofilm were characterised by the presence of large amounts of viable bacteria with an open void like biofilm structure. Dead cells were a small proportion of the cells on polished (4%) and SLActive surfaces (2%), but increased in proportion, to 10% on the SLA surface.

The CLSM imaging results for the PDT treatments are shown in figure 7.14: The total biomass of the 3 surfaces ranged between ca 23,000 μm^3 for the polished surface to ca. 26,000 μm^3 and ca. 28,000 μm^3 for the other two surfaces. These values were similar to those on the control surfaces. Compared to the control, the proportion of dead or dying cells was greater in the biofilms on polished (29% vs. 4%) and SLActive (21% vs. 2%) surfaces. Only a small increase in the proportion of dead cells (12% vs. 10%) was evident on the SLA surfaces compared with the control. The CLSM imaging of biofilm reflects the data generated from the Bioimage-L software package and was characterised by the presence of greater quantities of non-viable bacteria on polished and SLActive surfaces.

The CLSM imaging results for the combined (TB+PDT) are shown in Figure 7.15: The total biomass of the 3 surfaces ranged between ca. 1,000 μm^3 and ca. 7,000 μm^3 . These values were greatly reduced for all surfaces compared to the control biomass. The non-viable cells were in higher proportions on polished (8% vs. 4%), on SLA (52% vs. 2%) and SLActive surfaces (31% vs. 10%) compared to the control. The CLSM imaging of biofilm was characterised by the presence of a small amount of viable/non-viable bacteria on all surfaces.

The CLSM imaging results for the (Ti Brush) are shown in figure 7.16: The total biomass of the 3 surfaces varied greatly between the surfaces and ranged

between ca. 1,000 μm^3 and ca. 16,000 μm^3 . These values were greatly reduced for all surfaces compared to the biomass on the control. The proportion of non viable cells was small and did not exceed 5% on any of the three surfaces. The CLSM imaging of biofilms has characterised by the presence of a small amount of viable/non-viable bacteria on all surfaces.

The CLSM imaging results for the (CHX) are shown in figure 7.17: The total biomass of the 3 surfaces ranged between ca. 25,000 μm^3 and ca. 27,000 μm^3 and was similar to control surfaces. The proportion of dead or dying cells was higher on the SLA (8% vs. 3%) and SLActive (11% vs. 2%) surfaces compared to the control. CLSM imaging of the biofilms was characterised by the presence of a greater amount of viable/non-viable bacteria on all surfaces.

Overall, the Ti + PDT combination treatment was most effective at reducing total biofilm mass at reducing total biofilm biomass, with reductions of 93%, 80% and 74% evident with polished, SLA and SLActive surfaces, respectively. The Ti + PDT combination treatment also showed good antimicrobial efficacy. Compared to the control, the viable biomass was reduced by over 80% for all surfaces (93%, 90% and 81% for polished, SLA and SLActive surfaces, respectively).

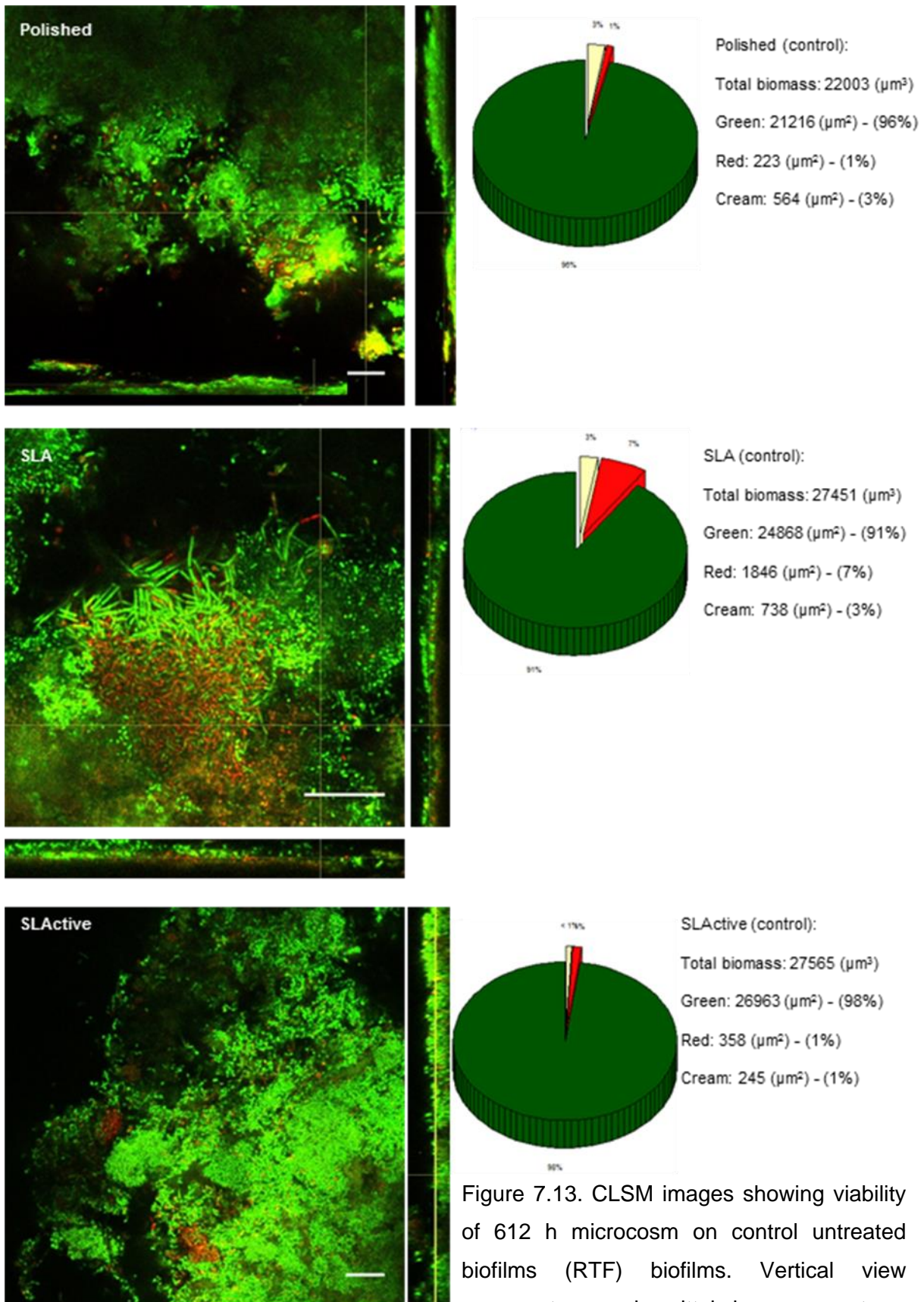


Figure 7.13. CLSM images showing viability of 612 h microcosm on control untreated biofilms (RTF) biofilms. Vertical view represents yz and sagittal view represents xz taken through layers of z axis. Scale bar represents 20 μm .

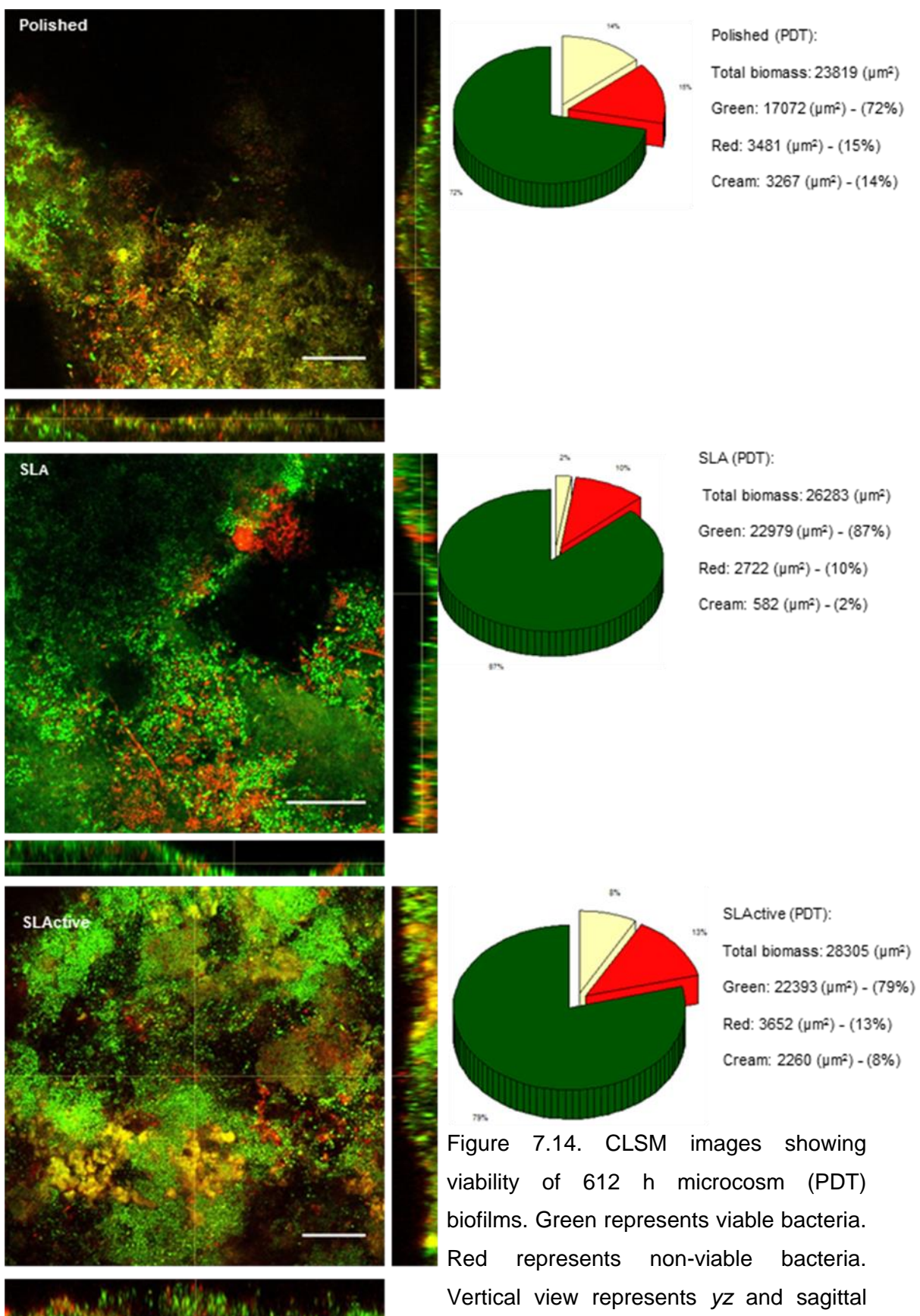


Figure 7.14. CLSM images showing viability of 612 h microcosm (PDT) biofilms. Green represents viable bacteria. Red represents non-viable bacteria. Vertical view represents yz and sagittal view represents xz taken through layers of z axis. Scale bar represents 20 μm .

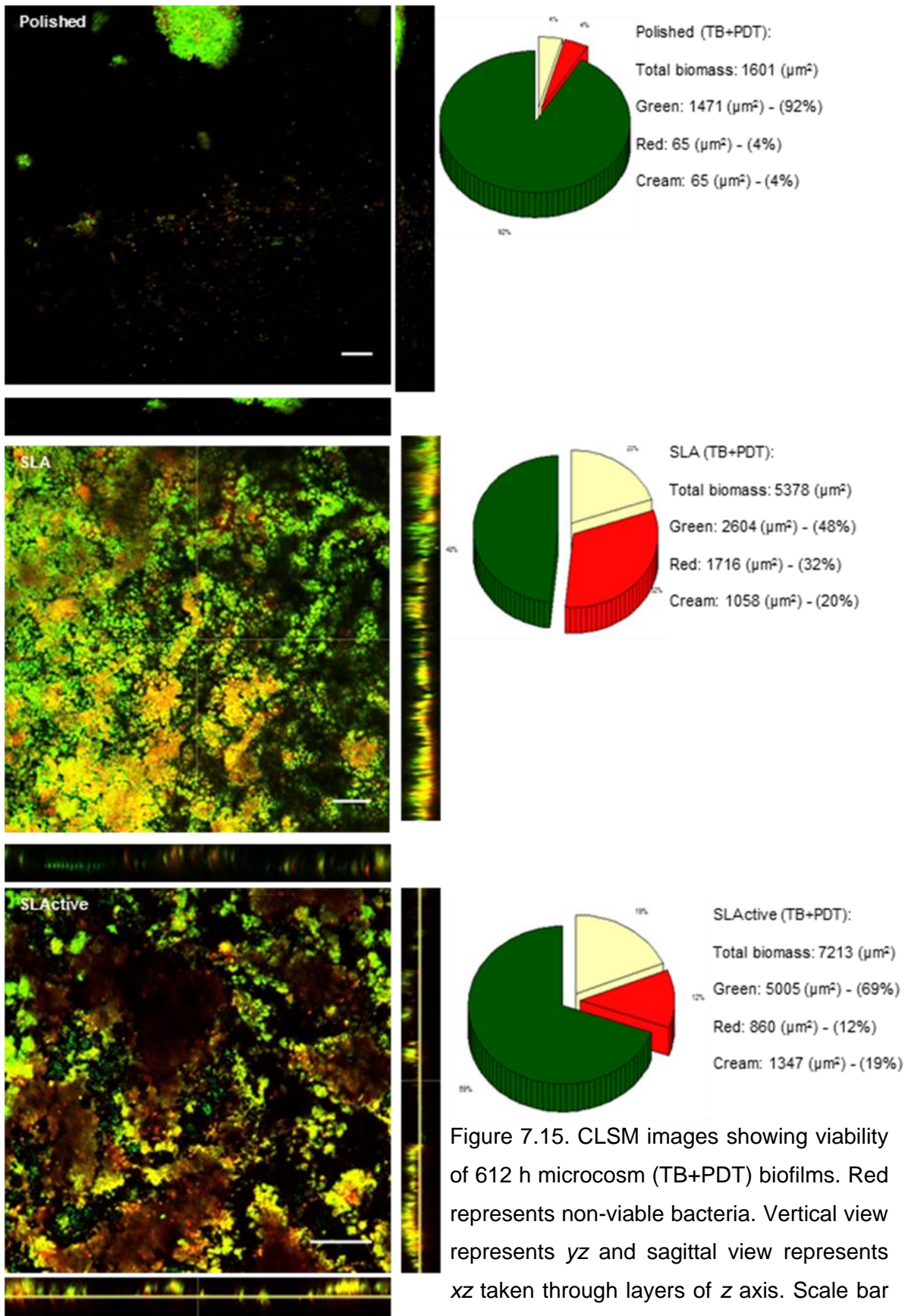


Figure 7.15. CLSM images showing viability of 612 h microcosm (TB+PDT) biofilms. Red represents non-viable bacteria. Vertical view represents *yz* and sagittal view represents *xz* taken through layers of *z* axis. Scale bar represents 20 μm .

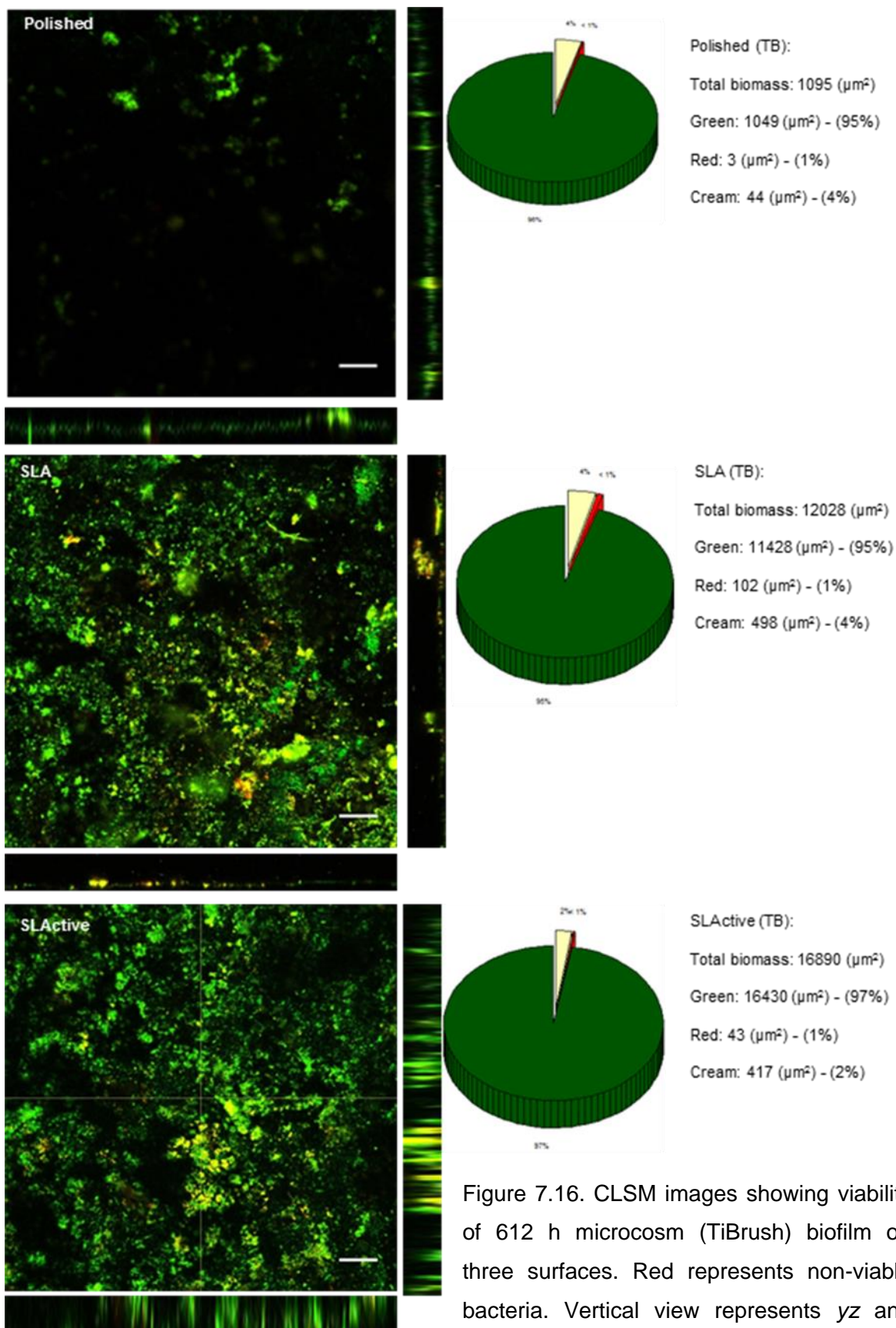


Figure 7.16. CLSM images showing viability of 612 h microcosm (TiBrush) biofilm on three surfaces. Red represents non-viable bacteria. Vertical view represents yz and sagittal view represents xz taken through layers of z axis. Scale bar represents 20 μm .

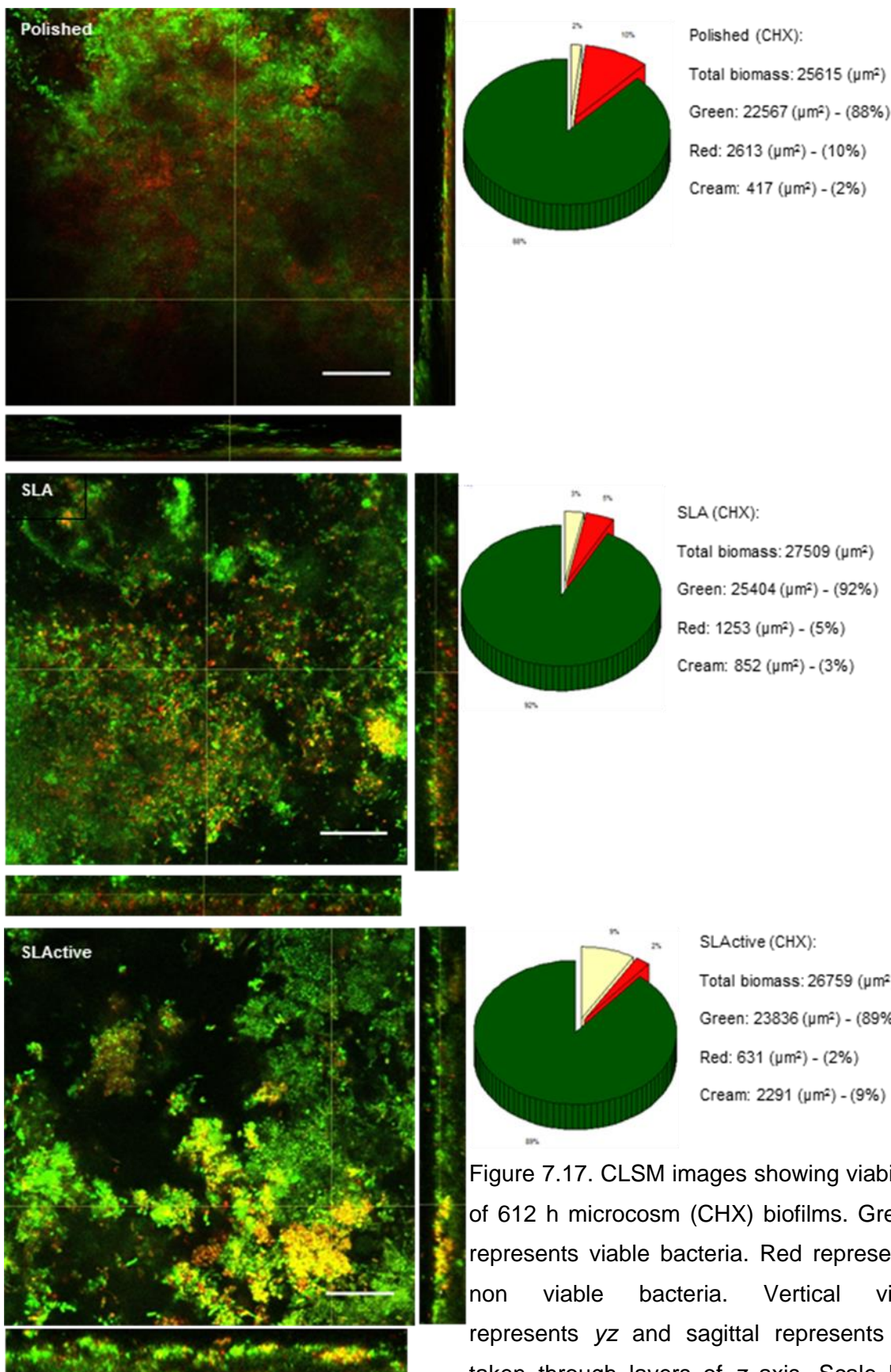


Figure 7.17. CLSM images showing viability of 612 h microcosm (CHX) biofilms. Green represents viable bacteria. Red represents non viable bacteria. Vertical view represents yz and sagittal represents xz taken through layers of z axis. Scale bar represents 20 μm .

7.3.3.1 Biofilm thickness

CLSM was used to analyse the biofilms of the different titanium surfaces, with two discs of each surface type being examined. The CLSM images were obtained from four sites per disc. In 3D section analysis, the z step size was 1 μm and the image stacks were converted into JPEG format and processed through the image J software analysis with orthogonal views, which calculated the biofilm thickness (Figure 7.18).

Biofilm thickness on the different titanium surfaces was investigated after 612 h of biofilm growth. The thickness of the biofilm was similar on all untreated surfaces (49 μm – 55 μm). When the surfaces were treated using the four test regimes, the mechanical approach using TiBrush therapy was the most effective at reducing the mean biofilm thickness (8.5 μm , ca. 16.25 μm , ca. 16.5 μm for polished, SLA and SLActive surfaces, respectively). The next most effective was combined technique treatment (TiBrush + PDT) which reduced the biofilm thickness to 8 μm , ca. 21.5 μm , 18 μm for polished, SLA, SLActive surfaces, respectively. When using mechanical regimes, the reduction in biofilm thickness was greatest with the polished followed by SLActive and SLA surfaces. On the whole, there were observable differences between the biofilm thicknesses on different titanium surfaces.

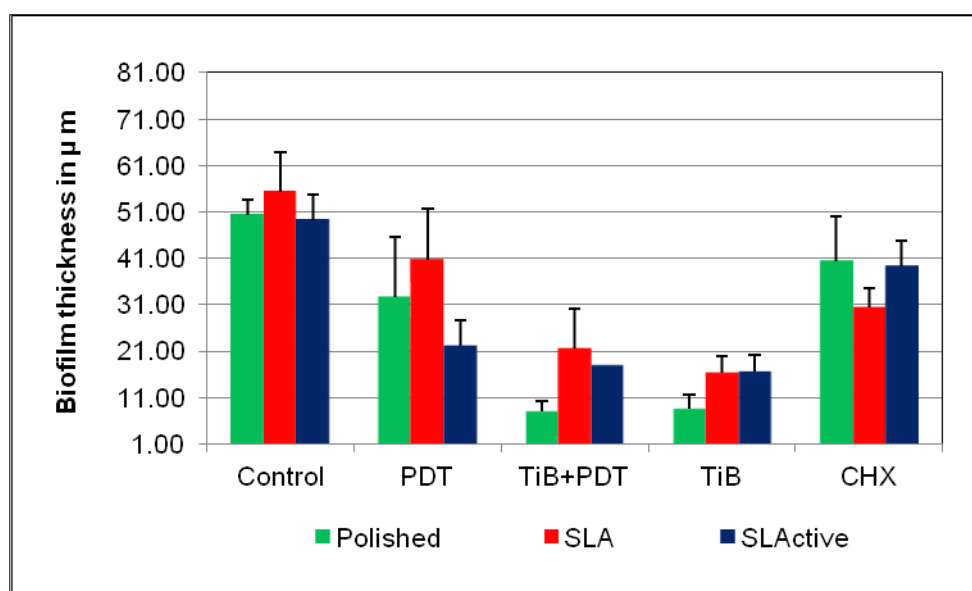


Figure 7.18. Thickness of biofilm μm grown on the three titanium surfaces after treatment regimes. Biofilms were 612 h old and grown under peri-implantitis conditions. Error bars represent standard deviation ($n = 4$).

7.3.4 Cell morphology

The results of decontamination and MG-63 cell culture were accompanied by imaging of both test and control discs by SEM. All Ti surfaces were examined after 7 days. The surface topography for the polished surface was moderately smooth ($R_a > 0.5 \mu\text{m}$) in appearance; SLA and SLActive surfaces were moderate rough ($R_a = 1.75 \mu\text{m}$) with the micro-pits, peaks and channels across the entire surface observed under 200 μm magnification were examined by the Straumann Company (Basel, Switzerland) (Figure 7.19).

Sterile discs- Figure 7.20: the MG-63 cells were grown on the three Ti surfaces. The cells grew well and assumed the appearance of (i) elongated cells scattered across the surface on polished surfaces, (ii) spindle shaped or polygonal cells on SLA surfaces and (iii) circular cells on SLActive surfaces.

Reduced transport fluid (RTF; control untreated biofilms) – Figure 7.21: the SEM of the polished surface revealed biofilm. The SLA was partially covered with an organic layer and the SLActive was completely covered with bacteria and MG-63 cells.

Photodynamic therapy (PDT) - Figure 7.22: the micrograph, at day 7 showed that the pits and troughs were entirely covered with an organic layer. The MG-63 cells were shown to be attached to the surface and dividing on polished and SLA surfaces. On SLActive surfaces, the presence of an organic layer with residual bacteria was observed.

Titanium brush and PDT (Ti + PDT) – Figure 7.23: no bacteria were observed on the polished Ti surfaces, but there was attachment of MG-63 cells (red arrow). The MG-63 cells were observed attached to the surface showing possible cell division. On SLA surfaces, the MG-63 cells were shown attached to other MG-63 cells. On SLActive surfaces the presence of an organic layer with residual bacteria was observed. Complete elimination of biofilm was not seen. There was no evidence of any surfaces changes brought about by the use of the Ti Brush.

Titanium brush (TiBrush) – Figure 7.24: from the SEM analysis, MG-63 cells were attached to all three surfaces. On all surfaces there were areas of

Chapter 7: An *in vitro* assessment of antibacterial treatment strategies

multilayered MG-63 cells. There was no evidence of any surface alteration brought about by the use of the Ti Brush.

Chlorhexidine (CHX) – Figure 7.25: SEM analysis of the polished surface showed an absence of MG-63 cells, and these surfaces were completely covered by layers of biofilm and organic material. SLA surfaces showed MG-63 cells covered with bacteria. The SLActive surface showed an absence of MG-63 cells and complete coverage with bacteria.

Overall, the SLA and SLActive surfaces were demonstrated most biocompatibility following treatment modalities. The Ti + PDT combination treatment and TiBrush treatment indicated good biocompatibility efficacy compared to the other therapies.

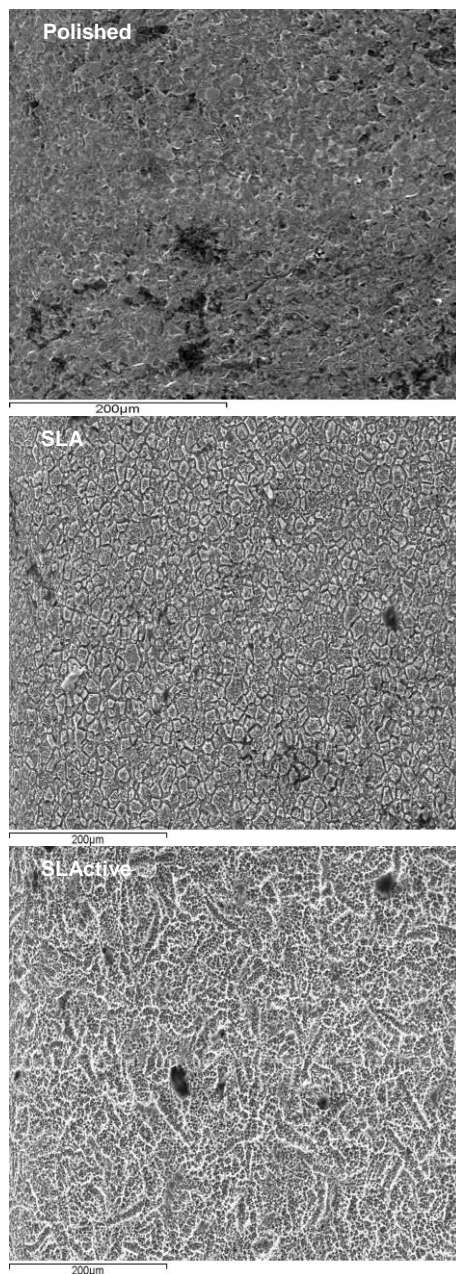


Figure 7.19. Sterile discs examined under SEM revealed that polished surfaces were relatively moderately smooth, whilst SLA and SLActive surfaces exhibited micropits, grooves and troughs (deemed moderately rough). Samples were viewed at $\times 200$ (Bar 200 μm).

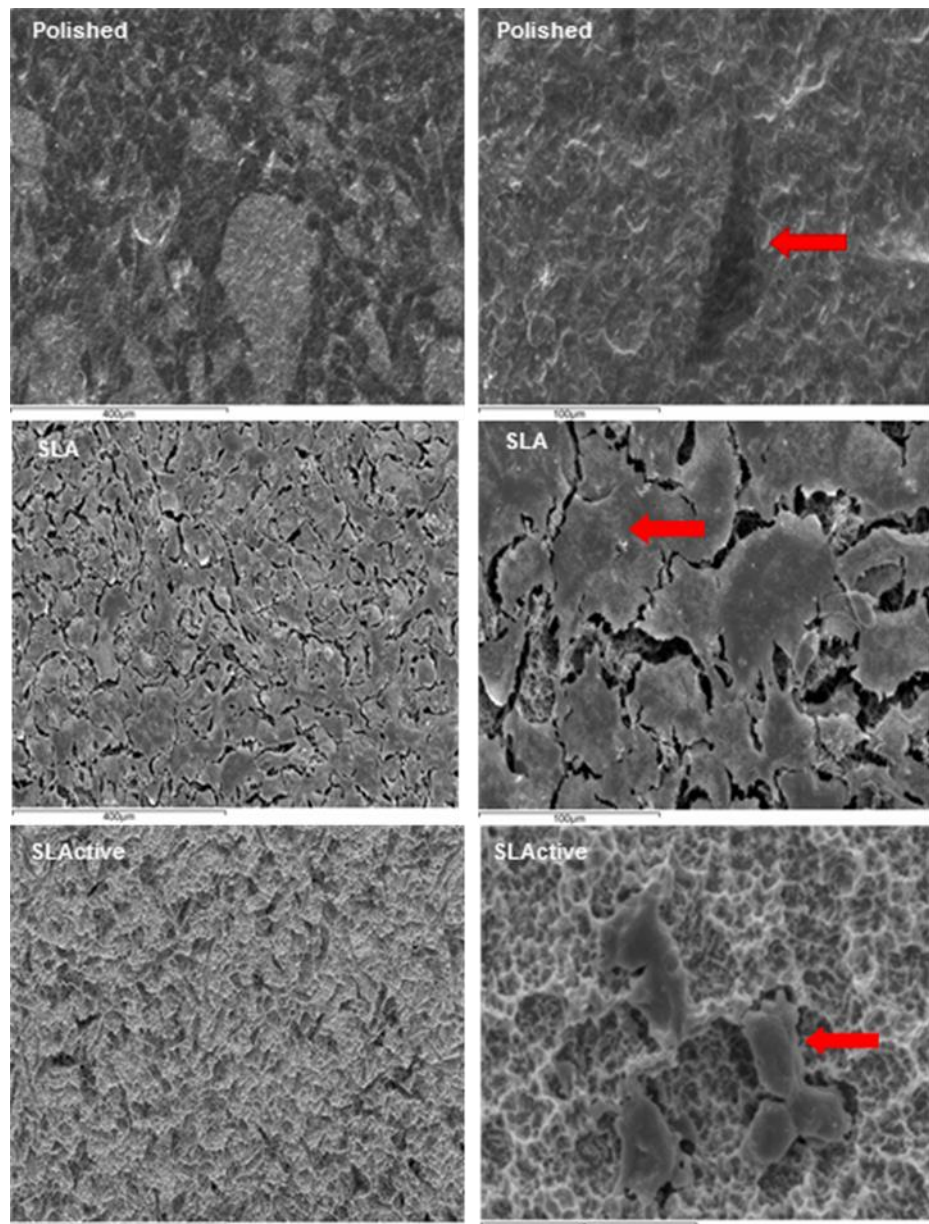


Figure 7.20. MG-63 cells (red arrows) attaching on three different sterile structural surfaces. Samples were viewed at $\times 1500$, $\times 500$, and $\times 150$ (Bar 40 μm , 100 μm , 400 μm , respectively).

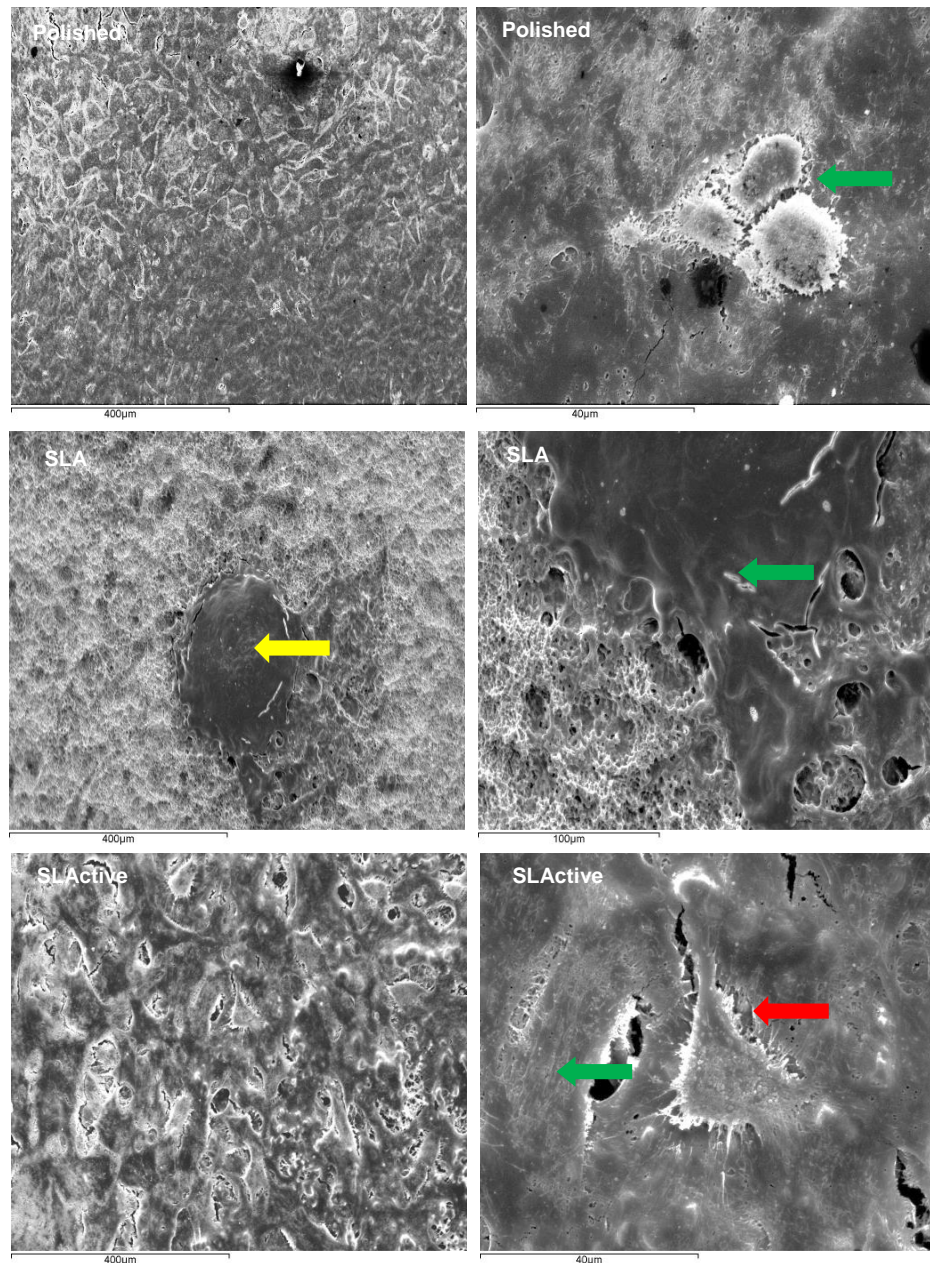


Figure 7.21. MG-63 cells grown on three untreated control biofilms surfaces (RTF) after 7 days in culture. Green arrow indicates residual biofilm, yellow arrow indicates organic layer made solid lamp, and red arrow indicates MG-63 cells. Samples were viewed at $\times 1500$, $\times 500$, and $\times 150$ (Bar 40 μm , 100 μm , 400 μm , respectively).

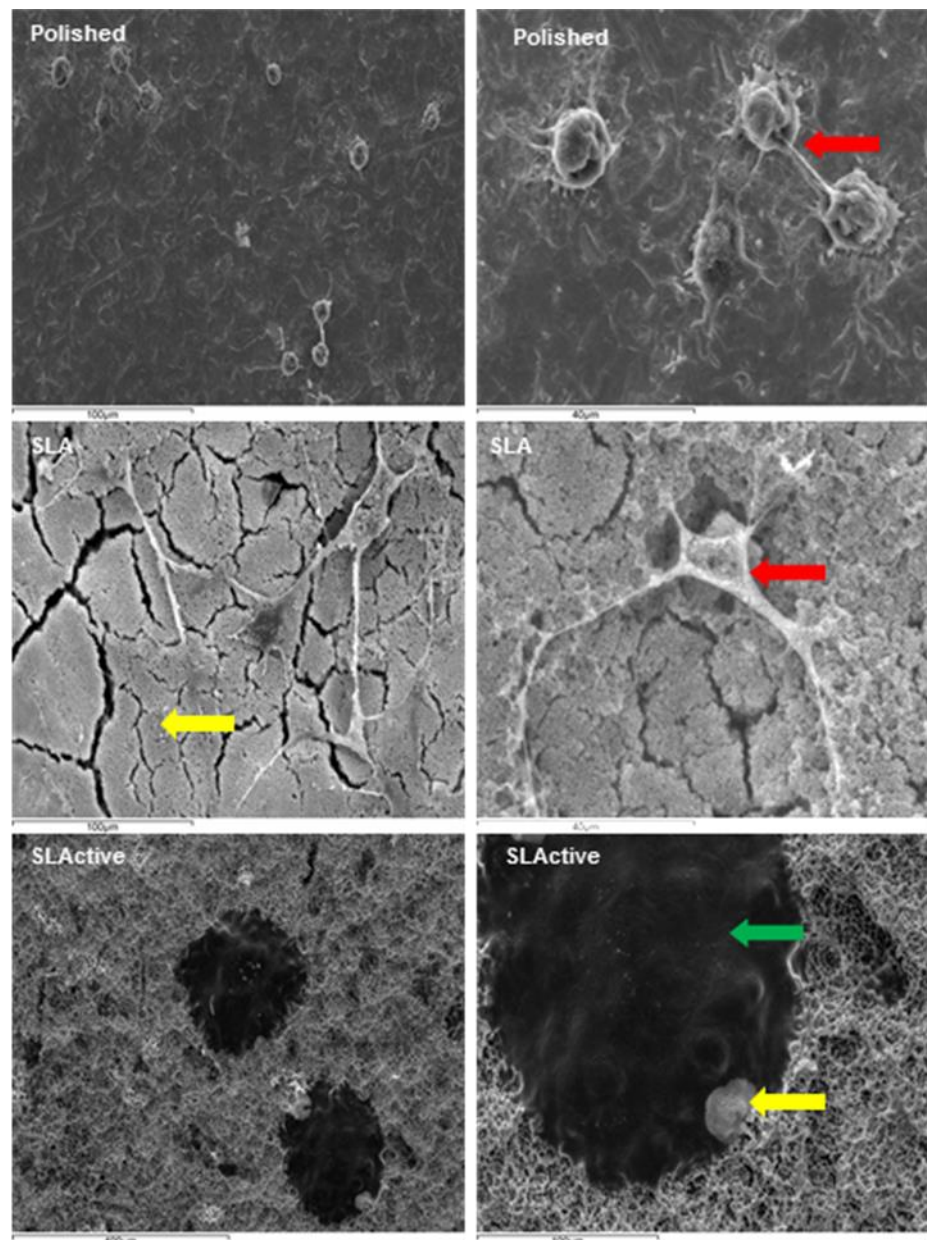


Figure 7.22. SEM images of MG-63 cell on three different titanium surfaces following PDT decontamination regimes after 7 days in culture. Red arrow indicates MG-63, yellow arrow indicates residual bacteria and biofilm, and green arrow indicates organic layer. Samples were viewed at $\times 1500$, $\times 500$, and $\times 150$ (Bar 40 μm , 100 μm , 400 μm , respectively).

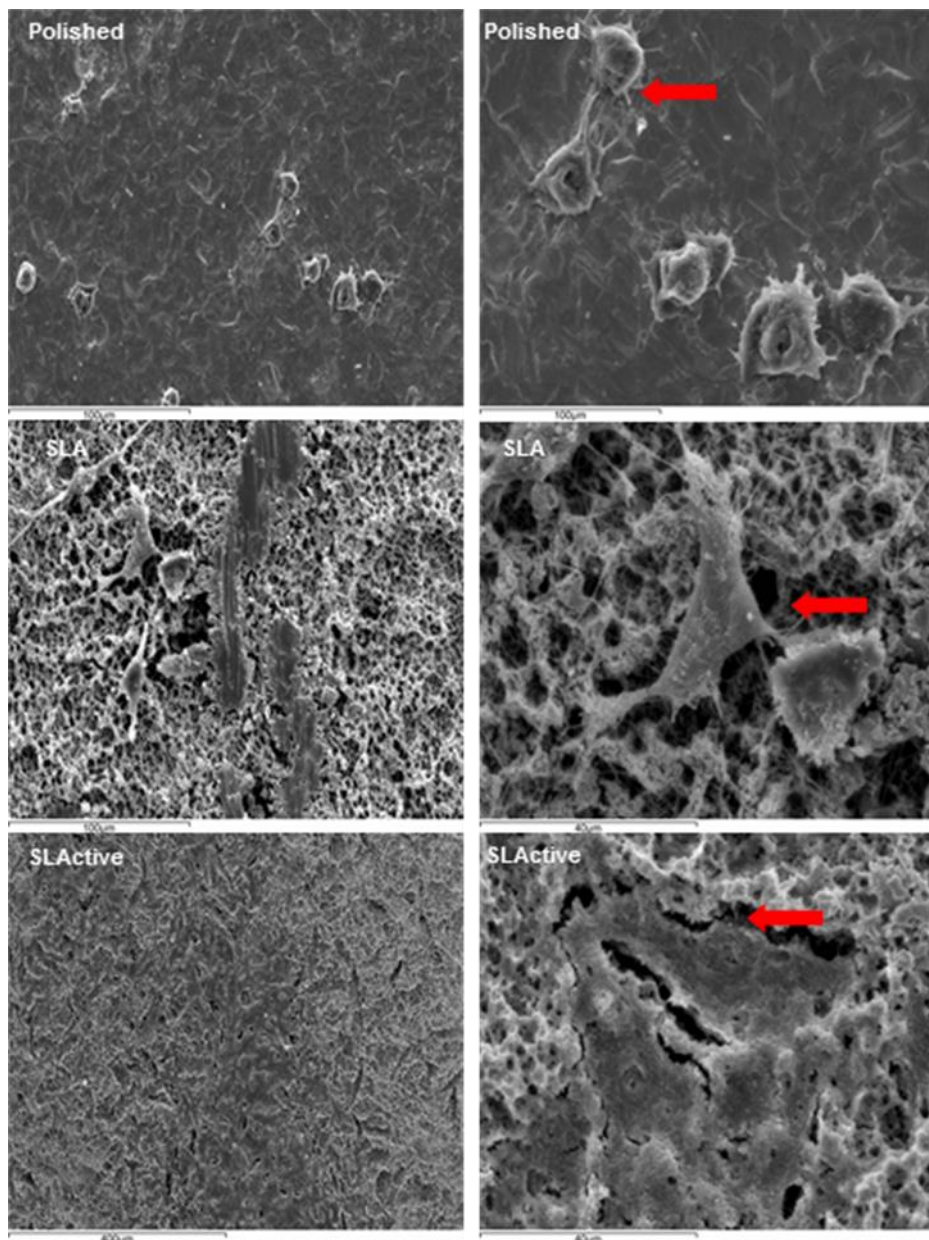


Figure 7.23. SEM images of MG-63 cells grown on three different titanium surfaces following TiBrush and PDT decontamination regimes after 7 days in culture. Red arrows indicates MG-63 cells division on polished surface, MG-63 attaching to the surface on SLA, and MG-63 split from the surface due to SEM sample processing. Samples were viewed at $\times 1500$, $\times 500$, and $\times 150$ (Bar 40 μm , 100 μm , 400 μm , respectively).

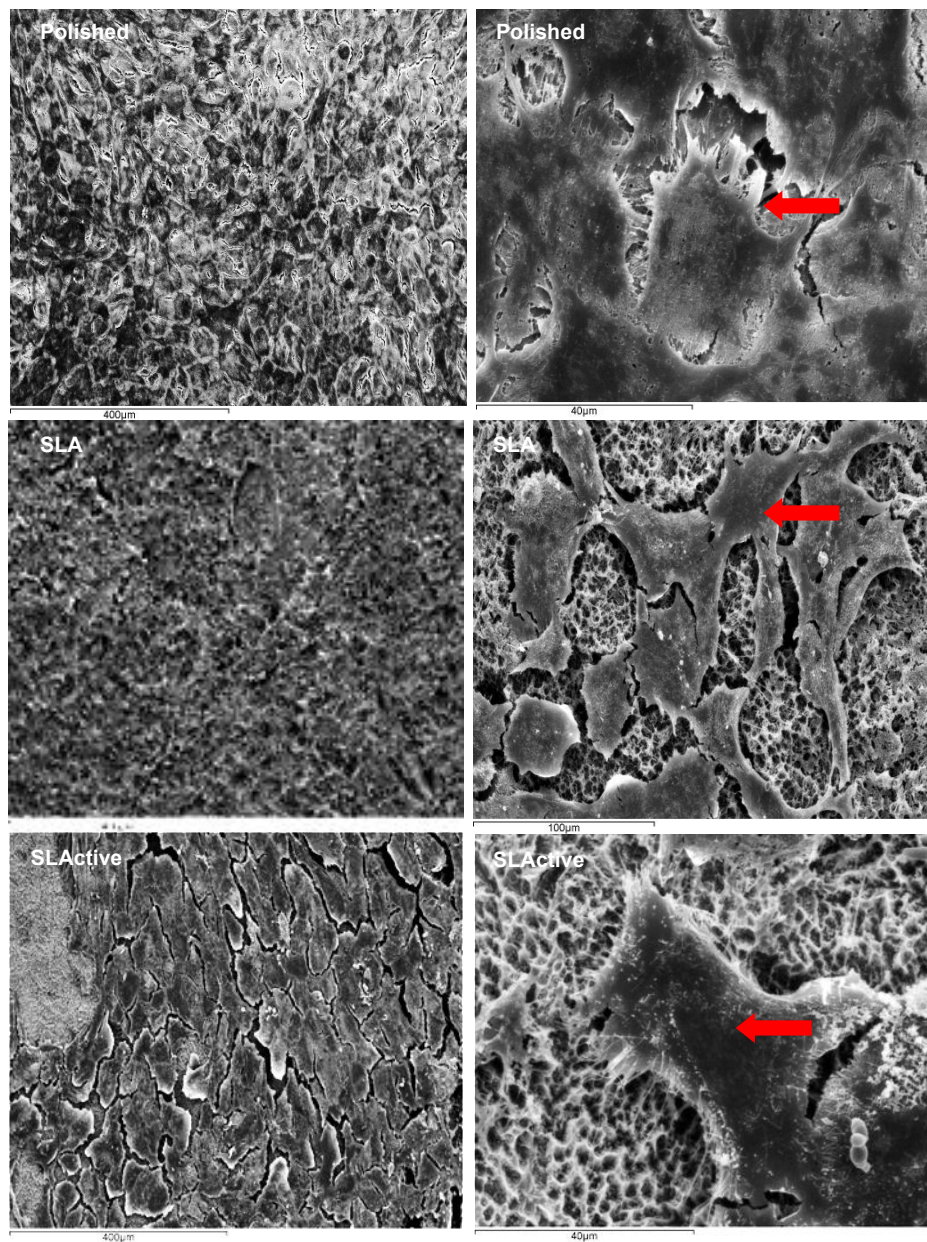


Figure 7.24. MG-63 cells (red arrows) attaching to three different titanium surfaces following TiBrush decontamination regime. Samples were viewed at $\times 1500$, $\times 500$, and $\times 150$ (Bar 40 μm , 100 μm , 400 μm , respectively).

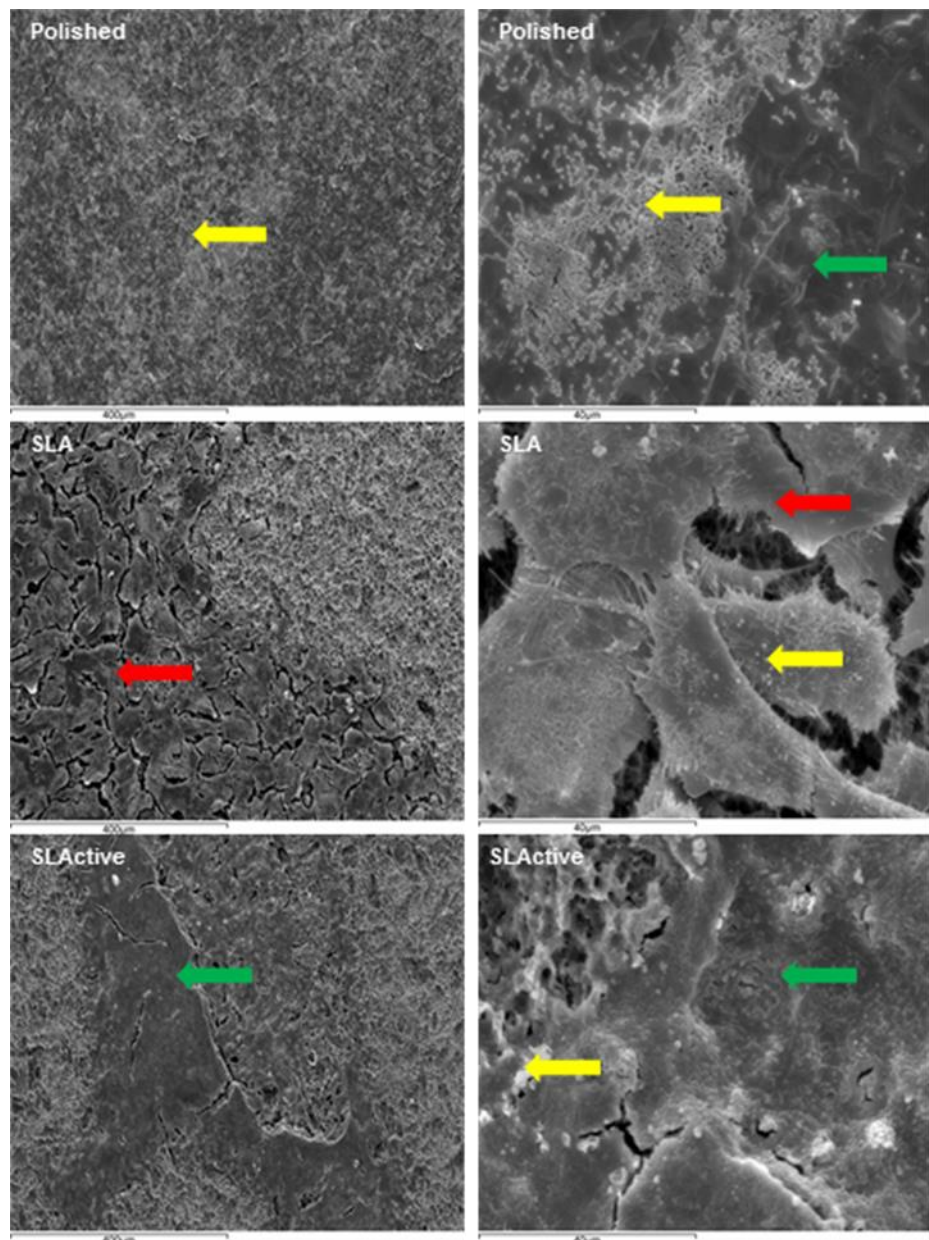


Figure 7.25. SEM images of MG-63 cells on three different titanium surfaces following CHX decontamination regimes after 7 days in culture. Red arrow indicates MG-63 attaching and splitting due to SEM process on SLA surface, yellow arrow indicate residual bacteria or biofilm, and green arrow indicates organic materials. Samples were viewed at $\times 1500$, $\times 500$, and $\times 150$ (Bar 40 μm , 100 μm , 400 μm , respectively).

7.3.5 Surface biocompatibility

The standard curve of fluorescence and number of MG-63 cells after 4 h incubation with Alamar blue was performed and the fluorescence measured (Figure 7.26).

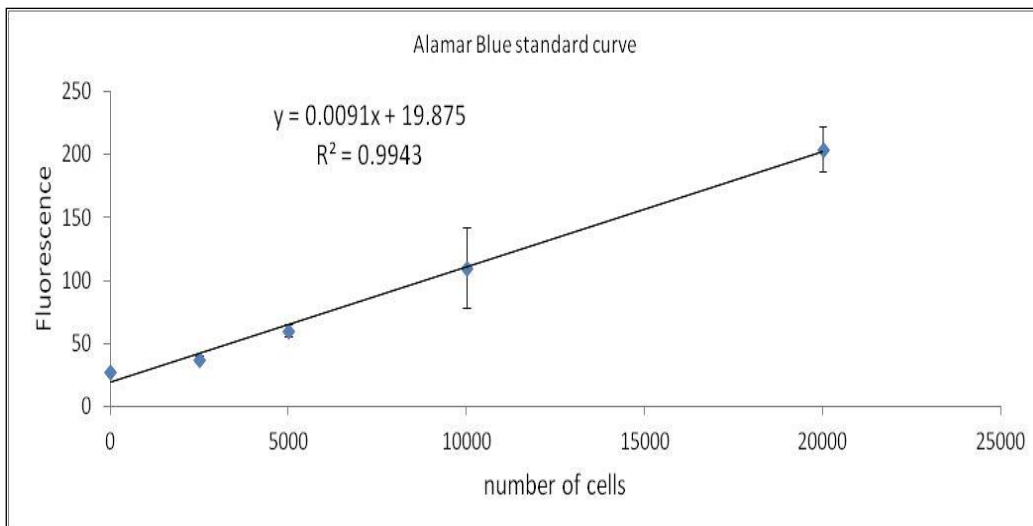


Figure 7.26. The standard curve of fluorescence and number of MG-63 cells after 4 h incubation with Alamar blue. The MG-63 cell number represents the mean \pm standard deviation ($n = 4$).

After sterilizing the discs for 30 min on each side by UV light (254 nm) exposure, MG-63 cells were then cultured on triplicate titanium discs with biofilm (control untreated) or devoid (sterile) of biofilm. All experiments were repeated twice under each of the two conditions (peri-implant mucositis and peri-implantitis). The MG-63 cells were further incubated and samples were harvested at different time periods (Day 1, 4 and 7), the harvested samples were subjected to the Alamar blue assay and analysed by fluoroscan. The data are shown in Table 7.2.

Under peri-implant mucositis conditions

The total numbers of MG-63 cell were determined for all three different titanium surfaces at day 1, 4 and 7 (Table 7.2).

On day 1: the cells count was highest on the control biofilms (6516 cells) grown on the polished surfaces, and lowest after PDT (2028 cells). The cells count on SLA surface was highest in the sterile control (8140 cells) and lowest (3114 cells) after PDT treatment. The highest cell count on SLActive surface was 12241 cells on control biofilms without treatment and lowest after (1780 cells) CHX treatment.

On day 4: the cells count was highest on polished (13202 cells) surfaces after CHX treatment and lowest (3461 cells) after PDT. The cell count on SLA surface was highest (19167 cells) on the sterile disc and lowest (5902 cells) following PDT. The cell count on SLActive surface was highest (21002 cells) on the sterile disc and less than 2847 cells following PDT.

On day 7: the cell count on polished surface was highest (82079 cells) on the sterile disc and lowest (19891 cells) following combined treatments (Ti + PDT). The cell count on SLA surface was highest (89629 cells) on the sterile disc and lowest (21303 cells) following PDT. The cell count on SLActive surface was highest (88508 cells) on sterile disc and lowest (3620 cells) following CHX treatment.

Under peri-implantitis conditions:

The total numbers of MG-63 cell were determined for all three different surfaces at day 1, 4 and 7 (Table 7.3).

On day 1: The highest cell count was on the polished surfaces was on the sterile disc (14552 cells) and was lowest (4893 cells) after CHX treatment. The cell count on the SLA surface was highest (18782 cells) for the untreated surface and lowest (7130 cells) following PDT. The cell count on the SLActive surface was highest (10666 cells) for the untreated surface and lowest (3524 cells) after combined treatment with the TiBrush and PDT.

On day 4: the cell count on the polished surface was highest (35634 cells) on the sterile discs and lowest (14326 cells) on untreated controls. The cell count on SLA surfaces was highest (41233 cells) on the sterile discs and lowest (31217 cells) following PDT. The cell count on SLActive surfaces was highest (31217 cells) following Tibrush treatment and lowest (4451 cells) after combined (TiBrush and PDT) treatments.

On day 7: the cell count on polished surface was 52920 cells on sterile surfaces and 14326 cells on untreated controls. The cell count on SLA surfaces was 70046 cells on untreated controls and 12272 cells after PDT. The cell count on SLActive surfaces was 45030 cells after TiBrush treatment and 7745 cells following the combined technique of TiBrush and PDT.

Overall, the sterile control (no biofilm ever grown on it) was shown to be as biocompatible as the biofilm control (original CFU ca.10⁸). There was no measurable difference between any of the decontamination regimes and controls for either of the sampling time points (366 h or 612 h) used.

Table 7.2. The number of cultured MG-63 cells on days 1, 4 and 7 on the three Ti surfaces. Biofilms were grown under peri-implant mucositis conditions prior to treatment. Control disc with untreated biofilm and sterile disc without biofilm; \pm standard deviation ($n = 2$).

Peri-implant mucositis conditions			
1st day biocompatibility test			
Treatment	Polished	SLA	SLActive
	Mean \pm SD	Mean \pm SD	Mean \pm SD
Control	6516 \pm 7790	4164 \pm 4271	12241 \pm 16245
PDT	2028 \pm 1831	3115 \pm 3629	3551 \pm 3448
TB + PDT	4268 \pm 4493	3698 \pm 4324	2677 \pm 2754
TB	6223 \pm 7801	4220 \pm 4910	3777 \pm 4701
CHX	4001 \pm 4664	4959 \pm 6340	1781 \pm 2499
Sterile	6298	8140	7624
4th day biocompatibility test			
Treatment	Polished	SLA	SLActive
	Mean \pm SD	Mean \pm SD	Mean \pm SD
Control	8010 \pm 7527	10079 \pm 9637	6383 \pm 3503
PDT	3462 \pm 1309	5902 \pm 3839	2848 \pm 385
TB + PDT	4353 \pm 2501	13271 \pm 14540	7107 \pm 6380
TB	10507 \pm 11440	11030 \pm 12938	13783 \pm 14717
CHX	13203 \pm 11015	17284 \pm 21577	3341 \pm 1047
Sterile	11860	19168	21003
7th day biocompatibility test			
Treatment	Polished	SLA	SLActive
	Mean \pm SD	Mean \pm SD	Mean \pm SD
Control	48459 \pm 68387	39477 \pm 51267	69199 \pm 93931
PDT	28866 \pm 40506	21304 \pm 27159	45954 \pm 59792
TB + PDT	19891 \pm 27292	35234 \pm 47260	46347 \pm 61257
TB	34525 \pm 48153	45476 \pm 60469	38164 \pm 49207
CHX	49141 \pm 67935	46614 \pm 62356	3620 \pm 915
Sterile	82080	89629	88508

Chapter 7: An *in vitro* assessment of antibacterial treatment strategies

Table 7.3. The number of cultured MG-63 cells on day 1, day 4, day 7 on the three Ti surfaces. Biofilms were grown under peri-implantitis conditions prior to treatment. Control untreated biofilm surfaces and sterile without biofilm surfaces; \pm standard deviation ($n = 2$).

Peri-implantitis conditions			
1st day biocompatibility test			
Treatment	Polished	SLA	SLActive
	Mean \pm SD	Mean \pm SD	Mean \pm SD
Control	6207 ± 3674	4164 ± 10257	10666 ± 7438
PDT	6630 ± 928	7130 ± 5943	6695 ± 6341
TB + PDT	8730 ± 6944	11997 ± 1795	3524 ± 3987
TB	13113 ± 8035	17162 ± 5975	8991 ± 731
CHX	4893 ± 3340	8040 ± 7391	6223 ± 5983
Sterile	14552 ± 2393	12847 ± 8596	6933 ± 8833
4th day biocompatibility test			
Treatment	Polished	SLA	SLActive
	Mean \pm SD	Mean \pm SD	Mean \pm SD
Control	8935 ± 7867	24481 ± 29162	28970 ± 13847
PDT	24141 ± 22432	13650 ± 16071	15654 ± 19499
TB + PDT	24580 ± 19605	21701 ± 10078	4451 ± 2120
TB	24794 ± 9542	20459 ± 16372	31217 ± 21485
CHX	28314 ± 37169	19384 ± 22679	11060 ± 10564
Sterile	35635 ± 785	41234 ± 34081	22871 ± 26978
7th day biocompatibility test			
Treatment	Polished	SLA	SLActive
	Mean \pm SD	Mean \pm SD	Mean \pm SD
Control	14327 ± 6877	70047 ± 8579	34327 ± 13388
PDT	49574 ± 26342	12271 ± 12846	29145 ± 34439
TB + PDT	24766 ± 5400	27975 ± 34665	7745 ± 3177
TB	45030 ± 2914	25694 ± 29995	40558 ± 19216
CHX	24265 ± 32171	28431 ± 36630	29108 ± 36418
Sterile	52920 ± 19107	33102 ± 31859	33701 ± 33110

7.4 Discussion

In this Chapter, microcosm biofilms were grown for 29 days and harvested. The biofilm covered discs were then treated using one of four treatment protocols (PDT, TiBrush + PDT, TiBrush, CHX) or left untreated (control; RTF). Ti discs (Polished, SLA or SLActive) were then subjected to microbiological analysis (selective and non-selective media), CLSM analysis and assessment of human fibroblast cell biocompatibility (SEM and Alamar blue assay). An *in vitro* study such as this is essential in the development of treatment modalities, as these are the basic steps with which to reveal the efficacy of different cleaning regimes on infected titanium surfaces.

7.4.1 Microbial culture data

The treatment of peri-implant infection is challenging because of the specific anatomical characteristics of the dental implants. Peri-implantitis is a common complication in dental implant therapy, and management of peri-implantitis is, at present, often difficult (Charalampakis et al., 2011).

In a single study, peri-implantitis was diagnosed in 16% of patients treated with turned (machined) Branemark implants 9 to 14 years after loading (Esposito et al., 2007). Surface roughness modifications have been made to implants for increased biocompatibility between the titanium surface and bone tissue in order to decrease the healing period (Shibli et al., 2008). The problem with these rougher surfaces is that they can favour bacterial colonisation (Esposito et al., 2012). Different treatment strategies for peri-implantitis have been suggested (Esposito et al., 2012) and include:

1. Mechanical debridement.
2. Pharmaceutical therapy (chlorhexidine irrigation, local or systemic antibiotics).
3. Surgical procedures.
4. Use of soft lasers.
5. Smoothing the implant surface (to decrease surface roughness).
6. 'Decontamination' or 'detoxification' of the implant surface using various chemical agents or laser.

The present study attempted to evaluate whether a range of decontamination regimes were effective in reducing the levels of bacterial biofilm formed on three different characteristic surfaces. In this study, it was shown that the combined treatment (TiBrush and PDT) was equal to, or better than the other treatments for removing peri-implant mucositis biofilms from all three implant surfaces.

Combined treatment (TiBrush and PDT) was also the most effective approach on polished and SLActive surfaces. Furthermore, the combined technique was the most effective of the four treatments for removing peri-implantitis biofilms from all implant surfaces. These results were perhaps expected because the combined technique included mechanical and chemical aspects. The rotating titanium brush with stiff titanium bristles allowed for effective biofilm clearance from the surfaces prior to chemical cleaning. The reduction in biofilm thickness may allow for better penetration and diffusion of the photosensitiser into the remaining biofilm, however complete elimination was not achieved.

The biofilms used in this study were multispecies, complex microbial communities embedded in a matrix of polymers of bacterial and salivary origin. In the case of biofilms, it is possible that the presence of extracellular matrix acts as a barrier to the diffusion of the photosensitiser through the biofilm (Wilson et al., 1996). There is also evidence that the bacterial phenotype changes once cells move from the planktonic growth state to the biofilm state making them more resistant to killing (Wilson et al., 1996, Zanin et al., 2005, Wood et al., 1999). A further contributing to microbial resilience on a surface is the influence of a high surface energy leading to higher binding force between bacterial cells and the surface thus leading to difficulties in removing of bacteria from the surface (Claffey et al., 2008).

The present results were in agreement with other *in vitro* PDT studies that clearly demonstrated that PDT alone was able to kill oral bacterial species (Takasaki et al., 2009). Marotti et al. (2013) had investigated sixty implants by means of PDT to analyse implant surface decontamination *in vitro*; the implants were irradiated with a low-level laser (660 nm, 30 mW) for 3 or 5 min (7.2 and 12 J). After 5 min in contact with methylene blue dye, the authors suggested that PDT can be considered an efficient method for reducing anaerobic bacteria on implant surfaces.

Al-Ahmed et al. (2013) had investigated the effectiveness of antimicrobial photodynamic therapy (APDT) using visible light together with water-filtered infrared-A (VIS+wIRA) to eradicate single species of planktonic bacteria and microorganisms during initial oral bacterial colonization *in situ*. Toluidine blue (TB) was utilised as a photosensitizer at concentrations of 5, 10, 25 and 50 µg/ml and applied for 1 min on planktonic cultures of *Streptococcus mutans* and *Enterococcus faecalis*. The authors found that up to 2 log₁₀ of *S. mutans* and *E. faecalis* were killed by APDT. This study had shown that APDT in combination

with TB and VIS+wIRA is a promising method for killing bacteria during initial oral colonization.

The nature of the pellicle formed on a substratum has been shown to depend on its hydrophobicity (van der Mei et al., 1993). Few *in vitro* studies of the binding of antiplaque agents to substrata have been reported. However, Freitas et al. (1993) showed that CHX binds to both hydrophobic and hydrophilic surfaces by hydrophobic and electrostatic interactions respectively via polar and non-polar regions of the molecule. The susceptibility of biofilm to an agent is dependent, amongst other factors, on a number of attributes of the agents including its rate of penetration into the biofilm which will depend on its charge, its size and its affinity for the biofilm matrix and its ability to exert an anticlerical effect in the microenvironment (pH, redox potential etc.). This may be attributable to specific agent/substrata and bacteria/substrata interactions.

Chlorhexidine (CHX) treatment resulted in bacterial reduction under peri-implant mucositis conditions on polished surfaces, when compared to the control. The limited ability of CHX to remove the whole biofilm from the SLA and SLActive surfaces could be attributed to the more mature biofilms which are known to be complex, diverse and less susceptible to antimicrobial agents due to several physical and biological factors that protect the complex bacteria communities. Bacteria living within biofilms are more resistant to antimicrobial treatments than bacteria suspended in solution. Furthermore, the biofilm-EPS matrix has repeatedly been cited as a barrier which may protect cells from the influence of a range of stress factors including antimicrobial agents. It has been stated that in order to kill microorganisms in a mature and well organised biofilm community, a higher concentration of the antimicrobial agent together with longer exposure times is required (Gera, 2008).

Oosterwaal et al. (1989) reported that CHX had a bacteriostatic effect when used at low concentrations and a bactericidal effect when used at very high concentrations (0.5 - 2% for 10 min) against periodontal pathogens. The results of a study by Henderson et al. (2012) support the current findings. These authors reported that 0.2% CHX had significant effects on biofilms when applied for 2 min on contaminated mirror polished surface covered with multilayers of *Staphylococcus epidermidis*. However, complete removal of the biofilm was not achieved. Also, studies by Zablotsky et al. (1992) and Wennström et al. (1987) provided similar supportive evidence.

The findings of this present study were in agreement with Zaura-Arite et al. (2001), who reported that CHX 0.2% treatment for 1 min had a significant effect

on 6 h biofilms and only in the outer layer of 48 h old *in situ* – grown biofilm. Limited diffusion of CHX into the biofilm may have been an issue as it has been shown that it can take up to 5 minutes to diffuse to the deeper layers of biofilm. Therefore, increasing the contact time of the CHX may increase its efficacy in the treatment of peri-implant pathologies in a way similar to periodontal treatment (Salvi et al., 2002). The only study on CHX diffusion into plaque was performed on *in vitro* condensed intra-orally grown plaque (Melsen et al., 1983), where it was reported that 0.2% CHX was able to penetrate rapidly (within 1 min) the outer 2 mm of a 5-mm-thick biofilm. However, in the present study, on undisturbed dental biofilm, with a thickness approximately 55 μ m, CHX had only a superficial bactericidal effect, especially in heavy-plaque-formers, where there might have been larger amounts of EPS.

Initial microbial colonisation of a surface readily occurs within surface irregularities, and it is difficult to completely remove plaque from these grooves (Quirynen et al., 1993). Furthermore, implant surfaces with greater roughness can promote the attachment of bacteria and hamper mechanical and chemical cleaning (Esposito et al., 1999).

In this study, the evaluation of the surfaces to determine the most effective treatment showed that the polished surface was easier to decontaminate than the SLA or SLActive surfaces. This was perhaps expected as the polished surfaces were smooth ($R_a < 0.5$) and therefore provided better access for the Ti brush. The moderate roughness of the SLA and SLActive surfaces ($R_a = 1.75 \mu$ m) possibly provided enough habitats in the forms of pits and troughs, to protect adherent bacterial cells from shear forces of the titanium brush and resisting photosensitizer exposure.

7.4.2 CLSM analysis

After treatment, the microbial biofilms were evaluated by CLSM and Baclight viability staining. The changes in bacterial viability and bacterial non-viability were monitored. The viability of untreated control biofilms was similar for all surfaces (Figure 7.13). The CLSM images of polished surfaces showed dense viable biofilm (green channel) with few dead bacteria and the other 2 surfaces followed this trend. Following PDT therapy, the lowest total biomass was on polished, followed by SLActive and SLA surfaces (Figure 7.14). CLSM imaging revealed dense biofilms with higher amounts of non-viable cells, particularly on polished surfaces, followed by SLA and SLActive surfaces. After exposure to TiBrush for 1 min, followed by PDT for 1 min, a greater reduction of total biomass

was observed for all surfaces compared to untreated control biofilms. CLSM imaging showed few residual bacteria and clusters (live and dead) remained on all surfaces. This was perhaps expected because preliminary mechanical removal of biofilm followed by a chemical treatment served to disturb the protective structures within the biofilm and allowed better access to the remaining bacterial cells (Figure 7.15). After TiBrush therapy for 1 min, an increased reduction of total biomass was observed for all surfaces (94% on polished, 57% on SLA and 39% on SLActive) compared to untreated control biofilms. CLSM analysis showed few residual bacteria and clusters (live and dead) were remained on all surfaces (Figure 7.16).

After CHX treatment, the total biomass proportion was 88% on polished, 92% on SLA and 89% on SLActive surfaces compared to untreated control biofilms. CLSM images revealed dense biofilm with residual bacteria of non-viable bacteria (red channel) on polished and few numbers on SLActive surfaces (Figure 7.17). The above data showed that the combined technique (Ti + PDT) was the better treatment. CLSM and total biomass proportions findings were in agreement with culture analysis.

One mechanism that is used to increase bone to implant contact and promote rapid osseointegration is to increase the implant surface roughness (Rasmusson et al., 2001). The effects of titanium surface roughness on biofilm thickness were assessed. One of the surfaces had a R_a value $< 0.5 \mu\text{m}$ (Figure 7.19, section 7.3.4) and therefore was classified as smooth (Albrektsson and Wennerberg, 2004). The biofilm thickness (obtained by measuring xz optical sections) was monitored after the different treatments regimes. The thickness of the biofilms ranged between $49 \mu\text{m} - 55 \mu\text{m}$ on all surfaces and control untreated biofilms (Figure 7.18). The average surface roughness is defined by the number and height of peaks on the surface. Based on this defined measurement, rough surfaces such as SLA and SLActive would potentially provide a greater surface area for potential bacterial interactions than the smooth surfaces (polished). However, developed surface area alone cannot wholly account for the observed difference in biofilm thickness, a one explanation of this was that topography (peaks and troughs) on the rougher surfaces provides the bacteria with protection from removal by shear forces (Bürgers et al., 2010).

The polished surface yielded the biofilm of lowest thickness ($8 \mu\text{m}$) following combined (TiBrush and PDT) treatment. The next lowest ($41 \mu\text{m}$) was after CHX treatment. The other two surfaces also followed this trend (Table 7.18). The differences between the three surfaces was supported by the fact that on the

moderately rough surfaces, much of the biofilm thickness (17 µm on SLA, 17 µm on SLActive surfaces) remained after mechanical removal with a titanium brush, whereas almost all the biofilm was removed from the polished surface (9 µm). Also, the results of the difference in biofilm thickness were supported by biomass levels (Figures 7.15 & 7.16) which showed an increased reduction of total biomass (94% on polished, 57% on SLA and 39% on SLActive) compared to untreated control biofilms. Results from a previous *in vivo* study also showed that rough titanium surface had significantly more bacteria remaining than smooth titanium surface (Amarante et al., 2008).

7.4.3 SEM

Surface biocompatibility was assessed on treated Ti discs for both communities (366 h peri-implant mucositis and 612 h peri-implantitis) by visualising MG-63 cells using SEM. Use of the human osteoblast-like cell line MG-63, had previously shown that an increased surface roughness of titanium discs led to reduced cell proliferation, whilst inducing cellular differentiation and matrix production (Martin et al., 1995, Herrero-Climent et al., 2013).

Overall, the MG-63 cells grew well on all three sterile titanium surfaces (Figure 7.20). On untreated control biofilms, polished surfaces, covered partially with biofilm there was no visible MG-63 presence. The SLA surface also demonstrated this observation. The SLActive discs (control untreated biofilm; RTF) were shown to be completely covered with bacteria and MG-63 cells (Figure 7.21). When the biofilm surfaces were exposed to PDT (Figure 7.22), fewer numbers of MG-63 cells were observed with signs of division on the polished surface. The MG-63 cells were found attached to the SLA surface, whilst on SLActive surfaces, only an organic layer was present. After application of combined technique (TiBrush + PDT), the MG-63 cells were observed on all three surfaces with no sign of surface alteration (Figure 7.23). After use of TiBrush (Figure 7.24), the same observation as seen with the combined technique was observed on all surfaces. Following CHX treatment, there were no MG-63 cells on polished and SLActive surfaces with the presence of organic matter and residual biofilm. On SLA surfaces, the MG-63 cells appeared to be separated from the surface, possibly due to the SEM processing method (Figure 7.25).

7.4.4 Cell culture

Surface biocompatibility was assessed on decontaminated Ti discs for both communities (366 h peri-implant mucositis and 612 h peri-implantitis) by assessing the viability of MG-63 cells and use of Alamar blue assay with reference to a standard curve. Cell culture experiments have become more attractive in recent years in an attempt to understand, control and direct interfacial interactions at biomaterial surfaces. In particular, cultures of osteoblasts, either primary or from tumor cell lines are frequently used to evaluate the effect of surface modifications on cell behaviour. Cell line, which is a human osteoblast-like cell line was selected for this study. Originally isolated from a human osteosarcoma, the cell line is widely used for testing biomaterials (Billiau et al., 1975) and in this study they mimic osteoblasts during re-osseointegration following the clinical therapy of peri-implantitis. Following application of a decontamination regime, the discs were placed under a UV light (30 min per side) to kill the cells prior to use in cell assay. This was to stop the bacteria infecting the human cell culture. Their viability of MG-63 cells was assessed using an Alamar blue assay. The aim of this was to MG-63 presence on decontaminated titanium surfaces. Despite the high numbers of bacteria (up to 10^8) that were present on the titanium disc surfaces, there appeared to be a high biocompatibility between the surfaces and the MG-63 based on the Alamar blue assay. This finding was unexpected and difficult to explain. Perhaps the most likely reason for these apparent high MG-63 biocompatibility levels was the continued existence of viable bacteria on the UV treated surfaces which subsequently contributed to the Alamar blue readings. After evaluating normal cellular growth by flourescan analysis, scanning electron microscopy evaluation was carried out for all surfaces. It is unknown what affect this had on the MG-63 cells or indeed the assay. Bacterial presence in the assay will contribute to the "cell number" measurement as they both possess resazurin, cell permeable compound that is blue in colour and virtually nonfluorescent. Upon entering cells, resazurin is reduced to resorufin, which produces a very bright red fluorescence. Viable cells continuously convert resazurin to resorufin.

This therefore means that the figures for the number of cells in the tables (7.2 and 7.3) are a sum of MG-63 cell line activity plus bacterial biofilm activity. Whenever fluorescence/absorbance is used as an end point measurement, as in the Alamar blue assay, awareness of contribution to such readings from other sources should be considered. Hence, the interpretation of the results following the Alamar Blue assay has to be done with caution. In addition, the results from

the SEM study revealed the presence of residual biofilm in the Alamar blue assay (Figs 7.22-7.25). It must be emphasized that there are many factors that could have influenced the results, such as the small number of samples used, and the inadequate killing effect of UV radiation for half an hour per side. The duration of UV exposure may not have been sufficient for the total elimination of microbial viability within the mature and complex biofilm (Renier et al., 2011). Indeed increased duration of irradiation doses has previously been shown to be needed to increase mortality within biofilms (Nandakumar et al., 2006).

7.5 Conclusions

From these data (culture and CLSM) it was shown that a combined (TiBrush and PDT) technique was the most efficient treatment regime for decontaminating all three surfaces. This might be expected, as the treatment was a combination of mechanical plus chemical techniques. Biofilm removal includes biomass reduction and disruption of protective structures (EPS etc.) that may be present in the community and may promote more efficient killing. Once the biomass of the biofilm had been reduced, there would conceivably be enhanced access to the remaining cells for the PDT. In evaluating the surfaces, polished surfaces showed the largest reduction of bacterial biofilm better than SLA and SLActive surfaces. The CLSM evaluation of biofilm biomass was supported with cultural data on all treated surfaces.

The results from this study have shown that it is possible to assess the efficacy of current treatment modalities *in vitro*. The treatments could be ranked in order of effectiveness, however further work would need to be carried out to assess whether this could be compared to clinical findings.

Chapter 8
Assessment of novel nanotechnology surface implant coatings to reduce
biofilm formation.

8.1 Introduction

Pure titanium is commonly used for artificial joints and implants in both dental and orthopaedic clinics because of its biocompatibility and mechanical properties (Allaker and Ren, 2008). The initial attachment and the colonisation of bacteria to an implant surface play an important role in the pathogenesis of infections related to biomaterials (Grössner-schreiber et al., 2001). Once formed, the complex structure of a biofilm, containing a polymicrobial community and extracellular matrix, makes it extremely resistant to host-defense mechanisms or to antibiotic treatment. Furthermore, the lower susceptibility of biofilms to antimicrobial agents adds to the increasing burden of multiple-drug resistance in bacteria (Costerton et al., 2005).

There is therefore a need to investigate novel alternatives to traditional antimicrobial agents. One such method could be to use antimicrobial metal nanoparticles (NPs) to control biofilm formation. Bacteria are less likely to acquire resistance against metal NPs than other conventional antibiotics (Allaker, 2013). Recent advances in the field of nanotechnology, particularly the ability to prepare highly ordered nanoparticulates of any size and shape, have led to the development of new biocidal agents (Jones et al., 2008). Indeed, studies have indicated that nanoparticulates can be used as effective bactericidal materials (Allaker, 2010). In order to achieve better disinfection with biocompatibility, one method could be to modify the surface material of the titanium-base implant. Modification of implant surfaces resulting in antibacterial properties is a promising approach in the development of new biomaterials (Allaker and Ren, 2008, Allaker, 2010). Surface coatings with antibacterial properties have previously been shown to be very effective in preventing bacterial adhesion (Allaker and Douglas, 2009, Ahearn et al., 1995). Examples of surface modification of titanium by active antibiotics are outlined below:

1. Use of aminopropylsilane to immobilize vancomycin on titanium surfaces (Jose et al., 2005).
2. Use of dry processes (Yoshinari et al., 2010) such as ion implantation, ion plating oxidation, and ion beam mixing to fabricate various surfaces on titanium modified with calcium, titanium oxide, alumina, silver, zinc, and fluorine have shown to be of benefit in clinical treatment by reducing bacterial numbers.

Metallic nanoparticles (metal oxides) have so far proven to have a long lasting biocidal activity with high thermal stability and relatively low toxicity to human cells. There are various coating techniques used, such as plasma spraying (Kobayashi et al., 2012), dip coating (Kobayashi et al., 2012), sputtering and

pulsed laser deposition (Ozeki et al., 2002, Zabetakis et al., 1994) and more recently, electrohydrodynamic spraying (Ozeki et al., 2002, Zabetakis et al., 1994). Plasma spraying is the most widely used commercially for producing hydroxylapatite coatings, but it requires high processing temperatures. The dip coating technique is cheap and fast, and also able to produce coatings on substrates of complex shape; but it also requires higher temperatures (Kobayashi et al., 2012).

Sputter coatings and pulsed laser deposition techniques are able to produce a uniform coating thickness on flat substrates, but both techniques are incapable of producing coatings on substrates of complex geometries (Ozeki et al., 2002, Zabetakis et al., 1994). Electrohydrodynamic spraying is simple and economical with the ability to produce a uniform coating at room temperature while easily covering a large area. Additionally, a wide variety of materials from metal, polymer, ceramic to composite can be processed (Huang et al., 2011).

There are at least three mechanisms by which nanoparticles can inhibit the formation of microbial plaque (Vargas-Reus et al., 2012):

1. Nanoparticles larger than 10 nm accumulate on the cell membrane and lead to leakage of the intracellular components which eventually causes cell death.
2. Nanoparticles smaller than 10 nm may penetrate membranes and accumulate intracellularly and lead to damaging effects on nucleic acids.
3. Through disruption of normal cellular function, nanoparticles trigger the production of reactive oxygen species such as O_2 and H_2O_2 which contribute to bacterial killing.

Recent advances in the field of nanotechnology, particularly the ability to prepare highly ordered nanoparticulates of any size and shape, have led to the development of new biocidal agents. Many studies have found that TiN (Titanium nitride) and ZrN (Zirconium nitride) coatings possess antibacterial activity against members of the oral microbiota, for example *Streptococcus* spp. (Grössner-Schreiber et al., 2001). Ag and Cu are known to be efficient antibacterial agents however, they have also been reported to be highly toxic to eukaryotic cells (Karlsson et al., 2008). Ren et al. (2009) reported that copper oxide (CuO) nanoparticles in suspension showed activity against a range of bacterial pathogens, including methicillin-resistant *Staphylococcus aureus* (MRSA) and *E. coli*, with minimum bactericidal concentrations (MBCs) ranging from 100 μ g/ml to 5000 μ g/ml.

Hydroxyapatite (HA) has shown a great deal of promise in the field of orthopaedics as it provides a very stable interface between bone and the implant. Hence, nano-scale HA simulates more closely the size and properties of HA crystals in natural bone (Li et al., 2007). HA has chemical similarities to the inorganic components of bone and teeth (Li et al., 2010). Indeed, Huang et al. (2011) concluded that nanoTiHA had the ability to inhibit growth of both Gram-negative and Gram-positive bacteria, including *S. aureus* and *S. epidermidis*.

Colon et al. (2006) developed zinc oxide (ZnO) nanostructures and compared their ability to inhibit bacterial growth to that of titanium oxide (TiO) nanostructures. Both surfaces reduced the adhesion of *S. epidermidis* by 69%. ZnO in the form of nanoparticles has shown promise as an antimicrobial agent against *E. coli* and *S. aureus* (Premanathan et al., 2011). The preliminary studies of (Brayner et al., 2006) showed that ZnO nanoparticles at a concentration of between 3 and 10 mM cause 100% inhibition of bacterial growth. It has been reported that antibacterial activity of ZnO increases with a reduction of particle size (Nair et al., 2009). Smaller ZnO nanoparticles have been found to be more effective than larger particles against both Gram-negative and Gram-positive bacteria (Nair et al., 2009). Nevertheless, the effect of metal nanoparticles on oral cavity is still under exploration.

In light of the above findings, it was hypothesized that a titanium surface coated with ZnO, HA, or 50% ZnO + 50% HA nanoparticles may exhibit antibacterial properties. To test this hypothesis, nanoparticle coatings were prepared on titanium surfaces using an electrodynamic deposition spraying method. The distribution of the nanoparticles was investigated with scanning electron microscopy (SEM). Furthermore, the antibacterial properties were evaluated using the *in vitro* peri-implantitis model developed in the previous chapters

8.2 Material and Methods

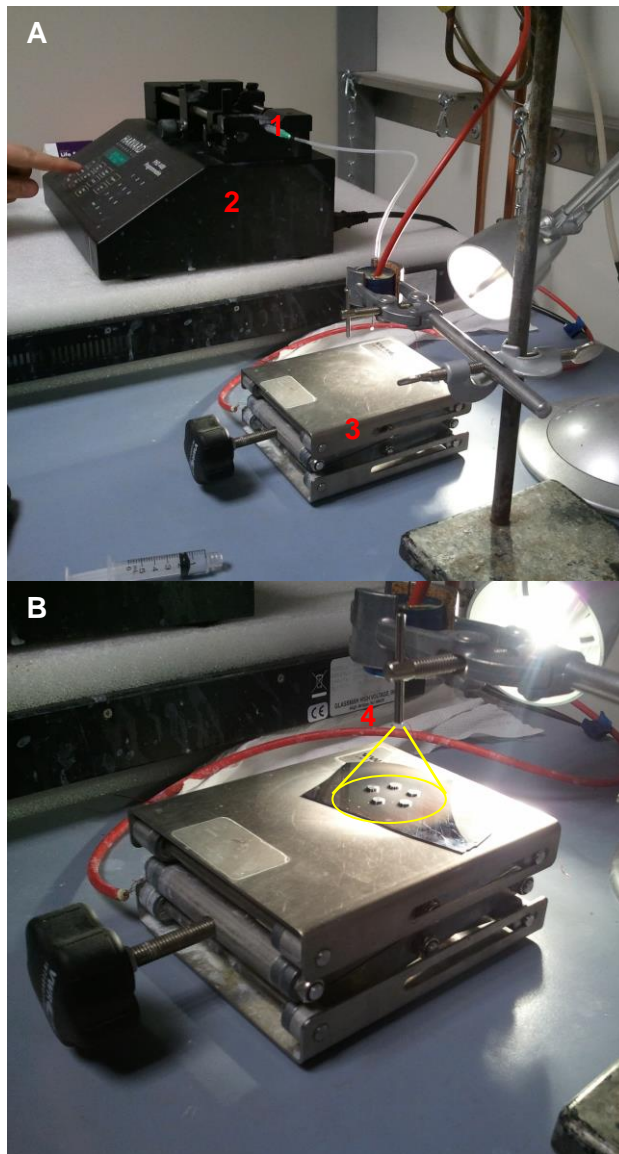
8.2.1 Nanoparticles

The nanoparticles were produced by collaboration between Queen Mary University of London, Barts & The London School of Medicine and Dentistry and the Departments of Mechanical Engineering, and Microbial Diseases, Eastman Dental Institute, UCL. The metal oxide particles had a size range of 20-100 nm. Handling and storage of these nanoparticles was carried out under industrial safe-working practices to avoid biological and environmental safety issues. The nanoparticles (NPs) tested included: ZnO, HA and combined 50% ZnO + 50% HA.

Coating of Ti discs with nanoparticles: The samples were coated using Electrohydrodynamic Deposition (EHD) at the Department of Mechanical Engineering, UCL. This is illustrated in Figure 8.1.

8.2.2 Electrohydrodynamic (EHD) spraying

HA nanoparticles (nanoHA), ZnO nanoparticles (nanoZnO) or combination of equal proportion of these (ZnO + HA) nanoparticles were used. In EHD the suspension is jetted from a needle under an electric field. The needle (stainless steel) had a diameter of approximately 300 μ m and is used to spray the content of the syringe onto the surface of the sample. Spraying was achieved as a result of the electrical field between the substrate (silicon) and the needle; this caused a cone shaped (8 mm) spray at the tip of the needle, which showed to be an optimal coating method in EHD (Figure 8.1). The distance between the substrate and the needle was maintained at 30 mm. Ten milligrams of the nanoparticles (NPs) were suspended in 10 ml of ethanol and sonicated for 10 min then pumped 1 ml using a syringe pump at the rate of 5 μ l/min. All the experiments were performed from a freshly prepared suspension. The voltage used for spraying was between 4.5 – 5 kV. Pure titanium discs of (5 mm diameter and 2 mm height) were coated for 60 s. Following coating, the nanoparticles were subjected to heat treatment in an oven at 600°C for 1 h followed by a cooling rate of 1°C/min as shown in Figure 8.2.



1. Syringe and Needle

2. Pump

3. Stage

4. Substratum and cone shape illustrating spray coverage.

Figure 8.1. Electrohydrodynamic Deposition (EHD). A, the coating setup shows the nanoparticles were placed into a syringe and needle arrangement on a syringe pump to allow a controlled flow rate. B, Ti discs were arranged within the nanoparticle spray. The yellow conical line illustrates the spray coverage.

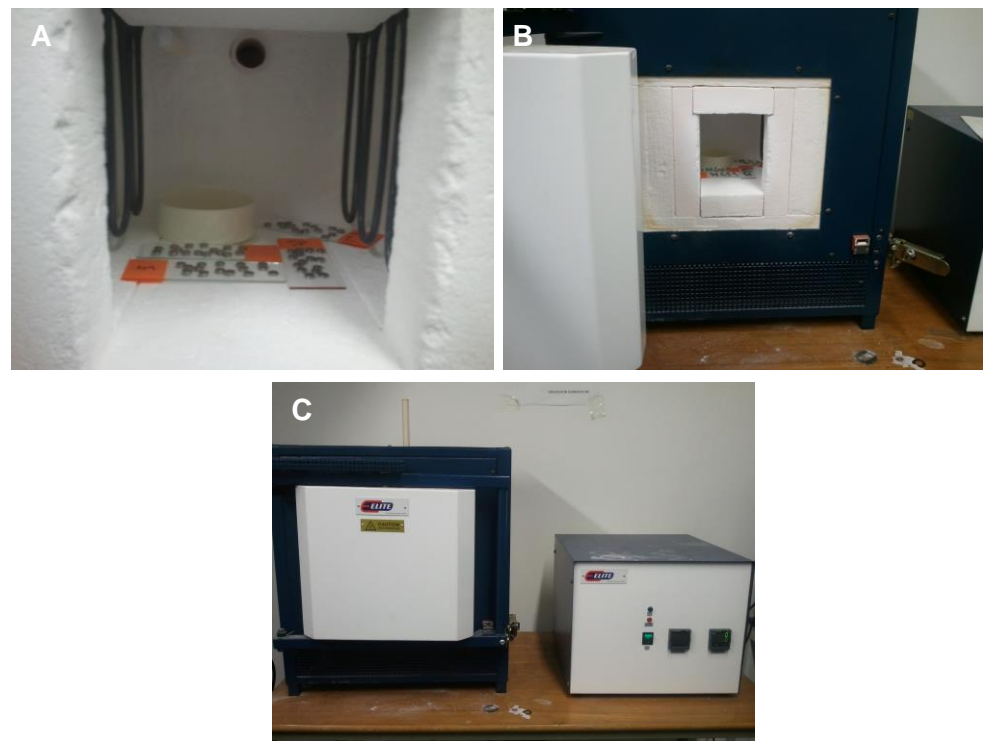


Figure 8.2. A & B, nano coated Ti discs prior to heat treatment (600°C for 1 h). C. cooling at a rate of 1°C/min.

8.2.3 CDFF set up

Various discs of titanium were prepared

- Pure titanium (control) ($n = 4$)
- Nano ZnO coated ($n = 4$)
- Nano HA ($n = 4$)
- 50% Nano ZnO plus 50% Nano HA coated ($n = 4$)

The three novel titanium discs coatings were prepared in addition to polished Ti (as control). The CDFF, described previously in Chapter 2 sections 2.2.1, was used to grow microcosm biofilms on these discs. The experiments were performed in two separate CDF runs. The discs were positioned on PTFE plugs and were held in place using vacuum silicone grease (Dow Corning) and recessed to a depth of 600 μm . Whole human saliva was used as an inoculum to provide microcosm biofilms. The nutrient source used for the experiments was mucin containing artificial saliva and 40 $\mu\text{l}/\text{min}$ of PISF used to mimic the healthy conditions associated with a dental implant under aerobic conditions for 5 days at 37 $^{\circ}\text{C}$.

8.2.4 Biofilm sampling

CDFF pans were removed and placed in sterile universal tubes and discs from each pan were used for determining the bacterial composition of the biofilms (section 2.2.4). The titanium discs were aseptically removed and placed into 1 ml of RTF containing five sterile glass beads and then vortexed for 1 min to disrupt the biofilm. This suspension was then serially diluted up to 10^7 and spread in duplicate onto FAA, blood and mitis salivarius culture media. All plates were incubated aerobically for 48 h with 5% CO_2 except fastidious anaerobic agar which was incubated for 4 to 5 days under anaerobic conditions. Following appropriate incubation the colonies on the agar plates were counted and CFU/biofilm calculated.

8.2.5 Characterisation of nanocoatings surfaces

The morphology of nano coatings was examined using scanning electron microscopy (SEM). The nanocoatings discs were mounted on carbon plugs. The coated discs were sputter-coated with gold and the surface morphology was observed.

8.2.6 Confocal laser scanning microscopy (CLSM)

The bacterial biofilm structures were studied by means CLSM (section 5.2.1.1 and 5.2.1.2). Each biofilm was analysed by Image J (<http://rsb.info.nih.gov/ij>) in combination with Image analysis software for Investigation of microbial biofilms (Chávez de Paz, 2009). A cell counting function was used to enumerate the total bacterial biomass and the distribution of the green (live) channel and red (dead) channel in one image. Other colours such as cream color were considered to be dying cells (Chávez de Paz, 2009).

8.3 Results

8.3.1 Culture analysis

The composition of inocula for two independent CDFF experiments was determined using fastidious anaerobe agar, blood agar and mitis salivarius agar. Following appropriate incubation, the colonies were counted and the CFU/ml was calculated to give viable counts as shown in table 8.1. The inoculum data showed that the numbers of anaerobe spp. was ca. 10^6 , aerobe spp. ca. 10^5 and *Streptococcus* spp. was ca. 10^5 .

Table 8.1. The mean \pm standard deviation ($n = 4$) (CFU/ml) of the salivary inoculum.

Bacteria species	Mean CFU/ml \pm SD
Anaerobe spp.	$6.88 \times 10^6 \pm 2.17 \times 10^6$
Aerobe spp.	$1.30 \times 10^5 \pm 9.56 \times 10^4$
Streptococcus spp.	$6.50 \times 10^5 \pm 1.73 \times 10^5$

8.3.2 Culture analysis of substratum

Samples were taken at 6 h, 24 h and 96 h and processed. Total anaerobes, total aerobes and total streptococci were enumerated. The differences between nanocoatings surfaces and control were revealed for 6 h, 24 h and 96 h peri-implant health microcosm are shown in Figures 8.3, 8.4 and 8.5. Analysis of biofilms sampled at 6 h showed a reduction of *Streptococcus* spp. on ZnO compared with control as shown in figure 8.5. Older biofilms, (24 h) showed a reduced number of anaerobes spp., aerobes spp. and streptococci on the discs coated with ZnO. At 96 h, there was a reduction of the aerobes on ZnO, combined ZnO + HA surfaces compared with control.

There was a reduction of anaerobes on ZnO, combined ZnO + HA surfaces compared with control. There was also a reduction of anaerobes on HA surfaces compared with control at 96 h. In terms of proportions, analysis of the data was performed:

1. At 6 h, the *Streptococcus* spp. were reduced on coated surfaces (74% on ZnO, 29% on HA and 33% on ZnO + HA surfaces) compared with control.

2. At 24 h on ZnO surfaces, the anaerobic bacteria counts were reduced by 76%; aerobic bacteria were reduced by 89% and *Streptococcus* spp. were reduced by 96% compared with control.
3. At 96 h, the number of anaerobes had reduced on coated surfaces (91% ZnO, 91% on HA and 95% on combined ZnO + HA surfaces); number of aerobes had also reduced (64% on ZnO, 50% on HA and 90% on ZnO +HA surfaces) and *Streptococcus* spp. were also reduced (92% on ZnO, 92% on HA, 95% on ZnO +HA surfaces) compared to the control.

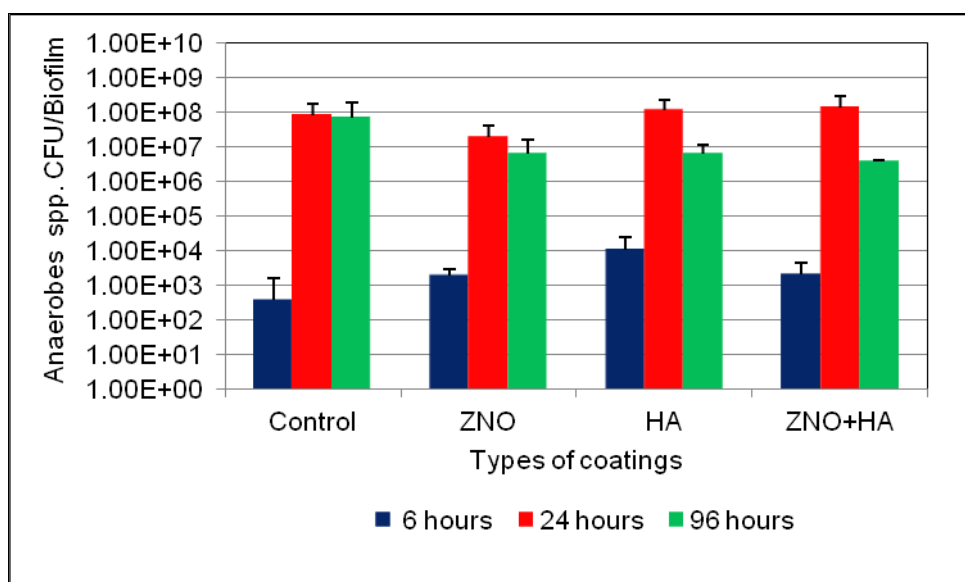


Figure 8.3. Total anaerobic bacteria counts on fastidious anaerobic agar under conditions simulating health for biofilm grown on control (uncoated polished titanium surfaces); ZnO surfaces, HA surfaces and combined ZnO + HA surfaces. Sampling points were 6, 24, 96 hours. Two separate experimental runs comprised of 4 replicates. Error bars represent the standard deviations ($n = 4$).

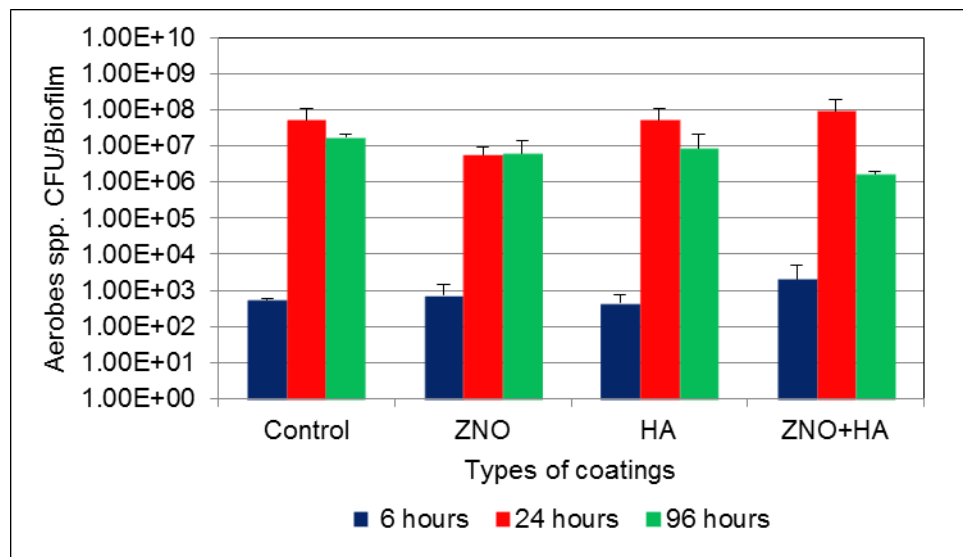


Figure 8.4. Total aerobic bacteria counts on blood agar under conditions simulating health for biofilm grown on control (uncoated polished titanium surfaces); ZnO surfaces, HA surfaces and combined ZnO + HA surfaces. Sampling points were 6, 24, 96 hours. Two separate experimental runs comprised of 4 replicates of each were used. Error bars represent the standard deviations ($n = 4$).

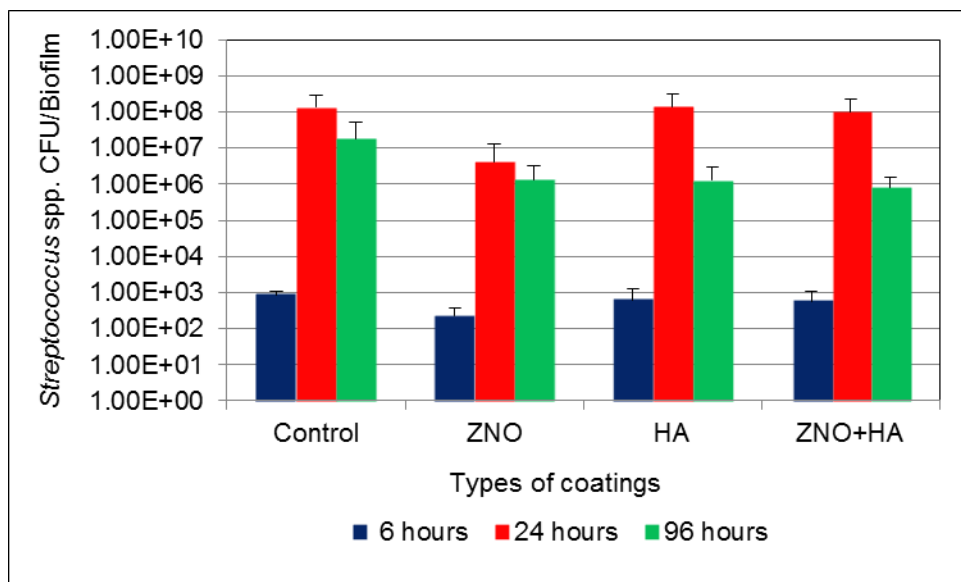


Figure 8.5. Total *Streptococcus* spp. counts on mitis salivarius agar under conditions simulating health for biofilm grown on control (uncoated polished titanium surfaces); ZnO surfaces, HA surfaces and combined ZnO + HA surfaces. Sampling points were 6, 24, 96 hours. Two separate experimental runs comprised of 4 replicates. Error bars represent the standard deviations ($n = 4$).

8.3.3 Characterisation of nanoparticles

The SEM micrographs showed nanoparticles deposited on the titanium surface, with a diameter of approximately 20-100 nm. Some nanoparticles formed aggregates as shown in figure 8.6 on both ZnO and HA nanoparticles surfaces.

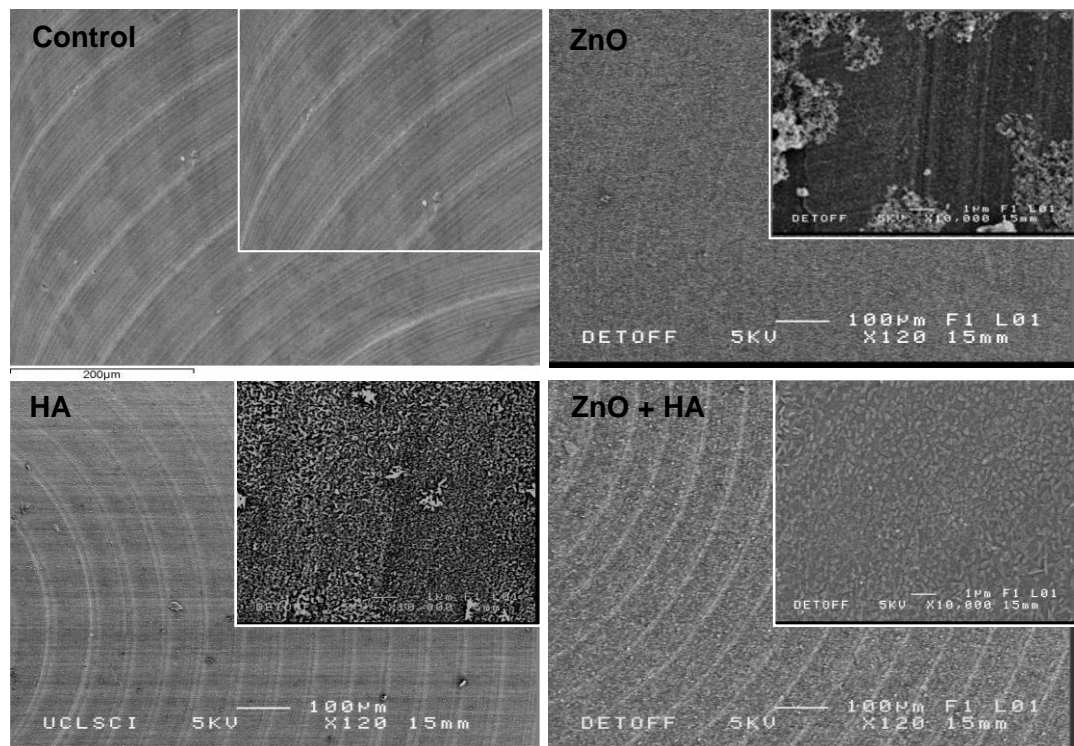


Figure 8.6. Scanning electron micrograph showing the microstructure of the nano surfaces on the Ti substrate prepared using the electrosprayed technique. Nano spray surfaces are shown at magnification of $\times 120$ (scale bar 100 μm). Inserts are higher magnification ($\times 10,000$ with scale bar 1 μm). Pure Ti (control) disc is shown a higher magnification, scale bar 200 μm .

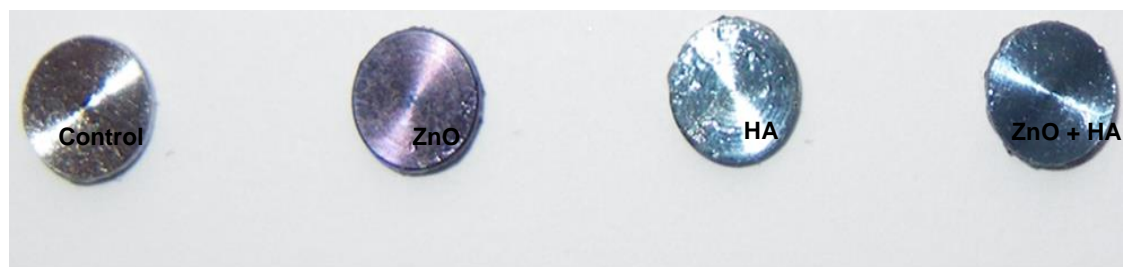


Figure 8.7. The surface colour of the Ti coated discs after 600°C treatment. ZnO coating become purple, HA become dark blue and combined ZnO + HA become blue/grey colour).

8.3.4 Biofilm structure analysis using CLSM

The biofilms (all surfaces and at each time point) were removed and prepared for visualization using CLSM. All biofilms were stained with live/dead stain. The confocal micrographs revealed that very few cells were present at 6 h (data not shown) and that far more were present at 24 h and 96 h. Initially cells were seemingly randomly distributed over the control surface while on other coated surfaces the cells were more likely to form as chains. The major community changes in the biofilms were of one initially dominated by rods (24 h) to one dominated with fusiform bacteria (96 h) are shown in Figures 8.8 - 8.11.

The cell counting function (section 8.2.6) was used for enumerating live (Green), dead (Red) or cream coloured cells (cream cells were assumed to be dying). The CLSM imaging results for the 24 h sampling point are shown in Figures 8.8 and 8.9.

The biomass volume of the 4 surfaces was highest on the control surface (ca. 15,000 μm^3) and lowest on the ZnO surface (ca. 5,000 μm^3). The dead and dying cells were highest on the control surface (39%) and lowest on the combined ZnO + HA surfaces (1%). The CLSM imaging results for the 96 h sampling point are shown in figures 8.10 and 8.11. The total biomass volume of the 4 surfaces was highest on the control surface (ca. 30,000 μm^3) and lowest on the HA surface (ca. 6,000 μm^3). The dead and dying cells were highest on the combined ZnO + HA surface (80%) and lowest on the HA coated discs (3%). Compared with 24 h samples, the dead or dying cells in the 96 h samples made up a greater proportion of the biofilm on the combined ZnO + HA surfaces (80% vs. 1%) and ZnO surfaces (56% vs. 37%). The proportion of dead and dying cells decreased for controls (39% vs. 13%) and HA coated discs (16% vs. 3%).

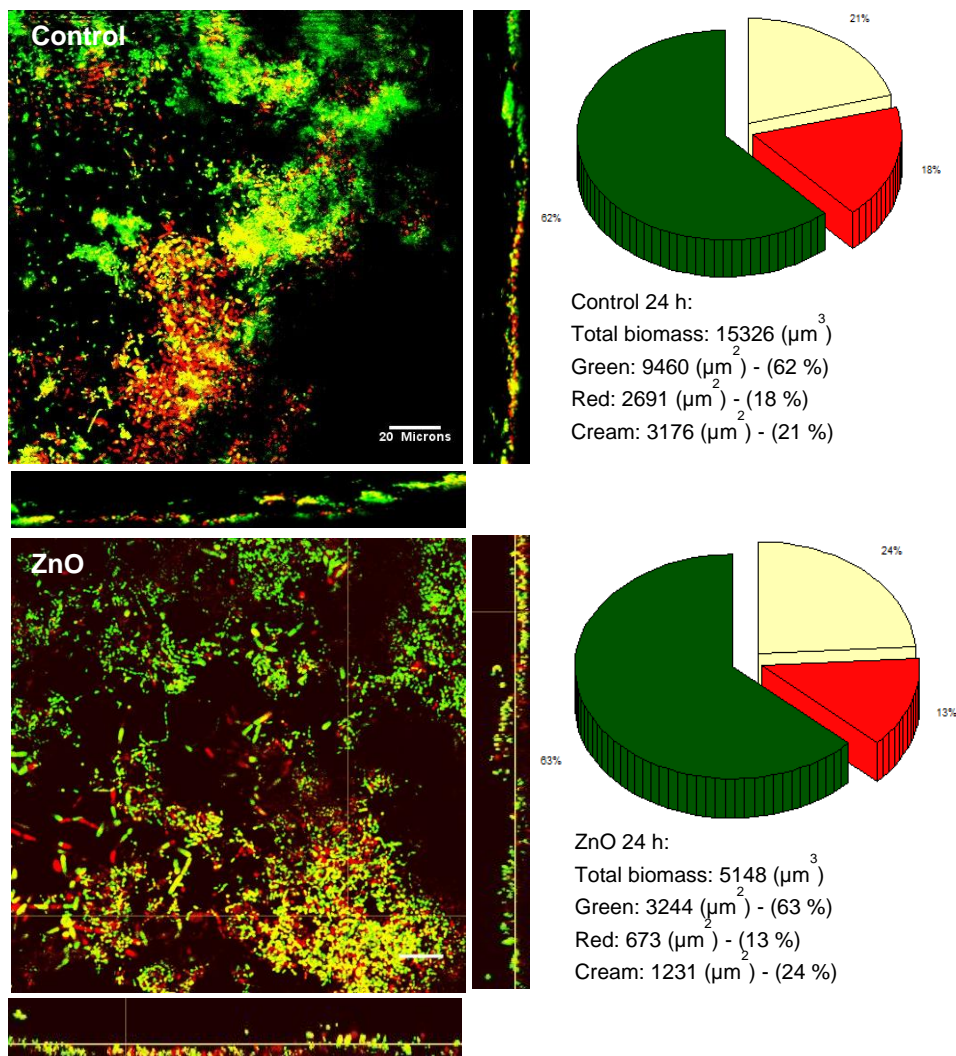


Figure 8.8. Live/dead staining of 24 h biofilm on control and ZnO nanoparticles. The lowest total viable biomass volume was on ZnO followed by HA nanoparticles surfaces. The highest total viable biomass volume was on combined ZNO + HA nanoparticles followed by control (pure titanium) surfaces. Scale bars 20 μm .

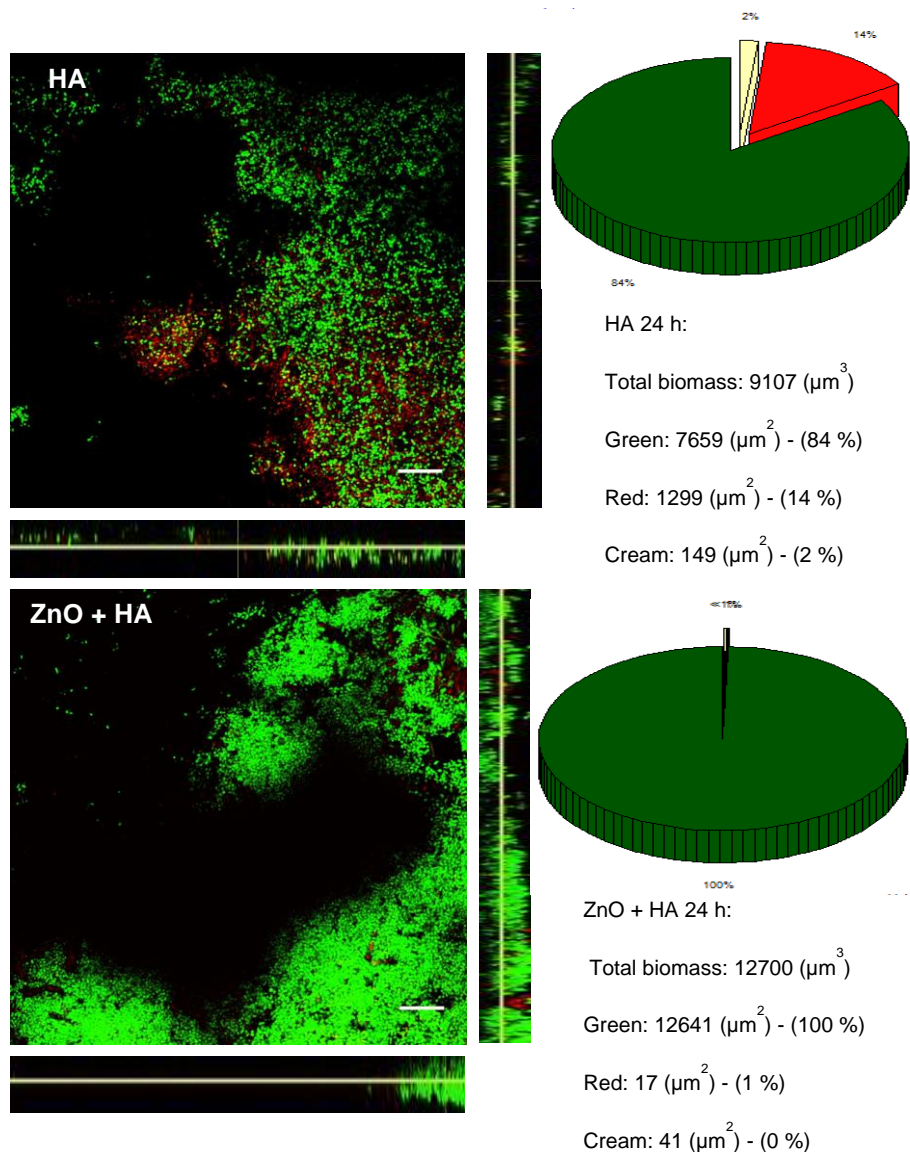


Figure 8.9. Live/dead staining of 24 h biofilm on HA and combined ZnO + HA nanoparticles. The lowest total viable biomass volume was on ZnO followed by HA nanoparticles surfaces. The highest total viable biomass volume was on combined ZNO + HA nanoparticles followed by control (pure titanium) surfaces. Scale bars 20 μm .

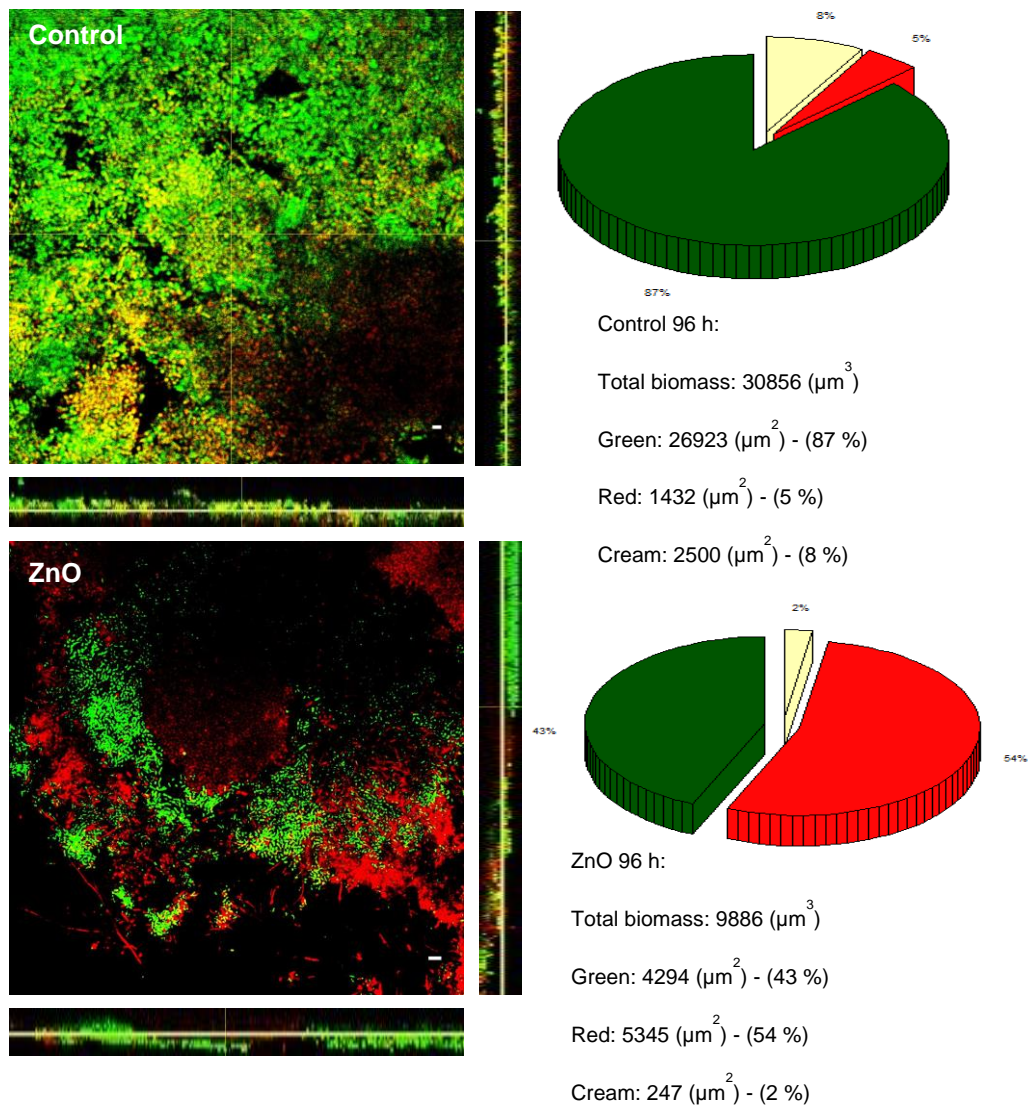


Figure 8.10. Live/dead staining of 96 h biofilm on control, ZnO nanoparticles. The lowest total viable biomass volume was on combined ZnO + HA followed by ZnO and HA nanoparticles surfaces compared with total viable biomass volume was on control (pure titanium) surfaces. Scale bars 20 μm .

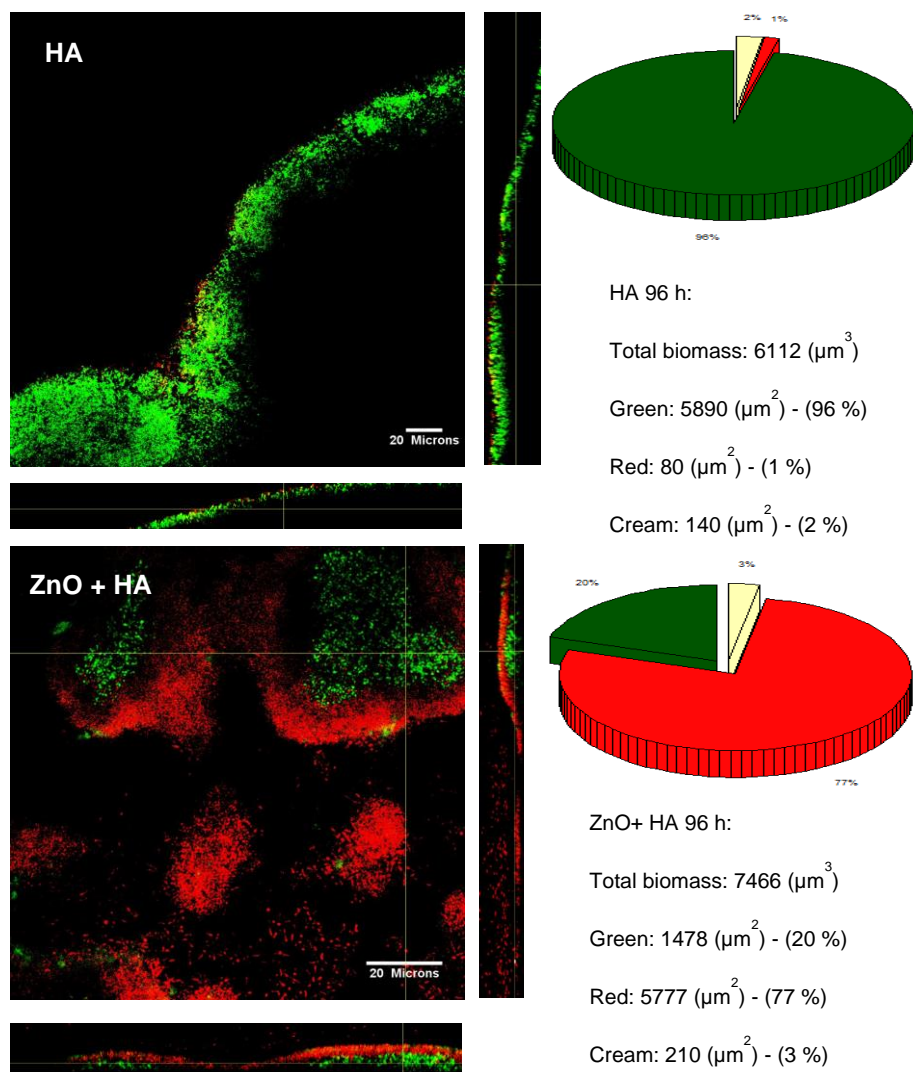


Figure 8.11. Live/dead staining of 96 h biofilm on HA and combined ZnO + HA nanoparticles. The lowest total viable biomass volume was on combined ZnO + HA followed by ZnO and HA nanoparticles surfaces compared with total viable biomass volume was on control (pure titanium) surfaces. Scale bars 20 μm .

8.3.5 Biofilm thickness analysis

The four titanium discs were examined by CLSM. Ten stocks of each nanocoatings surface were analysed. The image stacks were converted into JPEG format and processed through the image J software analysis with orthogonal views, which calculated the biofilm thickness as shown in Figure 8.12. At 24 h, biofilm depth was measured at around 35 µm for control, 13 µm for HA, 14 µm for ZnO and 7 µm for combined ZnO + HA. At 96 h biofilms depth was around 41 µm for control, 35 µm for HA, 24 µm for ZnO and 32 µm for combined ZnO + HA surfaces. Overall, the thickest biofilm was on control at 96 h (ca. 41 µm) and the thinner biofilm was on ZnO surfaces at the same sampling points (24 µm). There was a difference in depth of biofilm between the nanocoatings and control surfaces.

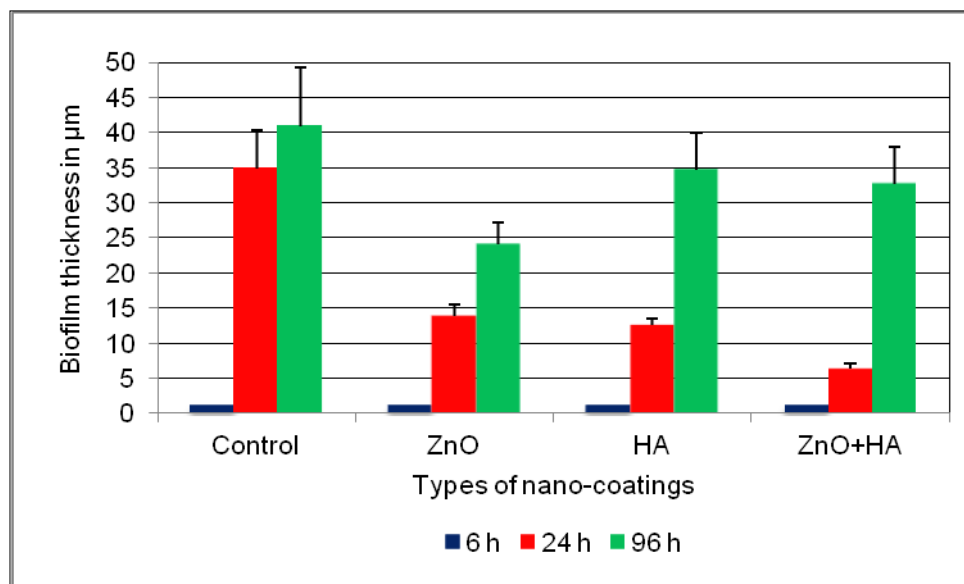


Figure 8.12. Thickness in µm of biofilms over time. Error bars represents the standard deviation ($n = 10$).

8.4 Discussion

8.4.1 Characterization of nanoparticles modified titanium surface

Electrohydrodynamic deposition techniques have been applied to deposit calcium phosphate coatings on metallic substrates (Leeuwenburgh et al., 2005), nano-metallic-oxides on silicone discs (Memarzadeh et al., 2012) and nano hydroxyapatite coatings on glass slides and TEM copper grids (Li et al., 2007, Li et al., 2008, Munir et al., 2011). The optimization of the conditions for spraying of nanoparticles suspensions, including the effects of needle size, the distance between the needle and substrate, the suspension flow rate and the voltage applied, have been systematically investigated and calibrated (Huang et al., 2011, Li et al., 2008 and 2007).

Overall, the coating surfaces exhibited uniform topography and no cracks were observed by SEM (Figure 8.6). The uniformity still prevailed on all surfaces, although aggregation of nanoparticles was found in particular on ZnO and HA discs. During the process of preparing the surfaces one noticeable change was the color of the Ti disc which became purple on ZnO and blue on HA and dark blue on combined ZnO + HA coatings (Figure 8.7).

8.4.2 Culture data

Saliva was used as an inoculum to provide a multispecies biofilm containing organisms found in the oral cavity. The nutrient source in both experiments was artificial saliva and PISF. The atmospheric parameters on both experiments were performed under aerobic conditions. The biofilms were grown on four titanium surfaces. The microcosm biofilms were treated in a similar manner, but were placed on to a various selective and non-selective media.

There are at least two mechanisms of inhibiting the formation of microbial plaque. The first is to inhibit the initial adhesion of bacteria, and the second is to inhibit the colonization of bacteria. *Streptococcus* spp. have been reported to be the most common initial biofilm coloniser of human enamel surfaces *in vivo* (Nyvad and Kilian, 1987). Indeed, the earlier study in Chapter 4 corroborated these findings and showed that *Streptococcus* spp. dominated biofilms in healthy dental implant conditions *in vitro*. Therefore, this model was deemed appropriate for testing the antibacterial properties of the novel Ti nanoparticles coating surfaces. Culture analysis at early time points 6, 24, 96 hours (health associated conditions) was performed to determine the antibacterial activity of three nanoparticles tested. The minimum inhibitory concentration (MIC) and minimum bactericidal concentration of ZnO nanoparticles was previously determined

(Memarzadeh et al., 2012). These previous studies tested ZnO against the *E. coli*, *P. aeruginosa*, *S. aureus*, and *S. epidermidis* and concluded that ZnO nanoparticles at a concentration of 10 mg/ml were bactericidal against *S. aureus* in suspension for 24 hours.

A biofilm analogous to other similar biofilms (Chapters 3 and 4) was produced on the control Ti surfaces. Biofilms grown on coated surfaces showed some differences compared to the controls. Broadly, the number of anaerobes and aerobes was similar for all discs and there was a significantly lower count of streptococci on the ZnO coated discs. This was unexpected as one might have expected the initial adherence and colonisation events to have had a greater effect as the bacteria would be in close proximity to the nano coatings and therefore perhaps more susceptible to their influence. There were no differences between any of the biofilms on coated surfaces and controls and the marginal significance of the ZnO disappeared even though there was a big difference (arguably larger than the 6 h biofilm) between this and control. After 96 h of biofilm growth a number of significant changes occurred and all three coatings had reduced numbers of anaerobes and 2 of them (ZnO and ZnO + HA) had fewer aerobes.

At 96 h the biofilm was expected to be in quasi steady state and it seems that in this case, the coatings were reducing the numbers by about a log. It could be argued that they were inhibiting the growth of the community and stopping the biofilm reaching a steady state. This was unexpected as in all previous studies, it was the early points 6 h - 24 h where effects was observed and was often lost in later time points. The experiment was designed to capture early community changes as a result of the coatings not, later, steady state changes. This was an interesting finding as it hints at a different mode of action driving the changes. Further experiments with extended sampling times would need to be performed to start to answer this question. This variation may be attributed to the greater surface area, which may have effect in enabling bacteria to contact with the surface of nanoparticles. Furthermore, it may be attributed to the selectivity of nanoparticles towards Gram-positive species rather than Gram negative spp. in particular ZnO nanoparticles (Premanathan et al., 2011). These data are also supported by CLSM findings.

It was also demonstrated a reduction of anaerobes occurred on combined ZnO+HA and ZnO surfaces at 96 h. At 24 h on ZnO surfaces, the proportion of anaerobe, aerobe and *Streptococcus* spp. had reduced (76%, 89%, 96%) compared with the control. This observation is consistent with the study of

Ahearn et al. (1995), who showed that following 24 h incubation of *S. aureus* and *E. coli* on Ti-nAg surface, 94% *S. aureus* and more than 95% *E. coli* in the bacteria suspension were killed.

8.4.3 CLSM data

The biofilms almost covered the entire discs at 24 h and 96 h as shown in Figures 8.8 - 8.11. An increase in time would be expected to promote an increase in bacterial extracellular polymers. Indeed, the total biomass of the biofilms on control surfaces at 24 h and 96 h time points was higher than the other surfaces. At 24 h, the total biomass of biofilm on ZnO was lower than that biofilm at 96 h. The proportion of dead or dying bacteria on ZnO surfaces was higher at 96 h compared with 24 h (56% vs. 37%). On HA surfaces, the proportion of dead or dying bacteria was lowest at 96 h compared with 24 h (3% vs. 16%). On combined ZnO+HA surfaces, the proportion of dead or dying bacteria was highest at 96 h compared with 24 h (80% vs. 1%). Overall the combined ZnO + HA surfaces was more bactericidal than other nanocoatings surfaces at 96 h. These data were supported by the culture data; it was observed that the proportion of killings CFU/ml of anaerobes spp., aerobes, and streptococci (95%, 95%, and 90%, respectively) on combined ZnO + HA surfaces compared with control. It was also observed that the control (pure titanium) biofilms at 96 h were thicker than all nanoparticles biofilms (ca. 41 μ m). The exceptions were biofilms grown on ZnO coatings at 96 h were thinner than all nanoparticles surfaces (24 μ m) as shown in Figure 8.12.

8.5 Conclusions

In the present study, novel nanoparticles-modified titanium surfaces were prepared using an electrodynamic deposition method. The microbial culture data indicated little antibacterial efficacy of either ZnO or combined nanoparticles against bacteria that initially attached. However, there was a significant reduction in the number of anaerobes at 96 h of which was also supported CLSM data. The data suggested that combined ZnO + HA and ZnO nanoparticles had some antibacterial properties and that they may have some clinical impact if used as implantable biomaterials in implant therapy.

Chapter 9
General discussion and conclusions

9.1 General discussion

Bacterial colonization and biofilm formation on dental hard tissues play a key role in the pathogenesis of caries, gingivitis, periodontitis (Marsh, 2005) and peri-implantitis (Heitz-Mayfield and Lang, 2010). In modern dentistry, titanium implants are one of the most common treatment options used for tooth replacement (Esposito et al., 2012). During the past two and a half decades, extensive clinical and laboratory research has been performed in the field of peri-implantitis microbiology. This has resulted in a significantly better understanding of the etiology and pathology of peri-implantitis (Koyanagi et al., 2013).

The biofilm that forms on these (and all other) oral surfaces is extremely complex and involves representatives of the entire oral microbial community, which is thought to be anything up to 1000 bacterial species (Wade, 2012). The bacterial community of the mouth is dominated by the phyla Firmicutes, Bacteroidetes, Proteobacteria, Actinobacteria, Spirochaetes and Fusobacteria, which account for 96% of species detected (Dewhirst et al., 2010). All of these organisms could have interactions with implant surfaces and are responsible for short or long term success and/or failure of osseointegration (Abrahamsson et al., 1998). The microbial load and host defense are extremely important and any perturbation to these may lead to infection of the implant (Mombelli, 1993, Heitz-Mayfield and Lang, 2010).

There are several limitations when analyzing the natural extent of inflammation around dental implants, as the implants themselves may reduce access for adequate clinical examination (Smith and Zarb, 1989). Since most peri-implant infections result in irreversible destruction of gingival tissue and resorption of alveolar bone, it is unethical to induce experimental peri-implantitis in humans and/or animals. There are numerous limitations when analysing the association of the microbiota at specific times and clinical conditions around implants at different time points and conditions around implants. Recent studies have shown that peri-implantitis includes a complex microbiota albeit less complex than that of periodontitis (Koyanagi et al., 2013). To overcome this, a laboratory model of peri-implantitis is required to help in the fundamental understanding of the microbiology associated with this condition. This could allow the testing of current and future treatments modalities and to test novel coating implants materials. Furthermore, a biofilm model system is essential to gain a better understanding of the mechanisms involved in biofilm formation and resistance to treatment regimes.

A number of biofilm-generating devices have been extensively used such as the Multiple Sorbarod Device (MSD) (McBain et al., 2005), various flow cells systems (Busscher and van der Mei, 1995), and the constant depth film fermentor (Peters and Wimpenny, 1988). The advantages of the CDFF system is that it provides many replicates in a single run, allows sampling of the biofilm at various intervals during the course of an experiment and inoculation can be of a single species; mixed species or microcosm (saliva or homogenous plaque). Given appropriate environmental conditions and substratum, the CDFF can be used to model numerous oral biofilm communities (Wilson, 1999). In the CDFF system, the development of a biofilm on a surface is limited to a predetermined depth by mechanically removing excess biofilm. This situation is regarded by some to reflect the movement of tongue over the teeth (Pratten, 2007).

The CDFF has been used comprehensively to study the ability of various antibacterial agents, to prevent biofilm formation (Pratten et al., 1998b), to kill bacteria in biofilms (Pratten et al., 1998a), to evaluate the erosion potential of oral biofilm (Wilson et al., 1997), to study the influence of surface characteristics (e.g. roughness) on biofilm formation (Morgan and Wilson, 2001), and to model shifts in microbial population associated with health or disease (Dalwai et al., 2006).

An important aspect of any study involving cultural-based microbiology is the assumption that all of the community is represented by the culture. Cultivation methods, traditionally considered as being the golden standard approaches, are limited as they do not detect viable non-culturable bacteria due to the inability of some species to grow reliably on selective media. Additionally, it has been reported that less than half of bacterial species in biological samples seem to be culturable (Rappé and Giovannoni, 2003, Flynn et al., 2012). In this present study, efforts have been made to identify the oral microbiota and assess their biofilm-related growth dynamics as well as their association with peri-implant disease conditions.

To overcome unculturable issues, culture independent microbiological characterisation methods were used. The comparative 16S rRNA gene cloning and sequencing approach has been used extensively in the study of the normal oral microbiota, oral infections, and the relationship of oral bacteria to systemic diseases. Molecular methods have been used to identify changes in the oral microbiota during growth and development (Aas et al., 2005). These methods have been used to study the microbiota of periodontal diseases (Spratt et al., 1999, Paster et al., 2001, Paster et al., 2006) and comparing between the

subgingival microbiota associated with moderate to severe chronic periodontitis with healthy controls (Kumar et al., 2005). These methods have been used for the detection of almost every species in a given sample and are able to indicate the presence of uncultivated and unknown bacteria (Aas et al., 2005), to determine the bacterial richness within the human subgingival crevice (Kroes et al., 1999), dentoalveolar abscesses (Dymock et al., 1996) and analysis of microbiota associated with peri-implantitis (Koyanagi et al., 2010, Koyanagi et al., 2013).

In the present investigation, biofilms were also imaged by confocal laser scanning microscopy (CLSM) to obtain structural analysis of natural, hydrated, and intact undisturbed microcosm biofilms formed on the titanium discs. CLSM offers several advantages over conventional light microscopy, including the ability to control depth of field, to eliminate or reduce background distortion, to collect serial optical images and generate 3D reconstructions from thick sections of specimens (Wood et al., 2000). CLSM is widely used in many scientific fields, especially in biology and medicine. CLSM has been used to determine the viability of biofilms (Hope and Wilson, 2003), to determine the structure of biofilms (Pratten et al., 2000) and in modeling shifts in microbial populations associated with health or disease (Dalwai et al., 2006).

In the present study, two software packages; Image J and Bioimage-L developed by Chávez de Paz (2009) were employed to image biofilms and analyse specific features. The features examined included mean biofilm thickness, viable and non-viable bacteria and total biomass. CLSM has also been used in the analysis of multispecies biofilm formation on customised titanium surfaces (Fröjd et al., 2011).

Multiplex qPCR has previously been used to assess the proportion and number of bacterial species present in communities associated with dental implants (Circi et al., 2010). Similar methodology was used in the present study to analyse *in vitro* biofilms at 15 separate time points over 29 days of culture. These experiments were conducted on two separate occasions (Circi et al., 2010). For generation of bacterial standard curves, the number of colony forming units (CFU/ml) was determined by plating serial dilutions of bacteria on agar media. Species-specific primers and probes homologous to regions in the 16S RNA gene portion and specific for *F. nucleatum*, *L. casei*, *V. dispar*, *N. subflava*, *P. intermedia* and total bacteria (universal) were determined. The exception to these were *S. sanguinis*, *S. mutans* where *sod(A)* gene was used and for *A. naeslundii* where *ure(C)* gene was used. To quantify *Capnocytophaga* spp., the

novel primers and dual labelled TaqMan probes were designed using the 16S rRNA gene sequence. Locked nucleic acid probes were employed in all assays except those for *A. naeslundii* and total bacteria. The advantage of using locked nucleic acid is that higher specificity and efficiency can be achieved (Circi et al., 2010).

As in periodontal diseases, various therapies have been proposed to reduce the number of pathogenic species (Mombelli et al., 2011). Several methods for implant disinfection, such as chemical conditioning, air-powered abrasive, plastic curettes and laser therapies, have been used in combination with regenerative techniques and/or antimicrobials. To assess the bacterial population after certain treatments of commercial titanium surfaces associated with the onset of peri-implant mucositis and peri-implantitis, the model was used to test the viable numbers of bacteria and fungi, remaining on three different titanium surfaces (polished, SLA and SLActive) following a range of decontamination regimes.

The biocompatibility of the three different titanium surfaces (following decontamination regimes) was analysed by assessing culture and proliferation of MG-63 cells. Standard curves of MG-63 cell numbers were used with all experiments to determine cell proliferation on the titanium surfaces. In addition, SEM was used to evaluate cell morphology following use of the decontamination regimes.

Bacterial attachment plays a significant role in determining the outcome and success of dental implants. Bacteria attached to a surface are able to replicate, move and form colonies beyond the biofilm. Therefore, surface modification of titanium to reduce the number of bacteria and microbial adhesion seems an efficient way to increase the benefit of clinical treatment. Generally, it is accepted that the most effective method to prevent biofilm buildup on dental implant surfaces is to inhibit initial bacterial adhesion, due to the fact that mature biofilms are more difficult to remove. Metal oxide particles (size range of 20-100 nm) were coated onto Ti discs using Electrohydrodynamic Deposition (EHD). The CDFF was then used to grow appropriate microcosm biofilms on these discs.

To fulfil the above aims a number of objectives needed to be achieved:

1. To grow appropriate microcosm biofilms on titanium discs.
2. To develop the model to allow progression from a health-associated community to a peri-implant mucositis-associated community and then to a peri-implantitis-associated community.

3. To develop microscopic and molecular biology methods to characterise these three communities.

4. To use the model to test both commercially available and novel antimicrobial nanotechnology surfaces.

9.1.1 Development of an *in vitro* model of peri-implantitis

To provide conditions associated with healthy dental implants, only modified artificial saliva was initially introduced into the CDFF. To model a healthy dental implant progressing to peri-implant mucositis, the nutrition provided was changed to also include peri-implant sulcular fluid. An increased flow of artificial tissue fluid with microaerophilic gas mixture was supplied to simulate peri-implant mucositis conditions.

The study showed that the number of anaerobes increased in the populations and that the number of aerobic bacteria and streptococci initially reduced; the anaerobic population, were however, dominated throughout.

The microstructure of non-supplemented biofilms was shown to be complex, with stacks of bacteria developing over time, separated by clear channels. The heterogeneous nature of the biofilm structure was observed by CLSM and was in agreement with the study of Wood et al. (2002). Under conditions emulating peri-implant mucositis, non-viable bacteria became more widely distributed throughout the substratum. This was in agreement with the specific finding of Auschill et al. (2001) who reported that the dead layers of dental implant biofilms were adjacent to the substratum surface. Furthermore, material derived from dead microorganisms was proposed to be important in the initial development of dental plaque biofilms (Auschill et al., 2001).

In the biofilms studied in this present research, the proportion of viable microorganisms was lower adjacent to the titanium surface and at the outer layers. A limited shift in the microbiota composition from health to peri-implant mucositis was unexpected; indeed the change of conditions was expected to elicit a greater change in the microbial population. It is possible that some members of the community were developed into a VBNC state or that perhaps the taxa that changed were part of the unculturable proportion of the population. The CLSM data relating to the changes in the populations did not agree with the culture data. The culture results showed that there was little or no differences between conditions, yet the CLSM data showed extensive differences in the structure and cell morphology in the biofilms.

The model was progressed from conditions associated with health, to those associated with mucositis and finally to conditions of peri-implantitis. The microbiological characterisation methods used were based on culturing the samples on a variety of media. The data showed no differences in the culture between peri-implant mucositis and peri-implantitis conditions. CLSM analysis showed that the biofilm associated with the anaerobic atmosphere had dense embedded clusters of long filaments on titanium disc surface. The culture data and the CLSM data did not agree in terms of community shifts associated with environmental changes. To more fully understand this, it was decided to analyse the biofilms by molecular techniques. It was thought that these culture independent methods should be able to resolve the issue and characterise the changing community.

Comparative 16S rRNA gene cloning and sequencing was performed to detect community changes between the 3 different conditions. A number of commonly reported bacterial genera present in this study were identified. Mainly, *Streptococcus mitis* and *Neisseria* species were the dominant species under health conditions, constituting classical dental plaque pioneer species. This is in agreement with a previous study of the peri-implant microbiota of successful implants using anaerobic culture techniques (Mombelli et al., 1988), that showed that implants were colonized by Gram-positive cocci. Also, these results are in agreement with findings of Quirynen et al. (2002) and Romeo et al. (2004), who identified that the plaque around successful dental implants was mainly composed of Gram-positive cocci e.g. *Streptococcus* with low numbers of Gram-negative anaerobes. These species are frequently detected *in vivo* in healthy dental implant biofilms (Lee et al., 1999) by culture independent techniques (Rams et al., 1984, Sanz et al., 1990).

In peri-implant mucositis, the biofilms were dominated mainly with *Capnocytophaga* spp. *Veillonella* spp., *Neisseria* spp., with some *Parvimonas micra* and *Streptococcus* spp. These findings were similar to those reported by Maximo et al. (2009) who used a checkerboard DNA-DNA hybridization technique and detected *S. sanguinis*, *S. gordonii*, *P. intermedia*, *Veillonella parvula* at elevated levels in peri-implant mucositis conditions. The same authors identified *N. mucosa*, *C. ochracea* and *Fusobacterium* spp. at higher levels in peri-implantitis.

In peri-implantitis, the microbial community was dominated by *Capnocytophaga* spp. and *Veillonella parvula*. Commensal gut species (e.g. *Klebsiella pneumonia*) were also detected in all conditions. Augthun and Conrads (1997) detected

Capnocytophaga, *F. nucleatum* and *Eikenella corrodens*, whilst Newman and Flemmig (1988) reported an increased incidence of *Capnocytophaga* spp. in infected implants. A further study by Alcoforado et al. (1991) reported potentially pathogenic bacteria such as *P. micra*, *Fusobacterium* sp. and *P. intermedia* associated with dental implants infections. The same authors reported significant numbers of enteric rods and *Capnocytophaga* spp. Using pyrosequencing, Kumar et al. (2012), showed lower levels of *Prevotella* spp. and *Leptotrichia* spp., and higher levels of *Actinomyces* spp., *Peptococcus* spp., *Campylobacter* spp., *Butyrivibrio* spp. and *Streptococcus* spp. in peri-implantitis. Another clinical study conducted by Koyanagi et al. (2010) found that the microbiota associated with peri-implantitis was more diverse than in healthy dental implants and included *F. nucleatum* and *Granulicatella adiacens*. These figures were also similar to those reported by Mombelli (2002) who detected higher levels of *Fusobacterium* spp. and *Prevotella* species in peri-implant infections.

Differences at the species level were observed in all three states and some, as yet unreported bacteria, were also detected, for example TM7 and *Vibrio* spp. were identified by the PCR-cloning technique. These bacteria are difficult to grow or not cultivable and therefore are not well characterised (Al-Radha et al., 2012, Kumar et al., 2012). The main differences in the microbial profiles of diseased states compared with healthy implants are the higher levels of periodontal pathogens and the lower proportions of host-compatible bacteria (Shibli et al., 2008). An important finding was the change in proportion of Gram-positive to Gram-negative species (67% under health condition, 43% under peri-implant mucositis condition and 30% under peri-implantitis condition). Several studies have indicated that during peri-implant biofilm formation the microbial composition shifts towards a higher proportion of Gram-negative anaerobes (Mombelli and Décailliet, 2011, Abrahamsson et al., 1998, Ericsson et al., 1992, Cortelli et al., 2013) and the results from the current study support this.

9.1.2 Assessing the change in proportions and total of specific bacteria in biofilms of the three communities using multiplex qPCR assays

There are a number of avenues which can be taken to progress this work and our understanding of peri-implantitis. To study the change in proportions of specific bacteria in biofilms of the three community's types, the quantification of eight key taxa as well as a universal bacterial assay was used to allow total number of bacteria present and the proportion of each taxon to be determined in each community. Three triplex qPCR assays were established by Cric et al.

(2010) to enumerate three organisms associated with gingivitis (*F. nucleatum*, *A. naeslundii*, *P. intermedia*), three organisms associated with oral health (*S. sanguinis*, *V. dispar*, *N. subflava*) and two organisms strongly implicated in dental caries (*S. mutans*, *L. casei*). A universal primer and probe were used to quantify total number of cells. The results showed that the most numerous taxa were *N. subflava* followed by *F. nucleatum*, *S. sanguinis* and *V. dispar* under healthy conditions. Under peri-implant mucositis conditions, the dominant taxa were *N. subflava*, *F. nucleatum*, *V. dispar* and *S. sanguinis*. Under peri-implantitis conditions the total numbers of organisms remained stable over the experiment. The number of *L. casei*, *S. mutans*, *P. intermedia* and *A. naeslundii* remained below the detectable limit through the course of the study.

A previous study suggested that these taxa did not grow well in biofilms cultured in the CDFF without introduction of carbohydrates such as glucose and sucrose. The lack of glucose or sucrose could be therefore the cause of the lower detection of rates of these organisms in the present study (Ciric et al., 2011).

The new multi-triplex qPCR method targeting microorganisms associated with dental implant health, peri-implant mucositis; and peri-implantitis has allowed for the quick and efficient targeted analysis of the microbial community structure. Based on the results, qPCR showed a significant difference between health and peri-implantitis conditions and between peri-implant mucositis and peri-implantitis. The use of qPCR to assess the species and genus numbers in these populations allowed particular organisms to be assessed more accurately than by culture analysis.

9.1.3 Design of novel TaqMan probe and primers to assess the proportions of *Capnocytophaga* species

To assess the numbers of *Capnocytophaga* present in the biofilms during the changes in the community, novel qPCR probes and primers were developed. The 16S ribosome RNA gene sequences of oral *Capnocytophaga* species were retrieved from Ribosomal Data Base and a number of primer pairs were designed for the target organism. The specificity of the primers for the target sequence were tested initially on target and reference strains using conventional PCR technique. The results showed that some of primer pairs had cross reactivity with other strains and others did not work, so alternative forward and reverse primers were produced. These primers were specific when assessed by conventional PCR method and with a specific TaqMan probe in qPCR.

These new primers were used to determine the number of *Capnocytophaga* in the biofilm community through the biofilm development. The results showed that *Capnocytophaga* numbers were lowest under conditions emulating health whilst numbers were higher in peri-implant mucositis condition and peri-implantitis.

This finding was also supported by the cell morphology observed in several of the CLSM images, where fusiform cells were observed in abundance (chapter 4, section 4.3.2.1, and figure 4.12). It is unclear why these data should not fit with the qPCR results. It may be that the CLSM images were not *Capnocytophaga* or indeed that there were, as yet, uncultured *Capnocytophaga* species present that did not amplify with the primer set used. The use of qPCR to assess the numbers of *Capnocytophaga* and other taxa in communities allows the fast and accurate assessment of the effects environmental changes on the population. It was shown that qPCR primer design for specific taxa has allowed analysis of complex communities. It also allows the primer set to be used in any *in vitro* or indeed *ex vivo* samples for detection and quantification of *Capnocytophaga*.

9.1.4 Testing of current and future decontamination modalities

The CDFF model was used to assess the effect of different commercial titanium surfaces on the community structure of biofilms. The biofilms were grown on three commercial titanium surfaces (polished, SLA and SLActive) then treated with one of four treatments protocols (PDT, TiBrush + PDT, TiBrush, CHX) or control untreated biofilms (RTF). Ti discs were subjected to traditional microbiological analysis, CLSM and biocompatibility analysis.

It was shown that a combination of Ti brush and PDT was the most effective treatments for removing biofilms. The present results are in agreement with another *in vitro* PDT study that clearly demonstrated that PDT alone was able of killing oral bacteria species (Takasaki et al., 2009). CHX treatment resulted in bacterial reduction under peri-implant mucositis conditions only on polished surfaces when compared to control. The poor ability of chlorhexidine to remove the whole biofilm from the SLA and SLActive surfaces could be attributed to the presence of more mature biofilms, which are widely regarded as being less to antibacterial agents. The biofilm-EPS matrix has repeatedly been cited as a protective barrier which may buffer cells from the influence of a range of stress factors including antimicrobial agents. In order to kill bacteria in mature biofilm, the need to higher concentrations of antimicrobials with longer exposure times has been shown (Gera, 2008). For example, Oosterwaal et al. (1989) reported

that CHX had a bacteriostatic effect when used at low concentrations and a bactericidal effect when used at very high concentrations (0.5 - 2% for 10 min) against periodontal pathogens. Biofilm thickness may affect the transfer of essential nutrients into biofilms by increasing the diffusion length of penetration to the base of the film. A thinner biofilm may, therefore, have a faster growth rate due to possible increase in nutrients from increased penetration. A number of investigations have concluded that slowly growing cells are less susceptible to the action of harmful agents (Gilbert and Brown, 1980). Hence, if bacteria are growing faster in a thin biofilm compared to a thick biofilm they may be more susceptible to the action of antibacterial agents.

The results of a study by Henderson et al. (2012) support the current findings in that 0.2% CHX had significant effects on the biofilms when applied for 2 min on the contaminated mirror polished surface covered with biofilms of *Staphylococcus epidermidis*. The effects on biofilm thickness were investigated by comparing three titanium surfaces of different roughness. One of the surfaces had an R_a value $< 0.5 \mu\text{m}$ and therefore was classified as smooth (Albrektsson and Wennerberg, 2004). The biofilm thickness ranged between $49 \mu\text{m} - 55 \mu\text{m}$ on all surfaces and controls. The polished surface showed greatest reduction in biofilm thickness following the combined treatment (Ti and PDT) and least with CHX. The other two surfaces also followed this trend. The differences between the three surfaces was supported by the fact that on the moderate rough surfaces much of the biofilm thickness remained after mechanical removal with a titanium brush, whereas almost all the bacteria were removed from the polished surface. Also the observed differences were supported based on total biomass volume proportions. Results from a previous *in vivo* study also showed that rough titanium surfaces retained significantly more bacteria than smooth surfaces (Amarante et al., 2008).

Surface biocompatibility was assessed on decontaminated Ti discs for both communities using MG-63 cells and assessed by SEM. The apparent high biocompatibility of the cells on surfaces treated with all decontamination regimes was difficult to explain. However, it is thought that the assays were contaminated with bacteria. The fluorescence/absorbance endpoint quantification procedure of the Alamar blue assay is related to total cell activity and that in this case it may well have been the sum of bacterial and MG-63 cells activity. This therefore may mean that the figures for the number of cells are a sum of MG-63 cells activity plus bacterial biofilm activity. Hence, the interpretation of the Alamar blue results

should be taken with caution. In addition, the results from the SEM study revealed the presence of residual biofilm in the Alamar blue assay. There are many factors that could influence this study, such as the low number of samples, and the conditions used for UV irradiation. In the case of the latter, it was likely that an insufficient time of UV exposure was employed to eliminate the mature and complex biofilm (Renier et al., 2011). The previous study found that the mortality increased with an increase in the duration of irradiation dose (Nandakumar et al., 2006). The exact proportion of each of these contributing factors is not quantifiable in the current data set. Therefore, very few meaningful conclusions can be drawn from these data.

9.1.5 To assess the initial attachment of bacterial biofilm on novel nanocoatings surfaces

NanoHA and NanoZnO or combined ZnO + HA nanoparticles were used. Samples were taken at 6 h, 24 h and 96 h and processed. Analysis of biofilms sampled at 6 h showed a reduction of *Streptococcus* spp. on ZnO compared with control. Older biofilms, (24 h) showed a reduced number of anaerobic spp., aerobes spp. and streptococci on the discs coated with ZnO. At 96 h, there was a reduction of both aerobic and anaerobic bacteria on the ZnO, combined ZnO + HA surfaces compared with control. The confocal micrographs revealed that dense layers of viable and non viable bacteria were present at 24 h and 96 h. The cells were seemingly randomly distributed over the control surface, whilst on other coated surfaces; the cells were more likely to form as chains. The major community changes in the biofilms were from one dominated by rods (24 h) to one dominated by fusiform bacteria (96 h). The total biomass of the 4 surfaces was highest on the control surface (ca. 30,000 μm^3). Compared with 24 h samples, the dead or dying cells in the 96 h samples made up a greater proportion of the biofilm on the combined ZnO + HA surfaces. In conclusion, the culture-based data indicated limited antibacterial activity against initial bacterial attachment, but at 96 h antibacterial effects were apparent. Traditionally, it is generally considered that surface coatings tend to function at early stages of biofilm formation and it was therefore surprising that the antimicrobial effects of these were only detected at 96 h in this study.

9.1.6 Conclusions

Based on the results of this study, the CDFF model of peri-implantitis has been developed to simulate the three communities (health, peri-implant mucositis

progressing to peri-implantitis). CLSM was successfully employed to characterise the biofilm structure, spatial distribution of viable and non-viable cells within the depth of the biofilms, thickness and cell enumerating associated with dental implant conditions. The newly designed probe and primers allowed the primer set to be used in any *in vitro* or indeed *ex vivo* samples for detection and quantification of *Capnocytophaga* species. The CDFF model was used successfully to test and assess current and novel treatments modalities. The novel antibacterial nanocoatings on Ti surfaces tested successfully. Use of this model may be of considerable value by reducing the need for large numbers of expensive clinical trials by selecting patients with peri-implantitis conditions. The screening of potential commercial or nanocoatings antibacterial surfaces for use in preventing and/or treating plaque related disease. Overall, a working peri-implantitis model has been developed.

9.1.7 Clinical relevance

A wide range of bacteria are associated with peri-implant diseases. The biofilm in peri-implantitis showed a more complex, aggressive microbial composition and several bacteria were identified as candidate pathogens in peri-implantitis. Decontamination of titanium surfaces is of key importance when trying to resolve peri-implantitis and obtain re-osseointegration.

The challenge is to find a treatment protocol that balances decontamination of the titanium surface with the stimulation and promotion of healing in peri-implant tissues. The therapeutic strategies for managing and preventing peri-implantitis could focus on limiting/reducing bacterial load, with the aim of impeding biofilm formation.

9.1.8 Future work

Consequent to the findings of this study, the following investigations are proposed:

1. To use new generation sequencing techniques (Mi-Seq system) to truly understand richness and diversity changes in biofilm development and the progression from healthy, peri-implant mucositis and peri-implantitis.
2. Use the CLSM and fluorescent *in situ* hybridisation technique (FISH) to resolve the spatial distribution and temporal changes on specific

Chapter 9: General discussion and conclusions

members of microbiota and population dynamics in health, peri-implant mucositis and peri-implantitis phases of biofilms.

3. Design a new protocol for the biocompatibility test (MG-63 cells and Alamar blue assay); further develop an *in vitro* model of bone to understand the effect of infected titanium surfaces on proliferation and viability of osteoblasts and osteoclasts cells.
4. Use the same technique to compare between clinical scenario and *in vitro* model of peri-implantitis.

References

AAS, J. A., PASTER, B. J., STOKES, L. N., OLSEN, I. & DEWHIRST, F. E. 2005. Defining the normal bacterial flora of the oral cavity. *J Clin Microbiol*, 43, 5721-32.

ABRAHAMSSON, I., BERGLUNDH, T. & LINDHE, J. 1998. Soft tissue response to plaque formation at different implant systems. A comparative study in the dog. *Clin Oral Implants Res*, 9, 73-9.

ADELL, R., LEKHOLM, U., ROCKLER, B. & BRÅNEMARK, P. I. 1981. A 15-year study of osseointegrated implants in the treatment of the edentulous jaw. *Int J Oral Surg*, 10, 387-416.

ADELL, R., LEKHOLM, U., ROCKLER, B., BRÅNEMARK, P. I., LINDHE, J., ERIKSSON, B. & SBORDONE, L. 1986. Marginal tissue reactions at osseointegrated titanium fixtures (I). A 3-year longitudinal prospective study. *Int J Oral Maxillofac Surg*, 15, 39-52.

ADONOGIANAKI, E., MOONEY, J., WENNSTRÖM, J. L., LEKHOLM, U. & KINANE, D. F. 1995. Acute-phase proteins and immunoglobulin G against *Porphyromonas gingivalis* in peri-implant crevicular fluid: a comparison with gingival crevicular fluid. *Clin Oral Implants Res*, 6, 14-23.

AGLIETTA, M., SICILIANO, V. I., ZWAHLEN, M., BRAGGER, U., PJETURSSON, B. E., LANG, N. P. & SALVI, G. E. 2009. A systematic review of the survival and complication rates of implant supported. *Clin Oral Implants Res*, 20, 441-51.

AHEARN, D. G., MAY, L. L. & GABRIEL, M. M. 1995. Adherence of organisms to silver-coated surfaces. *J Ind Microbiol*, 15, 372-6.

AHMADIAN, A., GHARIZADEH, B., GUSTAFSSON, A. C., STERKY, F., NYRÉN, P., UHLÉN, M. & LUNDEBERG, J. 2000. Single-nucleotide polymorphism analysis by pyrosequencing. *Anal Biochem*, 280, 103-10.

AL-AHMAD, A., TENNERT, C., KARYGIANNI, L., WRBAS, K. T., HELLWIG, E. & ALTBURGER, M. J. 2013. Antimicrobial photodynamic therapy using visible light plus water-filtered infrared-A (wIRA). *J Med Microbiol*, 62, 467-73.

AL-AHMAD, A., WIEDMANN-AL-AHMAD, M., FAUST, J., BÄCHLE, M., FOLLO, M., WOLKEWITZ, M., HANNIG, C., HELLWIG, E., CARVALHO, C. & KOHAL, R. 2010. Biofilm formation and composition on different implant materials in vivo. *J Biomed Mater Res B Appl Biomater*, 95, 101-9.

AL-RADHA, A. S. D., PAL, A., PETTEMERIDES, A. P. & JENKINSON, H. F. 2012. Molecular analysis of microbiota associated with peri-implant diseases. *J Dent*, 40, 989-998.

ALBREKTSSON, T. 1998. Surface roughness of intraoral dental implant fixtures. *Dent Implantol Update*, 9, 73-7.

ALBREKTSSON, T. & WENNERBERG, A. 2004. Oral implant surfaces: Part 1-- review focusing on topographic and chemical properties of different surfaces and in vivo responses to them. *Int J Prosthodont*, 17, 536-43.

ALBREKTSSON, T. & WENNERBERG, A. 2005. The impact of oral implants - past and future, 1966-2042. *J Can Dent Assoc*, 71, 327.

ALBREKTSSON, T., ZARB, G., WORTHINGTON, P. & ERIKSSON, A. R. 1986. The long-term efficacy of currently used dental implants: a review and proposed criteria of success. *Int J Oral Maxillofac Implants*, 1, 11-25.

ALCOFORADO, G. A., RAMS, T. E., FEIK, D. & SLOTS, J. 1991. Microbial aspects of failing osseointegrated dental implants in humans. *J Parodontol*, 10, 11-8.

ALJATEELI, M., FU, J. H. & WANG, H. L. 2012. Managing peri-implant bone loss: current understanding. *Clin Implant Dent Relat Res*, 14 Suppl 1, e109-18.

ALLAKER, R. P. 2010. The use of nanoparticles to control oral biofilm formation. *J Dent Res*, 89, 1175-86.

ALLAKER, R. P. 2013. Chapter 10 - Nanoparticles and the Control of Oral Biofilms. *Nanobiomaterials in Clinical Dentistry*. William Andrew Publishing.

ALLAKER, R. P. & DOUGLAS, C. W. 2009. Novel anti-microbial therapies for dental plaque-related diseases. *Int J Antimicrob Agents*, 33, 8-13.

ALLAKER, R. P. & REN, G. 2008. Potential impact of nanotechnology on the control of infectious diseases. *Trans R Soc Trop Med Hyg*, 102, 1-2.

ALSAADI, G., JACOBS, R., QUIRYNEN, M. & VAN STEENBERGHE, D. 2008. Soft tissue augmentation of the cheeks detected on intra- and extraoral radiographs: a case report. *Dentomaxillofac Radiol*, 37, 117-20.

AMARANTE, E. S., CHAMBRONE, L., LOTUFO, R. F. & LIMA, L. A. 2008. Early dental plaque formation on toothbrushed titanium implant surfaces. *Am J Dent*, 21, 318-22.

APSE, P., ELLEN, R. P., OVERALL, C. M. & ZARB, G. A. 1989. Microbiota and crevicular fluid collagenase activity in the osseointegrated dental implant sulcus: a comparison of sites in edentulous and partially edentulous patients. *J Periodontal Res*, 24, 96-105.

APSE, P., ZARB, G. A., SCHMITT, A. & LEWIS, D. W. 1991. The longitudinal effectiveness of osseointegrated dental implants. The Toronto Study: peri-implant mucosal response. *Int J Periodontics Restorative Dent*, 11, 94-111.

ARWEILER, N. B., HENNING, G., REICH, E. & NETUSCHIL, L. 2002. Effect of an amine-fluoride-triclosan mouthrinse on plaque regrowth and biofilm vitality. *J Clin Periodontol*, 29, 358-63.

ASAI, Y., JINNO, T., IGARASHI, H., OHYAMA, Y. & OGAWA, T. 2002. Detection and quantification of oral treponemes in subgingival plaque by real-time PCR. *J Clin Microbiol*, 40, 3334-40.

ASIKAINEN, S., ALALUUSUA, S. & SAXÉN, L. 1991. Recovery of A. actinomycetemcomitans from teeth, tongue, and saliva. *J Periodontol*, 62, 203-6.

ATA-ALI, J., FLICHY-FERNÁNDEZ, A. J., ALEGRE-DOMINGO, T., CANDEL-MARTI, M. E., PEÑARROCHA, D., BALAGUER-MARTINEZ, J. F. & PEÑARROCHA, M. A. 2011. Analysis of the peri-implant microbiota in 90 dental implants and its relationship to crevicular fluid volume. *Med Oral Patol Oral Cir Bucal*, 16, e944-7.

ATIEH, M. A., ALSABEEHA, N. H., FAGGION, C. M., JR. & DUNCAN, W. J. 2012. The Frequency of Peri-Implant Diseases: A Systematic Review and Meta-Analysis. *J Periodontol*.

AUGTHUN, M. & CONRADS, G. 1997. Microbial findings of deep peri-implant bone defects. *Int J Oral Maxillofac Implants*, 12, 106-12.

AUGTHUN, M., TINSCHERT, J. & HUBER, A. 1998. In vitro studies on the effect of cleaning methods on different implant surfaces. *J Periodontol*, 69, 857-64.

AUSCHILL, T. M., ARTWEILER, N. B., NETUSCHIL, L., BRECX, M., REICH, E. & SCULEAN, A. 2001. Spatial distribution of vital and dead microorganisms in dental biofilms. *Arch Oral Biol*, 46, 471-476.

BAIN, C. A. & MOY, P. K. 1993. The association between the failure of dental implants and cigarette smoking. *Int J Oral Maxillofac Implants*, 8, 609-15.

BALDWIN, B. R., NAKATSU, C. H. & NIES, L. 2003. Detection and enumeration of aromatic oxygenase genes by multiplex and real-time PCR. *Appl Environ Microbiol*, 69, 3350-8.

BARBOZA, E. P., CAÚLA, A. L. & CARVALHO, W. R. 2002. Crestal bone loss around submerged and exposed unloaded dental implants: a radiographic and microbiological descriptive study. *Implant Dent*, 11, 162-9.

BECKER, S., BÖGER, P., OEHLMANN, R. & ERNST, A. 2000. PCR bias in ecological analysis: a case study for quantitative Taq nuclease assays in analyses of microbial communities. *Appl Environ Microbiol*, 66, 4945-53.

BECKER, W., BECKER, B. E., NEWMAN, M. G. & NYMAN, S. 1990. Clinical and microbiologic findings that may contribute to dental implant failure. *Int J Oral Maxillofac Implants*, 5, 31-8.

BECKER, W., BECKER, B. E., NEWMAN, M. G. & NYMAN, S. 1991. [Clinical and microbiological findings, that can cause failure of dental implants]. *Quintessenz*, 42, 9-21.

BECKER, W. & SENNERBY, L. 2012. 300 years of experience. *Clin Implant Dent Relat Res*, 14, 1-2.

BEHNEKE, A., BEHNEKE, N., D'HOEDT, B. & WAGNER, W. 1997. Hard and soft tissue reactions to ITI screw implants: 3-year longitudinal results of a prospective study. *Int J Oral Maxillofac Implants*, 12, 749-57.

BERGLUNDH, T., PERSSON, L. & KLINGE, B. 2002. A systematic review of the incidence of biological and technical complications in implant dentistry reported in prospective longitudinal studies of at least 5 years. *J Clin Periodontol*, 29 Suppl 3, 197-212; discussion 232-3.

BERGLUNDH, T., ZITZMANN, N. U. & DONATI, M. 2011. Are peri-implantitis lesions different from periodontitis lesions? *J Clin Periodontol*, 38 Suppl 11, 188-202.

BILLIAU, A., CASSIMAN, J. J., WILLEMS, D., VERHELST, M. & HEREMANS, H. 1975. In vitro cultivation of human tumor tissues. *Oncology*, 31, 257-72.

BLUMENTHAL, N. M. 1993. A clinical comparison of collagen membranes with e-PTFE membranes in the treatment of human mandibular buccal class II furcation defects. *J Periodontol*, 64, 925-33.

BOGNER, A., JOUNEAU, P. H., THOLLET, G., BASSET, D. & GAUTHIER, C. 2007. A history of scanning electron microscopy developments: towards "wet-STEM" imaging. *Micron*, 38, 390-401.

BOSSHARDT, D. D. & SCULEAN, A. 2009. Does periodontal tissue regeneration really work? *Periodontol 2000*, 51, 208-19.

BOTERO, J. E., GONZÁLEZ, A. M., MERCADO, R. A., OLAVE, G. & CONTRERAS, A. 2005. Subgingival microbiota in peri-implant mucosa lesions and adjacent teeth in partially edentulous patients. *J Periodontol*, 76, 1490-1495.

BOUTAGA, K., SAVELKOUL, P. H., WINKEL, E. G. & VAN WINKELHOFF, A. J. 2007. Comparison of subgingival bacterial sampling with oral lavage for detection and quantification of periodontal pathogens by real-time polymerase chain reaction. *J Periodontol*, 78, 79-86.

BOUTAGA, K., VAN WINKELHOFF, A. J., VANDENBROUCKE-GRAULS, C. M. & SAVELKOUL, P. H. 2003. Comparison of real-time PCR and culture for detection of *Porphyromonas gingivalis* in subgingival plaque samples. *J Clin Microbiol*, 41, 4950-4.

BOWER, R. C. 1996. Peri-implantitis. *Ann R Australas Coll Dent Surg*, 13, 48-57.

BRADSHAW, D. J., HOMER, K. A., MARSH, P. D. & BEIGHTON, D. 1994. Metabolic cooperation in oral microbial communities during growth on mucin. *Microbiol*, 140 (Pt 12), 3407-12.

BRADSHAW, D. J. & MARSH, P. D. 1999. [22] Use of continuous flow techniques in modeling dental plaque biofilms. In: RON, J. D. (ed.) *Methods Enzymol*. Academic Press.

BRADSHAW, D. J., MARSH, P. D., ALLISON, C. & SCHILLING, K. M. 1996. Effect of oxygen, inoculum composition and flow rate on development of mixed-culture oral biofilms. *Microbiol*, 142 (Pt 3), 623-9.

BRADSHAW, D. J., MARSH, P. D., WATSON, G. K. & ALLISON, C. 1997. Oral anaerobes cannot survive oxygen stress without interacting with facultative/aerobic species as a microbial community. *Lett in Appl Microbiol*, 25, 385-387.

BRADSHAW, D. J., MCKEE, A. S. & MARSH, P. D. 1989. The use of defined inocula stored in liquid nitrogen for mixed culture chemostat studies. *J Microbiol Methods*, 9, 123-128.

BRAUN, A., KRAUSE, F., FRENTZEN, M. & JEPSEN, S. 2005a. Efficiency of subgingival calculus removal with the Vector-system compared to ultrasonic scaling and hand instrumentation in vitro. *J Periodontal Res*, 40, 48-52.

BRAUN, A., KRAUSE, F., FRENTZEN, M. & JEPSEN, S. 2005b. Removal of root substance with the Vector-system compared with conventional debridement in vitro. *J Clin Periodontol*, 32, 153-7.

BRAYNER, R., FERRARI-ILIOU, R., BRIVOIS, N., DJEDIAT, S., BENEDETTI, M. F. & FIÉVET, F. 2006. Toxicological impact studies based on *Escherichia coli* bacteria in ultrafine ZnO nanoparticles colloidal medium. *Nano Lett*, 6, 866-70.

BROWN, F. H., OGLETREE, R. C. & HOUSTON, G. D. 1992. Pneumoparotitis associated with the use of an air-powder prophylaxis unit. *J Periodontol*, 63, 642-4.

BRÅNEMARK, P. I., ADELL, R., ALBREKTSSON, T., LEKHOLM, U., LUNDKVIST, S. & ROCKLER, B. 1983. Osseointegrated titanium fixtures in the treatment of edentulousness. *Biomaterials*, 4, 25-8.

BRÅNEMARK, P. I., HANSSON, B. O., ADELL, R., BREINE, U., LINDSTRÖM, J., HALLÉN, O. & OHMAN, A. 1977. Osseointegrated implants in the treatment of the edentulous jaw. Experience from a 10-year period. *Scand J Plast Reconstr Surg Suppl*, 16, 1-132.

BUCHMANN, R., KHOURY, F., PINGEL, D. & LANGE, D. E. 2003. The microflora recovered from the outer-surfaces of the Frialit-2 implanto-prosthetic connector. *Clin Oral Implants Res*, 14, 28-34.

BUSER, D., JANNER, S. F. M., WITTNEBEN, J. G., BRÄGGER, U., RAMSEIER, C. A. & SALVI, G. E. 2012. 10-Year Survival and Success Rates of 511 Titanium Implants with a Sandblasted and Acid-Etched Surface: A Retrospective Study in 303 Partially Edentulous Patients. *Clin Implant Dent and Rel Res*.

BUSER, D., WEBER, H. P., BRAGGER, U. & BALSIGER, C. 1991. Tissue integration of one-stage ITI implants: 3-year results of a longitudinal study with Hollow-Cylinder and Hollow-Screw implants. *Int J Oral Maxillofac Implants*, 6, 405-12.

BUSER, D., WEBER, H. P. & LANG, N. P. 1990. Tissue integration of non-submerged implants. 1-year results of a prospective study with 100 ITI hollow-cylinder and hollow-screw implants. *Clin Oral Implants Res*, 1, 33-40.

BUSSCHER, H. J., RINASTITI, M., SISWOMIHARDJO, W. & VAN DER MEI, H. C. 2010. Biofilm formation on dental restorative and implant materials. *J Dent Res*, 89, 657-65.

BUSSCHER, H. J. & VAN DER MEI, H. C. 1995. Use of flow chamber devices and image analysis methods to study microbial adhesion. *Methods Enzymol*, 253, 455-77.

BYRNE, G. 2012. Effectiveness of different treatment regimens for peri-implantitis. *J Am Dent Assoc*, 143, 391-2.

BÜRGERS, R., GERLACH, T., HAHNEL, S., SCHWARZ, F., HANDEL, G. & GOSAU, M. 2010. In vivo and in vitro biofilm formation on two different titanium implant surfaces. *Clin Oral Implants Res*, 21, 156-64.

BÜRGERS, R., WITECY, C., HAHNEL, S. & GOSAU, M. 2012. The effect of various topical peri-implantitis antiseptics on *Staphylococcus epidermidis*, *Candida albicans*, and *Streptococcus sanguinis*. *Arch Oral Biol*, 57, 940-947.

CASADO, P. L., CANULLO, L., DE ALMEIDA FILARDY, A., GRANJEIRO, J. M., BARBOZA, E. P. & LEITE DUARTE, M. E. 2013a. Interleukins 1 β and 10 Expressions in the Periimplant Crevicular Fluid From Patients With Untreated Periimplant Disease. *Implant Dent*.

CASADO, P. L., VILLAS-BOAS, R., DE MELLO, W., DUARTE, M. E. & GRANJEIRO, J. M. 2013b. Peri-implant Disease and Chronic Periodontitis: Is Interleukin-6 Gene Promoter Polymorphism the Common Risk Factor in a Brazilian Population? *Int J Oral Maxillofac Implants*, 28, 35-43.

CHAN, Y. & LAI, C. H. 2003. Bactericidal effects of different laser wavelengths on periodontopathic germs in photodynamic therapy. *Lasers Med Sci*, 18, 51-5.

CHARALAMPakis, G., RABE, P., LEONHARDT, A. & DAHLÉN, G. 2011. A follow-up study of peri-implantitis cases after treatment. *J Clin Periodontol*, 38, 864-71.

CHONDROS, P., NIKOLIDAKIS, D., CHRISTODOULIDES, N., RÖSSLER, R., GUTKNECHT, N. & SCULEAN, A. 2009. Photodynamic therapy as adjunct to

non-surgical periodontal treatment in patients on periodontal maintenance: a randomized controlled clinical trial. *Lasers Med Sci*, 24, 681-8.

CHÁVEZ DE PAZ, L. E. 2009. Image analysis software based on color segmentation for characterization of viability and physiological activity of biofilms. *Appl Environ Microbiol*, 75, 1734-9.

CIANCIO, S. G., LAUCIELLO, F., SHIBLY, O., VITELLO, M. & MATHER, M. 1995. The effect of an antiseptic mouthrinse on implant maintenance: plaque and peri-implant gingival tissues. *J Periodontol*, 66, 962-5.

CIANTAR, M., SPRATT, D. A., NEWMAN, H. N. & WILSON, M. 2001a. Assessment of five culture media for the growth and isolation of *Capnocytophaga* spp. *Clin Microbiol Infect*, 7, 158-60.

CIANTAR, M., SPRATT, D. A., NEWMAN, H. N. & WILSON, M. 2001b. *Capnocytophaga granulosa* and *Capnocytophaga haemolytica*: novel species in subgingival plaque. *J Clin Periodontol*, 28, 701-5.

CIMASONI, G. 1983. Crevicular fluid updated. *Monogr Oral Sci*, 12, III-VII, 1-152.

CIRIC, L., PRATTEN, J., WILSON, M. & SPRATT, D. 2010. Development of a novel multi-triplex qPCR method for the assessment of bacterial community structure in oral populations. *Environ Microbiol Reports*, 2, 770-774.

CIRIC, L., TYMON, A., ZAURA, E., LINGSTRÖM, P., STAUDER, M., PAPETTI, A., SIGNORETTO, C., PRATTEN, J., WILSON, M. & SPRATT, D. 2011. In vitro assessment of shiitake mushroom (*Lentinula edodes*) extract for its antigingivitis activity. *J Biomed Biotechnol*, 2011, 507908.

CLAFFEY, N., CLARKE, E., POLYZOIS, I. & RENVERT, S. 2008. Surgical treatment of peri-implantitis. *J Clin Periodontol*, 35, 316-32.

COCHIS, A., FINI, M., CARRASSI, A., MIGLIARIO, M., VISAI, L. & RIMONDINI, L. 2012. Effect of air polishing with glycine powder on titanium abutment surfaces. *Clin Oral Implants Res*.

COLON, G., WARD, B. C. & WEBSTER, T. J. 2006. Increased osteoblast and decreased *Staphylococcus epidermidis* functions on nanophase ZnO and TiO₂. *J Biomed Mater Res A*, 78, 595-604.

CONSORTIUM, H. M. P. 2012. Structure, function and diversity of the healthy human microbiome. *Nature*, 486, 207-14.

COOPER, L. F., MASUDA, T., WHITSON, S. W., YLIHEIKKILÄ, P. & FELTON, D. A. 1999. Formation of mineralizing osteoblast cultures on machined, titanium oxide grit-blasted, and plasma-sprayed titanium surfaces. *Int J Oral Maxillofac Implants*, 14, 37-47.

CORTELLI, S. C., CORTELLI, J. R., HOLZHAUSEN, M., FRANCO, G. C., REBELO, R. Z., SONAGERE, A. S., QUEIROZ, C. A. S. & COSTA, F. O. 2009. Essential oils in one-stage full-mouth disinfection: double-blind, randomized clinical trial of long-term clinical, microbial and salivary effects. *J Clin Periodontol*, 36, 333-42.

CORTELLI, S. C., CORTELLI, J. R., ROMEIRO, R. L., COSTA, F. O., AQUINO, D. R., ORZECHOWSKI, P. R., ARAÚJO, V. C. & DUARTE, P. M. 2013. Frequency of periodontal pathogens in equivalent peri-implant and periodontal clinical statuses. *Arch Oral Biol*, 58, 67-74.

COSTERTON, J. W., MONTANARO, L. & ARCIOLA, C. R. 2005. Biofilm in implant infections: its production and regulation. *Int J Artif Organs*, 28, 1062-8.

CRAWFORD, B. J. & BURKE, R. D. 2004. TEM and SEM methods. *Methods Cell Biol*, 74, 411-41.

CURTIS, M. A., GRIFFITHS, G. S., PRICE, S. J., COULTHURST, S. K. & JOHNSON, N. W. 1988. The total protein concentration of gingival crevicular fluid. Variation with sampling time and gingival inflammation. *J Clin Periodontol*, 15, 628-32.

D'ERCOLE, S., CATAMO, G., TRIPODI, D. & PICCOLOMINI, R. 2008. Comparison of culture methods and multiplex PCR for the detection of periodontopathogenic

bacteria in biofilm associated with severe forms of periodontitis. *New Microbiol*, 31, 383-91.

DALWAI, F., SPRATT, D. A. & PRATTEN, J. 2006. Modeling shifts in microbial populations associated with health or disease. *Appl Environ Microbiol*, 72, 3678-84.

DALWAI, F., SPRATT, D. A. & PRATTEN, J. 2007. Use of quantitative PCR and culture methods to characterize ecological flux in bacterial biofilms. *J Clin Microbiol*, 45, 3072-6.

DANSER, M. M., TIMMERMAN, M. F., VAN WINKELHOFF, A. J. & VAN DER VELDEN, U. 1996. The effect of periodontal treatment on periodontal bacteria on the oral mucous membranes. *J Periodontol*, 67, 478-85.

DANSER, M. M., VAN WINKELHOFF, A. J., DE GRAAFF, J., LOOS, B. G. & VAN DER VELDEN, U. 1994. Short-term effect of full-mouth extraction on periodontal pathogens colonizing the oral mucous membranes. *J Clin Periodontol*, 21, 484-9.

DANSER, M. M., VAN WINKELHOFF, A. J. & VAN DER VELDEN, U. 1997. Periodontal bacteria colonizing oral mucous membranes in edentulous patients wearing dental implants. *J Periodontol*, 68, 209-16.

DARVEAU, R. P., TANNER, A. & PAGE, R. C. 1997. The microbial challenge in periodontitis. *Periodontol 2000*, 14, 12-32.

DE BOEVER, A. L. & DE BOEVER, J. A. 2006. Early colonization of non-submerged dental implants in patients with a history of advanced aggressive periodontitis. *Clin Oral Implants Res*, 17, 8-17.

DECKER, E. M. 2001. The ability of direct fluorescence-based, two-colour assays to detect different physiological states of oral streptococci. *Lett Appl Microbiol*, 33, 188-92.

DENG, D. M. & TEN CATE, J. M. 2004. Demineralization of dentin by *Streptococcus mutans* biofilms grown in the constant depth film fermentor. *Caries Res*, 38, 54-61.

DEVIDES, S. L. & FRANCO, A. T. 2006. Evaluation of peri-implant microbiota using the polymerase chain reaction in completely edentulous patients before and after placement of implant-supported prostheses submitted to immediate load. *Int J Oral Maxillofac Implants*, 21, 262-9.

DEWHIRST, F. E., CHEN, T., IZARD, J., PASTER, B. J., TANNER, A. C., YU, W. H., LAKSHMANAN, A. & WADE, W. G. 2010. The human oral microbiome. *J Bacteriol*, 192, 5002-17.

DIGE, I., NILSSON, H., KILIAN, M. & NYVAD, B. 2007. In situ identification of streptococci and other bacteria in initial dental biofilm by confocal laser scanning microscopy and fluorescence in situ hybridization. *Eur J Oral Sci*, 115, 459-67.

DODDS, M. W., JOHNSON, D. A. & YEH, C. K. 2005. Health benefits of saliva: a review. *J Dent*, 33, 223-33.

DONOS, N., LAURELL, L. & MARDAS, N. 2012. Hierarchical decisions on teeth vs. implants in the periodontitis-susceptible. *Periodontol 2000*, 59, 89-110.

DYMOCK, D., WEIGHTMAN, A. J., SCULLY, C. & WADE, W. G. 1996. Molecular analysis of microflora associated with dentoalveolar abscesses. *J Clin Microbiol*, 34, 537-42.

DÖRTBUDAK, O., HAAS, R., BERNHART, T. & MAILATH-POKORNY, G. 2001. Lethal photosensitization for decontamination of implant surfaces in the treatment of peri-implantitis. *Clin Oral Implants Res*, 12, 104-8.

DÖRTBUDAK, O., HAAS, R. & MALLATH-POKORNY, G. 2000. Biostimulation of bone marrow cells with a diode soft laser. *Clin Oral Implants Res*, 11, 540-5.

EDWARDS, R. A., RODRIGUEZ-BRITO, B., WEGLEY, L., HAYNES, M., BREITBART, M., PETERSON, D. M., SAAR, M. O., ALEXANDER, S., ALEXANDER, E. C. & ROHWER, F. 2006. Using pyrosequencing to shed light on deep mine microbial ecology. *BMC Genomics*, 7, 57.

EMRANI, J., CHEE, W. & SLOTS, J. 2009. Bacterial colonization of oral implants from nondental sources. *Clin Implant Dent Relat Res*, 11, 106-12.

ERICSSON, I., BERGLUNDH, T., MARINELLO, C., LILJENBERG, B. & LINDHE, J. 1992. Long-standing plaque and gingivitis at implants and teeth in the dog. *Clin Oral Implants Res*, 3, 99-103.

ERICSSON, I., PERSSON, L. G., BERGLUNDH, T., EDLUND, T. & LINDHE, J. 1996. The effect of antimicrobial therapy on periimplantitis lesions. An experimental study in the dog. *Clin Oral Implants Res*, 7, 320-8.

ESPOSITO, M., GRUSOVIN, M. G. & WORTHINGTON, H. V. 2012. Interventions for replacing missing teeth: treatment of peri-implantitis. *Cochrane Database Syst Rev*, 1, CD004970.

ESPOSITO, M., HIRSCH, J., LEKHOLM, U. & THOMSEN, P. 1999. Differential Diagnosis and Treatment Strategies for Biologic Complications and Failing Oral Implants: A Review of the Literature. *Int J of Oral and Maxillofac Implants*, 14, 473-490.

ESPOSITO, M., HIRSCH, J. M., LEKHOLM, U. & THOMSEN, P. 1998. Biological factors contributing to failures of osseointegrated oral implants. (I). Success criteria and epidemiology. *Eur J Oral Sci*, 106, 527-51.

ESPOSITO, M., MURRAY-CURTIS, L., GRUSOVIN, M. G., COULTHARD, P. & WORTHINGTON, H. V. 2007. Interventions for replacing missing teeth: different types of dental implants. *Cochrane Database Syst Rev*, CD003815.

ESPOSITO, M., THOMSEN, P., ERICSON, L. E., SENNERBY, L. & LEKHOLM, U. 2000. Histopathologic observations on late oral implant failures. *Clin Implant Dent Relat Res*, 2, 18-32.

FARDAL, O., JOHANNESSEN, A. C. & OLSEN, I. 1999. Severe, rapidly progressing peri-implantitis. *J Clin Periodontol*, 26, 313-7.

FELO, A., SHIBLY, O., CIANCIO, S. G., LAUCIELLO, F. R. & HO, A. 1997. Effects of subgingival chlorhexidine irrigation on peri-implant maintenance. *Am J Dent*, 10, 107-10.

FERREIRA, S. D., SILVA, G. L., CORTELLI, J. R., COSTA, J. E. & COSTA, F. O. 2006. Prevalence and risk variables for peri-implant disease in Brazilian subjects. *J Clin Periodontol*, 33, 929-35.

FEY, A., EICHLER, S., FLAVIER, S., CHRISTEN, R., HÖFLE, M. G. & GUZMÁN, C. A. 2004. Establishment of a real-time PCR-based approach for accurate quantification of bacterial RNA targets in water, using *Salmonella* as a model organism. *Appl Environ Microbiol*, 70, 3618-23.

FICARA, A. J., LEVIN, M. P., GROWER, M. F. & KRAMER, G. D. 1975. A comparison of the glucose and protein content of gingival fluid from diabetics and nondiabetics. *J Periodontal Res*, 10, 171-5.

FLEMMING, R. G., CAPELLI, C. C., COOPER, S. L. & PROCTOR, R. A. 2000. Bacterial colonization of functionalized polyurethanes. *Biomaterials*, 21, 273-81.

FLYNN, T. R., PASTER, B. J., STOKES, L. N., SUSARLA, S. M. & SHANTI, R. M. 2012. Molecular methods for diagnosis of odontogenic infections. *J Oral Maxillofac Surg*, 70, 1854-9.

FOLWACZNY, M., AGGSTALLER, H., MEHL, A. & HICKEL, R. 2003. Removal of bacterial endotoxin from root surface with Er:YAG laser. *Am J Dent*, 16, 3-5.

FOX, S. C., MORIARTY, J. D. & KUSY, R. P. 1990. The effects of scaling a titanium implant surface with metal and plastic instruments: an *in vitro* study. *J Periodontol*, 61, 485-90.

FREITAS, L. B., RUNDEGREN, J. & ARNEBRANT, T. 1993. The binding of delmopinol and chlorhexidine to *Streptococcus mutans* and *Actinobacillus actinomycetemcomitans* strains with varying degrees of surface hydrophobicity. *Oral Microbiol Immunol*, 8, 355-60.

FRIBERG, B., JEMT, T. & LEKHOLM, U. 1991. Early failures in 4,641 consecutively placed Bränemark dental implants: a study from stage 1 surgery to the connection of completed prostheses. *Int J Oral Maxillofac Implants*, 6, 142-6.

FRIEDMANN, A., ANTIC, L., BERNIMOULIN, J. P. & PURUCKER, P. 2006. In vitro attachment of osteoblasts on contaminated rough titanium surfaces treated by Er:YAG laser. *Journal of Biomedical Materials Research - Part A*, 79, 53-60.

FROUM, S. J. & ROSEN, P. S. 2012. A proposed classification for peri-implantitis. *Int J Periodontics Restorative Dent*, 32, 533-40.

FRÖJD, V., CHÁVEZ DE PAZ, L., ANDERSSON, M., WENNERBERG, A., DAVIES, J. R. & SVENSÄTER, G. 2011. In situ analysis of multispecies biofilm formation on customized titanium surfaces. *Mol Oral Microbiol*, 26, 241-52.

FÜRST, M. M., SALVI, G. E., LANG, N. P. & PERSSON, G. R. 2007. Bacterial colonization immediately after installation on oral titanium implants. *Clin Oral Implants Res*, 18, 501-8.

GATTANI, D. & ANSARI, S. T. 2010. Peri-implant Diseases: Pathogenesis and Treatment. *Int J Clin Implant Dent*, 2(1), 23- 30.

GERA, I. 2008. [The bacterial biofilm and the possibilities of chemical plaque control. Literature review]. *Fogorv Sz*, 101, 91-9.

GIANNELLI, M., CHELLINI, F., MARGHERI, M., TONELLI, P. & TANI, A. 2008. Effect of chlorhexidine digluconate on different cell types: a molecular and ultrastructural investigation. *Toxicol In Vitro*, 22, 308-17.

GIGLIO, S., MONIS, P. T. & SAINT, C. P. 2003. Demonstration of preferential binding of SYBR Green I to specific DNA fragments in real-time multiplex PCR. *Nucleic Acids Res*, 31, e136.

GILBERT, P. & BROWN, M. R. 1980. Cell wall-mediated changes in sensitivity of *Bacillus megaterium* to chlorhexidine and 2-phenoxyethanol, associated with growth rate and nutrient limitation. *J Appl Bacteriol*, 48, 223-30.

GOODSON, J. M. 2003. Gingival crevice fluid flow. *Periodontol 2000*, 31, 43-54.

GOULD, T. R., BRUNETTE, D. M. & WESTBURY, L. 1981. The attachment mechanism of epithelial cells to titanium in vitro. *J Periodontal Res*, 16, 611-6.

GRIFFITHS, R. I., WHITELEY, A. S., O'DONNELL, A. G. & BAILEY, M. J. 2000. Rapid method for coextraction of DNA and RNA from natural environments for analysis of ribosomal DNA- and rRNA-based microbial community composition. *Appl Environ Microbiol*, 66, 5488-91.

GRÖSSNER-SCHREIBER, B., GRIEPENTROG, M., HAUSTEIN, I., MÜLLER, W. D., LANGE, K. P., BRIEDIGKEIT, H. & GÖBEL, U. B. 2001. Plaque formation on surface modified dental implants. An in vitro study. *Clin Oral Implants Res*, 12, 543-51.

GRÖSSNER-SCHREIBER, B. & TUAN, R. S. 1991. [The influence of the titanium implant surface on the process of osseointegration]. *Dtsch Zahnärztl Z*, 46, 691-3.

GUGGENHEIM, B., GIERTSEN, E., SCHÜPBACH, P. & SHAPIRO, S. 2001. Validation of an in vitro biofilm model of supragingival plaque. *J Dent Res*, 80, 363-70.

GUGGENHEIM, M., THURNHEER, T., GMÜR, R., GIOVANOLI, P. & GUGGENHEIM, B. 2011. Validation of the Zürich burn-biofilm model. *Burns*, 37, 1125-33.

GÜNCÜ, G. N., AKMAN, A. C., GÜNDAY, S., YAMALIK, N. & BERKER, E. 2012. Effect of inflammation on cytokine levels and bone remodelling markers in peri-implant sulcus fluid: a preliminary report. *Cytokine*, 59, 313-6.

HAAS, R., BARON, M., DÖRTBUDAK, O. & WATZEK, G. 2000. Lethal photosensitization, autogenous bone, and e-PTFE membrane for the treatment of peri-implantitis: preliminary results. *Int J Oral Maxillofac Implants*, 15, 374-82.

HAAS, R., DÖRTBUDAK, O., MENSDORFF-POUILLY, N. & MAILATH, G. 1997. Elimination of bacteria on different implant surfaces through photosensitization and soft laser. An in vitro study. *Clin Oral Implants Res*, 8, 249-54.

HAFFAJEE, A. D. & SOCRANSKY, S. S. 2005. Microbiology of periodontal diseases: introduction. *Periodontol 2000*, 38, 9-12.

HALLSTRÖM, H., PERSSON, G. R., LINDGREN, S., OLOFSSON, M. & RENVERT, S. 2012. Systemic antibiotics and debridement of peri-implant mucositis. A randomized clinical trial. *J Clin Periodontol*, 39, 574-81.

HANNIG, C., HANNIG, M., REHMER, O., BRAUN, G., HELLWIG, E. & AL-AHMAD, A. 2007. Fluorescence microscopic visualization and quantification of initial bacterial colonization on enamel in situ. *Arch Oral Biol*, 52, 1048-56.

HARDT, C. R., GRÖNDAL, K., LEKHOLM, U. & WENNSTRÖM, J. L. 2002. Outcome of implant therapy in relation to experienced loss of periodontal bone support: a retrospective 5- year study. *Clin Oral Implants Res*, 13, 488-94.

HAYEK, R. R. A., ARAÚJO, N. S., GIOSO, M. A., FERREIRA, J., BAPTISTA-SOBRINHO, C. A., YAMADA JR, A. M. & RIBEIRO, M. S. 2005. Comparative study between the effects of photodynamic therapy and conventional therapy on microbial reduction in ligature-induced peri-implantitis in dogs. *J Periodontol*, 76, 1275-1281.

HEITZ, F., HEITZ-MAYFIELD, L. J. & LANG, N. P. 2004. Effects of post-surgical cleansing protocols on early plaque control in periodontal and/or periimplant wound healing. *J Clin Periodontol*, 31, 1012-8.

HEITZ-MAYFIELD, L. J. 2008a. Diagnosis and management of peri-implant diseases. *Aust Dent J*, 53 Suppl 1, S43-8.

HEITZ-MAYFIELD, L. J. 2008b. Peri-implant diseases: diagnosis and risk indicators. *J Clin Periodontol*, 35, 292-304.

HEITZ-MAYFIELD, L. J. A. & LANG, N. P. 2010. Comparative biology of chronic and aggressive periodontitis vs. peri-implantitis. *Periodontol 2000*, 53, 167-181.

HENDERSON, E., SCHNEIDER, S., PETERSEN, F. C., HAUGEN, H. J., WOHLFAHRT, J. C., EKSTRAND, K. & EKFELDT, A. 2012. Chemical debridement of contaminated titanium surfaces: An *in vitro* study. *Acta Odontol Scand*.

HERRERO-CLIMENT, M., LÁZARO, P., VICENTE RIOS, J., LLUCH, S., MARQUÉS, M., GUILLEM-MARTÍ, J. & GIL, F. J. 2013. Influence of acid-etching

after grit-blasted on osseointegration of titanium dental implants: in vitro and in vivo studies. *J Mater Sci Mater Med.*

HEUER, W., ELTER, C., DEMLING, A., NEUMANN, A., SUERBAUM, S., HANNIG, M., HEIDENBLUT, T., BACH, F. W. & STIESCH-SCHOLZ, M. 2007. Analysis of early biofilm formation on oral implants in man. *J Oral Rehabilit*, 34, 377-382.

HEUER, W., KETTENRING, A., STUMPP, S. N., EBERHARD, J., GELLERMANN, E., WINKEL, A. & STIESCH, M. 2012. Metagenomic analysis of the peri-implant and periodontal microflora in patients with clinical signs of gingivitis or mucositis. *Clin Oral Investig*, 16, 843-50.

HOLLAND, P. M., ABRAMSON, R. D., WATSON, R. & GELFAND, D. H. 1991. Detection of specific polymerase chain reaction product by utilizing the 5'----3' exonuclease activity of *Thermus aquaticus* DNA polymerase. *Proc Natl Acad Sci U S A*, 88, 7276-80.

HOPE, C. K., CLEMENTS, D. & WILSON, M. 2002. Determining the spatial distribution of viable and nonviable bacteria in hydrated microcosm dental plaques by viability profiling. *J Appl Microbiol*, 93, 448-55.

HOPE, C. K. & WILSON, M. 2002. Comparison of the interproximal plaque removal efficacy of two powered toothbrushes using in vitro oral biofilms. *Am J Dent*, 15 Spec No, 7B-11B.

HOPE, C. K. & WILSON, M. 2003. Measuring the thickness of an outer layer of viable bacteria in an oral biofilm by viability mapping. *J Microbiol Methods*, 54, 403-410.

HOPE, C. K. & WILSON, M. 2006. Biofilm structure and cell vitality in a laboratory model of subgingival plaque. *J Microbiol Methods*, 66, 390-398.

HULTIN, M., GUSTAFSSON, A., HALLSTRÖM, H., JOHANSSON, L. A., EKFELDT, A. & KLINGE, B. 2002. Microbiological findings and host response in patients with peri-implantitis. *Clin Oral Implants Res*, 13, 349-58.

HÄMMERLE, C. H. & JUNG, R. E. 2003. Bone augmentation by means of barrier membranes. *Periodontol 2000*, 33, 36-53.

IZU, K. H., THOMAS, S. J., ZHANG, P., IZU, A. E. & MICHALEK, S. 2004. Effectiveness of sodium hypochlorite in preventing inoculation of periapical tissues with contaminated patency files. *J Endod*, 30, 92-4.

JERVØE-STORM, P. M., KOLTZSCHER, M., FALK, W., DÖRFLER, A. & JEPSEN, S. 2005. Comparison of culture and real-time PCR for detection and quantification of five putative periodontopathogenic bacteria in subgingival plaque samples. *J Clin Periodontol*, 32, 778-83.

JONES, N., RAY, B., RANJIT, K. T. & MANNA, A. C. 2008. Antibacterial activity of ZnO nanoparticle suspensions on a broad spectrum of microorganisms. *FEMS Microbiol Lett*, 279, 71-6.

JOSE, B., ANTOCI, V., ZEIGER, A. R., WICKSTROM, E. & HICKOK, N. J. 2005. Vancomycin covalently bonded to titanium beads kills *Staphylococcus aureus*. *Chem Biol*, 12, 1041-8.

JUNG, R. E., PJETURSSON, B. E., GLAUSER, R., ZEMBIC, A., ZWAHLEN, M. & LANG, N. P. 2008. A systematic review of the 5-year survival and complication rates of implant-supported single crowns. *Clin Oral Implants Res*, 19, 119-30.

KALYKAKIS, G. K., MOJON, P., NISENGARD, R., SPIEKERMANN, H. & ZAFIROPOULOS, G. G. 1996. Clinical and microbial findings on osseointegrated implants; comparisons between partially dentate and edentulous subjects. *European Transactions on Electrical Power*, 6, 155-159.

KANDELER, E., DEIGLMAYR, K., TSCHERKO, D., BRU, D. & PHILIPPOT, L. 2006. Abundance of narG, nirS, nirK, and nosZ genes of denitrifying bacteria during primary successions of a glacier foreland. *Appl Environ Microbiol*, 72, 5957-62.

KARLSSON, H. L., CRONHOLM, P., GUSTAFSSON, J. & MÖLLER, L. 2008. Copper oxide nanoparticles are highly toxic: a comparison between metal oxide nanoparticles and carbon nanotubes. *Chem Res Toxicol*, 21, 1726-32.

KAUFMAN, E. & LAMSTER, I. B. 2000. Analysis of saliva for periodontal diagnosis-a review. *J Clin Periodontol*, 27, 453-65.

KAZOR, C. E., MITCHELL, P. M., LEE, A. M., STOKES, L. N., LOESCHE, W. J., DEWHIRST, F. E. & PASTER, B. J. 2003. Diversity of bacterial populations on the tongue dura of patients with halitosis and healthy patients. *J Clin Microbiol*, 41, 558-63.

KEIJSER, B. J. F., ZAURA, E., HUSE, S. M., VAN DER VOSSEN, J. M. B. M., SCHUREN, F. H. J., MONTIJN, R. C., TEN GATE, J. M. & CRIELAARD, W. 2008. Pyrosequencing analysis of the oral microflora of healthy adults. *J Dent Res*, 87, 1016-1020.

KELLER, W., BRÄGGER, U. & MOMBELLI, A. 1998. Peri-implant microflora of implants with cemented and screw retained suprastructures. *Clin Oral Implants Res*, 9, 209-17.

KIM, Y. T., CHA, J. K., PARK, J. C., JUNG, U. W., KIM, C. S., CHO, K. S. & CHOI, S. H. 2012. In situ dental implant installation after decontamination in a previously peri-implant diseased site: a pilot study. *J Periodontal Implant Sci*, 42, 13-9.

KINNIMENT, S. L., WIMPENNY, J. W., ADAMS, D. & MARSH, P. D. 1996a. Development of a steady-state oral microbial biofilm community using the constant-depth film fermenter. *Microbiol*, 142 (Pt 3), 631-8.

KINNIMENT, S. L., WIMPENNY, J. W., ADAMS, D. & MARSH, P. D. 1996b. The effect of chlorhexidine on defined, mixed culture oral biofilms grown in a novel model system. *J Appl Bacteriol*, 81, 120-5.

KLAPPENBACH, J. A., DUNBAR, J. M. & SCHMIDT, T. M. 2000. rRNA operon copy number reflects ecological strategies of bacteria. *Appl Environ Microbiol*, 66, 1328-33.

KLAPPENBACH, J. A., SAXMAN, P. R., COLE, J. R. & SCHMIDT, T. M. 2001. rrndb: the Ribosomal RNA Operon Copy Number Database. *Nucleic Acids Res*, 29, 181-4.

KLINGE, B., GUSTAFSSON, A. & BERGLUNDH, T. 2002. A systematic review of the effect of anti-infective therapy in the treatment of peri-implantitis. *J Clin Periodontol*, 29 Suppl 3, 213-25; discussion 232-3.

KLINGE, B., HULTIN, M. & BERGLUNDH, T. 2005. Peri-implantitis. *Dent Clin North Am*, 49, 661-76, vii-viii.

KOBAYASHI, A., KURODA, T., KIMURA, H. & INOUE, A. 2012. Effect of Zr on microstructure of metallic glass coatings prepared by gas tunnel type plasma spraying. *J Nanosci Nanotechnol*, 12, 4883-6.

KOCAR, M., SEME, K. & HREN, N. I. 2010. Characterization of the normal bacterial flora in peri-implant sulci of partially and completely edentulous patients. *Int J Oral Maxillofac Implants*, 25, 690-8.

KOLDSLAND, O. C., SCHEIE, A. A. & AASS, A. M. 2010. Prevalence of peri-implantitis related to severity of the disease with different degrees of bone loss. *J Periodontol*, 81, 231-8.

KOLENBRANDER, P. E., PALMER, R. J., RICKARD, A. H., JAKUBOVICS, N. S., CHALMERS, N. I. & DIAZ, P. I. 2006. Bacterial interactions and successions during plaque development. *Periodontol 2000*, 42, 47-79.

KONOPKA, K. & GOSLINSKI, T. 2007. Photodynamic therapy in dentistry. *J Dent Res*, 86, 694-707.

KOURTIS, S. G., SOTIRIADOU, S., VOLIOTIS, S. & CHALLAS, A. 2004. Private practice results of dental implants. Part I: Survival and evaluation of risk factors - Part II: Surgical and prosthetic complications. *Implant Dent*, 13, 373-385.

KOYANAGI, T., SAKAMOTO, M., TAKEUCHI, Y., MARUYAMA, N., OHKUMA, M. & IZUMI, Y. 2013. Comprehensive microbiological findings in peri-implantitis and periodontitis. *J Clin Periodontol*, 40, 218-26.

KOYANAGI, T., SAKAMOTO, M., TAKEUCHI, Y., OHKUMA, M. & IZUMI, Y. 2010. Analysis of microbiota associated with peri-implantitis using 16S rRNA gene clone. *J Oral Microbiol*, 2.

KREISLER, M., AL HAJ, H. & D'HOEDT, B. 2002a. Temperature changes at the implant-bone interface during simulated surface decontamination with an Er:YAG laser. *Int J Prosthodont*, 15, 582-7.

KREISLER, M., AL HAJ, H., GÖTZ, H., DUSCHNER, H. & D'HOEDT, B. 2002b. Effect of simulated CO₂ and GaAlAs laser surface decontamination on temperature changes in Ti-plasma sprayed dental implants. *Lasers Surg Med*, 30, 233-9.

KREISLER, M., GÖTZ, H. & DUSCHNER, H. 2002c. Effect of Nd:YAG, Ho:YAG, Er:YAG, CO₂, and GaAlAs laser irradiation on surface properties of endosseous dental implants. *Int J Oral Maxillofac Implants*, 17, 202-11.

KREISLER, M., KOHNEN, W., CHRISTOFFERS, A. B., GÖTZ, H., JANSEN, B., DUSCHNER, H. & D'HOEDT, B. 2005. In vitro evaluation of the biocompatibility of contaminated implant surfaces treated with an Er : YAG laser and an air powder system. *Clin Oral Implants Res*, 16, 36-43.

KREISLER, M., KOHNEN, W., MARINELLO, C., GÖTZ, H., DUSCHNER, H., JANSEN, B. & D'HOEDT, B. 2002d. Bactericidal effect of the Er:YAG laser on dental implant surfaces: an *in vitro* study. *J Periodontol*, 73, 1292-8.

KROES, I., LEPP, P. W. & RELMAN, D. A. 1999. Bacterial diversity within the human subgingival crevice. *Proc Natl Acad Sci U S A*, 96, 14547-52.

KRONSTRÖM, M., SVENSON, B., HELLMAN, M. & PERSSON, G. R. 2001. Early implant failures in patients treated with Bränemark System titanium dental implants: a retrospective study. *Int J Oral Maxillofac Implants*, 16, 201-7.

KRONSTRÖM, M., SVENSSON, B., ERICKSON, E., HOUSTON, L., BRAHAM, P. & PERSSON, G. R. 2000. Humoral immunity host factors in subjects with failing or successful titanium dental implants. *J Clin Periodontol*, 27, 875-82.

KUMAR, P. S., GRIFFEN, A. L., MOESCHBERGER, M. L. & LEYS, E. J. 2005. Identification of candidate periodontal pathogens and beneficial species by quantitative 16S clonal analysis. *J Clin Microbiol*, 43, 3944-55.

KUMAR, P. S., LEYS, E. J., BRYK, J. M., MARTINEZ, F. J., MOESCHBERGER, M. L. & GRIFFEN, A. L. 2006. Changes in periodontal health status are associated with bacterial community shifts as assessed by quantitative 16S cloning and sequencing. *J Clin Microbiol*, 44, 3665-3673.

KUMAR, P. S., MASON, M. R., BROOKER, M. R. & O'BRIEN, K. 2012. Pyrosequencing reveals unique microbial signatures associated with healthy and failing dental implants. *J Clin Periodontol*, 39, 425-33.

KUTYAVIN, I. V., AFONINA, I. A., MILLS, A., GORN, V. V., LUKHTANOV, E. A., BELOUSOV, E. S., SINGER, M. J., WALBURGER, D. K., LOKHOV, S. G., GALL, A. A., DEMPCY, R., REED, M. W., MEYER, R. B. & HEDGPETH, J. 2000. 3'-minor groove binder-DNA probes increase sequence specificity at PCR extension temperatures. *Nucleic Acids Res*, 28, 655-61.

KÄMPER, M., VETTERKIND, S., BERKER, R. & HOPPERT, M. 2004. Methods for in situ detection and characterization of extracellular polymers in biofilms by electron microscopy. *J Microbiol Methods*, 57, 55-64.

LAMFON, H., PORTER, S. R., MCCULLOUGH, M. & PRATTEN, J. 2003. Formation of *Candida albicans* biofilms on non-shedding oral surfaces. *Eur J Oral Sci*, 111, 465-71.

LANE, D. J. 1991. 16S/23S rRNA sequencing. *Nucleic Acid Techniques in Bacterial Systematics*, Goodfellow, E.S.M. (ed). Chichester, UK: John Wiley & Sons., 115-175.

LANG, N. P. & BERGLUNDH, T. 2011. Periimplant diseases: Where are we now? - Consensus of the Seventh European Workshop on Periodontology. *J Clin Periodontol*, 38, 178-181.

LANG, N. P., BERGLUNDH, T. & PERIODONTOLOGY, W. G. O. S. E. W. O. 2011. Periimplant diseases: where are we now?--Consensus of the Seventh European Workshop on Periodontology. *J Clin Periodontol*, 38 Suppl 11, 178-81.

LANG, N. P., BRÄGGER, U., WALTHER, D., BEAMER, B. & KORNMAN, K. S. 1993. Ligature-induced peri-implant infection in cynomolgus monkeys. I. Clinical and radiographic findings. *Clin Oral Implants Res*, 4, 2-11.

LANG, N. P., MOMBELLI, A., TONETTI, M. S., BRÄGGER, U. & HÄMMERLE, C. H. 1997. Clinical trials on therapies for peri-implant infections. *Ann Periodontol*, 2, 343-56.

LANG, N. P., PJETURSSON, B. E., TAN, K., BRÄGGER, U., EGGER, M. & ZWAHLEN, M. 2004. A systematic review of the survival and complication rates of fixed partial dentures (FPDs) after an observation period of at least 5 years: II. Combined tooth-implant-supported FPDs. *Clin Oral Implants Res*, 15, 643-653.

LANG, N. P., WILSON, T. G. & CORBET, E. F. 2000. Biological complications with dental implants: their prevention, diagnosis and treatment. *Clin Oral Implants Res*, 11 Suppl 1, 146-55.

LAWRENCE, J. R., KORBER, D. R., HOYLE, B. D., COSTERTON, J. W. & CALDWELL, D. E. 1991. Optical sectioning of microbial biofilms. *J Bacteriol*, 173, 6558-67.

LEADBETTER, E. R., HOLT, S. C. & SOCRANSKY, S. S. 1979. *Capnocytophaga*: new genus of gram-negative gliding bacteria. I. General characteristics, taxonomic considerations and significance. *Arch Microbiol*, 122, 9-16.

LEDDER, R. G., GILBERT, P., HUWS, S. A., AARONS, L., ASHLEY, M. P., HULL, P. S. & MCBAIN, A. J. 2007. Molecular analysis of the subgingival microbiota in health and disease. *Appl Environ Microbiol*, 73, 516-23.

LEE, A. & WANG, H. L. 2010. Biofilm related to dental implants. *Implant Dent*, 19, 387-393.

LEE, D. Y., SPÅNGBERG, L. S., BOK, Y. B., LEE, C. Y. & KUM, K. Y. 2005. The sustaining effect of three polymers on the release of chlorhexidine from a controlled release drug device for root canal disinfection. *Oral Surg Oral Med Oral Pathol Oral Radiol Oral Endod*, 100, 105-11.

LEE, K. H., MAIDEN, M. F., TANNER, A. C. & WEBER, H. P. 1999. Microbiota of successful osseointegrated dental implants. *J Periodontol*, 70, 131-8.

LEE, Y. H., PARK, H. W., LEE, J. H., SEO, H. W. & LEE, S. Y. 2012. The photodynamic therapy on *Streptococcus mutans* biofilms using erythrosine and dental halogen curing unit. *Int J Oral Sci*, 4, 0.

LEEUWENBURGH, S., WOLKE, J., SCHOONMAN, J. & JANSEN, J. A. 2005. Influence of deposition parameters on chemical properties of calcium phosphate coatings prepared by using electrostatic spray deposition. *J Biomed Mater Res A*, 74, 275-84.

LEITE, M. F., SANTOS, M. C., DE SOUZA, A. P. & LINE, S. R. 2008. Osseointegrated implant failure associated with MMP-1 promotor polymorphisms (-1607 and -519). *Int J Oral Maxillofac Implants*, 23, 653-8.

LEONHARDT, A., BERGLUNDH, T., ERICSSON, I. & DAHLÉN, G. 1992. Putative periodontal pathogens on titanium implants and teeth in experimental gingivitis and periodontitis in beagle dogs. *Clin Oral Implants Res*, 3, 112-9.

LEONHARDT, A., DAHLÉN, G. & RENVERT, S. 2003. Five-year clinical, microbiological, and radiological outcome following treatment of peri-implantitis in man. *J Periodontol*, 74, 1415-22.

LEONHARDT, A., OLSSON, J. & DAHLÉN, G. 1995. Bacterial colonization on titanium, hydroxyapatite, and amalgam surfaces in vivo. *J Dent Res*, 74, 1607-12.

LEONHARDT, A., RENVERT, S. & DAHLÉN, G. 1999. Microbial findings at failing implants. *Clin Oral Implants Res*, 10, 339-45.

LI, X., HUANG, J., AHMAD, Z. & EDIRISINGHE, M. 2007. Electrohydrodynamic coating of metal with nano-sized hydroxyapatite. *Biomed Mater Eng*, 17, 335-46.

LI, X., HUANG, J. & EDIRISINGHE, M. 2008. Development of nano-hydroxyapatite coating by electrohydrodynamic atomization spraying. *J Mater Sci Mater Med*, 19, 1545-51.

LI, X., KOLLER, G., HUANG, J., DI SILVIO, L., RENTON, T., ESAT, M., BONFIELD, W. & EDIRISINGHE, M. 2010. A novel jet-based nano-hydroxyapatite patterning technique for osteoblast guidance. *J R Soc Interface*, 7, 189-97.

LINDHE, J., BERGLUNDH, T., ERICSSON, I., LILJENBERG, B. & MARINELLO, C. 1992. Experimental breakdown of peri-implant and periodontal tissues. A study in the beagle dog. *Clin Oral Implants Res*, 3, 9-16.

LINDHE, J. & MEYLE, J. 2008. Peri-implant diseases: Consensus Report of the Sixth European Workshop on Periodontology. *J Clin Periodontol*, 35, 282-285.

LINDHE, J., MEYLE, J. & PERIODONTOLOGY, G. D. O. E. W. O. 2008. Peri-implant diseases: Consensus Report of the Sixth European Workshop on Periodontology. *J Clin Periodontol*, 35, 282-5.

LINDQUIST, L. W., CARLSSON, G. E. & JEMT, T. 1997. Association between marginal bone loss around osseointegrated mandibular implants and smoking habits: a 10-year follow-up study. *J Dent Res*, 76, 1667-74.

LISTGARTEN, M. A. 1976. Structure of the microbial flora associated with periodontal health and disease in man. A light and electron microscopic study. *J Periodontol*, 47, 1-18.

LISTGARTEN, M. A. 1994. The structure of dental plaque. *Periodontol 2000*, 5, 52-65.

LISTGARTEN, M. A., LOESCHE, W. J. & SOCRANSKY, S. S. 1963. morphology of *treponema microdentium* as revealed by electron microscopy of ultrathin sections. *J Bacteriol*, 85, 932-9.

LIVAK, K. J., FLOOD, S. J., MARMARO, J., GIUSTI, W. & DEETZ, K. 1995. Oligonucleotides with fluorescent dyes at opposite ends provide a quenched probe system useful for detecting PCR product and nucleic acid hybridization. *PCR Methods Appl*, 4, 357-62.

LOESCHE, W. J. 1968. Importance of nutrition in gingival crevice microbial ecology. *Periodontics*, 6, 245-9.

LOESCHE, W. J. 1992. DNA probe and enzyme analysis in periodontal diagnostics. *J Periodontol*, 63, 1102-9.

LOESCHE, W. J., GUSBERTI, F., METTRAUX, G., HIGGINS, T. & SYED, S. 1983. Relationship between oxygen tension and subgingival bacterial flora in untreated human periodontal pockets. *Infect Immun*, 42, 659-67.

LYONS, S. R., GRIFFEN, A. L. & LEYS, E. J. 2000. Quantitative real-time PCR for *Porphyromonas gingivalis* and total bacteria. *J Clin Microbiol*, 38, 2362-5.

MACHTEI, E. E., FRANKENTHAL, S., LEVI, G., ELIMELECH, R., SHOSHANI, E., ROSENFELD, O., TAGGER-GREEN, N. & SHLOMI, B. 2012. Treatment of peri-implantitis using multiple applications of chlorhexidine chips: a double-blind, randomized multi-centre clinical trial. *J Clin Periodontol*, 39, 1198-205.

MAEDA, H., FUJIMOTO, C., HARUKI, Y., MAEDA, T., KOKEGUCHI, S., PETELIN, M., ARAI, H., TANIMOTO, I., NISHIMURA, F. & TAKASHIBA, S. 2003. Quantitative real-time PCR using TaqMan and SYBR Green for *Actinobacillus actinomycetemcomitans*, *Porphyromonas gingivalis*, *Prevotella intermedia*, tetQ gene and total bacteria. *FEMS Immunol Med Microbiol*, 39, 81-6.

MANDEL, I. D. 1994. Antimicrobial mouthrinses: overview and update. *J Am Dent Assoc*, 125 Suppl 2, 2S-10S.

MANOR, Y., OUBAID, S., MARDINGER, O., CHAUSHU, G. & NISSAN, J. 2009. Characteristics of early versus late implant failure: a retrospective study. *J Oral Maxillofac Surg*, 67, 2649-52.

MAROTTI, J., TORTAMANO, P., CAI, S., RIBEIRO, M. S., FRANCO, J. E. & DE CAMPOS, T. T. 2013. Decontamination of dental implant surfaces by means of photodynamic therapy. *Lasers Med Sci*, 28, 303-9.

MARSH, P. D. 1994. Microbial ecology of dental plaque and its significance in health and disease. *Adv Dent Res*, 8, 263-71.

MARSH, P. D. 2003. Are dental diseases examples of ecological catastrophes? *Microbiol*, 149, 279-294.

MARSH, P. D. 2005. Dental plaque: biological significance of a biofilm and community life-style. *J Clin Periodontol*, 32, 7-15.

MARSH, P. D. 2010. Microbiology of Dental Plaque Biofilms and Their Role in Oral Health and Caries. *Dental Clinics of North America*, 54, 441-454.

MARSH, P. D. & PERCIVAL, R. S. 2006. The oral microflora — friend or foe? Can we decide? *Int Dent J*, 56, 233-239.

MARTIN, J. Y., SCHWARTZ, Z., HUMMERT, T. W., SCHRAUB, D. M., SIMPSON, J., LANKFORD, J., DEAN, D. D., COCHRAN, D. L. & BOYAN, B. D. 1995. Effect of titanium surface roughness on proliferation, differentiation, and protein synthesis of human osteoblast-like cells (MG63). *J Biomed Mater Res*, 29, 389-401.

MARX, R. E., CARLSON, E. R., EICHSTAEDT, R. M., SCHIMMELE, S. R., STRAUSS, J. E. & GEORGEFF, K. R. 1998. Platelet-rich plasma: Growth factor enhancement for bone grafts. *Oral Surg Oral Med Oral Pathol Oral Radiol Endod*, 85, 638-46.

MCBAIN, A. J., SISSONS, C., LEDDER, R. G., SREENIVASAN, P. K., DE VIZIO, W. & GILBERT, P. 2005. Development and characterization of a simple perfused oral microcosm. *J Appl Microbiol*, 98, 624-34.

MEFFERT, R. M. 1988a. Four case studies: use of chlorhexidine gluconate (0.12%) (Peridex Oral Rinse) to control plaque and maintain oral hygiene in post restorative phases of endosseous implant therapy. *J Indiana Dent Assoc*, 67, 9-11.

MEFFERT, R. M. 1988b. The soft tissue interface in dental implantology. *J Dent Educ*, 52, 810-1.

MEFFERT, R. M. 1996. Periodontitis vs. peri-implantitis: the same disease? The same treatment? *Crit Rev Oral Biol Med*, 7, 278-91.

MELSEN, B., KAAE, O. & RÖLLA, G. 1983. Penetration of fluoride and chlorhexidine in human dental plaque in vitro. *Caries Res*, 17, 113-7.

MEMARZADEH, K., VARGAS, M., HUANG, J., FAN, J. & ALLAKER, R. P. Nano metallic-oxides as antimicrobials for implant coatings. 23rd Symposium and Annual Meeting of International Society for Ceramics in Medicine, ISCM 2011, November 6, 2011 - November 9, 2011, 2012 Istanbul, Turkey. Trans Tech Publications Ltd, 489-494.

MIR-MARI, J., MIR-ORFILA, P., FIGUEIREDO, R., VALMASEDA-CASTELLÓN, E. & GAY-ESCODA, C. 2012. Prevalence of peri-implant diseases. A cross-sectional study based on a private practice environment. *J Clin Periodontol*, 39, 490-4.

MOIMAZ, S. A., ZINA, L. G., SALIBA, O. & GARBIN, C. A. 2009. Smoking and periodontal disease: clinical evidence for an association. *Oral Health Prev Dent*, 7, 369-76.

MOMBELLI, A. 1987. [Costs calculation with bar codes. The use of microcomputers in dental practice]. *Schweiz Monatsschr Zahnmed*, 97, 1001-4.

MOMBELLI, A. 1993. Microbiology of the dental implant. *Adv Dent Res*, 7, 202-6.

MOMBELLI, A. 1994. ["The objective is not to create a system of superdentists". Interview by Kurt Venner and Serge Roh]. *Schweiz Monatsschr Zahnmed*, 104, 1551, 1567-8.

MOMBELLI, A. 1998. [Antibiotics in periodontal therapy. Their use within the framework of a treatment concept]. *Schweiz Monatsschr Zahnmed*, 108, 968-81.

MOMBELLI, A. 1999. In vitro models of biological responses to implant microbiological models. *Adv Dent Res*, 13, 67-72.

MOMBELLI, A. 2002. Microbiology and antimicrobial therapy of peri-implantitis. *Periodontol 2000*, 28, 177-89.

MOMBELLI, A. 2012. Antimicrobial advances in treating periodontal diseases. *Front Oral Biol*, 15, 133-48.

MOMBELLI, A., BRÄGGER, U. & LANG, N. P. 1992. Microbiota associated with residual clefts and neighboring teeth in patients with cleft lip, alveolus, and palate. *Cleft Palate Craniofac J*, 29, 463-9.

MOMBELLI, A., BUSER, D. & LANG, N. P. 1988. Colonization of osseointegrated titanium implants in edentulous patients. Early results. *Oral Microbiol Immunol*, 3, 113-20.

MOMBELLI, A., CIONCA, N. & ALMAGHLOUTH, A. 2011a. Does adjunctive antimicrobial therapy reduce the perceived need for periodontal surgery? *Periodontol 2000*, 55, 205-16.

MOMBELLI, A. & DÉCAILLET, F. 2011. The characteristics of biofilms in peri-implant disease. *J Clin Periodontol*, 38 Suppl 11, 203-13.

MOMBELLI, A., DÉCAILLET, F., ALMAGHLOUTH, A., WICK, P. & CIONCA, N. 2011b. [Efficient, minimally invasive periodontal therapy. An evidence based treatment concept]. *Schweiz Monatsschr Zahnmed*, 121, 145-57.

MOMBELLI, A., FELOUTZIS, A., BRAGGER, U. & LANG, N. P. 2001. Treatment of peri-implantitis by local delivery of tetracycline. Clinical. *Clin Oral Implants Res*, 12, 287-94.

MOMBELLI, A. & LANG, N. P. 1992. Antimicrobial treatment of peri-implant infections. *Clin Oral Implants Res*, 3, 162-8.

MOMBELLI, A. & LANG, N. P. 1998. The diagnosis and treatment of peri-implantitis. *Periodontol 2000*, 17, 63-76.

MOMBELLI, A., LANG, N. P., BÜRGIN, W. B. & GUSBERTI, F. A. 1990. Microbial changes associated with the development of puberty gingivitis. *J Periodontal Res*, 25, 331-8.

MOMBELLI, A. & MERICSKE-STERN, R. 1990. Microbiological features of stable osseointegrated implants used as abutments for overdentures. *Clin Oral Implants Res*, 1, 1-7.

MOMBELLI, A., MÜLLER, N. & CIONCA, N. 2012. The epidemiology of peri-implantitis. *Clin Oral Implants Res*, 23 Suppl 6, 67-76.

MOMBELLI, A., NYMAN, S., BRÄGGER, U., WENNSTRÖM, J. & LANG, N. P. 1995. Clinical and microbiological changes associated with an altered subgingival environment induced by periodontal pocket reduction. *J Clin Periodontol*, 22, 780-7.

MOMBELLI, A., SCHMID, B., RUTAR, A. & LANG, N. P. 2002. Local antibiotic therapy guided by microbiological diagnosis. *J Clin Periodontol*, 29, 743-9.

MOMBELLI, A., VAN OOSTEN, M. A., SCHURCH, E. & LAND, N. P. 1987. The microbiota associated with successful or failing osseointegrated titanium implants. *Oral Microbiol Immunol*, 2, 145-51.

MOORE, W. E. & MOORE, L. V. 1994. The bacteria of periodontal diseases. *Periodontol 2000*, 5, 66-77.

MORGAN, T. D. & WILSON, M. 2001. The effects of surface roughness and type of denture acrylic on biofilm formation by *Streptococcus oralis* in a constant depth film fermentor. *J Appl Microbiol*, 91, 47-53.

MORIKAWA, M., CHIBA, T., TOMII, N., SATO, S., TAKAHASHI, Y., KONISHI, K., NUMABE, Y., IWATA, K. & IMAI, K. 2008. Comparative analysis of putative periodontopathic bacteria by multiplex polymerase chain reaction. *J Periodontal Res*, 43, 268-74.

MOSHREFI, A. 2002. Chlorhexidine. *J West Soc Periodontol Periodontal Abstr*, 50, 5-9.

MOUHYI, J., SENNERBY, L., NAMOUR, S., GUILLAUME, P. & VAN RECK, J. 1999. Temperature increases during surface decontamination of titanium implants using CO₂ laser. *Clin Oral Implants Res*, 10, 54-61.

MUNIR, G., KOLLER, G., DI SILVIO, L., EDIRISINGHE, M. J., BONFIELD, W. & HUANG, J. 2011. The pathway to intelligent implants: osteoblast response to nano silicon-doped hydroxyapatite patterning. *J R Soc Interface*, 8, 678-88.

MÁXIMO, M. B., DE MENDONÇA, A. C., ALVES, J. F., CORTELLI, S. C., PERUZZO, D. C. & DUARTE, P. M. 2008. Peri-implant diseases may be associated with increased time loading and generalized periodontal bone loss: preliminary results. *J Oral Implantol*, 34, 268-73.

MÁXIMO, M. B., DE MENDONÇA, A. C., RENATA SANTOS, V., FIGUEIREDO, L. C., FERES, M. & DUARTE, P. M. 2009. Short-term clinical and microbiological evaluations of peri-implant diseases before and after mechanical anti-infective therapies. *Clin Oral Implants Res*, 20, 99-108.

MÜLLER, P., GUGGENHEIM, B. & SCHMIDLIN, P. R. 2007. Efficacy of gasiform ozone and photodynamic therapy on a multispecies oral biofilm *in vitro*. *Eur J Oral Sci*, 115, 77-80.

NADKARNI, M. A., MARTIN, F. E., JACQUES, N. A. & HUNTER, N. 2002. Determination of bacterial load by real-time PCR using a broad-range (universal) probe and primers set. *Microbiol*, 148, 257-66.

NAIR, S., SASIDHARAN, A., DIVYA RANI, V. V., MENON, D., MANZOOR, K. & RAINA, S. 2009. Role of size scale of ZnO nanoparticles and microparticles on toxicity toward bacteria and osteoblast cancer cells. *J Mater Sci Mater Med*, 20 Suppl 1, S235-41.

NAKAZATO, G., TSUCHIYA, H., SATO, M. & YAMAUCHI, M. 1989. In vivo plaque formation on implant materials. *Int J Oral Maxillofac Implants*, 4, 321-6.

NAKOU, M., MIKX, F. H., OOSTERWAAL, P. J. & KRUIJSEN, J. C. 1987. Early microbial colonization of permucosal implants in edentulous patients. *J Dent Res*, 66, 1654-7.

NANDAKUMAR, K., KEELER, W., SCHRAFT, H. & LEUNG, K. T. 2006. Visible laser and UV-A radiation impact on a PNP degrading Moraxella strain and its rpoS mutant. *Biotechnol Bioeng*, 94, 793-802.

NAPEÑAS, J. J., BRENNAN, M. T. & FOX, P. C. 2009. Diagnosis and treatment of xerostomia (dry mouth). *Odontolo*, 97, 76-83.

NEWMAN, H. N. 1972a. Clinical significance of microorganisms and organic films on human enamel. *Proc R Soc Med*, 65, 908-11.

NEWMAN, H. N. 1972b. Structure of approximal human dental plaque as observed by scanning electron microscopy. *Arch Oral Biol*, 17, 1445-53.

NEWMAN, M. G. & FLEMMIG, T. F. 1988. Periodontal considerations of implants and implant associated microbiota. *J Dent Educ*, 52, 737-44.

NIBALI, L. & DONOS, N. 2011. Radiographic bone fill of peri-implantitis defects following nonsurgical therapy: report of three cases. *Quintessence Int*, 42, 393-7.

NOBBS, A. H., LAMONT, R. J. & JENKINSON, H. F. 2009. *Streptococcus* adherence and colonization. *Microbiol Mol Biol Rev*, 73, 407-50, Table of Contents.

NOGUEROL, B., MUÑOZ, R., MESA, F., DE DIOS LUNA, J. & O'VALLE, F. 2006. Early implant failure. Prognostic capacity of Periotest: retrospective study of a large sample. *Clin Oral Implants Res*, 17, 459-64.

NONNENMACHER, C., DALPKE, A., MUTTERS, R. & HEEG, K. 2004. Quantitative detection of periodontopathogens by real-time PCR. *J Microbiol Methods*, 59, 117-25.

NOROWSKI, P. A., JR. & BUMGARDNER, J. D. 2009. Biomaterial and antibiotic strategies for peri-implantitis: a review. *J Biomed Mater Res B Appl Biomater*, 88, 530-43.

NOVAES, P. D., ALMEIDA, O. P., JAEGER, R. G. & ITO, V. S. 1991. An electron microscopic study of dental plaque of the rat incisor. *Arch Oral Biol*, 36, 693-6.

NYVAD, B. & FEJERSKOV, O. 1989. Structure of dental plaque and the plaque-enamel interface in human experimental caries. *Caries Res*, 23, 151-8.

NYVAD, B. & KILIAN, M. 1987. Microbiology of the early colonization of human enamel and root surfaces in vivo. *Scand J Dent Res*, 95, 369-80.

NYVAD, B., TEN CATE, J. M. & FEJERSKOV, O. 1989. Microradiography of experimental root surface caries in man. *Caries Res*, 23, 218-24.

O'NEILL, J. F., HOPE, C. K. & WILSON, M. 2002. Oral bacteria in multi-species biofilms can be killed by red light in the presence of toluidine blue. *Lasers Surg Med*, 31, 86-90.

OFFENBACHER, S. 1996. Periodontal diseases: pathogenesis. *Ann Periodontol*, 1, 821-78.

OKAYASU, K. & WANG, H. L. 2011. Decision tree for the management of periimplant diseases. *Implant Dent*, 20, 256-61.

ONAGAWA, M., ISHIHARA, K. & OKUDA, K. 1994. Coaggregation between *Porphyromonas gingivalis* and *Treponema denticola*. *Bull Tokyo Dent Coll*, 35, 171-81.

ONG, E. S., NEWMAN, H. N., WILSON, M. & BULMAN, J. S. 1992. The occurrence of periodontitis-related microorganisms in relation to titanium implants. *J Periodontol*, 63, 200-5.

OOSTERWAAL, P. J., MIKX, F. H., VAN DEN BRINK, M. E. & RENGLI, H. H. 1989. Bactericidal concentrations of chlorhexidine-digluconate, amine fluoride gel and stannous fluoride gel for subgingival bacteria tested in serum at short contact times. *J Periodontal Res*, 24, 155-60.

OZEKI, K., YUHTA, T., FUKUI, Y., AOKI, H. & NISHIMURA, I. 2002. A functionally graded titanium/hydroxyapatite film obtained by sputtering. *J Mater Sci Mater Med*, 13, 253-8.

PAES LEME, A. F., KOO, H., BELLATO, C. M., BEDI, G. & CURY, J. A. 2006. The role of sucrose in cariogenic dental biofilm formation--new insight. *J Dent Res*, 85, 878-87.

PASTER, B. J., BOCHES, S. K., GALVIN, J. L., ERICSON, R. E., LAU, C. N., LEVANOS, V. A., SAHASRABUDHE, A. & DEWHIRST, F. E. 2001. Bacterial diversity in human subgingival plaque. *J Bacteriol*, 183, 3770-83.

PASTER, B. J. & DEWHIRST, F. E. 2009. Molecular microbial diagnosis. *Periodontol 2000*, 51, 38-44.

PASTER, B. J., OLSEN, I., AAS, J. A. & DEWHIRST, F. E. 2006. The breadth of bacterial diversity in the human periodontal pocket and other oral sites. *Periodontol 2000*, 42, 80-7.

PERSSON, G. R., SALVI, G. E., HEITZ-MAYFIELD, L. J. & LANG, N. P. 2006. Antimicrobial therapy using a local drug delivery system (Arestin) in the treatment of peri-implantitis. I: Microbiological outcomes. *Clin Oral Implants Res*, 17, 386-93.

PERSSON, G. R., SAMUELSSON, E., LINDAHL, C. & RENVERT, S. 2010. Mechanical non-surgical treatment of peri-implantitis: a single-blinded randomized longitudinal clinical study. II. Microbiological results. *J Clin Periodontol*, 37, 563-73.

PERSSON, L. G., ERICSSON, I., BERGLUNDH, T. & LINDHE, J. 2001. Osseointegration following treatment of peri-implantitis and replacement of implant components. An experimental study in the dog. *J Clin Periodontol*, 28, 258-63.

PERSSON, L. G., LEKHOLM, U., LEONHARDT, A., DAHLÉN, G. & LINDHE, J. 1996. Bacterial colonization on internal surfaces of Bränemark system implant components. *Clin Oral Implants Res*, 7, 90-5.

PETERS, A. C. & WIMPENNY, J. W. 1988. A constant-depth laboratory model film fermentor. *Biotechnol Bioeng*, 32, 263-70.

PITARU, S., TAL, H., SOLDINGER, M., AZAR-AVIDAN, O. & NOFF, M. 1987. Collagen membranes prevent the apical migration of epithelium during periodontal wound healing. *J Periodontal Res*, 22, 331-3.

POLZ, M. F. & CAVANAUGH, C. M. 1998. Bias in template-to-product ratios in multitemplate PCR. *Appl Environ Microbiol*, 64, 3724-30.

PONTORIERO, R., TONELLI, M. P., CARNEVALE, G., MOMBELLI, A., NYMAN, S. R. & LANG, N. P. 1994. Experimentally induced peri-implant mucositis. A clinical study in humans. *Clin Oral Implants Res*, 5, 254-9.

PORRAS, R., ANDERSON, G. B., CAFFESSE, R., NARENDRAN, S. & TREJO, P. M. 2002. Clinical response to 2 different therapeutic regimens to treat peri-implant mucositis. *J Periodontol*, 73, 1118-25.

POYART, C., QUESNE, G., BOUMAILA, C. & TRIEU-CUOT, P. 2001. Rapid and accurate species-level identification of coagulase-negative staphylococci by using the sodA gene as a target. *J Clin Microbiol*, 39, 4296-301.

POYART, C., QUESNE, G., COULON, S., BERCHE, P. & TRIEU-CUOT, P. 1998. Identification of streptococci to species level by sequencing the gene encoding the manganese-dependent superoxide dismutase. *J Clin Microbiol*, 36, 41-7.

PRATTEN, J. 2007. Growing oral biofilms in a constant depth film fermentor (CDFF). *Curr Protoc Microbiol*, Chapter 1, Unit 1B.5.

PRATTEN, J., ANDREWS, C. S., CRAIG, D. Q. & WILSON, M. 2000. Structural studies of microcosm dental plaques grown under different nutritional conditions. *FEMS Microbiol Lett*, 189, 215-8.

PRATTEN, J., BARNETT, P. & WILSON, M. 1998a. Composition and susceptibility to chlorhexidine of multispecies biofilms of oral bacteria. *Appl Environ Microbiol*, 64, 3515-9.

PRATTEN, J., PASU, M., JACKSON, G., FLANAGAN, A. & WILSON, M. 2003a. Modelling oral malodour in a longitudinal study. *Arch Oral Biol*, 48, 737-43.

PRATTEN, J., SMITH, A. W. & WILSON, M. 1998b. Response of single species biofilms and microcosm dental plaques to pulsing with chlorhexidine. *J Antimicrob Chemother*, 42, 453-9.

PRATTEN, J., WILLS, K., BARNETT, P. & WILSON, M. 1998c. In vitro studies of the effect of antiseptic-containing mouthwashes on the formation and viability of *Streptococcus sanguis* biofilms. *J Appl Microbiol*, 84, 1149-55.

PRATTEN, J., WILSON, M. & SPRATT, D. A. 2003b. Characterization of in vitro oral bacterial biofilms by traditional and molecular methods. *Oral Microbiol Immunol*, 18, 45-9.

PREMANATHAN, M., KARTHIKEYAN, K., JEYASUBRAMANIAN, K. & MANIVANNAN, G. 2011. Selective toxicity of ZnO nanoparticles toward Gram-positive bacteria and cancer cells by apoptosis through lipid peroxidation. *Nanomedicine*, 7, 184-92.

PRICE, R. R., VISCOUNT, H. B., STANLEY, M. C. & LEUNG, K. P. 2007. Targeted profiling of oral bacteria in human saliva and in vitro biofilms with. *Biofouling*, 23, 203-13.

QIN, Y., LUAN, X., BI, L., HE, G., BAI, X., ZHOU, C. & ZHANG, Z. 2008. Toluidine blue-mediated photoinactivation of periodontal pathogens from supragingival plaques. *Lasers Med Sci*, 23, 49-54.

QUIRYNEN, M. & BOLLEN, C. M. 1995. The influence of surface roughness and surface-free energy on supra- and subgingival plaque formation in man. A review of the literature. *J Clin Periodontol*, 22, 1-14.

QUIRYNEN, M., DE SOETE, M. & VAN STEENBERGHE, D. 2002. Infectious risks for oral implants: a review of the literature. *Clin Oral Implants Res*, 13, 1-19.

QUIRYNEN, M. & LISTGARTEN, M. A. 1990. Distribution of bacterial morphotypes around natural teeth and titanium implants ad modum Bränemark. *Clin Oral Implants Res*, 1, 8-12.

QUIRYNEN, M., VAN DER MEI, H. C., BOLLEN, C. M., SCHOTTE, A., MARECHAL, M., DOORNBUSCH, G. I., NAERT, I., BUSSCHER, H. J. & VAN STEENBERGHE, D. 1993. An in vivo study of the influence of the surface roughness of implants on the microbiology of supra- and subgingival plaque. *J Dent Res*, 72, 1304-9.

RAMBERG, P., LINDHE, J., BOTTICELLI, D. & BOTTICELLI, A. 2009. The effect of a triclosan dentifrice on mucositis in subjects with dental implants: a six-month clinical study. *J Clin Dent*, 20, 103-7.

RAMS, T. E., BABALOLA, O. O. & SLOTS, J. 1990. Subgingival occurrence of enteric rods, yeasts and staphylococci after systemic doxycycline therapy. *Oral Microbiol Immunol*, 5, 166-8.

RAMS, T. E. & LINK, C. C. 1983. Microbiology of failing dental implants in humans: electron microscopic observations. *J Oral Implantol*, 11, 93-100.

RAMS, T. E., ROBERTS, T. W., FEIK, D., MOLZAN, A. K. & SLOTS, J. 1991. Clinical and microbiological findings on newly inserted hydroxyapatite-coated and pure titanium human dental implants. *Clin Oral Implants Res*, 2, 121-7.

RAMS, T. E., ROBERTS, T. W., TATUM, H. & KEYES, P. H. 1984. The subgingival microbial flora associated with human dental implants. *J Prosthet Dent*, 51, 529-34.

RANI, S. A., PITTS, B. & STEWART, P. S. 2005. Rapid diffusion of fluorescent tracers into *Staphylococcus epidermidis* biofilms visualized by time lapse microscopy. *Antimicrob Agents Chemother*, 49, 728-32.

RAPPÉ, M. S. & GIOVANNONI, S. J. 2003. The uncultured microbial majority. *Annu Rev Microbiol*, 57, 369-94.

RASMUSSEN, L., KAHNBERG, K. E. & TAN, A. 2001. Effects of implant design and surface on bone regeneration and implant stability: an experimental study in the dog mandible. *Clin Implant Dent Relat Res*, 3, 2-8.

RENIER, S., HÉBRAUD, M. & DESVAUX, M. 2011. Molecular biology of surface colonization by *Listeria monocytogenes*: an additional facet of an opportunistic Gram-positive foodborne pathogen. *Environ Microbiol*, 13, 835-50.

RENVERT, S., LESSEM, J., DAHLÉN, G., RENVERT, H. & LINDAHL, C. 2008. Mechanical and repeated antimicrobial therapy using a local drug delivery system in the treatment of peri-implantitis: a randomized clinical trial. *J Periodontol*, 79, 836-44.

RENVERT, S., POLYZOIS, I. & CLAFFEY, N. 2011. How do implant surface characteristics influence periimplant disease? *J of Clinical Periodontol*, 38, 214-222.

RENVERT, S., POLYZOIS, I. & MAGUIRE, R. 2009. Re-osseointegration on previously contaminated surfaces: a systematic review. *Clin Oral Implants Res*, 20 Suppl 4, 216-27.

RENVERT, S., ROOS-JANSÅKER, A. M., LINDAHL, C., RENVERT, H. & RUTGER PERSSON, G. 2007. Infection at titanium implants with or without a clinical diagnosis of inflammation. *Clin Oral Implants Res*, 18, 509-516.

RICKARD, A. H., GILBERT, P. & HANDLEY, P. S. 2004. Influence of growth environment on coaggregation between freshwater biofilm bacteria. *J Appl Microbiol*, 96, 1367-73.

RINKE, S., OHL, S., ZIEBOLZ, D., LANGE, K. & EICKHOLZ, P. 2011. Prevalence of periimplant disease in partially edentulous patients: a practice-based cross-sectional study. *Clin Oral Implants Res*, 22, 826-33.

RODU, B. 1990. The polymerase chain reaction: the revolution within. *Am J Med Sci*, 299, 210-6.

ROMANOS, G., KO, H. H., FROUM, S. & TARNOW, D. 2009. The use of CO(2) laser in the treatment of peri-implantitis. *Photomed Laser Surg*, 27, 381-6.

ROMEO, E., GHISOLFI, M. & CARMAGNOLA, D. 2004. Peri-implant diseases. A systematic review of the literature. *Minerva Stomatol*, 53, 215-30.

ROOS-JANSÅKER, A. M., RENVERT, H., LINDAHL, C. & RENVERT, S. 2006. Nine- to fourteen-year follow-up of implant treatment. Part III: factors associated with peri-implant lesions. *J Clin Periodontol*, 33, 296-301.

ROOS-JANSÅKER, A. M., RENVERT, S. & EGELBERG, J. 2003. Treatment of peri-implant infections: a literature review. *J Clin Periodontol*, 30, 467-85.

ROSENBERG, E. S., TOROSIAN, J. P. & SLOTS, J. 1991. Microbial differences in 2 clinically distinct types of failures of osseointegrated implants. *Clin Oral Implants Res*, 2, 135-44.

ROSLING, B., DAHLÉN, G., VOLPE, A., FURUICHI, Y., RAMBERG, P. & LINDHE, J. 1997a. Effect of triclosan on the subgingival microbiota of periodontitis-susceptible subjects. *J Clin Periodontol*, 24, 881-7.

ROSLING, B., WANNFORS, B., VOLPE, A. R., FURUICHI, Y., RAMBERG, P. & LINDHE, J. 1997b. The use of a triclosan/copolymer dentifrice may retard the progression of periodontitis. *J Clin Periodontol*, 24, 873-80.

ROSS, N. M., CHARLES, C. H. & DILLS, S. S. 1989. Long-term effects of Listerine antiseptic on dental plaque and gingivitis. *J Clin Dent*, 1, 92-5.

RUPF, S., IDLIBI, A. N., MARRAWI, F. A., HANNIG, M., SCHUBERT, A., VON MUELLER, L., SPITZER, W., HOLTMANN, H., LEHMANN, A., RUEPPELL, A. & SCHINDLER, A. 2011. Removing biofilms from microstructured titanium ex vivo: a novel approach using atmospheric plasma technology. *PLoS One*, 6, e25893.

RUPP, F., AXMANN, D., ZIEGLER, C. & GEIS-GERSTORFER, J. 2002. Adsorption/desorption phenomena on pure and Teflon AF-coated titania surfaces studied by dynamic contact angle analysis. *J Biomed Mater Res*, 62, 567-78.

RUSSELL, C. & COULTER, W. A. 1975. Continuous monitoring of pH and Eh in bacterial plaque grown on a tooth in an artificial mouth. *Appl Microbiol*, 29, 141-4.

RÜDIN, H. J., OVERDIEK, H. F. & RATEITSCHAK, K. H. 1970. Correlation between sulcus fluid rate and clinical and histological inflammation of the marginal gingiva. *Helv Odontol Acta*, 14, 21-6.

RÜHLING, A., KOCHER, T., KREUSCH, J. & PLAGMANN, H. C. 1994. Treatment of subgingival implant surfaces with Teflon-coated sonic and ultrasonic scaler tips and various implant curettes. An in vitro study. *Clin Oral Implants Res*, 5, 19-29.

SAFII, S. H., PALMER, R. M. & WILSON, R. F. 2010. Risk of implant failure and marginal bone loss in subjects with a history of periodontitis: a systematic review and meta-analysis. *Clin Implant Dent Relat Res*, 12, 165-74.

SAKAMOTO, M., HUANG, Y., UMEDA, M., ISHIKAWA, I. & BENNO, Y. 2002. Detection of novel oral phylotypes associated with periodontitis. *FEMS Microbiol Lett*, 217, 65-9.

SAKAMOTO, M., TAKEUCHI, Y., UMEDA, M., ISHIKAWA, I. & BENNO, Y. 2001. Rapid detection and quantification of five periodontopathic bacteria by real-time PCR. *Microbiol Immunol*, 45, 39-44.

SAKAMOTO, M., UMEDA, M. & BENNO, Y. 2005. Molecular analysis of human oral microbiota. *J Periodontal Res*, 40, 277-85.

SALCETTI, J. M., MORIARTY, J. D., COOPER, L. F., SMITH, F. W., COLLINS, J. G., SOCRANSKY, S. S. & OFFENBACHER, S. 1997. The Clinical, Microbial, and Host Response Characteristics of the Failing Implant. *International Journal of Oral and Maxillofacial Implants*, 12, 32-42.

SALVI, G. E., FÜRST, M. M., LANG, N. P. & PERSSON, G. R. 2008. One-year bacterial colonization patterns of *Staphylococcus aureus* and other bacteria at implants and adjacent teeth. *Clin Oral Implants Res*, 19, 242-8.

SALVI, G. E., MOMBELLI, A., MAYFIELD, L., RUTAR, A., SUVAN, J., GARRETT, S. & LANG, N. P. 2002. Local antimicrobial therapy after initial periodontal treatment. *J Clin Periodontol*, 29, 540-50.

SALVI, G. E., PERSSON, G. R., HEITZ-MAYFIELD, L. J., FREI, M. & LANG, N. P. 2007. Adjunctive local antibiotic therapy in the treatment of peri-implantitis II: clinical and radiographic outcomes. *Clin Oral Implants Res*, 18, 281-5.

SANZ, M., NEWMAN, M. G., NACHNANI, S., HOLT, R., STEWART, R. & FLEMMIG, T. 1990. Characterization of the subgingival microbial flora around endosteal sapphire dental implants in partially edentulous patients. *Int J Oral Maxillofac Implants*, 5, 247-53.

SAXTON, C. A. 1973. Scanning electron microscope study of the formation of dental plaque. *Caries Res*, 7, 102-19.

SCARANO, A., PIATTELLI, M., CAPUTI, S., FAVERO, G. A. & PIATTELLI, A. 2004. Bacterial adhesion on commercially pure titanium and zirconium oxide disks: an in vivo human study. *J Periodontol*, 75, 292-6.

SCHWARZ, F., AOKI, A., SCULEAN, A. & BECKER, J. 2009a. The impact of laser application on periodontal and peri-implant wound healing. *Periodontol 2000*, 51, 79-108.

SCHWARZ, F. & BECKER, J. 2005. Treatment of periodontitis and peri-implantitis with an Er:YAG laser: Experimental and clinical studies. *Medical Laser Application*, 20, 47-59.

SCHWARZ, F., BIELING, K., NUESRY, E., SCULEAN, A. & BECKER, J. 2006. Clinical and histological healing pattern of peri-implantitis lesions following non-surgical treatment with an Er:YAG laser. *Lasers Surg Med*, 38, 663-71.

SCHWARZ, F., BIELING, K., SCULEAN, A., HERTEN, M. & BECKER, J. 2004. [Treatment of periimplantitis with laser or ultrasound. A review of the literature]. *Schweiz Monatsschr Zahnmed*, 114, 1228-35.

SCHWARZ, F., FERRARI, D., POPOVSKI, K., HARTIG, B. & BECKER, J. 2009b. Influence of different air-abrasive powders on cell viability at biologically contaminated titanium dental implants surfaces. *J Biomed Mater Res B Appl Biomater*, 88, 83-91.

SCHWARZ, F., JOHN, G., MAINUSCH, S., SAHM, N. & BECKER, J. 2012. Combined surgical therapy of peri-implantitis evaluating two methods of surface debridement and decontamination. A two-year clinical follow up report. *J Clin Periodontol*, 39, 789-97.

SCHWARZ, F., SAHM, N., IGLHAUT, G. & BECKER, J. 2011. Impact of the method of surface debridement and decontamination on the clinical outcome following combined surgical therapy of peri-implantitis: a randomized controlled clinical study. *J Clin Periodontol*, 38, 276-84.

SCHWARZ, F., SCULEAN, A., BIELING, K., FERRARI, D., ROTHAMEL, D. & BECKER, J. 2008. Two-year clinical results following treatment of peri-implantitis lesions using a nanocrystalline hydroxyapatite or a natural bone mineral in combination with a collagen membrane. *J Clin Periodontol*, 35, 80-7.

SCHWARZ, F., SCULEAN, A., ROMANOS, G., HERTEN, M., HORN, N., SCHERBAUM, W. & BECKER, J. 2005. Influence of different treatment approaches on the removal of early plaque biofilms and the viability of SAOS2 osteoblasts grown on titanium implants. *Clin Oral Investig*, 9, 111-7.

SCHÄR, D., RAMSEIER, C. A., EICK, S., ARWEILER, N. B., SCULEAN, A. & SALVI, G. E. 2013. Anti-infective therapy of peri-implantitis with adjunctive local drug delivery or photodynamic therapy: six-month outcomes of a prospective randomized clinical trial. *Clin Oral Implants Res*, 24, 104-10.

SEGATA, N., HAAKE, S. K., MANNON, P., LEMON, K. P., WALDRON, L., GEVERS, D., HUTTENHOWER, C. & IZARD, J. 2012. Composition of the adult digestive tract bacterial microbiome based on seven mouth surfaces, tonsils, throat and stool samples. *Genome Biol*, 13, R42.

SHALABI, M. M., GORTEMAKER, A., VAN'T HOF, M. A., JANSEN, J. A. & CREUGERS, N. H. 2006. Implant surface roughness and bone healing: a systematic review. *J Dent Res*, 85, 496-500.

SHIBLI, J. A., MELO, L., FERRARI, D. S., FIGUEIREDO, L. C., FAVERI, M. & FERES, M. 2008. Composition of supra- and subgingival biofilm of subjects with healthy and diseased implants. *Clin Oral Implants Res*, 19, 975-82.

SHIBLI, J. A., VITUSSI, T. R., GARCIA, R. V., ZENÓBIO, E. G., OTA-TSUZUKI, C., CASSONI, A., PIATTELLI, A. & D'AVILA, S. 2007. Implant surface analysis and microbiologic evaluation of failed implants retrieved from smokers. *J Oral Implantol*, 33, 232-8.

SIGUSCH, B. W., PFITZNER, A., ALBRECHT, V. & GLOCKMANN, E. 2005. Efficacy of photodynamic therapy on inflammatory signs and two selected periodontopathogenic species in a beagle dog model. *J Periodontol*, 76, 1100-5.

SILVERSTEIN, L. H., KURTZMAN, D., GARNICK, J. J., SCHUSTER, G. S., STEFLIK, D. E. & MOSKOWITZ, M. E. 1994. The microbiota of the peri-implant region in health and disease. *Implant dentistry*, 3, 170-174.

SIMONIS, P., DUFOUR, T. & TENENBAUM, H. 2010. Long-term implant survival and success: a 10-16-year follow-up of non-submerged dental implants. *Clin Oral Implants Res*, 21, 772-7.

SISSONS, C. H., CUTRESS, T. W., HOFFMAN, M. P. & WAKEFIELD, J. S. 1991. A multi-station dental plaque microcosm (artificial mouth) for the study of plaque growth, metabolism, pH, and mineralization. *J Dent Res*, 70, 1409-16.

SISSONS, C. H. & YAKUB, S. 2000. Suppression of urease levels in *Streptococcus salivarius* by cysteine, related compounds and by sulfide. *Oral Microbiol Immunol*, 15, 317-24.

SLOTS, J. 2002. Selection of antimicrobial agents in periodontal therapy. *J Periodontal Res*, 37, 389-98.

SMITH, C. J. & OSBORN, A. M. 2009. Advantages and limitations of quantitative PCR (Q-PCR)-based approaches in microbial ecology. *FEMS Microbiol Ecol*, 67, 6-20.

SMITH, D. E. & ZARB, G. A. 1989. Criteria for success of osseointegrated endosseous implants. *J Prosthet Dent*, 62, 567-72.

SOCRANSKY, S. S. 1970. Relationship of bacteria to the etiology of periodontal disease. *J Dent Res*, 49, 203-22.

SOCRANSKY, S. S. & HAFFAJEE, A. D. 1992. The bacterial etiology of destructive periodontal disease: current concepts. *J Periodontol*, 63, 322-31.

SOCRANSKY, S. S., HAFFAJEE, A. D., CUGINI, M. A., SMITH, C. & KENT, R. L. 1998. Microbial complexes in subgingival plaque. *J Clin Periodontol*, 25, 134-44.

SOGIN, M. L., MORRISON, H. G., HUBER, J. A., MARK WELCH, D., HUSE, S. M., NEAL, P. R., ARRIETA, J. M. & HERNDL, G. J. 2006. Microbial diversity in the deep sea and the underexplored "rare biosphere". *Proc Natl Acad Sci U S A*, 103, 12115-20.

SOUKOS, N. S. & GOODSON, J. M. 2011. Photodynamic therapy in the control of oral biofilms. *Periodontol 2000*, 55, 143-66.

SPANGBERG, L., ENGSTRÖM, B. & LANGELAND, K. 1973. Biologic effects of dental materials. 3. Toxicity and antimicrobial effect of endodontic antiseptics in vitro. *Oral Surg Oral Med Oral Pathol*, 36, 856-71.

SPRATT, D. A. 2004. Significance of bacterial identification by molecular biology methods. *Endodo Topics*, 9, 5-14.

SPRATT, D. A., WEIGHTMAN, A. J. & WADE, W. G. 1999. Diversity of oral asaccharolytic *Eubacterium* species in periodontitis--identification of novel phylotypes representing uncultivated taxa. *Oral Microbiol Immunol*, 14, 56-9.

STANFORD, C. M. 2008. Surface modifications of dental implants. *Aust Dent J*, 53 Suppl 1, S26-33.

STEWART, P. S. 2003. Diffusion in biofilms. *J Bacteriol*, 185, 1485-91.

SUBRAMANI, K., JUNG, R. E., MOLENBERG, A. & HAMMERLE, C. H. 2009. Biofilm on dental implants: a review of the literature. *Int J Oral Maxillofac Implants*, 24, 616-26.

SUGIYAMA, M. & SIGESATO, G. 2004. A review of focused ion beam technology and its applications in transmission electron microscopy. *J Electron Microsc (Tokyo)*, 53, 527-36.

SUZUKI, M. T., TAYLOR, L. T. & DELONG, E. F. 2000. Quantitative analysis of small-subunit rRNA genes in mixed microbial populations via 5'-nuclease assays. *Appl Environ Microbiol*, 66, 4605-14.

SUZUKI, N., NAKANO, Y., YOSHIDA, A., YAMASHITA, Y. & KIYOURA, Y. 2004. Real-time TaqMan PCR for quantifying oral bacteria during biofilm formation. *J Clin Microbiol*, 42, 3827-30.

SVERZUT, A. T., STABILE, G. A., DE MORAES, M., MAZZONETTO, R. & MOREIRA, R. W. 2008. The influence of tobacco on early dental implant failure. *J Oral Maxillofac Surg*, 66, 1004-9.

SYED, S. A. & LOESCHE, W. J. 1972. Survival of human dental plaque flora in various transport media. *Appl Microbiol*, 24, 638-44.

SYED, S. A. & LOESCHE, W. J. 1978. Bacteriology of human experimental gingivitis: effect of plaque age. *Infect Immun*, 21, 821-9.

TABANELLA, G., NOWZARI, H. & SLOTS, J. 2009. Clinical and microbiological determinants of ailing dental implants. *Clin Implant Dent Relat Res*, 11, 24-36.

TAGUCHI, K., KOMINE, F., FUSHIKI, R., BLATZ, M. B., KAMIO, S. & MATSUMURA, H. 2013. Fracture resistance of single-tooth implant-supported zirconia-based indirect composite-layered molar restorations. *Clin Oral Implants Res*.

TAKASAKI, A. A., AOKI, A., MIZUTANI, K., SCHWARZ, F., SCULEAN, A., WANG, C. Y., KOSHY, G., ROMANOS, G., ISHIKAWA, I. & IZUMI, Y. 2009. Application of antimicrobial photodynamic therapy in periodontal and peri-implant diseases. *Periodontol 2000*, 51, 109-40.

TAKEUCHI, H. & YAMAMOTO, K. 2001. Ultrastructural analysis of structural framework in dental plaque developing on synthetic carbonate apatite applied to human tooth surfaces. *Eur J Oral Sci*, 109, 249-59.

TANNER, A., MAIDEN, M. F., LEE, K., SHULMAN, L. B. & WEBER, H. P. 1997. Dental implant infections. *Clin Infect Dis*, 25 Suppl 2, S213-7.

TANNER, A., MAIDEN, M. F., PASTER, B. J. & DEWHIRST, F. E. 1994. The impact of 16S ribosomal RNA-based phylogeny on the taxonomy of oral bacteria. *Periodontol 2000*, 5, 26-51.

TER STEEG, P. F., VAN DER HOEVEN, J. S., DE JONG, M. H., VAN MUNSTER, P. J. & JANSEN, M. J. 1987. Enrichment of subgingival microflora on human serum leading to accumulation of *Bacteroides* species, *Peptostreptococci* and *Fusobacteria*. *Antonie Van Leeuwenhoek*, 53, 261-72.

THEILADE, J., FEJERSKOV, O. & HORSTED, M. 1976. A transmission electron microscopic study of 7-day old bacterial plaque in human tooth fissures. *Arch Oral Biol*, 21, 587-98.

THIERBACH, R. & EGER, T. 2013. Clinical outcome of a nonsurgical and surgical treatment protocol in different types of peri-implantitis: A case series. *Quintessence Int*, 44, 137-48.

TOMSON, P. L., BUTTERWORTH, C. J. & WALMSLEY, A. D. 2004. Management of peri-implant bone loss using guided bone regeneration: a clinical report. *J Prosthet Dent*, 92, 12-6.

TÖZÜM, T. F., GÜNCÜ, G. N., YAMALIK, N., TURKYILMAZ, I. & GÜNCÜ, M. B. 2008. The impact of prosthetic design on the stability, marginal bone loss, peri-implant sulcus fluid volume, and nitric oxide metabolism of conventionally loaded endosseous dental implants: a 12-month clinical study. *J Periodontol*, 79, 55-63.

UITTO, V. J. 2003. Gingival crevice fluid--an introduction. *Periodontol 2000*, 31, 9-11.

UMEDA, M., TOMINAGA, Y., HE, T., YANO, K., WATANABE, H. & ISHIKAWA, I. 1996. Microbial flora in the acute phase of periodontitis and the effect of local administration of minocycline. *J Periodontol*, 67, 422-7.

UNGVÁRI, K., PELSÖCZI, I. K., KORMOS, B., OSZKÓ, A., RAKONCZAY, Z., KEMÉNY, L., RADNAI, M., NAGY, K., FAZEKAS, A. & TURZÓ, K. 2010. Effects on titanium implant surfaces of chemical agents used for the treatment of peri-implantitis. *J Biomed Mater Res B Appl Biomater*, 94, 222-9.

VALENZA, V., D'ANGELO, M., FARINA-LIPARI, E., FARINA, F. & MARGIOTTA, V. 1987. [Morphostructural changes in human gingival epithelium due to the local application of citric acid during periodontal therapy]. *G Stomatol Ortognatodonzia*, 6, 11-4.

VAN DE SANDE, F. H., AZEVEDO, M. S., LUND, R. G., HUYSMANS, M. C. & CENCI, M. S. 2011. An in vitro biofilm model for enamel demineralization and antimicrobial dose-response studies. *Biofouling*, 27, 1057-63.

VAN DER MEI, H. C., DE VRIES, J. & BUSSCHER, H. J. 1993. Hydrophobic and electrostatic cell surface properties of thermophilic dairy streptococci. *Appl Environ Microbiol*, 59, 4305-12.

VAN STEENBERGHE, D., JACOBS, R., DESNYDER, M., MAFFEI, G. & QUIRYNEN, M. 2002. The relative impact of local and endogenous patient-related factors on implant failure up to the abutment stage. *Clin Oral Implants Res*, 13, 617-22.

VAN WINKELHOFF, A. J. 2012. Antibiotics in the treatment of peri-implantitis. *Eur J Oral Implantol*, 5 Suppl, S43-50.

VAN WINKELHOFF, A. J., GOENÉ, R. J., BENSCHOP, C. & FOLMER, T. 2000. Early colonization of dental implants by putative periodontal pathogens in partially edentulous patients. *Clin Oral Implants Res*, 11, 511-20.

VAN WINKELHOFF, A. J. & WOLF, J. W. 2000. *Actinobacillus actinomycetemcomitans*-associated peri-implantitis in an edentulous patient. A case report. *J Clin Periodontol*, 27, 531-5.

VARGAS-REUS, M. A., MEMARZADEH, K., HUANG, J., REN, G. G. & ALLAKER, R. P. 2012. Antimicrobial activity of nanoparticulate metal oxides against peri-implantitis pathogens. *Int J Antimicrob Agents*, 40, 135-9.

WADE, W. G. 2013. The oral microbiome in health and disease. *Pharmacol Res*, 69, 137-43.

WENNERBERG, A. & ALBREKTSSON, T. 2000. Suggested guidelines for the topographic evaluation of implant surfaces. *Int J Oral Maxillofac Implants*, 15, 331-44.

WENNSTRÖM, J. L., HEIJL, L., DAHLÉN, G. & GRÖNDahl, K. 1987. Periodic subgingival antimicrobial irrigation of periodontal pockets (I). Clinical observations. *J Clin Periodontol*, 14, 541-50.

WILSON, M. 1999. [21] Use of constant depth film fermentor in studies of biofilms of oral bacteria. In: RON, J. D. (ed.). *Methods Enzymol*. Academic Press. 310, 264-279.

WILSON, M., BURNS, T. & PRATTEN, J. 1996. Killing of *Streptococcus sanguis* in biofilms using a light-activated antimicrobial agent. *J Antimicrob Chemother*, 37, 377-81.

WILSON, M., BURNS, T., PRATTEN, J. & PEARSON, G. J. 1995. Bacteria in supragingival plaque samples can be killed by low-power laser light in the presence of a photosensitizer. *J Appl Bacteriol*, 78, 569-74.

WILSON, M., PATEL, H., KPENDEMA, H., NOAR, J. H., HUNT, N. P. & MORDAN, N. J. 1997. Corrosion of intra-oral magnets by multi-species biofilms in the presence and absence of sucrose. *Biomaterials*, 18, 53-57.

WILSON, T. G. 2009. The positive relationship between excess cement and peri-implant disease: a prospective clinical endoscopic study. *J Periodontol*, 80, 1388-92.

WITTWER, C. T., HERRMANN, M. G., MOSS, A. A. & RASMUSSEN, R. P. 1997. Continuous fluorescence monitoring of rapid cycle DNA amplification. *Biotechniques*, 22, 130-1, 134-8.

WOO, P. C., LAU, S. K., TENG, J. L., TSE, H. & YUEN, K. Y. 2008. Then and now: use of 16S rDNA gene sequencing for bacterial identification and discovery of novel bacteria in clinical microbiology laboratories. *Clin Microbiol Infect*, 14, 908-34.

WOOD, S., NATTRESS, B., KIRKHAM, J., SHORE, R., BROOKES, S., GRIFFITHS, J. & ROBINSON, C. 1999. An in vitro study of the use of photodynamic therapy for the treatment of natural oral plaque biofilms formed in vivo. *J Photochem Photobiol B*, 50, 1-7.

WOOD, S. R., KIRKHAM, J., MARSH, P. D., SHORE, R. C., NATTRESS, B. & ROBINSON, C. 2000. Architecture of intact natural human plaque biofilms studied by confocal laser scanning microscopy. *J Dent Res*, 79, 21-7.

WOOD, S. R., KIRKHAM, J., SHORE, R. C., BROOKES, S. J. & ROBINSON, C. 2002. Changes in the structure and density of oral plaque biofilms with increasing plaque age. *FEMS Microbiol Ecol*, 39, 239-244.

XIMÉNEZ-FYVIE, L. A., HAFFAJEE, A. D. & SOCRANSKY, S. S. 2000. Comparison of the microbiota of supra- and subgingival plaque in health and periodontitis. *J Clin Periodontol*, 27, 648-57.

YOSHIDA, A., KAWADA, M., SUZUKI, N., NAKANO, Y., OHO, T., SAITO, T. & YAMASHITA, Y. 2004. TaqMan real-time polymerase chain reaction assay for the correlation of *Treponema denticola* numbers with the severity of periodontal disease. *Oral Microbiol Immunol*, 19, 196-200.

YOSHINARI, M., KATO, T., MATSUZAKA, K., HAYAKAWA, T. & SHIBA, K. 2010. Prevention of biofilm formation on titanium surfaces modified with conjugated molecules comprised of antimicrobial and titanium-binding peptides. *Biofouling*, 26, 103-10.

ZABETAKIS, P. M., COTELL, C. M., CHRISEY, D. B. & AUYEUNG, R. C. 1994. Pulsed laser deposition of thin film hydroxyapatite. Applications for flexible catheters. *ASAIO J*, 40, M896-9.

ZABLOTSKY, M. H., DIEDRICH, D. L. & MEFFERT, R. M. 1992. Detoxification of endotoxin-contaminated titanium and hydroxyapatite-coated surfaces utilizing various chemotherapeutic and mechanical modalities. *Implant Dent*, 1, 154-8.

ZANIN, I. C., GONÇALVES, R. B., JUNIOR, A. B., HOPE, C. K. & PRATTEN, J. 2005. Susceptibility of *Streptococcus mutans* biofilms to photodynamic therapy: an in vitro study. *J Antimicrob Chemother*, 56, 324-30.

ZARB, G. A. & ALBERKTSSON, T. 1990. [Criteria for determining clinical success with osseointegrated dental implants]. *Cah Prothese*, 19-26.

ZAURA, E., BUIJS, M. J., HOOGENKAMP, M. A., CIRIC, L., PAPETTI, A., SIGNORETTO, C., STAUDER, M., LINGSTRÖM, P., PRATTEN, J., SPRATT, D. A. & WILSON, M. 2011. The effects of fractions from shiitake mushroom on composition and cariogenicity of dental plaque microcosms in an *in vitro* caries model. *J Biomed Biotechnol*, 2011, 135034.

ZAURA, E., KEIJSER, B. J., HUSE, S. M. & CRIELAARD, W. 2009. Defining the healthy "core microbiome" of oral microbial communities. *BMC Microbiol*, 9, 259.

ZAURA-ARITE, E., VAN MARLE, J. & TEN CATE, J. M. 2001. Conofocal microscopy study of undisturbed and chlorhexidine-treated dental biofilm. *J Dent Res*, 80, 1436-40.

ZECHNER, W., KNEISSEL, M., KIM, S., ULM, C., WATZEK, G. & PLENK, H. 2004. Histomorphometrical and clinical comparison of submerged and nonsubmerged implants subjected to experimental peri-implantitis in dogs. *Clin Oral Implants Res*, 15, 23-33.

ZEE, K. Y. 1996. Predominant cultivable supragingival plaque in Chinese "rapid" and "slow" plaque formers. *J Clin Periodontol*, 23, 1025-1031.

ZEE, K. Y., SAMARANAYAKE, L. P., ATTSTRÖM, R. & DAVIES, W. I. 1996. Predominant cultivable microflora of supragingival dental plaque in Chinese individuals. *Arch Oral Biol*, 41, 647-53.

ZIJNGE, V., VAN LEEUWEN, M. B., DEGENER, J. E., ABBAS, F., THURNHEER, T., GMÜR, R. & HARMSEN, H. J. 2010. Oral biofilm architecture on natural teeth. *PLoS One*, 5, e9321.

ZINELIS, S., SILIKAS, N., THOMAS, A., SYRES, K. & ELIADES, G. 2012. Surface characterization of SLActive dental implants. *Eur J Esthet Dent*, 7, 72-92.

ZITZMANN, N. U. & BERGLUNDH, T. 2008. Definition and prevalence of peri-implant diseases. *J Clin Periodontol*, 35, 286-91.

ZYLBER, L. J. & JORDAN, H. V. 1982. Development of a selective medium for detection and enumeration of *Actinomyces viscosus* and *Actinomyces naeslundii* in dental plaque. *J Clin Microbiol*, 15, 253-9.

Appendix: Consent form

Informed Consent Form for Participants

Title of Project:

NUTRIDENT: Towards functional foods for oral healthcare

This study has been approved by
the UCL Research Ethics
Committee [Project ID Number]:

1364/001

Participant's Statement

I agree that I have (please tick):

read the information sheet and/or the project has been explained to me orally;

had the opportunity to ask questions and discuss the study;

received satisfactory answers to all my questions or have been advised of an individual to contact for answers to pertinent questions about the research and my rights as a participant and whom to contact in the event of a research-related injury.

I agree to be contacted in the future by UCL researchers who would like to invite me to participate in follow-up studies.

I understand that I am free to withdraw from the study without penalty if I so wish and I consent to the processing of my personal information for the purposes of this study only and that it will not be used for any other purpose. I understand that such information will be treated as strictly confidential and handled in accordance with the provisions of the Data Protection Act 1998.

Signed: Date:

Investigator's Statement

I confirm that I have carefully explained the purpose of the study to the participant and outlined any reasonably foreseeable risks or benefits (where applicable).

UCL Eastman Dental Institute
256 Gray's Inn Road London WC1X 8LD
Tel: +44 (0)20 7915 1050 Fax: +44 (0)20 7915
1127
www.eastman.ucl.ac.uk



The Institute hosts a World Health Organization
Collaborating Centre for Research, Education and
Service in Oral Health, Disability and Culture.

Signed:

Date: